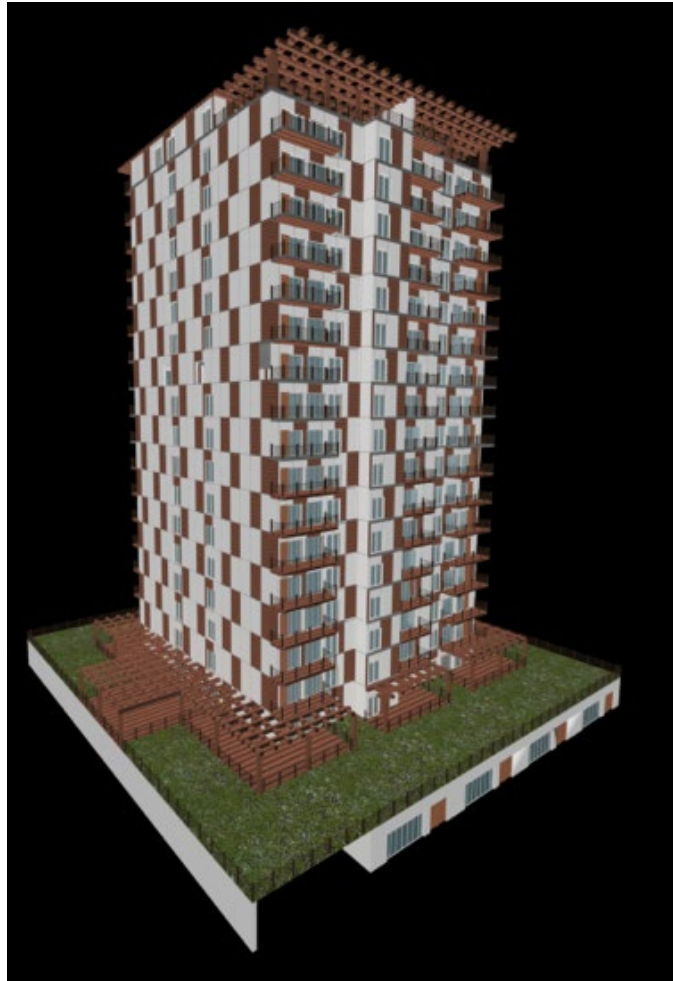


# Application of Analysis Tools from NEWBuildS Research Network in Design of a High-Rise Wood Building



NSERC Strategic Research Network on Innovative Wood Products and Building Systems (NEWBuildS)

In Partnership with FPInnovations



---

# FOREWORD

In 2009, through the Forest Sector R&D Initiative and in partnership with FPInnovations, a research network on Innovative Wood Products and Building Systems, known as NEWBuildS, was established by the Natural Sciences and Engineering Research Council of Canada (NSERC). The team of NEWBuildS researchers is investigating new applications for traditional light-weight wood frame in mid-rise construction, as well as heavier systems built with engineered wood products. Innovative construction that combines wood with other building materials to create hybrid building systems is also being investigated. The research team consists of 25 university professors and 19 researchers from FPInnovations, National Research Council (NRC) and the Canadian Wood Council (CWC). These researchers, with expertise in architecture, structural engineering, fire engineering, building acoustic and building envelope, supervise about 70 graduate students and post-doctoral fellows from 13 Canadian universities. The vision of NEWBuildS is to generate technical information that supports the use of wood products in multi-storey buildings for residential and non-residential purposes in Canada and other markets.

In 2013, NEWBuildS in partnership with FPInnovations initiated a project to demonstrate the application of the analysis tools and other technical information from the NEWBuildS research program in the analysis and design of a high-rise wood hybrid building. The three key objectives of the demonstration project are:

1. To demonstrate the use of tools developed and adopted within the NEWBuildS research program in designing tall wood buildings, thereby potentially making them available for future use by designers and code authorities for evaluating building designs under the alternative solution path. The work was carried out in accordance with the key reference document ‘Technical Guide for the Design and Construction of Tall Wood Buildings in Canada’ published by FPInnovations.
2. To identify additional challenges related specifically to the type of building considered and future research needs.
3. To provide a real-world training environment for NEWBuildS graduate students and post-doctoral fellows (PDF).

In this project, a conceptual but realistic 20-storey building of hybrid construction incorporating massive timber panels and other structural materials was identified. The project team, consisting of three practicing consultants and 6 graduate student and post-doctoral researchers from NEWBuildS, undertook an analysis and engineering design of the demonstration building. An advisory group that includes FPInnovations scientists, NEWBuildS supervisors of the graduate students and Post Doctoral Fellows, provides technical support to the project team. The performance attributes addressed in the project were structural performance under seismic and wind load, fire resistance and building envelope. . This publication documents the analysis and design of the demonstration building, and identifies technical issues that require further study.

## **Lynn Embury-Williams**

Executive Director  
WoodWORKS! British Columbia  
and  
Chair,  
Board of Directors  
NEWBuildS

## **Erol Karacabey**

Research Manager  
Advanced Building Systems Department  
FPInnovations  
and  
Member,  
Board of Directors  
NEWBuildS

# PROJECT TEAM

NAME	AFFILIATION	ROLE
Robert Drew	Perkins + Wills	Architectural consultant
Eric Karsh	Equilibrium Consulting	Structural consultant
Andrew Harmsworth	GHL Consultants	Fire consultant
Dr. Mohamed Nadim Adi	University of Alberta	NEWBuildS HQP, architecture
Sabrina D'Ambra	Concordia University	NEWBuildS HQP, building envelope
Dr. Zhiyong Chen	University of New Brunswick	NEWBuildS HQP, structural
Dr. Minghao Li	University of British Columbia	NEWBuildS HQP, structural
Alejandro Medina	Carleton University	NEWBuildS HQP, fire
Xiao Li	Carleton University	NEWBuildS HQP, fire
Christian Dagenais	FPIInnovations	Advisor, fire
Dr. Marjan Popovski	FPIInnovations	Advisor, structural
Dr. Jieying Wang	FPIInnovations	Advisor, building envelope
Conroy Lum	FPIInnovations	Advisor, structural
Dr. Frank Lam	University of British Columbia	HQP supervisor
Dr. Ying-Hei Chui	University of New Brunswick	HQP supervisor
Dr. George Hadjisophocleous	Carleton University	HQP supervisor
Dr. Mohamed Al-Hussein	University of Alberta	HQP supervisor
Dr. Hua Ge	Concordia University	HQP supervisor
Gary Chen	GHL Consultants	Advisor, fire
Dr. Mahmoud Rezai	Equilibrium Consulting	Advisor, structural
Caroline Frenette	Cecobois	Advisor, building envelope

---

## **ACKNOWLEDGEMENTS**

This project was conducted with financial support of NSERC through its Strategic Network Enhancement Initiative (SNEI) program, and BC Forestry Innovation Investment (FII) through its Wood First program.

---

# CONTENTS

## Pages

1	<b>Foreword</b>	
2	<b>Project Team</b>	
3	<b>Acknowledgements</b>	
6 - 14	<b>Chapter 1   Architectural Details</b>	Mohammed Nadeem Adi   Robert Drew   Mohammed Al-Hussein
15 - 36	<b>Chapter 2   Development of Lateral Load Resisting System</b>	Zhiyong Chen   Ying-He Chui   Marjan Popovski
37 - 47	<b>Chapter 3   Analysis and Design of Gravity Load Resisting System</b>	Zhiyong Chen   Minghao Li   Ying-He Chui   Marjan Popovski
49 - 63	<b>Chapter 4   Fire Risk Assessment</b>	Xiao Li   George Hadjisophocleous   Alejandro Medinar   Andrew Harmsworth   Christian Dagenais
65 - 80	<b>Chapter 5   Fire Resistance Design</b>	Alejandro Medina   George Hadjisophocleous   Christian Dagenais
81 - 106	<b>Chapter 6   Design of Energy Efficient and Durable Envelope</b>	Hua Ge   Sabrina D'Ambra   Lin Wang
107 - 114	<b>Appendix A   Architectural Drawings</b>	
115 - 125	<b>Appendix B   Structural Drawings</b>	

# CHAPTER 1

## ARCHITECTURAL DETAILS

---

**Mohamad Nadim Adi** | University of Alberta

**Robert Drew** | Perkins + Will

**Mohamed Al-Hussein** | University of Alberta

---

## 1. INTRODUCTION

Wood is one of the most widely used building materials in the Canadian construction market, with the majority of homes being wood-framed. Despite its popularity in low-rise buildings, tall buildings made from wood are a rare occurrence. In tall buildings wood is used primarily as a finishing material. The lack of tall wood-framed buildings is partially due to the fact that most building codes do not permit their construction. In the research presented in this chapter, a team of experts representing the areas of architecture, civil engineering, fire safety, construction, and building envelope has collaborated to provide a tall wooden building design. The aim is to demonstrate the opportunity to use wood as a structural, load-bearing element within tall buildings and transcend the traditional view of wood which would limit its application to light framing and finishing. The main output of this chapter is the design of the high-rise tower itself. The appearance of the building (materials, wood ratio, window ratio, and interior) is a direct result of consultations among the different building groups to provide the plans, elevations, and 3D models of what is the first tall wood building in Canada.

## 2. CONTEXT

For this project, a 20-storey mixed-use project is chosen to demonstrate the feasibility of using wooden products as the main structural building material in high-rise construction. A site in North Vancouver, Canada is selected as the theoretical location for the building. Subject to wet, windy environmental conditions and seismic activity, this location offers a specific set of challenges which have historically been considered barriers to wood-framed high-rise construction. The team followed the British Columbia Building Code in designing the high-rise building. It is believed that applying evolving building science and engineering methodologies to develop a viable design solution in the Pacific Northwest context will serve as a catalyst for exploring the feasibility of wood high-rise construction in other construction markets across North America.

## 3. ARCHITECTURAL DESIGN

The project comprises a 19-storey residential tower over a 1-storey commercial podium above an underground parkade. For the purpose of this study both the parkade and podium are designed to be constructed with concrete. The residential tower is designed to be constructed using structural engineered wood products. At 20 storeys, the tower falls under the 60 m height limit set by the design team.

The typical floor comprises residential suites situated around a compact central core encompassing the building users' vertical circulation. The design incorporates the use of cross-laminated timber (CLT) panels as the main structural system. The main objective of this project is to demonstrate the viability of wood as an efficient and suitable primary structural component that can be used in place of traditional structural building materials for tall buildings (e.g., concrete, steel).

The suites are sized and configured in a manner that is typical for residential suites in the Vancouver market. While the wood

structure is clad with gypsum board where it adjoins the suite demising walls, it is left exposed where it is an in-suite interior wall. Windows are mainly placed on the north and south façades. This is done to capitalize on the view in these directions as well as to maximize sunlight levels in the units. Structural wooden elements are purposely left exposed when possible for aesthetic reasons. While this project markets wood as a viable and economical structural system for tall buildings, leaving such elements exposed also enhances the design value. Having a simple and symmetrical design layout provides a design model that is not overly complicated (since overly complex designs may deter developers and clients).

## 4. PRELIMINARY DESIGNS

Early designs of the project explored several issues, such as the respective proportions and positions of windows and wood panels in the tower. Through discussions among the experts on the research team the design of the tower was fine-tuned. For instance, although the team had originally concentrated the wooden elements on the corners of the tower where the balconies were situated, the fire safety group pointed out that having a wooden exterior that ran continuously on the façade would pose a fire hazard. The orientation of the units was modified as well to capitalize on the benefits of the north and south views. The team also explored the possibility of having a green roof on the penthouse level, but then decided to include it on the lower level of the tower instead so that it would be accessible to the residents of the first tower floor. Figures 1 to 4 show the progression of design during the early stages of the project.



FIGURE 1: TOWER DESIGN STAGE 1

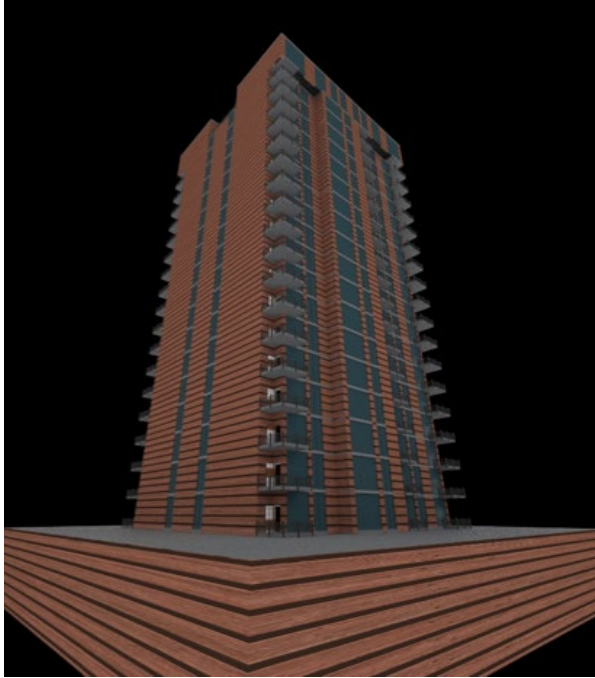


FIGURE 2: TOWER DESIGN STAGE 2

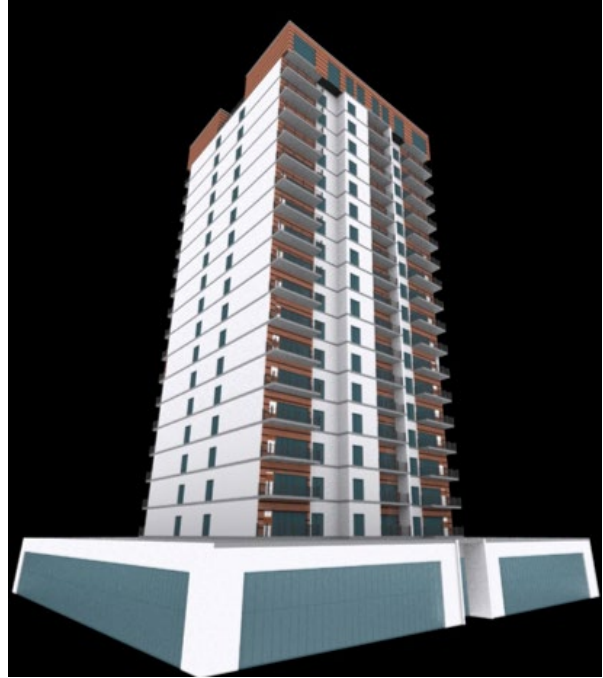


FIGURE 3: TOWER DESIGN STAGE 3



FIGURE 4: VARIATIONS OF EXTERIOR APPEARANCE FOR TOWER DESIGN STAGE 4

## 5. FINAL DESIGN

### PODIUM – LEVEL 1:

The single-storey 2250 m<sup>2</sup> podium comprises the main residential entry and commercial retail space facing the street, as well as key loading, parkade access, and service spaces facing the laneway. As noted above, the design of the podium assumes concrete construction.

The design of this floor includes minimal partitions, ensuring a flexible space that can be easily adapted for various purposes. Visitor parking is available in the back of the building. Residents enter through the courtyard to a lobby where they have access to the mail area. They can also access the parking through the back. This level also includes storage and service rooms. The main building entrance is located in the southeast corner.

The areas of the respective rooms are as follows:

- Room 1: 172 m<sup>2</sup>
- Room 2: 172 m<sup>2</sup>
- Room 3: 202 m<sup>2</sup>
- Room 4: 213 m<sup>2</sup>
- Service: 121 m<sup>2</sup>
- Total storage area: 240 m<sup>2</sup>

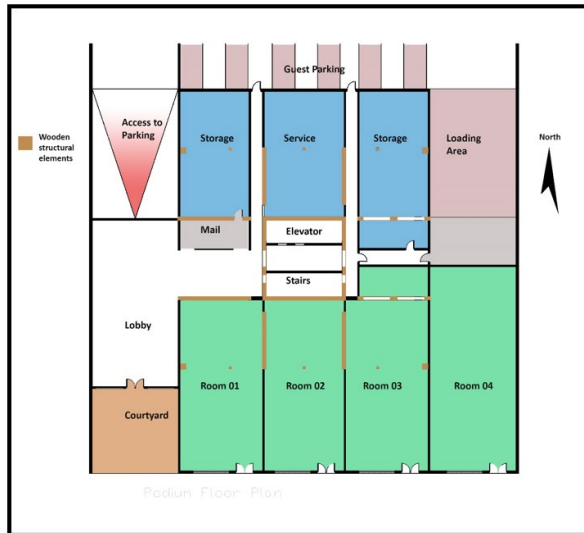


FIGURE 5: PODIUM FLOOR PLAN

### TOWER – LEVEL 2:

With a total area of 712 m<sup>2</sup>, this floor includes four one-bedroom units and two two-bedroom units, each with a large deck typical of large podium roof-top areas. It also has a communal deck and a utility room for the use of residents. Decks on this floor are shaded by pergolas, an addition which offers the added benefit of privacy. Green roof is used to cover the remainder of the podium floor. This provides a beautiful view both to occupants of this floor and to those on higher floors. The areas of the units on the podium floor are as follows:

- One-bedroom units: 66 – 70 m<sup>2</sup>
- Two-bedroom units: 100 – 102 m<sup>2</sup>
- Utility room: 64 m<sup>2</sup>
- Communal Deck: 86 m<sup>2</sup>

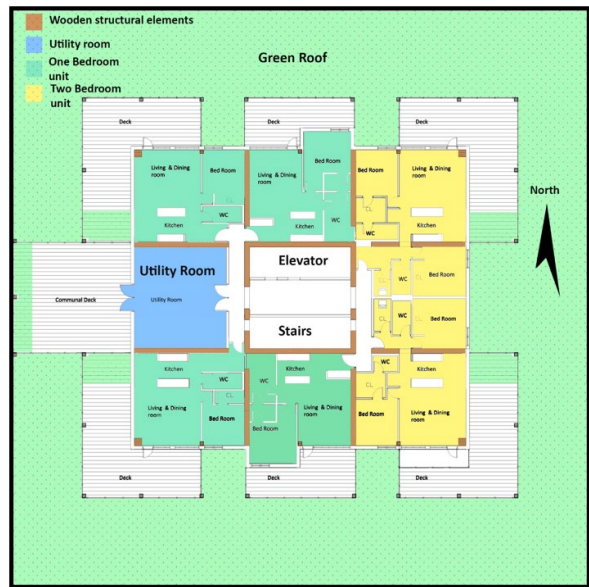


FIGURE 6: LEVEL ONE TOWER FLOOR PLAN

**TOWER - LEVELS 3 TO 19:**

Each with a total area of 712 m<sup>2</sup>, these floors each consist of six condo units—two one-bedroom units and four two-bedroom units. Condos in these floors have either north- or south-facing balconies to capitalize on the views. The floor areas of the respective units are as follows:

One-bedroom units: 70 m<sup>2</sup>

Two-bedroom units: 100 – 102 m<sup>2</sup>

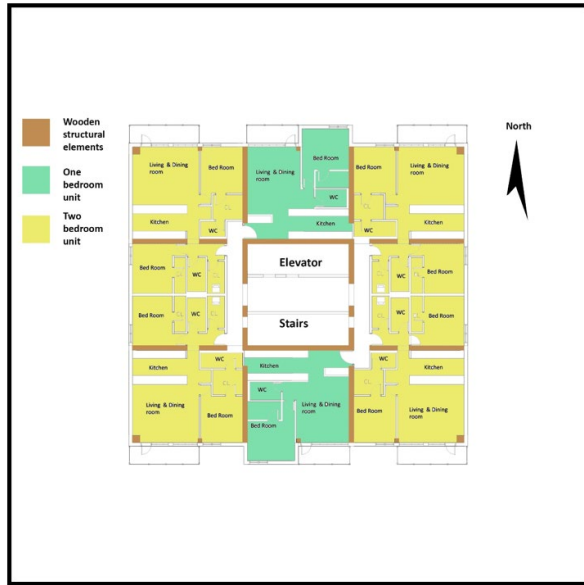


**FIGURE 7:** LEVELS TWO TO EIGHTEEN TOWER FLOOR PLAN

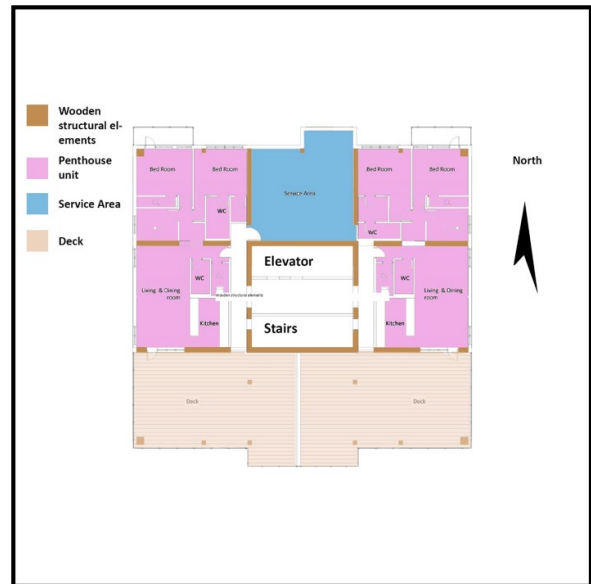
**TOWER – LEVEL 20 (PENTHOUSE):**

With a total area of 627 m<sup>2</sup>, this floor has two penthouse units with large south-facing decks. Each penthouse unit has two bedrooms, a living/dining area, two bathrooms, a kitchen, a study that can double as a third bedroom, and a north-facing balcony. The decks of the penthouse units are covered with pergolas to provide shading and enhance the aesthetic appeal. A general service room for the entire tower is also located on this level. The floor areas of the different spaces on this level are provided below.

Penthouse units: 157 m<sup>2</sup>

Penthouse decks: 100 m<sup>2</sup>

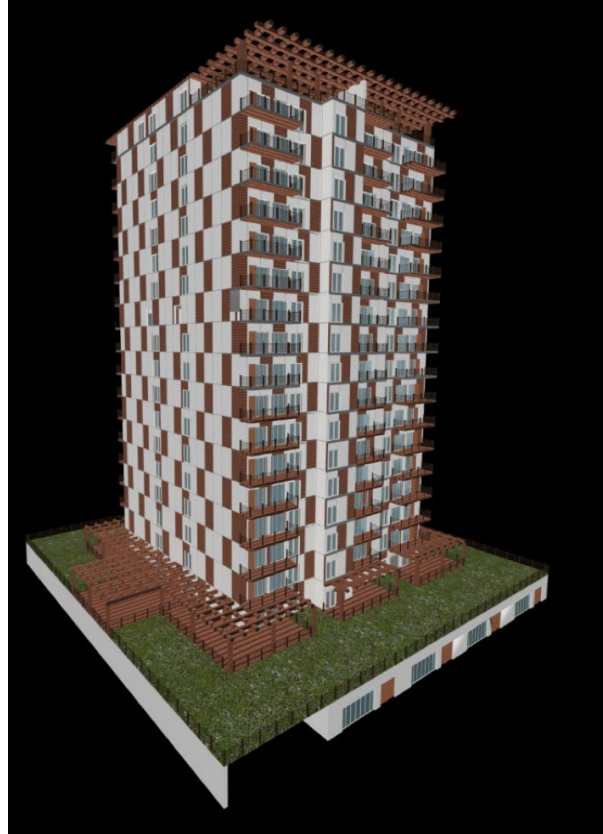
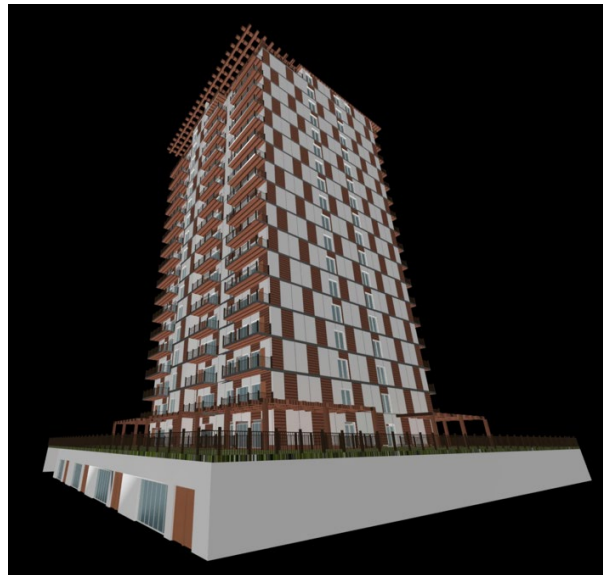
Service room: 76 m<sup>2</sup>



**FIGURE 8:** PENTHOUSE FLOOR PLAN

**EXTERIOR:**

A panel system was chosen for the cladding of the tower, with some portions of it being regular wall (gypsum panels) and others being engineered cedar cladding. This system can be produced offsite and installed quickly once it arrives at the building site, thereby contributing to the overall efficiency of the project. (The building materials considered in the design, including their properties, commercial brands, and suppliers, will be discussed in the building envelope chapter.) After discussions with experts in the team it was decided to limit the percentage of wooden cladding to 30% of the total surface area, with the panels separated by areas without wooden cladding for fire safety reasons, as discussed above. A checker pattern was chosen, as it provided a strong and distinguishing visual statement. Wood cladding was also selected for both the ceilings and floors of the balcony areas, also partly for aesthetic reasons. The inclusion of wooden-clad balcony ceilings presented an opportunity to showcase the prominent use of wood materials to passersby. Glazing was generally placed on the north and south façades, ensuring pleasing views for residents, as well as optimal natural lighting. Figures 9 to 11 show the exterior of the tower.

**FIGURE 9:** SOUTHEAST VIEW OF THE TOWER**FIGURE 10:** SOUTHWEST VIEW OF THE TOWER**FIGURE 11:** SOUTHEAST LOWER VIEW OF THE TOWER SHOWING THE WOODEN CLADDING ON THE BALCONIES

Figures 12 to 15 show the façades of the tower. The tower design was kept symmetrical with the exception of the penthouse level. This was done partly to simplify the prefabrication process for the construction of the tower, but also in consideration of the fact that symmetrical design provides a more stable and structurally sound building.

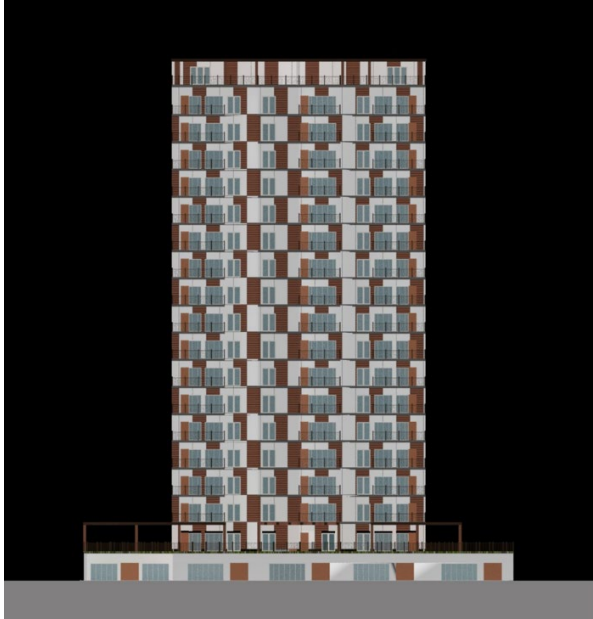


**FIGURE 12:** SOUTH FACADE

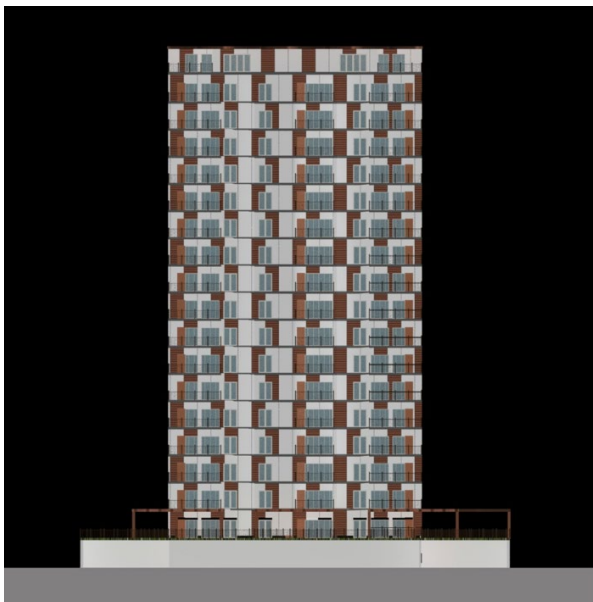


**FIGURE 13:** NORTH FACADE



**FIGURE 14:** WEST FACADE



**FIGURE 15:** EAST FACADE

**INTERIOR:**

Figure 16 shows an interior view of one of the one-bedroom units. As mentioned above, the columns were left exposed as a design statement, and the load-bearing wooden wall visible in the figure was left exposed for the same reason. This design of the interior space with exposed structural elements highlights the dual benefit of structural wood elements both as a structurally suitable and economical option, and a finishing element the texture and appearance of which make it highly desirable to buyers and occupants. Since the wood building materials used—cedar, CLT, and glulam—all offer appealing texture and appearance; the design team deemed it undesirable to cover these materials with drywall or paint. After talks with the fire safety experts it was decided to limit the use of wood as a finishing material to either the floors or the ceilings, as using wood for both would significantly increase the fire hazard as well as the cost of construction. In light of these considerations, hardwood was chosen for the floors, with a non-wood finishing material selected for the ceilings.



**FIGURE 16:** INTERIOR VIEW OF ONE-BEDROOM UNIT

**7. ACKNOWLEDGEMENTS**

The authors would like to thank members of the University of Alberta research team's support staff for their technical editing assistance.

**6. RECOMMENDATIONS AND CONCLUSIONS**

Wood as a structural material was found to enhance rather than hinder the design process and overall product. Having structural elements made from wood provided the design team with an abundance of design elements to utilize both inside and outside of the units. There are still some concerns regarding weather proofing of the exterior panels that must be answered by building envelope experts. Fire hazards will always be an issue of concern with combustible elements, but that will be answered in the fire safety chapter. Having interior wood panels and finishing, particularly for the floors, also raises concerns about the acoustic quality of the interior space and particularly the potential for increased noise transfer between living spaces and floors. In this regard, it is recommended that a detailed acoustic study and analysis of the space be carried out. It should also be kept in mind that residents will also alter the acoustics and other properties of the space through the addition of décor, furniture, and other fixtures. As a concluding remark, wood is found to be a suitable choice for this type of high-rise project that satisfies the structural requirements while providing flexibility and aesthetic appeal.

# CHAPTER 2

## DEVELOPMENT OF LATERAL LOAD RESISTING SYSTEM

---

**Zhiyong Chen** | University of New Brunswick

**Ying-Hei Chui** | University of New Brunswick

**Marjan Popovski** | FPInnovations / University of British Columbia (Adjunct Professor)

## 1. INTRODUCTION

### 1.1 BACKGROUND

Wood as a structural material can date back to more than 7000 years. The oldest standing wood structure is the Horyu-ji Temple, which was built about 1,400 years ago and is located in Nara, Japan. The tallest one is the Pagoda of Fogong Temple (commonly known as Yingxian Wood Pagoda, Fig. 1) with nine storeys and 67.31m in height that was built in Shanxi, China, in 1056 AD (Chen 2011).

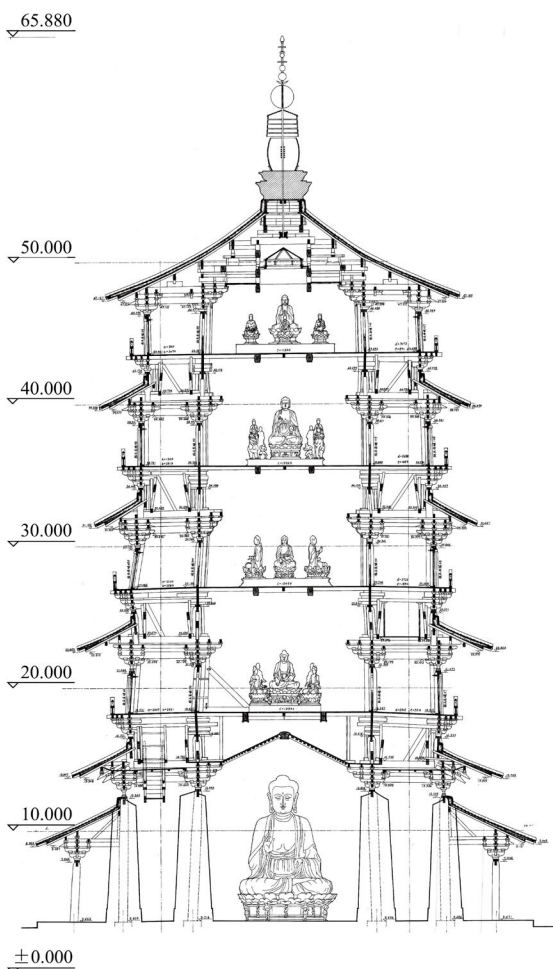


**FIGURE 1:** VERTICAL SECTION IN EAST-WEST DIRECTION (IN M MEASURED IN 1991) OF YINGXIAN WOOD PAGODA

Nowadays in Canada, however, wood structures are usually built to a maximum of 4 storeys due to restriction by building codes primarily because of concerns about fire safety. Even though the provinces of British Columbia, Ontario and Quebec have raised the storey limit of wood buildings from four to six, there is still a large potential for taller wood structures to be built.

Due to escalating land costs and costs of developing new sub-divisions, local authority and developers are favoring

tall buildings in inner cities. This has created interest in exploring use of wood in high-rise building projects. These structures pose big challenges to designers, especially from the perspective of their resistance against lateral loads, arising from wind and earthquake. In this chapter, the development of a lateral load resisting system (LLRS) and the structural design and numerical simulation of the system in the demonstration tall wood building are described.

### 1.2 TECHNOLOGY ROADMAP

The structural design of the building is performed following the procedure shown in Fig. 2.

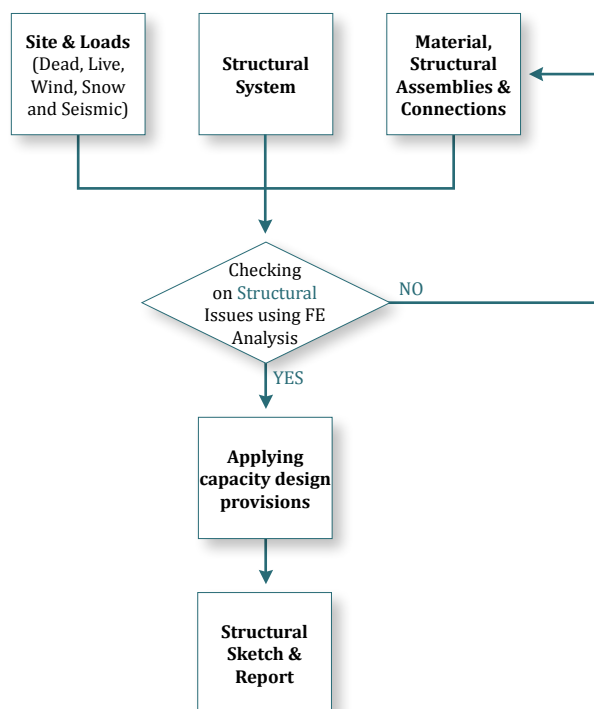


**FIGURE 2:** FLOW CHART OF THE STRUCTURAL DESIGN

The structural material and system are selected according to availability, site and loading conditions. Initially, the structural assemblies and connections are first determined based on experience. Then, the structural performances of the buildings are checked by performing an analysis, using an appropriate model, such as finite element (FE) Analysis. If any targets are not fulfilled with the design criteria, the assemblies and connections will be re-designed based on the FE analysis result. As long as all the design criteria have been met, a structure with suitable assemblies and connections is obtained. For a common high-rise building, 1 to 2 iterations for the assemblies and connections are usually enough. However, since tall wood building is a relatively new experience, more iterations would be expected.

This 20-storey demonstration building includes a 19-storey massive timber structure and 1 storey concrete podium structure. Since a concrete structure can be regarded to have

a much higher lateral stiffness than that of a wood structure, the structural design of this building focuses on the timber structure only.

## 2. CONCEPTUAL DESIGN OF LLRS FOR TALL WOOD BUILDING

### 2.1 STRUCTURAL SYSTEM

Appropriate structural analysis and design will lead to the development of a safe and economical structure. The right structural system can provide the best performance under loads with less material and simplest details. There are different types of structural system for high-rise buildings. They include moment resisting frame, braced frame, shear wall, core and outrigger system, tubular system (framed tube, trussed tube and bundle tubes), and hybrid system. The type of system to use will depend on the height and use of the building.

Taking into account the material of wood and the 19 storeys, shear wall with a core system was chosen as the LLRS for this tall wood building. These two subsystems, shear wall and core, are connected by steel beams with hinge joints, as illustrated in Fig. 3. In order to reduce the size of the horizontal connections between panels, which may be huge and complicated because of the large lateral load, the balloon framing construction technique and massive timber panels with full length were selected to build the shear wall and core.

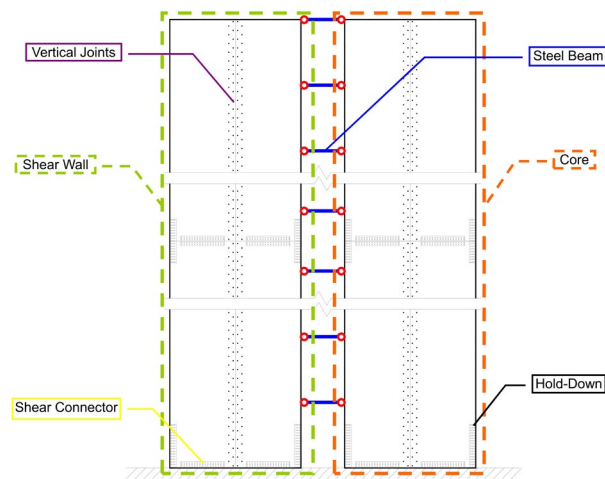


FIGURE 3: SCHEMATIC DIAGRAM OF THE LLRS

### 2.2 CONNECTION SYSTEM

Usually, the length of shear wall or/and core is larger than the width of the current massive panels (2.44m for laminated strand lumber, LSL and 3.00m for cross laminated timber, CLT), vertical joints (Fig. 3) are needed to connect adjacent panels horizontally. To resist the shear between panels or between panel and the podium, as well as the overturning uplift force, shear connectors and hold-downs are required, as shown in Fig. 3.

As it is known that the mechanical connections of timber structures are often the weakest link and source of ductility of the whole structural system, the connection type and the failure order among the connections affect the structural performance of the buildings under seismic and wind actions.

In an attempt to design this tall wood building with higher stiffness, strength and ductility, dowel-type connections and HSK (Wood–Steel–Composite) system (Fig. 4), are used in the vertical joints of the shear wall and core, respectively. The HSK system is also used as the shear connectors and hold-down connections. The vertical joints of shear wall (dowel-type connections) and the core (HSK system) are assumed to yield sequentially, and the ultimate limit state of the building is defined as the failure of the shear connectors and hold-downs.



FIGURE 4: HSK SYSTEM

### 3. STRUCTURAL DESIGN OF LLRS

#### 3.1 DESIGN INFORMATION AND PROCEDURE

##### 3.1.1 Design Data

The tall wood building is composed of 19 standard timber storey and 1 concrete podium. The total height is 60 m with 3 m per storey, and the standard plane dimensions are 27 m × 27 m with 9 m grids. This 20-storey demonstration building is assumed to be located at the junction of 15<sup>th</sup> St. W. and Lonsdale St., North Vancouver, BC, which has high earthquake, wind and rain load. The importance category of “Normal” and a site class of “D” were used in the design. The design data (Table 1) is based on the NBCC (NRC 2010) for North Vancouver. The design criteria are given in Table 2.

ITEM	VALUE	SOURCE	
<b>Dead Load</b>			
Roof	3.00 kPa	Including allowance for roof top units and screens	
Floor	5.00 kPa	Including 125mm concrete topping	
Partition	0.50 kPa		
<b>Live Load</b>			
Roof	1.82 kPa		
Floor	1.90 kPa		
<b>Ground Snow Load</b>			
Importance factor, $I_s$	ULS	1.0	Table 4.1.6.2
	SLS	0.9	
$S_s$		3.00 kPa	Table C-2
$S_r$		0.30 kPa	
<b>Wind Load</b>			
Importance factor, $I_w$	ULS	1.0	Table 4.1.7.1
	SLS	0.75	
Hourly Wind Pressure	1/10	0.35 kPa	Table C-2
	1/50	0.45 kPa	
<b>Earthquake Load</b>			
Importance factor, $I_E$	ULS	1.00	Table 4.1.8.5
	$S_a(0.2)$	0.88	
Spectral acceleration (5%)	$S_a(0.5)$	0.61	Table C-2
	$S_a(1.0)$	0.33	
	$S_a(2.0)$	0.17	
Peak Ground Acceleration	PGA	0.44 g	

TABLE 1: DESIGN DATA OF NORTH VANCOUVER

LOAD	ITEM	VALUE	SOURCE (NBCC)
Wind	Inter-storey drift	$h_n/500$	4.1.3.5-3
	Peak acceleration	$1.5\% \times g$	Commentary I
Seismic	Inter-storey drift	$h_n/40$	4.1.8.13-3

Note:  $h_n$  is the storey height.

TABLE 2: DESIGN CRITERIA

##### 3.1.2 Design Procedure

The analysis and design procedure of the building for lateral load resistance is illustrated in Fig. 5.

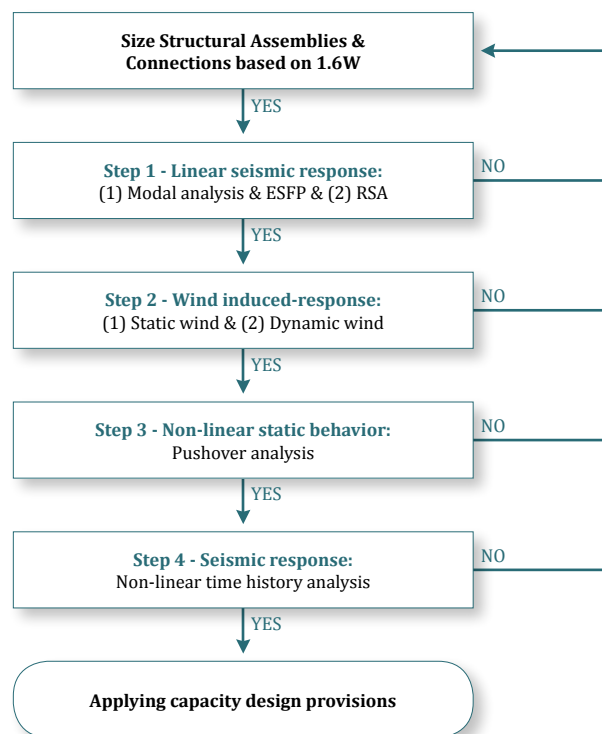


FIGURE 5: ANALYSIS AND DESIGN PROCEDURE

At the initial point, the structural assemblies and connections were sized based on 1.6 times design wind load, since high-rise building design is usually determined by serviceability limit states of wind action and the design strengths for structural components or connections are approximately equal to their average ultimate load-carrying capacity divided by a load factor of 1.6 (CWC 2010).

Step 1: Equivalent static force procedure (ESFP) and response spectrum analysis (RSA) were performed to determine the seismic load applied on the structure based on the natural periods calculated from modal analysis. If necessary, revise assembly sizes and connection details.

Step 2: Wind-induced response was investigated by conducting static and dynamic wind analysis. If necessary, revise assembly sizes and connection details and return to step 1.

Step 3: The structural performance, in terms of stiffness, strength and ductility, of the building was analyzed by conducting non-linear pushover analysis. If necessary, revise assembly sizes and connection details and return to step 1.

Step 4: Non-linear time history analysis was performed to investigate the seismic response of the building. If necessary, revise assembly sizes and connection details and return to step 1.

Since the LLRS's in the two major directions are nearly the same, only the LLRS in the East-West direction was designed and analyzed. In this report only the final design results are presented.

### 3.2 STRUCTURAL SYSTEM

#### 3.2.1 Wind Design

Three different procedures of determining design wind load on buildings are indicated in NBCC 4.1.7, Wind Load: Static Procedure, Dynamic Procedure and Experimental Procedure. They are selected for this project according to the height/width ratio, height and the lowest natural frequency of the building. Usually, the static procedure can be used for buildings with natural frequency higher than 1 Hz, the dynamic procedure will be used for cases of 0.25 – 1 Hz, while the experimental procedure shall be used for other buildings (natural frequency < 0.25 Hz).

##### (1) Static Procedure

As an initial step, static procedure was performed to derive the wind load applied on the tall wood building. The specified external pressure or suction due to wind on a building was calculated using equation 1.

$$p = I_w q C_e C_g C_p \quad [1]$$

where,  $p$  is the specified external pressure acting statically and in a direction normal to the surface, either as a pressure directed towards the surface or as a suction directed away from the surface;  $I_w$  is the importance factor for wind load, as provided in Table 1;  $q$  is the reference velocity pressure, as provided in Table 1;  $C_e$  is the exposure factor,  $0.7(h/12)^{0.3}$  but not less than 0.7 since the location is classed as rough terrain;  $C_g$  is the gust effect factor, 2.0;  $C_p$  is the external pressure coefficient, averaged over the area of the surface considered, 0.8 and -0.5 for windward and leeward sides, respectively.

Only one partial loading case (Fig. 6) was considered. The wind load and the shear at each storey are shown in Table 3.



FIGURE 6: FULL WIND PRESSURE APPLIED IN EAST-WEST DIRECTION (NRC 2010)

STOREY	$h_p, m$	$C_e$	$F_p, kN$	$V_p, kN$	$X_p, mm$	$X_r, mm$	$F_r X_r, mm^2$	$W_r X_r^2, t \cdot mm^2$
20	60	1.13	72	72	31.2	1.72	124	652
19	57	1.12	71	143	29.5	1.72	123	977
18	54	1.10	70	213	27.8	1.75	122	1008
17	51	1.08	69	282	26.0	1.78	123	1050
16	48	1.06	67	350	24.2	1.82	123	1091
15	45	1.04	66	416	22.4	1.85	122	1125
14	42	1.02	65	481	20.6	1.89	122	1171
13	39	1.00	63	544	18.7	1.87	118	1154
12	36	0.97	62	606	16.8	1.86	115	1139
11	33	0.95	60	666	14.9	1.84	111	1121
10	30	0.92	58	724	13.1	1.82	106	1095
9	27	0.89	56	780	11.3	1.78	101	1049
8	24	0.86	54	835	9.5	1.72	93	976
7	21	0.83	52	887	7.8	1.60	83	848
6	18	0.79	49	936	6.2	1.51	75	750
5	15	0.75	47	983	4.7	1.41	65	652
4	12	0.70	45	1027	3.3	1.28	58	539
3	9	0.70	45	1072	2.0	1.10	49	396
2	6	0.70	45	1117	0.9	0.88	40	256
1	3	0.70	45	1162				
<b>Sum</b>							1874	17049

TABLE 3: CALCULATION OF STATIC WIND LOAD

FE analysis (4.2.1 Static Wind) was conducted to calculate the deformation of the building,  $X_r$ , (Table 3) under static wind load, since the deformation equation for estimating the lateral deformation of the massive panel system is unavailable. It can be seen that, the inter-storey drift,  $x_r$ , of each storey is less than  $h_r/500$  ( $= 6mm$ ).

In order to check whether the dynamic procedure is needed or not, the lowest natural frequency of the building was calculated using Rayleigh's method based on the deformation under static wind load. The lowest natural frequency,  $f_n$ , in Hz can be estimated using equation 2.

$$f_n = \frac{1}{2\pi} \sqrt{\frac{\sum_{i=1}^n F_i \frac{X_i}{X_n}}{X_n \sum_{i=1}^n W_i \left(\frac{X_i}{X_n}\right)^2}} = \frac{1}{2\pi} \sqrt{\frac{\sum_{i=1}^N F_i X_i}{\sum_{i=1}^N W_i X_i^2}} \quad [2]$$

where,  $n$  is the storey number;  $F_i$  is the associated wind force of each storey, which was computed using the static procedure,  $N$ ;  $X_i$  is the horizontal deflection of each storey caused by  $F_i$  and computed using FE Analysis under static wind load, in m;  $W_i$  is the associated mass of each storey, in N.

The lowest natural frequency is 0.528 Hz. Since it is in the range of 0.25 to 1 Hz, dynamic procedure was performed below. It is important to note that the period determined with equation 2 is to be used only for estimating the lowest natural frequency that triggers the requirement to use the dynamic procedure for design for wind forces and should not be used in the calculation of design seismic loads.

#### (2) Dynamic Procedure

In the dynamic procedure for calculating wind load on the building structure, the wind load is estimated by equation 1 as well. The exposure factor,  $C_e$ , and external gust effect factor,  $C_g$ , are different from the factors used in the static procedure, but the pressure coefficient,  $C_p$ , is the same.  $C_p = 0.8$  and  $-0.5$  for windward and leeward sides, respectively.

In the dynamic procedure, the exposure factor,  $C_e$ , is based on the profile of mean wind speed, which varies considerably with the general roughness of the terrain over which the wind has been blowing before it reaches the building. Since this building is located at exposure A (rough exposure) terrain,  $C_e$  can be calculated by equation 3.

$$C_e = 0.5 \left( \frac{h}{12.7} \right)^{0.50} \quad \text{for } 0.5 \leq C_e \leq 2.5 \quad [3]$$

The gust effect factor,  $C_g$ , is defined as the ratio of the maximum effect of the loading to the mean effect of the loading. It takes into account: (a) random fluctuating wind forces caused by turbulence in the approaching wind and acting for short durations over all or part of the structure, (b) fluctuating forces induced by the wake of the structure itself, (c) additional inertial forces arising from motion of the structure itself as it responds to the fluctuating wind forces, and (d) additional aerodynamic forces due to alterations in the air flow around the structure caused by its motions (aero-elastic effects). It can be estimated using equation 4.

$$C_g = 1 + g_p (\sigma / \mu) \quad [4]$$

where,  $g_p$  is statistical peak factor for the loading effect,  $\mu$  is mean loading effect, and  $\sigma$  is "root-mean-square" loading effect.

The coefficient of variation,  $\sigma / \mu$ , can be expressed by

$$\sigma / \mu = \sqrt{\frac{K}{C_{eH}} \left( B + \frac{SF}{\beta} \right)} \quad [5]$$

where,  $K$  is a factor related to the surface roughness coefficient of the terrain, = 0.10 for Exposure B;  $C_{eH}$  is exposure factor at the top of the building evaluated according to equation 4;  $B$  is background turbulence factor as a function of  $w/H$  and obtained by

$$B = \frac{4}{3} \int_0^{914/H} \left( \frac{1}{1 + \frac{xh}{457}} \right) \left( \frac{1}{1 + \frac{xw}{122}} \right) \left[ \frac{x}{(1+x^2)^{4/3}} \right] dx \quad [6]$$

where  $w$  is the effective width of the windward face of the building, as defined in NBCC Sentence 4.1.7.2.(2);  $H$  is the height of the windward face of the building;  $S$  is the size reduction factor as a function of  $w/H$  and reduced frequency  $f_{nd}H/V_H$ , and is calculated by

$$S = \frac{\pi}{3} \left( \frac{1}{1 + \frac{8f_n H}{3V_H}} \right) \left( \frac{1}{1 + \frac{10f_n w}{V_H}} \right) \quad [7]$$

$f_{nd}$  is natural frequency of vibration in the along-wind direction, in Hz;  $V_H$  is mean wind speed, in m/s, at the top of structure,  $H$ , evaluated by

$$V_H = \bar{V} \sqrt{C_{eH}} = 39.2 \sqrt{I_w q C_{eH}} \quad [8]$$

$F$  is gust energy ratio at the natural frequency of the structure as a function of the wave number,  $f_{nd}/V_H$ , and is obtained from

$$F = \frac{x_0^2}{(1+x_0^2)^{4/3}} \quad [9]$$

$$x_0 = 1220 f_n / V_H \quad [10]$$

$\beta$  is critical damping ratio in the along-wind direction, which is based mainly on experiments on real structures, 1%.

The peak factor,  $g_p$  is a function of average fluctuation rate and can be calculated using

$$g_p = \sqrt{2 \ln(3600v)} + \frac{0.577}{\sqrt{2 \ln(3600v)}} \quad [11]$$

where  $v$  is the average fluctuation rate and can be estimated as follows

$$v = f_n \sqrt{\frac{SF}{SF + \beta B}} \quad [12]$$

The gust effect factor,  $C_g$ , of this building under dynamic wind load is 2.36. Similar to static procedure, the wind load, the shear and deformation,  $X_i$ , which was derived by conducting FE Analysis (4.2.2 Dynamic Wind) under dynamic wind load, at each storey are shown in Table 4. It can be seen that, the inter-storey drift,  $x_i$ , of each storey is also less than  $h_i/500$  (=6mm).

In the dynamic procedure, not only the wind-induced lateral deformation, but also the vibration and vortex-shedding effect are checked. While the maximum lateral wind loading and deflection are generally in the direction parallel to the wind (i.e. the along-wind direction), the maximum acceleration of a building leading to possible human perception of motion or even discomfort may occur in the direction perpendicular to the wind (i.e. the across-wind direction). Across-wind accelerations are likely to exceed along-wind accelerations if the building is slender about both axes, that is if  $\sqrt{wd}/H$  is less than one-third, where  $w$  and  $d$  are the across-wind effective width and along-wind effective depth, respectively and  $H$  is the height of the building. The across- and along-wind

accelerations,  $a_w$  and  $a_d$  ( $m/s^2$ ), are calculated from equations 13 and 14.

$$a_w = f_{nw}^2 g_p \sqrt{wd} \left( \frac{a_r}{\rho_B g \sqrt{\beta_w}} \right) \quad [13]$$

$$a_d = 4\pi^2 f_{nd}^2 g_p \sqrt{\frac{K_s F}{C_{eH} \beta_D}} \frac{\Delta}{C_g} \quad [14]$$

STOREY	$h_i, m$	$C_e$	$P_i, kN$	$V_i, kN$	$X_i, mm$	$x_i, mm$
20	60	1.09	82	82	33.7	1.89
19	57	1.06	80	163	31.8	1.89
18	54	1.03	78	241	29.9	1.92
17	51	1.00	76	317	28.0	1.95
16	48	0.97	74	390	26.0	1.99
15	45	0.94	71	462	24.0	2.02
14	42	0.91	69	530	22.0	2.06
13	39	0.88	66	597	19.9	2.04
12	36	0.84	64	661	17.9	2.02
11	33	0.81	61	722	15.9	2.00
10	30	0.77	58	780	13.9	1.97
9	27	0.73	55	835	11.9	1.92
8	24	0.69	52	887	10.0	1.85
7	21	0.64	49	936	8.1	1.71
6	18	0.60	45	981	6.4	1.60
5	15	0.54	41	1022	4.8	1.48
4	12	0.50	38	1060	3.4	1.33
3	9	0.50	38	1098	2.0	1.13
2	6	0.50	38	1136	0.9	0.90
1	3	0.50	38	1174		

TABLE 4: CALCULATION OF DYNAMIC WIND LOAD

where,  $\alpha_r = 78.5 \times 10^{-3} [V_H / f_{nW} \sqrt{wd}]^{3.3}$ , in  $N/m^3$ ;  $\rho_b$  is average density of the building, in  $kg/m^3$ ;  $\beta_w$  and  $\beta_d$  are fraction of critical damping in across- and along-wind directions, respectively, and are taken as 0.015;  $f_{nW}$  and  $f_{nD}$  and fundamental natural frequencies in across-wind and along-wind directions, respectively, in Hz;  $\Delta$  is maximum wind-induced lateral deflection at the top of the building in along-wind direction, in m, which was obtained by conducting FE Analysis on the tall wood building under dynamic wind load shown in Table 4; and  $g$  is acceleration due to gravity = 9.81  $m/s^2$ . Substituting the values of the parameters into equations 13 and 14,  $\alpha_w$  and  $\alpha_d$  are 0.9% and 1.1% of  $g$ , which are both less than the acceleration limits of 1.5% (Table 2) for residential occupancy.

### 3.2.2 Seismic Design

The Equivalent Static Force Procedure was utilized to estimate the seismic load applied on the tall wood building, since the building height is equal to 60m and the fundamental natural period is less than 2 s. In addition, response spectrum analysis and non-linear time history analysis were conducted as well to confirm the seismic performance of the building.

#### (1) Fundamental Natural Period, $T_a$

The fundamental natural period,  $T_a$ , which was estimated using equation 15 according to NBCC, of this tall wood building is 1.04 s.

$$T_a = 0.05 (h_n)^{3/4} \quad [15]$$

Using the frequency analysis (4.3.1), the period of the FEM of the building was 1.97 s. It is almost twice that estimated by equation 15, which also usually happens to mid-rise light wood frame structures and fulfills the requirement of Sentence 4.1.8.11. 3).d).iii) in NBCC. This is because equation 15 was derived from measurements on concrete structures rather than timber structures which are lighter and generally more flexible.

#### (2) Seismic Force Modification Factors

To account for potential energy-absorbing capacity in a structure, the concept of seismic force modification factors  $R_o R_d$  is adopted in NBCC. The ductility-related force modification factor,  $R_d$ , is used to reflect the capability of a structure to dissipate energy through inelastic behavior; while the overstrength-related force modification factor,  $R_o$ , is employed to account for the dependable portion of reserve strength in a structure designed according to the NBCC provisions.

However, there is no specification on the value of  $R_o R_d$  specifically for massive timber panel system by NBCC, since this type of structural system is new. The only one available document, CLT Handbook (Gagnon and Pirvu 2011), recommends  $R_o = 1.5$  and  $R_d = 2.0$  for CLT panel system with simple and standard connections. The tall wood report also argued that a higher  $R_d$  value (3.5) could be used (Green and Karsh 2012).

Based on the results of pushover analysis (4.3.3) using FEM, the ductility ratio of this building system was 2.55, and as a result, the  $R_d$  was 2.55. Therefore  $R_o R_d = 3.0$  ( $1.5 \times 2.0$ ) was used in the seismic design of this report.

#### (3) Design Seismic Force

Using the Equivalent Static Force Procedure the minimum lateral earthquake force,  $V$ , shall be calculated by equation 16.

$$V = S(T_a) M_V J_E W / (R_d R_o) \quad [16]$$

except

- a) for walls, coupled walls and wall-frame systems,  $V$  shall not be less than

$$V = S(4.0) M_V J_E W / (R_d R_o) \quad [17]$$

- b) for buildings located on a site other than Class F and having an LLRS with a  $R_d$  equal to or greater than 1.5,  $V$  need not be greater than

$$V = \frac{2}{3} S(0.2) J_E W / (R_d R_o) \quad [18]$$

Therefore, the specified design base shear is about 4900kN. The base shear of this building model under seismic action for the location derived from response spectrum analysis (4.3.2) is about 4500kN, which is close to the specified design base shear. This result justifies the use of the Equivalent Static Force Procedure, which takes into account the high mode effect by adding the  $F_t$  at the top of the building, to estimate the seismic load applied to this tall wood building.

Since the period of this building exceeds 0.7 s, the total lateral seismic force,  $V$ , shall be distributed such that a portion of the load,  $F_t$ , shall be assumed to be concentrated at the top of the building, where  $F_t$  is equal to  $0.07 T_a V$  but need not exceed  $0.25V$ ; the remainder,  $V - F_t$ , shall be distributed along the height of the building, including the top level, in accordance with the following formula:

$$F_x = (V - F_t) W_x h_x / \left( \sum_{i=1}^n W_i h_i \right) \quad [19]$$

The structure shall be designed to resist overturning effects caused by the earthquake forces and the overturning moment at level  $x$ ,  $M_x$ , shall be determined using the following equation:

$$M_x = J_x \sum_{i=1}^n F_i (h_i - h_x) \quad [20]$$

where,  $J_x = 1.0$  for  $h_x \geq 0.6h_n$ , and  $J_x = J + (1 - J)(h_x / 0.6h_n)$  for  $h_x < 0.6h_n$

The seismic force, shear for each storey, and the moments at the boundaries between panel and the podium, and between panels are shown in Table 5.

STOREY	$W_i, t$	$h_i, m$	$W_i h_i, t.m$	$\frac{W_i h_i}{\text{sum}, t.m}$	$F_i, kN$	$V_i, kN$	$M_{i,1}, kN.m$	$M_1, kN.m$	$M_{i,2}, kN.m$	$M_2, kN.m$	$M_{i,3}, kN.m$	$M_3, kN.m$
20	220	57	12548	0.069	976	976	55628	55628	37085	37085	18543	18543
19	329	54	17791	0.098	412	1388	22268	77896	14433	51518	6598	25141
18	329	51	16803	0.093	389	1778	19863	97759	12463	63981	5063	30204
17	329	48	15815	0.087	367	2144	17594	115353	10630	74611	3666	33869
16	329	45	14826	0.082	344	2488	15464	130817	8935	83546	2405	36275
15	329	42	13838	0.076	321	2809	13471	144288	7377	90923	1283	37558
14	329	39	12849	0.071	298	3107	11615	155903	5956	96879	298	37855
13	329	36	11861	0.065	275	3381	9897	165800	4674	101553		
12	329	33	10873	0.06	252	3633	8316	174116	3528	105081		
11	329	30	9884	0.054	229	3863	6873	180989	2520	107601		
10	329	27	8896	0.049	206	4069	5567	186556	1649	109250		
9	329	24	7907	0.044	183	4252	4399	190954	916	110167		
8	329	21	6919	0.038	160	4412	3368	194322	321	110487		
7	329	18	5930	0.033	137	4550	2474	196796				
6	329	15	4942	0.027	115	4664	1718	198514				
5	329	12	3954	0.022	92	4756	1100	199614				
4	329	9	2965	0.016	69	4825	619	200233				
3	329	6	1977	0.011	46	4871	275	200508				
2	329	3	988	0.005	23	4893	69	200576				
<b>sum</b>	6151		181568	1	4893							

TABLE 5: CALCULATION OF SEISMIC LOAD

#### (4) Maximum Inter-Storey Drift

The lateral deflection,  $X_i$ , of each storey derived by response spectrum analysis is shown in Table 6. According to NBCC, since it was obtained from a linear elastic analysis, it shall be multiplied by  $R_d R_o / I_E$  to give realistic values of anticipated deflections. The inter-storey drift,  $x_i$ , shown in Table 6 is less than  $2.5\%h_s$  ( $=75\text{mm}$ ). Hence, the seismic design of this building is appropriate.

### 3.3 CONNECTION SYSTEM

In applying the concept of capacity design the massive timber panels would be over-designed to ensure that the connections would yield and fail prior to failure in the panels. Hence, the vertical joints, shear connectors, hold-downs were arranged with sufficient stiffness and strength to resist the shear forces and moments induced by wind and earthquake, shown in Tables 3 to 5.

STOREY	$X_i$ ,mm	$X_i R_d R_o / I_E$ ,mm	$x_i$ ,mm	$x_i / h_i$ ,%
20	143.8	431	24.2	0.81
19	135.7	407	24.3	0.81
18	127.6	383	25.0	0.83
17	119.3	358	25.7	0.86
16	110.7	332	26.2	0.87
15	102.0	306	26.6	0.89
14	93.1	279	27.0	0.90
13	84.1	252	26.5	0.88
12	75.3	226	26.2	0.87
11	66.6	200	25.8	0.86
10	58.0	174	25.3	0.84
9	49.5	149	24.6	0.82
8	41.3	124	23.6	0.79
7	33.5	100	21.6	0.72
6	26.3	79	20.1	0.67
5	19.6	59	18.5	0.62
4	13.4	40	16.4	0.55
3	8.0	24	13.5	0.45
2	3.4	10	10.3	0.34

TABLE 6: LATERAL DEFLECTION DUE TO SEISMIC LOAD

Based on the observation of pushover analysis (4.3.3), the system ductility of this tall wood building was affected not only by the connection ductility, but also by the failure sequence. In order to achieve a less flexible, more ductile and sufficiently strong LLRS, three design principles were followed for the connection system design (see Figure 3 for type of connection).

- Ensure that vertical joints of shear wall sub-system yield first and produce most of the plastic deformation:** Dowel-type connections with low strength and high deformation ability was assigned to the shear wall vertical joints;
- Assign high stiffness and strength to vertical joints of core and ensure they yield after (a):** HSK connection system with high stiffness and strength was used as the vertical joints of the core sub-system;
- Ensure that shear connectors and hold-downs of sub-systems provide the major stiffness and strength to the whole system and fail after yielding of the vertical joints with somewhat plastic deformation:** HSK connection system with superior stiffness and strength as well as high ductility was utilized.

### 3.4 DESIGN RESULTS

Based on the wind and seismic loads with consideration of fire issue, the design results are discussed below.

Grade 2.1E “TimberStrand® LSL” (CCMC 1994) with dimensions

of 19 m (length) × 2.44 m (width) × 89 mm (thickness) was used to build the shear wall and core sub-system. The specified strengths and modulus are shown in Table 7. Three layers of LSL panels are combined together to build the shear wall and the core to achieve a total wall thickness of 267 mm. Steel beam S5x10 of Grade 50 with specified strength of 345 MPa (CSA 2009) was used to connect the shear wall and core sub-system, Fig. 7 and 8.

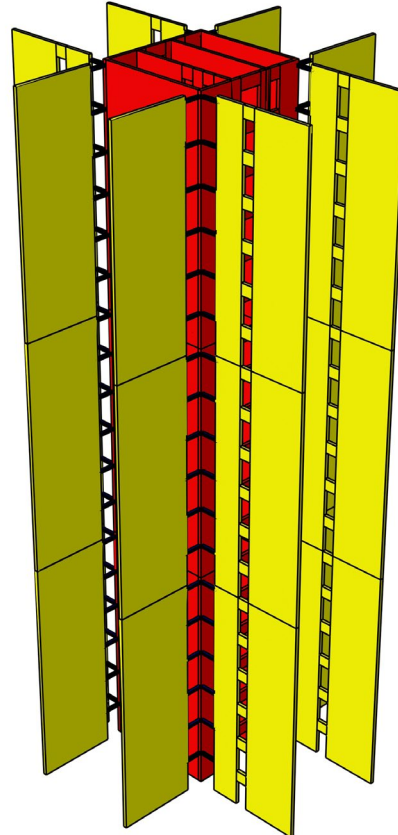


FIGURE 7: LLRS OF TALL WOOD BUILDING

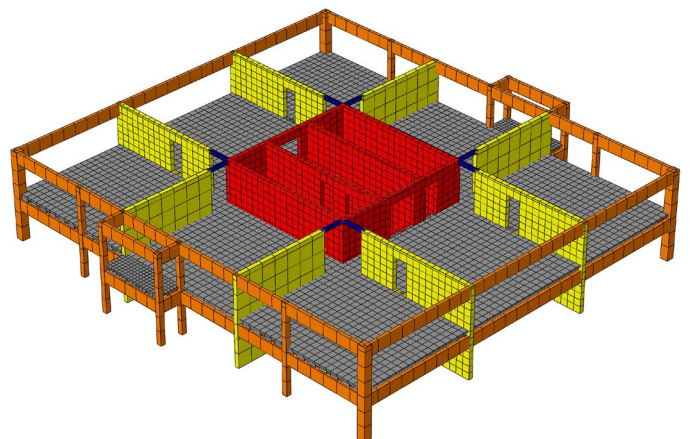


FIGURE 8: TYPICAL STOREY

MOE	AXIAL		JOIST OR BEAM			PLANK		
	Tension Parallel to Grain, $F_t$	Comp. Parallel to Grain, $F_c$	Flexure $F_b$	Shear, $F_v$	Comp. Perp. to Grain, $F_c$	Flexure, $F_b$	Shear, $F_v$	Comp. Perp. to Grain, $F_c$
14480	31.85	36.05	44.60	5.15	11.05	50.00	1.95	6.40

TABLE 7: SPECIFIED STRENGTHS AND MODULUS OF LSL, MPa

Dowel-type connection of LSL, Pa11A (Moses 2000), was used as the vertical joints of shear wall, while the HSK system was used as vertical joints of core, shear connectors and hold-downs for the whole system. For the dowel-type connection, the diameter of dowel is 19mm, and the stiffness and maximum strength of each dowel are 25.5kN/mm and 32.5kN respectively. The HSK system is a patented product of TiComTec GmbH, the performance parameters were provided by Prof. Bathon. The stiffness and maximum strength of each hole of the HSK system parallel to the grain are 7.4 kN/mm and 0.8 kN; while those in the perpendicular direction are 2.5 kN/mm and 0.8 kN respectively. All the connections were designed with an assumed design value that is taken as the test strength divided by 1.6. Structural details are illustrated in Appendix B, Structural Drawings.

## 4. RESPONSES UNDER LATERAL LOADS

### 4.1 DEVELOPMENT OF THE FINITE ELEMENT MODEL

A two-dimensional (2D) modeling approach was adopted to develop the FE model of the tall wood building using ABAQUS program (Hibbitt et al. 2011). Since the LLRS's in the two directions are nearly identical, only the LLRS in the east-west direction was analyzed. The 2D FE model is shown in Fig. 9.

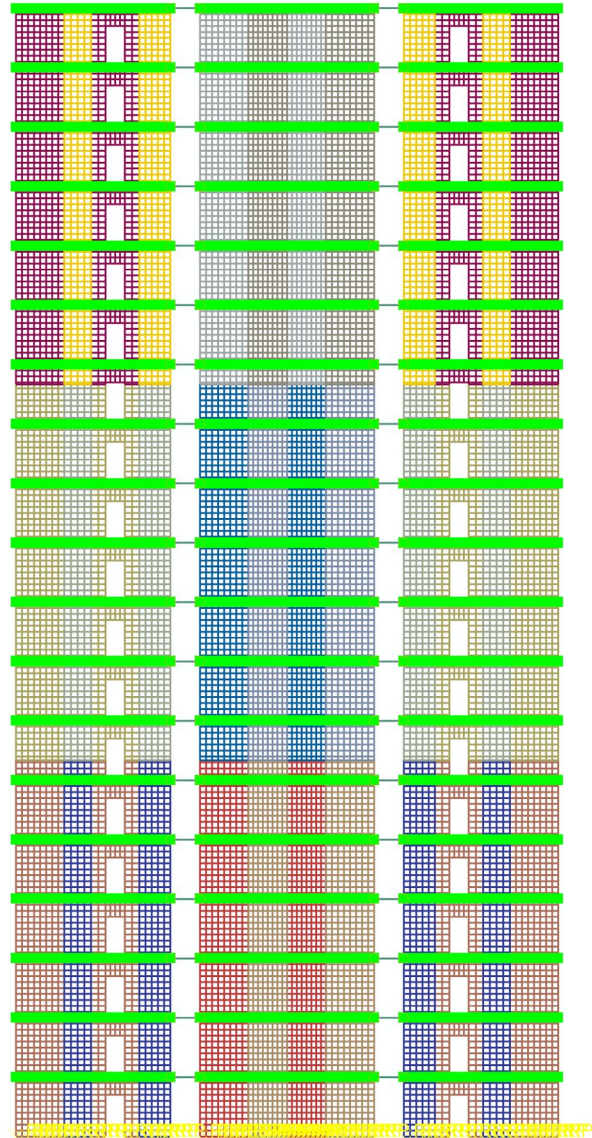


FIGURE 9: FE MODEL (2D) OF TALL WOOD BUILDING

### (1) Material models

As has been shown by tests, failure usually occurs at connections which are the vulnerable part of the massive timber panel building system. Therefore, the constitutive model of LSL was assumed to be orthotropic elasticity, Fig. 10a, while steel was regarded as an isotropic, idealized elasto-plastic material, Fig. 10b. The parameters of these two material models are shown in Table 8.

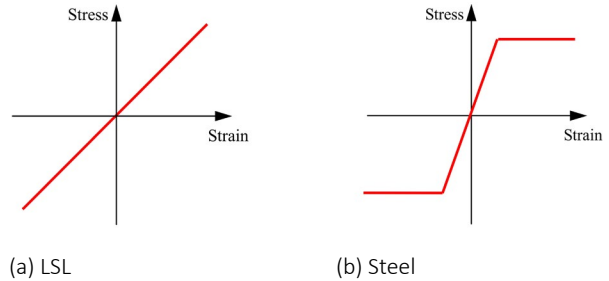


FIGURE 10: MATERIAL MODELS

MATERIAL	$E_1$ , MPa	$E_2$ , MPa	$\nu_{12}$	$G_{12}$ , MPa	$f_y$ , MPa
LSL	14,480	810	0.741	905	-
Steel	206,000	206,000	0.3	79,230	345

TABLE 8: MATERIAL PARAMETERS

### (2) Connection models

Connections play a significant role in the structural performance of the mass timber panel system, therefore the constitutive relationship between the force and deformation of the connection is the most important part of development of the FE model for the tall wood building.

As shown in Fig. 9, all the LSL panels in different colors are connected together by vertical joints in the height direction and shear connectors and hold-downs horizontally. The panels are attached to the concrete podium using shear connectors and hold-downs. A 2D, 2-node connector element (CONN2D2) was used to simulate the vertical joints, shear connectors and hold-downs.

Because the test data of HSK system and specific LSL dowel connection were unavailable, idealized models as shown in Fig 11 were used to model the reversed cyclic response of the connections. The behavior of the vertical joints and the shear connectors under shear was assumed to be idealized elasto-plastic with isotropic hardening, see Fig. 11a. In order to assign a specific ductility ratio to these connections, damage behavior was employed by the connection models with a motion-based linear damage evolution law. Meanwhile, the ELEMENT DELETION TECHNIQUE was used to delete a connection from the mesh once it was damaged completely. The hold-down connections were assumed to behave similar to the shear connectors and vertical joints under tension, but resist compression without deformation (Fig. 11b), since most of the compression deformation happens by bearing in LSL and very small deformation occurs in HSK system. The parameters of these connection models are shown in Table 9.

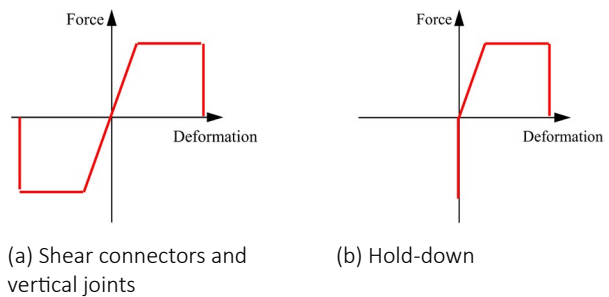


FIGURE 11: CONNECTION MODELS

TYPE	NO	CORE/WALL	CONNECTOR	$K$ , kN/mm	$P_{max}$ , kN	$\Delta_y$ , mm	$\Delta_{max}$ , mm	$\mu$
Vertical Joint	1	Core	HSK <sub>Par</sub>	1,780	192	±0.1	±0.5	5
		Wall	Dowel	67	100	±1.5	±3.0	2
	2	Core	HSK <sub>Par</sub>	1,780	192	±0.1	±0.5	5
		Wall	Dowel	57	85	±1.5	±3.0	2
	3	Core	HSK <sub>Par</sub>	1,180	128	±0.1	±0.5	5
		Wall	Dowel	40	60	±1.5	±3.0	2
Shear Connector	1	Core	HSK <sub>Per</sub>	600	192	±0.3	±1.6	5
		Wall		300	96			
	2	Core		600	192			
		Wall		300	96			
	3	Core		400	128			
		Wall		200	64			
Hold-Down	1	Core	HSK <sub>Par</sub>	50,000	5,410	±0.1	±0.5	5
		Wall		25,000	2,700			
	2	Core		2,400	259			
		Wall		1,200	130			
	3	Core		2,000	216			
		Wall		1,000	108			

Note: 'HSK<sub>Par</sub>' and 'HSK<sub>Per</sub>' indicate the major direction of HSK connection parallel or perpendicular to LSL grain.

TABLE 9: CONNECTION MODEL PARAMETERS

The steel beams are used to connect shear walls and the core, and to transfer the lateral load. Hence, the connections between steel beams and LSL panels were simulated by hinge joints.

### (3) Interaction models

As the behavior of the connections between panels and between panel and the concrete podium was simulated by the connection models above, the interaction relationship between connecting components was simplified into frictionless in tangential direction and hard contact in normal direction. The hard contact relationship (Fig. 12) minimizes the penetration of the slave surface into the master surface at the constraint locations, and does not allow the transfer of tensile stress across the interface.

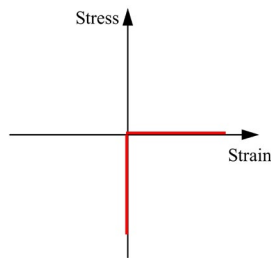


FIGURE 12: HARD CONTACT MODEL

### (4) Elements

The shear core and shear walls were meshed using a 4-node bilinear plane stress element (CPS4R) with reduced integration and hourglass control. The steel beams were modeled using a 2-node linear Timoshenko (shear flexible) beam element (B21). Point mass element (MASS) was used to assign the corresponding mass to each storey at the floor or roof level. The FE model was meshed with a total of about 30,000 elements, including the shell, beam, connector and mass elements.

### (5) Other Simulation Issues

In order to take into account the core effect, usually two methods, i.e. equivalent modulus of elasticity or I-shape section, can be used to develop the FE analysis model. In this project, I-shape section was assigned to the shear core panels, in which an equivalent length of the shear core in the other direction was input as the thickness of the elements at the two ends of the core. The openings for doorway were assumed as punched-out from the LSL panel.

In summary, even though this FE model is a 2D model, nonlinearity of material and boundary, in terms of plastic properties, damage behavior and element deletion, as well as the nonlinear analysis method as indicated below are involved in this analysis, it is still a huge and complex numerical simulation exercise. Moreover, due to the relative symmetry of the building in the N-S and E-W directions, 2-D analysis is considered adequate.

## 4.2 WIND-INDUCED RESPONSE

### 4.2.1 Static Wind

Because there are no analytical equations to estimate the lateral deformation for the massive timber panel system, FE analysis was performed to calculate the lateral deformation of the tall wood building under static wind load plus gravity load. The wind load,  $P_i$ , shown in Table 3 was applied at the floor or roof level, as illustrated in Fig. 13.

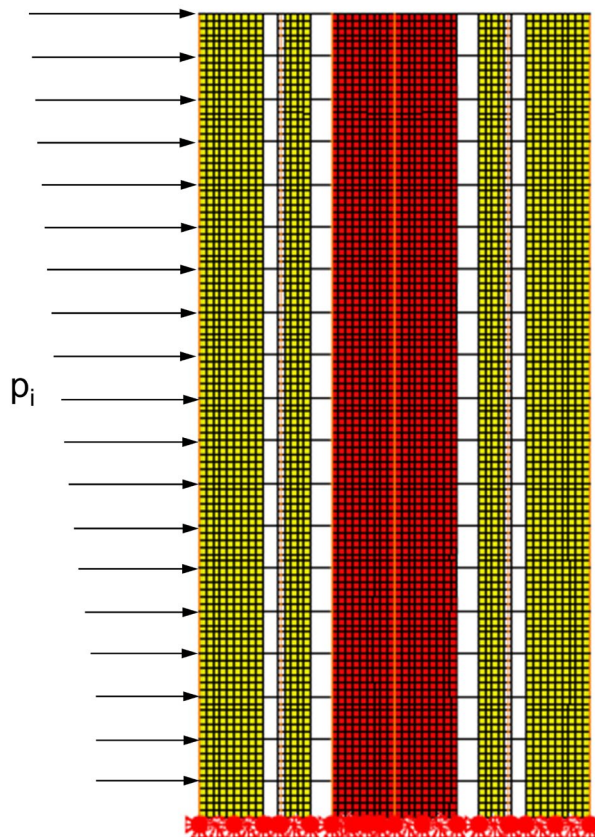
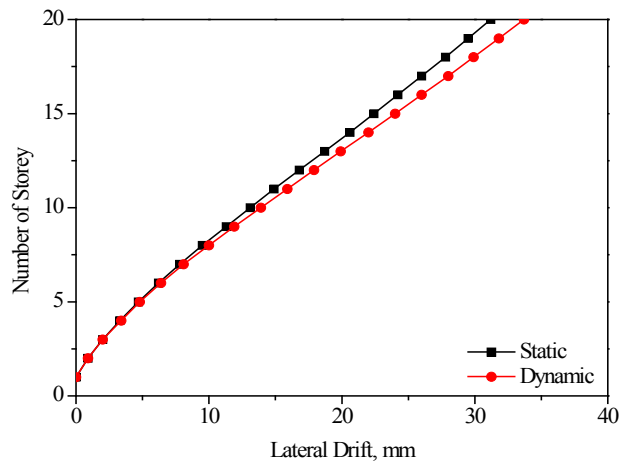
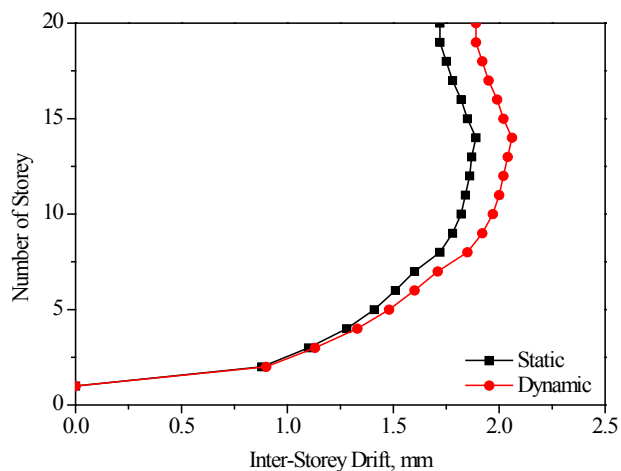


FIGURE 13: WIND LOAD APPLIED ON THE FE MODEL

The static stress analysis procedure was adopted for conducting the simulation. Under the wind load, the load applied on the tall wood building increased linearly with increasing lateral deformation. The deformation and inter-storey drift of the FE model under the design static wind load are shown in Table 3 and Fig. 14. It can be seen that the roof drift is 31.2 mm ( $\approx h_n/1800$ ) and the inter-storey drift of each storey is less than  $h_i/500$  ( $=6\text{mm}$ ).



(a) Storey drifts



(b) Inter-storey drifts

FIGURE 14: LATERAL DEFORMATION OF TALL WOOD BUILDING UNDER WIND

### 4.2.2 Dynamic Wind

A numerical simulation of the FE model under dynamic wind load plus gravity load was also performed using the static stress analysis procedure. The wind load,  $P_i$ , shown in Table 4 was applied at the floor or roof level, Fig. 13.

Under the dynamic wind load, the load applied on the tall wood building increased linearly with increasing lateral deformation. The deformation and inter-storey drift of the FEM under the design dynamic wind load are shown in Table 4 and Fig. 14. It can be seen that the storey drift and inter-storey drift of the building under dynamic wind load are slightly larger than those induced by the static wind load. It indicates that the dynamic procedure can derive a more conservative result comparing with the static procedure. The roof drift is 33.7 mm ( $\approx h_n/1700$ ) and the inter-storey drift of each storey is less than  $h_i/500$  ( $=6\text{mm}$ ).

Under either static or dynamic wind load, the tall wood building behaves linear elastically since the applied force did

not exceed the load-carrying capacity of the materials and connections. The deformation shape of the shear wall system calculated by the building model under static or dynamic wind load is similar to that of a cantilever.

### 4.3 SEISMIC RESPONSE

#### 4.3.1 Frequency Analysis

The periods of the tall wood building FE model were derived by conducting frequency analysis using LANCZOS method of

eigenvalue extraction (Hibbitt et al. 2011) and the results are shown in Table 10 and Fig. 15.

It shows that the lateral fundamental natural period of the building FEM is 1.97 s, which is almost twice that estimated by equation 15. This level of discrepancy is usually found for mid-rise light wood frame structures and fulfills the requirement of Sentence 4.1.8.11. 3).d).iii) in NBCC. This discrepancy is not surprising since equation 15 was derived based on measurements from primarily concrete structures.

Mode i	1	2	3	4	5	6	7	8	9	10
$f_i$ , Hz	0.508	1.829	2.659	2.932	3.250	3.570	4.219	4.230	4.541	4.631
$T_i$ , s	1.968	0.547	0.376	0.341	0.308	0.280	0.237	0.236	0.220	0.216
Mode i	11	12	13	14	15	16	17	18	19	20
$f_i$ , Hz	4.672	5.201	6.090	6.123	6.635	6.788	7.121	7.126	7.741	7.744
$T_i$ , s	0.214	0.192	0.164	0.163	0.151	0.147	0.140	0.140	0.129	0.129

TABLE 10: NATURAL FREQUENCIES AND PERIODS OF THE TALL WOOD BUILDING

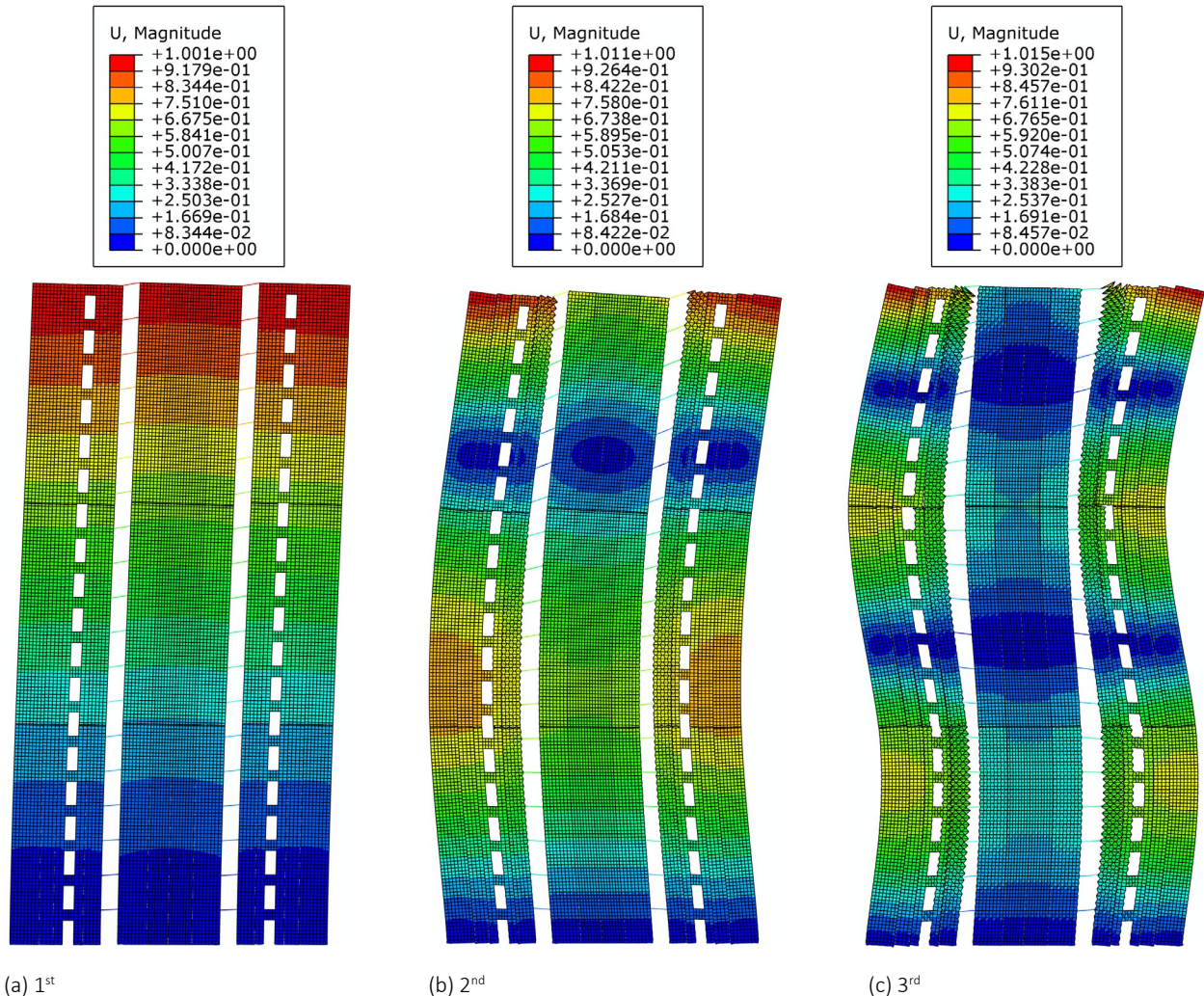


FIGURE 15: THE FIRST THREE MODE-SHAPES IN THE LATERAL DIRECTION

### 4.3.2 Response Spectrum Analysis

The response spectrum analysis is typically used by structural engineers to analyze response of a building under a seismic event. It can provide an estimate of the peak linear response of a structure to dynamic motion of fixed points (“base motion”). It assumes that the system’s response is linear so that it can be analyzed in the frequency domain using its natural modes, which are extracted in a previous eigenfrequency extraction step (Frequency Analysis, 4.3.1).

In order to derive accurate results from response spectrum analysis, the number of modes extracted must be sufficient to model the dynamic response of the system adequately. A criterion to determine the number of modes involved is that at least 90% of the mass participated in the modal analysis in the specific direction. Therefore, 20 modes of the building FE model were extracted and the frequencies are shown in Table 10.

Another factor affecting the response spectrum analysis is the spectrum of acceleration. The design spectrum with 5% damping for North Vancouver, shown in Fig. 16, was used to perform the response spectrum analysis.

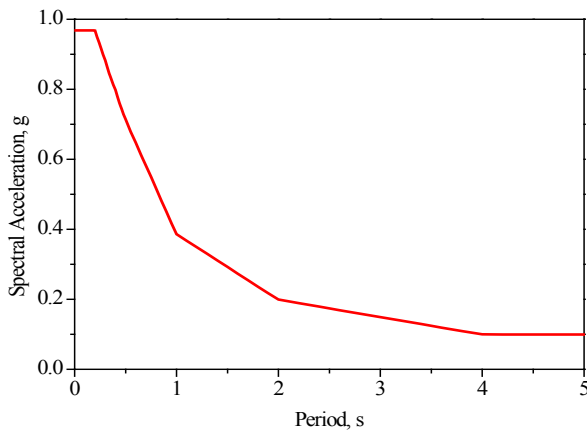
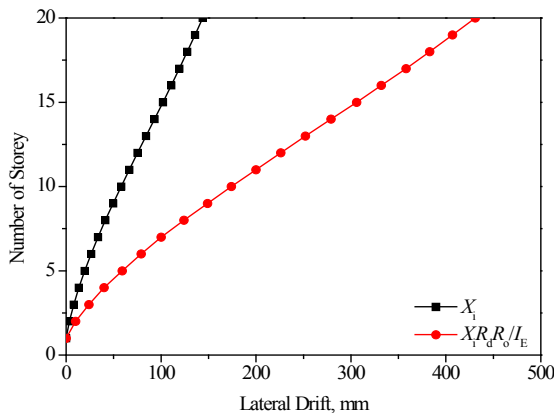
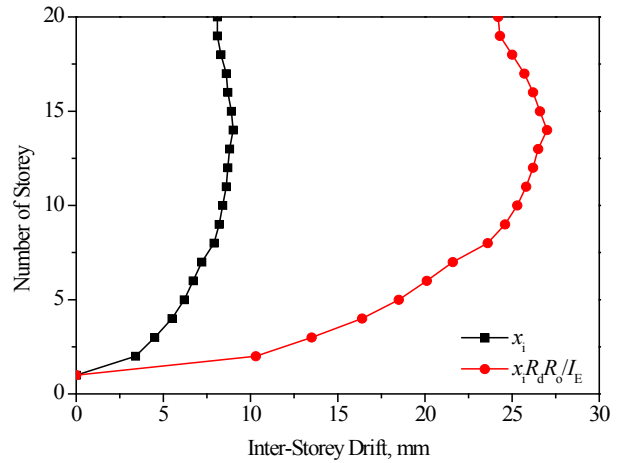


FIGURE 16: DESIGN SPECTRAL ACCELERATION OF NORTH VANCOUVER

The lateral deflection,  $X_i$ , of each storey is shown in Table 6 and Fig. 17a. According to NBCC, it shall be multiplied by  $R_d R_o / I_E$  to give realistic values of anticipated deflections, since it was obtained from a linearly elastic analysis. The inter-storey drift,  $x_r$ , shown in Table 6 and Fig. 17b is less than  $2.5\%h_s$  ( $=75\text{mm}$ ).



(a) Storey drifts



(b) Inter-storey drifts

FIGURE 17: LATERAL DEFORMATION OF TALL WOOD BUILDING UNDER EARTHQUAKE

The base shear of this building model under seismic is about 4500kN, which is similar to the design seismic force derived by Equivalent Static Force Procedure (3.2.2).

### 4.3.3 Pushover Analysis

In general, linear elastic analysis procedures are applicable when the structure is expected to remain nearly elastic for the level of ground motion or when the design results in nearly uniform distribution of nonlinear response throughout the structure. As the performance objective of the structure implies greater inelastic demands, the uncertainty with linear procedure increases to a point that requires a high level of conservatism in demand assumptions and acceptability criteria to avoid unintended performance. Therefore, analysis procedure incorporating inelastic analysis can reduce the uncertainty and conservatism. Such an approach is usually known as “pushover” analysis. A pattern of forces is applied to a structural model that incorporates non-linear properties (such as material or connection yield), and the total force is plotted against a reference displacement to define a capacity curve. This can show the structural performance, in terms of the stiffness, yield strength and deformation, maximum strength and deformation, and the failure / collapse deformation, of the building under lateral load.

In an attempt to derive the best design for the structural and connection system, pushover analysis was performed on the building FE model under an inverse triangular loading pattern

(Fig. 18) with a ratio of  $w_i h_i / \sum_{i=1}^n w_i h_i$  shown in Table 5. Under

the lateral load, the load-displacement curve of the FE model is shown in Fig. 19.

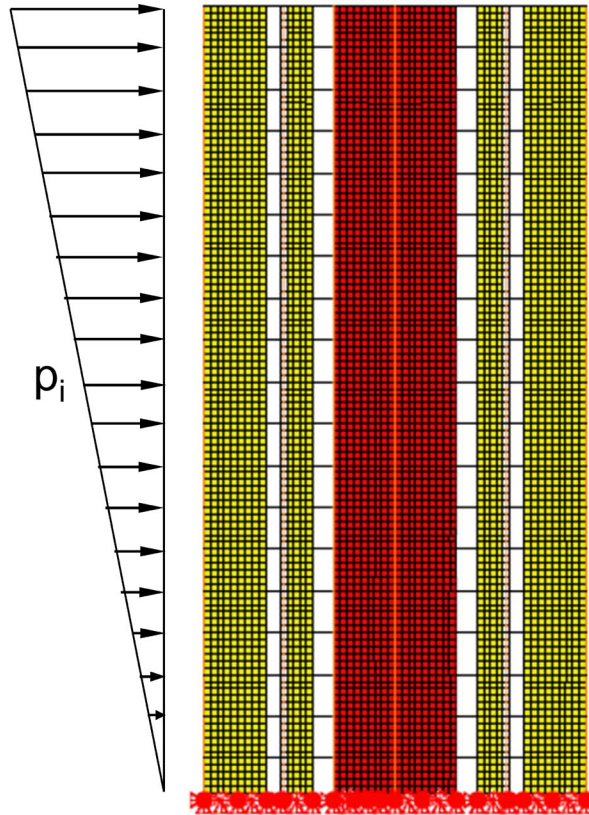


FIGURE 18: LATERAL LOAD APPLIED ON THE FEM

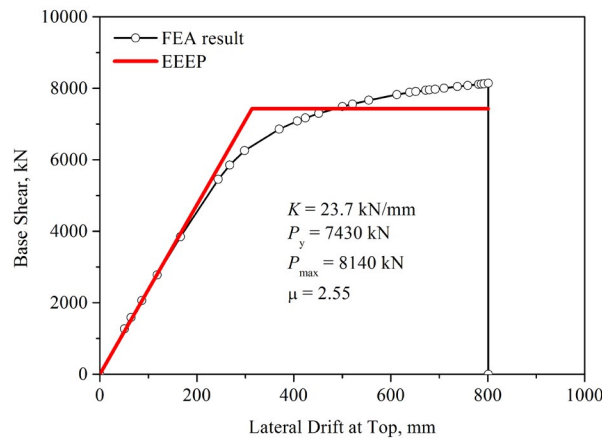
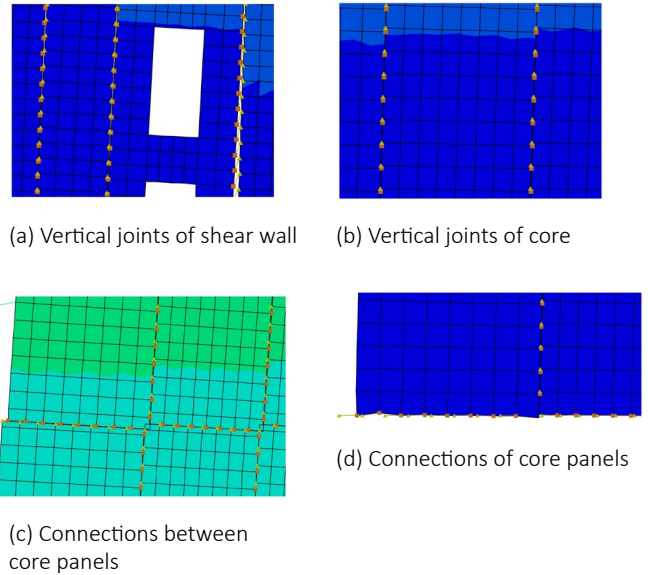
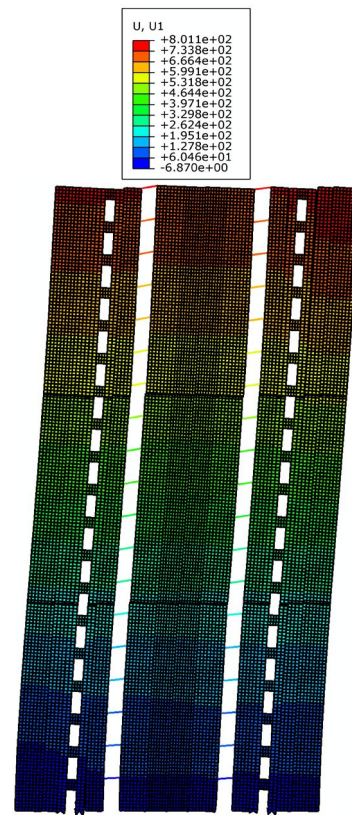


FIGURE 19: LATERAL LOAD-DISPLACEMENT CURVE

As shown in Fig. 19, the load increases linearly with displacement in the initial elastic stage (0 to 5,500kN). Then, the relationship between load and displacement becomes nonlinear, as the vertical joints of shear wall and core yield sequentially (Fig. 20a, b). Once the shear connectors and hold-downs yield and then fail completely (Fig. 20c, d), the building loses its lateral resistance, as shown in Fig. 20e. This analysis has proven that the structure would fail according to the intended sequence, thereby verifying the adopted capacity design approach.



(c) Connections between core panels



(e) Deformation of FE model

FIGURE 20: DEFORMATION OF CONNECTIONS AND BUILDING FE MODEL (SCALE FACTOR IS 5)

The equivalent energy elastic-perfectly-plastic (EEEP) curve of this building was derived in accordance with ASTM Standard E2126. The yield load,  $F_y$ , as defined in ASTM E2126 can be determined as follows, see Fig. 19.

$$F_y = \left( \Delta_u - \sqrt{\Delta_u^2 - \frac{2E}{K_y}} \right) K_y \quad [21]$$

where  $K_y$  is the initial (yield) stiffness, which is the secant stiffness between zero and 40% of the ultimate load;  $E$  is the energy dissipated at the ultimate displacement; and  $\Delta_u$  is the ultimate displacement in post-maximum load region where the load drops to 80% of the maximum load,  $F_{max}$ .

As shown in Fig. 19, the maximum load reached is 8,140 kN and is about 1.6 times the design seismic force derived by the Equivalent Static Force Procedure (Seismic Design, 3.2.2). The ductility ratio of this building FE model is 2.55. Using Equation 22 for medium and long period buildings (Newmark and Hall 1982, Chen et al 2014), the  $R_d$  factor is 2.55. A conservative value of 2.0 was used for seismic design (3.2.2).

$$R_d = \mu \quad [22]$$

#### 4.3.4 Non-linear Time History Analysis

Since the response spectrum analysis is a linear perturbation procedure and is, therefore, not appropriate if the excitation is so severe that nonlinear effects in the system are important. While nonlinear dynamic analysis utilizes a combination of ground motion records with a detailed structural model, therefore is capable of producing results with relatively

low uncertainty. In non-linear dynamic analysis, the non-linear properties of the structure are considered as part of a time domain analysis. This approach is the most rigorous, and is required by some building codes for buildings of unusual configuration or of special importance. Since this demonstration high-rise wood building is innovative, performing non-linear time history analysis would be useful.

However, the calculated response can be very sensitive to the characteristics of the individual ground motion used as seismic input; therefore, several analyses are required using different ground motion records to achieve a reliable estimation of the probabilistic distribution of structural response. Ten “Far-Field” earthquake records (Table 11) in the fault normal (FN) direction (ATC 2009) were scaled at the corresponding fundamental period of the building model (1.97 s) to match the spectral acceleration,  $S_a$ , of the North Vancouver design spectrum (Fig. 16), as shown in Fig. 21.

NO.	NGA #	YEAR	EVENT	STATION	SITE	MAG.	PGA,g	MECHANISM	SCALE FACTOR
1	1602	1999	Duzce- Turkey	Bolu	D	7.1	0.82	Strike-Slip	0.695
2	1787	1999	Hector Mine	Hector	C	7.1	0.34	Strike-Slip	1.173
3	169	1979	Imperial Valley-06	Delta	D	6.5	0.35	Strike-Slip	1.011
4	1111	1995	Kobe- Japan	Nishi-Akashi	C	6.9	0.51	Strike-Slip	1.111
5	1158	1999	Kocaeli- Turkey	Duzce	D	7.5	0.36	Strike-Slip	0.602
6	900	1992	Landers	Yermo Fire Station	D	7.3	0.24	Strike-Slip	1.434
7	752	1989	Loma Prieta	Capitola	D	6.9	0.53	Reverse-Oblique	1.555
8	721	1987	Superstition Hills-02	El Centro Imp. Co. Cent	D	6.5	0.36	Strike-Slip	0.773
9	829	1992	Cape Mendocino	Rio Dell Overpass - FF	D	7.0	0.55	Reverse	2.026
10	1244	1999	Chi-Chi- Taiwan	CHY101	D	7.6	0.44	Reverse-Oblique	0.586

TABLE 11: SUMMARY OF SELECTED HORIZONTAL GROUND MOTION RECORDS

An explicit dynamic analysis using the central-difference operator provided by ABAQUS/Explicit was adopted for performing the non-linear time history analysis, since it is computationally efficient for the analysis of large models with relatively short dynamic response times and for the analysis of extremely discontinuous events or processes, such as the tall wood building case.

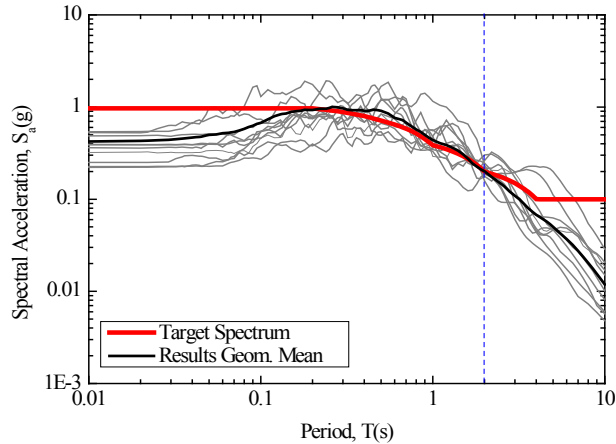
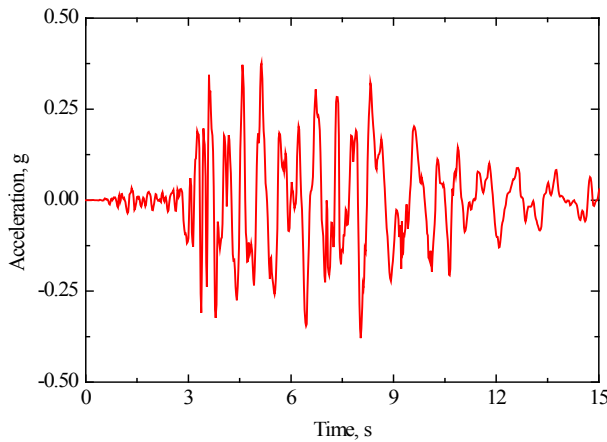
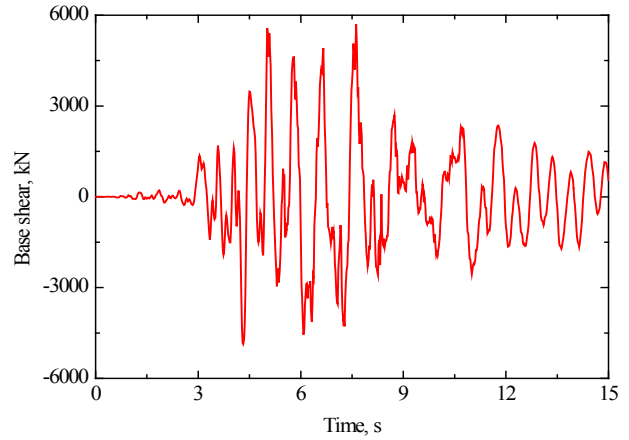


FIGURE 21: SCALING EARTHQUAKE RECORDS ( $T_0=1.97s$ )

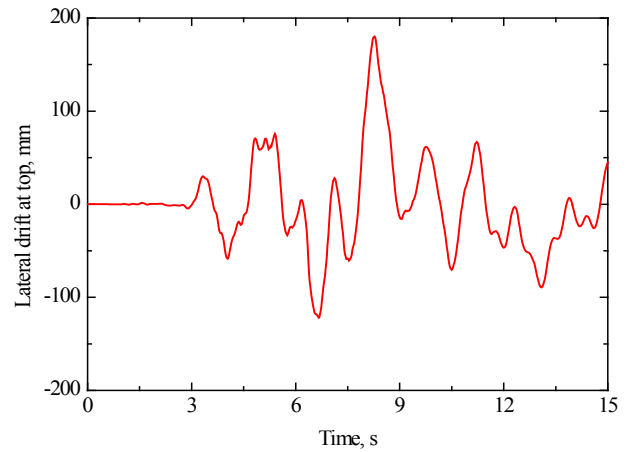
Fig. 22 shows the scaled acceleration of No. 1 earthquake (NGA #: 1602) with the duration between 0 to 15 s, as well as the structural response, in terms of base shear, lateral drift at top and inter-storey drift ratio, of the tall wood building.



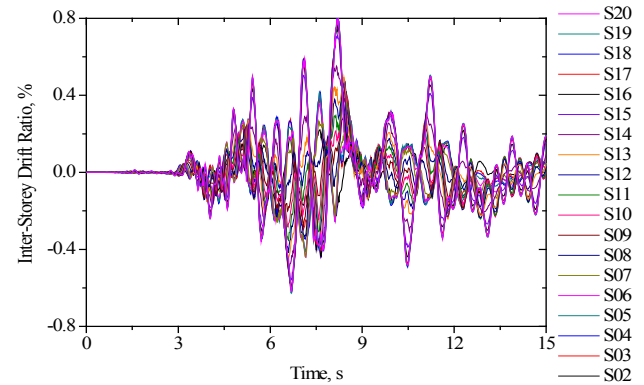
(a) Scaled earthquake acceleration (NGA #: 1602)



(b) Base shear



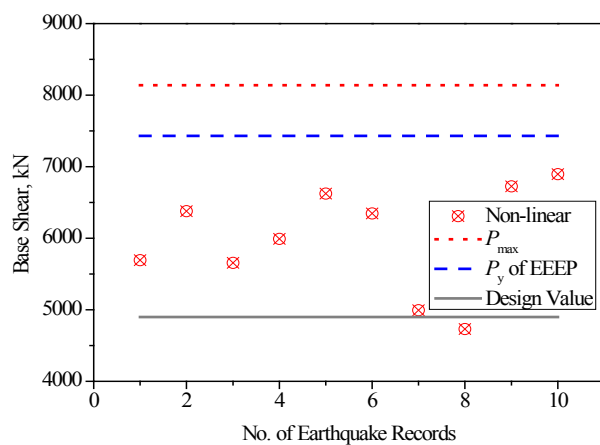
(c) Lateral drift at top



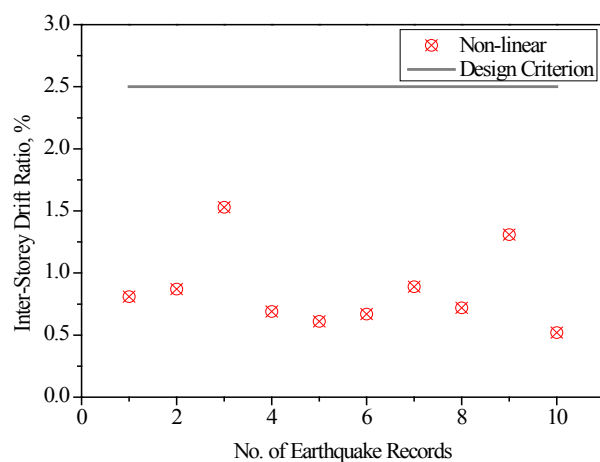
(d) Inter-storey drift ratio

FIGURE 22: SEISMIC RESPONSE OF THE FE MODEL UNDER EARTHQUAKE (NGA #: 1602)

The statistics results of the base shear and inter-storey drift ratio of the tall wood building under ten earthquake excitations are shown in Fig. 23. Fig. 23a illustrates that most (nine) of the base shears of the building are higher than the design value (3.2.2 Seismic Design). It was induced by the uncertainty of the earthquake excitations. It indicates that, on the other hand, it would be better to perform non-linear time history analysis on the buildings with innovative structural system to investigate the seismic behavior. However, all the base shears are less than the yield load of EEEP and the maximum capacity of the building which was derived by performing Pushover Analysis (4.3.3), and all the inter-storey drift ratios (Fig. 23b) are less than the design criterion, 2.5% (Table 2). Under the ten earthquake actions, only the vertical joints of the tall wood building yield. Hence, the seismic design of this tall wood building is justified.



(a) Base shear



(b) Inter-storey drift ratio

**FIGURE 23:** SEISMIC RESPONSE OF THE TALL WOOD BUILDING

## 5. RECOMMENDATIONS

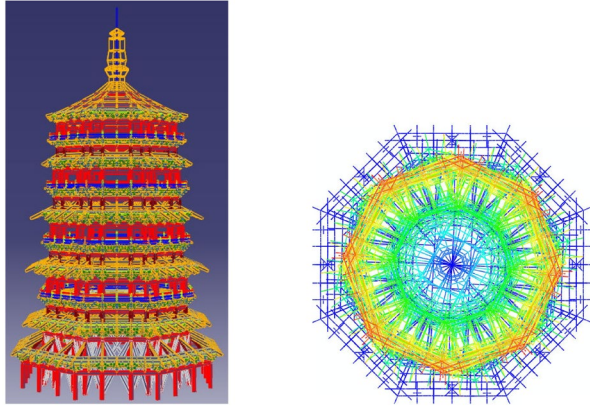
Based on the structural design and the FE analysis of this demonstration building, some recommendations are derived.

### 5.1 STRUCTURAL SYSTEM

- (1) The shear wall plus core system built with massive panels is suitable for the 20-storey high-rise timber wood building with sufficient stiffness, strength and ductility.
- (2) The 2D finite element modeling approach is appropriate to investigate the structural behavior, in terms of fundamental natural period, wind-induced response, seismic response and failure path, of the high-rise wood building.

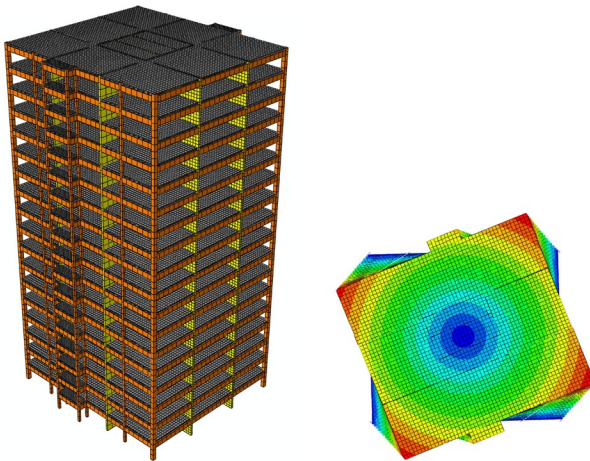
For further investigation,

- (1) Conducting three-dimensional (3D) modeling would give more comprehensive results and allow any potential torsional effects to be studied (see 3 below).
- (2) Non-linear time history analysis should be performed on the 3D FE model under dynamic wind load to take into account the cross-wind effect etc.
- (3) A torsional effect issue may need to be considered, since the Yingxian Wood Pagoda has a torsional period that is close to the lateral fundamental natural frequency, Fig. 24 (Chen 2011). Frequency analysis was performed on the 3D model in Chapter 3, and a similar phenomenon was found on this demonstration building, Fig. 25. If a building fails in the torsional way, it would collapse suddenly without any ductility. Therefore, additional strengthening, such as adding shear walls at the exterior, may be required to increase the torsional stiffness of this tall wood building.
- (4) It seems that the influence of the so-called “rotational” effect, of the bending of massive panels and hold-down connections on the “nominal” inter-storey drift,  $x_i$ , which is taken as  $X_i - X_{i-1}$ , is significant, and increases with increasing building height. It induces the maximum “nominal” inter-storey drift to occur at the top storey, as shown in Figs. 14, 17 and 22d. This raises a question: how to use the inter-storey drift criteria shown in Table 2 to design and evaluate the tall wood building. Should the criteria be compared with the “nominal” inter-storey drift or the “nominal” drift minus the rotational effect? To be conservative, the comparison between the criteria and the “nominal” inter-storey drift was performed in this project. Further discussion or/and investigation should be conducted.



(a) FEM

(b) Rotational mode shape

**FIGURE 24:** ROTATIONAL MODE-SHAPE OF YINGXIAN WOOD PAGODA (CHEN 2011)

(a) FEM

(b) Rotational mode shape

**FIGURE 25:** ROTATIONAL MODE SHAPE OF TALL WOOD BUILDING

## 5.2 CONNECTION SYSTEM

- (1) The connection systems, including vertical joints, shear connectors and hold-downs, are suitable for the 20-storey high-rise tall wood building with sufficient stiffness, strength and ductility.
- (2) The modeling approach using connector elements is appropriate to investigate the behaviour of the structural as well as the connection systems, in terms of fundamental natural period, wind-induced response, seismic response and failure path, of the high-rise building.

The work presented in this chapter has shown that the connection systems have a strong influence on the structural performance of the building. A capacity design approach should be adopted for tall wood buildings to ensure that first yield and failure does not occur at the base shear connections and hold-downs. To that end, connection system with high stiffness and high ductility or deformation ability and low

strength should be used in vertical joints; while strong and stiff connection system should be used as shear connectors and hold-downs.

## 6. ACKNOWLEDGEMENTS

The authors greatly acknowledge the expert advice provided by Mr. Eric Karsh and Dr. Mahmoud Rezai of Equilibrium Consulting Inc, Vancouver, BC. Mechanical specifications and test data on the HSK connection system were provided by Prof. Leander Bathon, University of Wiesbaden, Germany. Thanks are also extended to Mr. Mark McCormick, P.Eng from exp Services Inc., Fredericton, NB, for providing technical advice.

## REFERENCES

- Applied Technology Council (ATC). (2009). Quantification of building seismic performance factors. ATC-63/FEMA P-695 Project Rep., Redwood City.
- ASTM. (2005). Standard test methods for cyclic (reversed) load test for shear resistance of framed walls for buildings. ASTM E2126, West Conshohocken.
- Canadian Construction Materials Centre (CCMC). (1994). TimberStrand® LSL. Evaluation Report CCMC 12627-R. Weyerhaeuser, Boise.
- Canadian Standards Association (CSA). (2014). Engineering design in wood. CSA O86-14, Toronto.
- CSA. (2009). Design of steel structures. CSA S16-09. Toronto.
- Canadian Wood Council (CWC). (2010). Wood design manual 2010. Eton System, Nepean.
- Chen, Z. Y. (2011). Behaviour of typical joints and the structure of Yingxian Wood Pagoda. Ph.D. dissertation, School of Civil Engineering, Harbin Institute of Technology, Harbin.
- Chen, Z. Y., Chui, Y.H., Ni, C. and Xu, J. (2014). Seismic Response of Midrise Light Wood-Frame Buildings with Portal Frames. *J. Struct. Eng., ASCE*. DOI: 10.1061/(ASCE)ST.1943-541X.0000882, A4013003.
- Gagnon, S., and Pirvu, C. (2011). CLT handbook Canadian Edition. FPIInnovations Special Publication SP-528E, Quebec.
- Green, M.C. and Karsh, J.E. (2012). The case for tall wood buildings. Forestry Innovation Investment (FII) report, Vancouver.
- Hibbitt, D., Karlsson, B. and Sorensen, P. (2011). ABAQUS Analysis User's Manual (Version 6.11). Dassault Systemes Simulia Corp., Pawtucket.
- Karacabeyli E. and Lum C. (2014). Technical guide for the design and construction of tall wood buildings in Canada. FPIInnovations report, Quebec.
- Moses, D. M. (2000). Constitutive and analytical models for structural composite lumber with applications to bolted connections. Ph.D. dissertation, Department of civil Engineering, University of British Columbia, Vancouver.
- National Research Council (NRC). (2010). National Building Code of Canada, Canadian Commission on Building and Fire Codes, NRC, Ottawa.
- Newmark, N. M. and Hall, W. J. (1982). Earthquake Spectra and Design. Earthquake Engineering Research Institute, Berkeley.
- Skidmore, Owings & Merrill, LLP. (2013). Timber tower research project. Hedrich Blessing, Chicago.

# CHAPTER 3

# ANALYSIS AND DESIGN OF GRAVITY LOAD RESISTING SYSTEM

---

**Zhiyong Chen** | University of New Brunswick

**Minghao Li** | University of Canterbury

**Ying-Hei Chui** | University of New Brunswick

**Marjan Popovski** | FPInnovations / University of British Columbia (Adjunct Professor)

## 1. INTRODUCTION

The gravity load resisting system (GLRS) of the demonstration building is investigated in this chapter. Two major issues, vertical deformation caused by gravity load and long span of the composite floor system were also addressed.

The structural design of GLRS of this tall wood building was performed following the procedure shown in Fig. 2 (Chapter 2). Similar to the LLRS of Chapter 2, the structural design of GLRS of this building was only performed on the timber structural system.

## 2. CONCEPTUAL DESIGN OF GLRS FOR TALL WOOD BUILDING

### 2.1 STRUCTURAL SYSTEM

The GLRS of this demonstration building consists of the beam-column frame sub-system and the LLRS that includes Laminated Strand Lumber (LSL) shear wall and core sub-systems. In sizing the structural members, two major technical issues were considered. These were the vertical compression deformation and the long span of the composite floor system.

### 2.2 VERTICAL DEFORMATION

Ancient timber structures, such as Yingxian Wood Pagoda (67.31m tall), have demonstrated the feasibility of constructing durable tall timber structures. For such structures however a major problem in the form of vertical compressive deformation under gravity load needs to be addressed (Chen 2011). Since the 1920's, the height of Yingxian Wood Pagoda has decreased by about 1090mm, and the deformation rate is increasing. This is mainly caused by the low compressive stiffness perpendicular to grain of wood in the Dou-Gong layer of the floor system of the pagoda, Fig. 1 (Chapter 2). This problem also happens in multi-storey timber structures, especially in platform style buildings.

Usually, two approaches can be used to minimize the vertical deformation induced by compressive stress perpendicular to grain of wood assemblies. The first one is to insert steel or other high strength connectors at the joints between columns and floor system. In this case, only the specific floor loads are transferred from floor system to column, and the loads of other floors are transferred from the upper columns to the high strength connections, and in turn to the lower columns. The second one is to avoid perpendicular to grain stress by using continuous vertical assemblies (columns and walls). Using this approach, the beams at the same level are divided by the columns or walls.

Because of the large lateral load, the horizontal connections between vertical assemblies in the height direction may be huge and complicated. In order to reduce the number of the horizontal connections of the vertical assemblies, the balloon framing construction technique was adopted to develop the GLRS, as shown in Fig. 1 and 2.

Although the balloon framing technique leads to smaller vertical compression, there is still a need to check the compression

deformation due to gravity load. The shortening is caused by short-term deformation, long-term creep and shrinkage. It will reduce the storey height at the bottom storeys. Even worse, if there is a differential shortening between adjacent members, it will make the floor un-level and induce unintended stresses in structural members and connections. This phenomenon is referred to as 'differential shortening' in high-rise steel and concrete structures. Therefore, the gravity load should be distributed to the vertical gravity resisting elements appropriately. Furthermore, performing finite element (FE) analysis on the GLRS may be useful to verify the differential shortening and investigate the 3-d system effects.

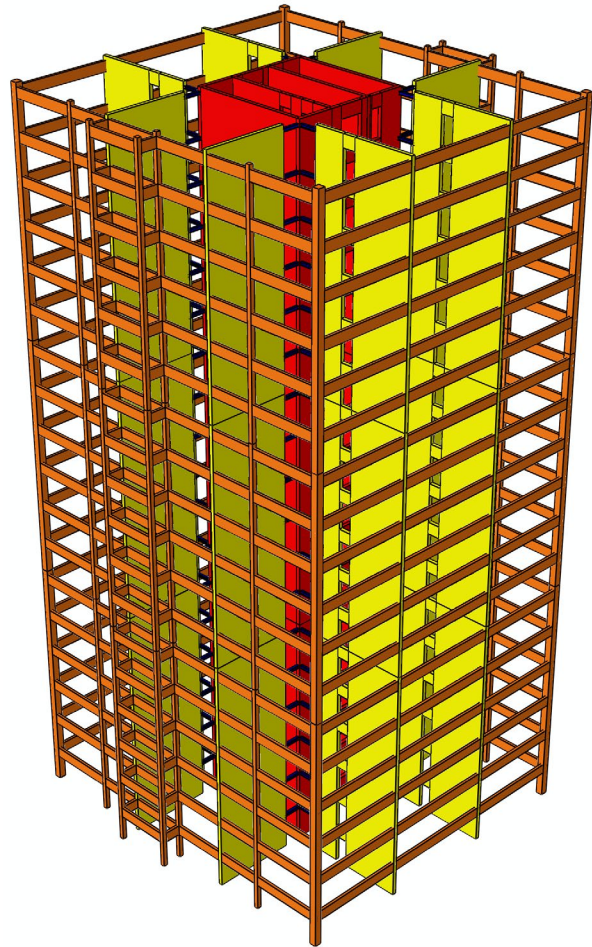


FIGURE 1: GLRS OF TALL WOOD BUILDING

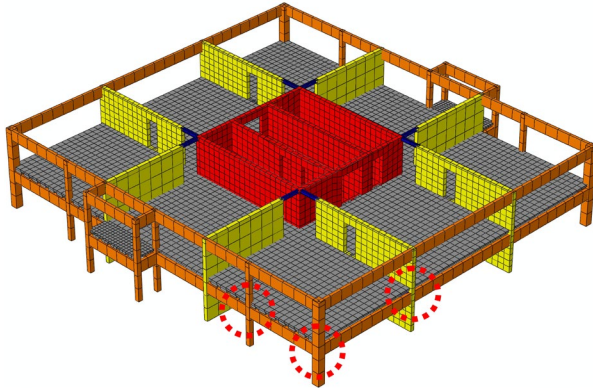


FIGURE 2: TYPICAL STOREY

### 2.3 LONG-SPAN FLOOR SYSTEM

Open space is one of the most attractive features for occupants of a building but a challenge for the structural engineers. Since a long-span floor system is required, it may induce serviceability problems such as excessive vibration. Generally, the common spans of timber floor systems are between 3 and 6 m. However, the maximum floor span of this demonstration building is about 9m.

Basically, strength criterion will not govern the structural design of a long-span floor system. Glulam beam, cross laminated timber (CLT), and even truss system can be used. But the problem is that such a floor system would be quite thick. On the other hand, the vibration and the acoustic issues will still need to be addressed.

To make up for the lightweight of wood that induces excessive floor vibration levels, concrete topping or wood-concrete-composite floor system would be one of the best approaches. TiComTec GmbH has developed a series of wood-concrete-composite with glued-in HBV (wood-concrete-composite) - shear connectors. They are HBV – Acoustic, Beam, Plate, Hollow Box, Box, Rib and Vario Floors. TiComTec GmbH claims that all HBV floor systems are suitable for a span of 15m or more (TiComTec GmbH 2011). The HBV – Vario floor system illustrated in Fig. 3 was adopted in this project.

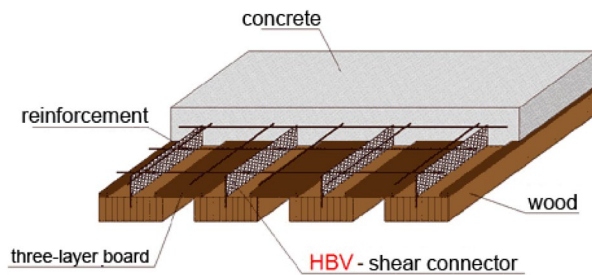


FIGURE 3: SYSTEM LAYOUT OF HBV – VARIO FLOOR (TICOMTEC GMBH 2001)

The specific features of the Vario floor system are summarized below:

- Higher static load bearing capacity resulting from a relatively close beam spacing and full composite action between concrete and timber;
- Strong and stiff diaphragm action;
- Improvement of the sound insulation as a result of the separate casting of the ceiling's under layer and the heavy mass of concrete;
- Stiffness properties for vibration;
- Low section height.

## 3. STRUCTURAL DESIGN OF GLRS

### 3.3.1 DESIGN INFORMATION AND METHOD

The design information was shown in Chapter 2, 3.1.1, Design Data. Because the balloon framing construction technique and the HBV – Vario floor system were adopted for the GLRS of the tall wood building, the horizontal elements, beams and floor, are 'cut' into single-span beams by vertical elements, columns and walls, correspondingly.

Moreover, the stiffness and strength of the joints between beam and column / shear wall, and between floor and beam are low. As a result, these joints are treated as pin joints for either the design or FE analysis modeling purposes.

Therefore, the GLRS can be designed by simple design calculation assuming the gravity load is assigned based on the respective tributary area. In addition, the sections of all assemblies of the GLRS were enlarged in order to meet fire resistance requirement for heavy timber. Therefore, the design of GLRS is superfluous. However, FE analysis was still desirable to check the stress and the deformation of GLRS.

### 3.2 DIAPHRAGM SYSTEM

#### 3.2.1 Wood-Concrete Composite Floor

Wood-concrete composite systems are engineered to benefit from composite action. In a wood-concrete system, the concrete component (slab) is designed to resist primarily compression stresses, while the wood component (a beam or plate) is mainly in tension providing exceptional strength relative to added weight of the overall composite system.

The stiffness of the connection plays a key role in the composite action between the wood and the concrete. Soft connectors, which allow substantial horizontal slip at the junction between the two materials, produce only a small degree of structural efficiency. Conversely, the highest degree of efficiency is achieved by using rigid connectors. The HBV connection can be considered as semi-rigid but close to a rigid connection due to the use of adhesive, according to the test results of the wood-concrete composite beam with HBV connector (Clouston et al. 2005). Their results suggested that the test composite wood-concrete beam performed with near full composite action – specifically, 97% effective stiffness and 99% strength of that of a beam with full composite action.

### (1) Design principle

To date, no formal design guidelines are available in North America for the design of wood-concrete composite sections. However, formulas to estimate design parameters of a bio-material system with semi-rigid shear connectors are provided by the European Standard for Timber Design, Eurocode 5 (DIN 1994). These formulas were derived from elastic composite beam theory and are independent of design method.

According to EC5, the effective composite bending stiffness  $(EI)_{ef}$  is calculated as

$$(EI)_{ef} = \sum_{i=1}^2 (EI_i + \gamma_i E_i A_i a_i^2) \quad [1]$$

where, referencing Fig. 4: subscripts 1 and 2 refer to the respective component;  $E$  = modulus of elasticity;  $I$  = moment of inertia;  $A$  = cross-sectional area;  $a$  = distance from centroid of respective component to overall neutral axis; and  $\gamma$  = shear connector reduction factor. The values of  $\gamma$  range between 0 (signifying no composite action) and 1 (full composite action) and are calculated as

$$\gamma_i = \begin{cases} \frac{1}{1 + \frac{\pi^2 E_1 A_1}{K' L^2}} & i = 1 \\ 1 & i = 2 \end{cases} \quad [2]$$

where  $K'$  = slip modulus  $K$  of one HSK connector measured from a push-out test divided by the length of the connectors; and  $L$  = beam span.

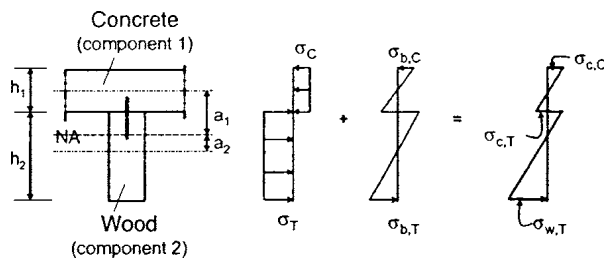


FIGURE 4: STRESS DISTRIBUTION WITHIN WOOD-CONCRETE COMPOSITE T-BEAM (CLOUSTON ET AL. 2001)

The distance between the wood member and the overall neutral axis  $a_2$  depends on the shear reduction factor  $\gamma_1$  and is calculated as

$$a_2 = \frac{\gamma_1 E_1 A_1 (h_1 + h_2)}{2 \sum_{i=1}^2 \gamma_i E_i A_i} \quad [3]$$

where,  $h$  = height of the respective member. The distance  $a_1$  is determined from the geometry of the composite beam and Eq. 4, and for HBV – Vario Floor system is calculated as

$$a_1 = (h_1 + h_2) / 2 - a_2 \quad [4]$$

The basic mechanical behaviour of the composite beam is assumed to be elastic. Referring to Fig. 4, the normal stress distribution in each component of the composite system is determined by algebraic addition. It is designed such that the concrete layer undergoes compression and bending, the wood member undergoes tension and bending, and the connector experiences shear. The maximum tensile stress in the wood is calculated as

$$\sigma_{w,T} = \sigma_T + \sigma_{b,T} = \frac{M_{max}}{(EI)_{ef}} E_2 a_2 + \frac{M_{max}}{(EI)_{ef}} E_2 \frac{h_2}{2} \quad [5]$$

where  $\sigma_{w,T}$  = total normal stress in the wood;  $\sigma_T$  = tensile stress in the wood as a result of the force couple in the composite section;  $\sigma_{b,T}$  = bending stress in the wood as a result of force couple about the wood section; and  $M_{max}$  = maximum bending moment in the beam.

The maximum compressive stress in the concrete is calculated in a similar manner as

$$\sigma_{c,C} = \sigma_C + \sigma_{b,C} = \frac{M_{max}}{(EI)_{ef}} \gamma_1 E_1 a_1 + \frac{M_{max}}{(EI)_{ef}} E_1 \frac{h_1}{2} \quad [6]$$

where  $\sigma_{c,C}$  = total normal stress in the concrete;  $\sigma_C$  = compressive stress in the concrete as a result of the force couple in the composite section; and  $\sigma_{b,C}$  = bending stress in the concrete as a result of force couple about the concrete section.

The shear flow in the connection may be computed as

$$q = \frac{\gamma_1 E_1 A_1 a_1 V_{max}}{(EI)_{ef}} \quad [7]$$

where  $q$  = maximum shear flow in the connection and  $V_{max}$  = maximum shear force in the beam.

### (2) Design procedure

#### • Design of the concrete and glulam beam

The depth (125 mm) of the concrete slab and the cross-sectional dimensions (175 × 532 mm) of the glulam beam were estimated by checking the bending capacity and deformation using  $\gamma_1 = 0.9$ . Since the floor is a single-span system, it can be simplified to a T-section beam. The width of the top-flange is equal to the glulam beam spacing which is 800mm. The effective bending stiffness of the T-section beam can be calculated using equation 1 with the shear reduction factor  $\gamma_1 = 0.9$ , as described below.

#### • Design of the HSK connector

In order to get a better composite action, a higher shear reduction factor  $\gamma_1$  is required. The shear reduction factor for the HSK connection was calculated according to equation 2. Using  $E_1 = 30,500$  MPa (B25 class; Clouston et al., 2001),  $A_1 = 100,000$  mm<sup>2</sup> (= 800 mm × 125 mm),  $k' = (415,460$  N/mm)/(400 mm) (Clouston et al. 2001),  $L = 8800$ mm, a reduction factor  $\gamma_1 = 0.9$  is obtained using 3 rows of HSK connectors with a spacing of 120mm.

### 3.2.2 Cross Laminated Timber (CLT) Floor and Roof

The roof design loads are smaller than those applied on the floor (see Table 1) and the floor span of the shear core is much shorter than other floors, therefore CLT (Fig. 5) diaphragms were used for the roof and floor structural systems for these two cases. Based on the specified roof snow load, 3.0 kPa, and the specified occupancy live load, 1.9 kPa, SLT 9 and SLT 5 CrossLam roof panel of single span were selected respectively, according to Cross Laminated Timber Design Guide (Structurlam, 2011). The CLT roof (SLT 9, 309 mm) and the wood-concrete composite floor (300 mm) have almost the same thickness.

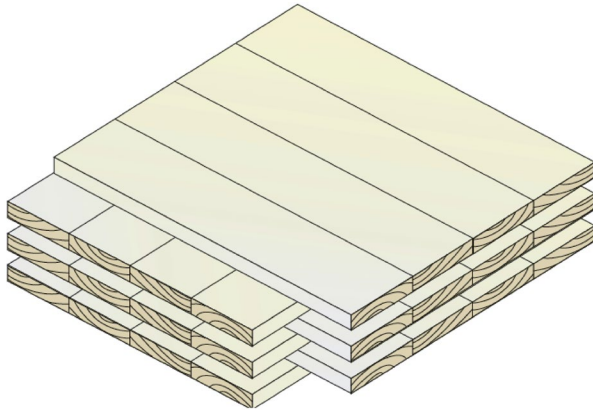


FIGURE 5: CLT (GAGNON AND PIRVU 2011)

### 3.3 FRAMES AND WALLS

#### 3.3.1 Beams

Glulam members are frequently used for intermediate and long-span bending applications. In this building, the beam span is 8.8 m. The design of glulam beams can be governed by:

- Bending moment resistance
- Shear resistance, or
- Deflection limit

In accordance with CSA O86-14 (CSA 2014), the factored bending moment resistance,  $M_r$ , of glued-laminated timber members shall be taken as the lesser of  $M_{r1}$  or  $M_{r2}$  that is the moment resistance on the tension or compression side of beam, as follows:

$$M_{r1} = \phi F_b S K_x K_{zbg} \quad [8]$$

$$M_{r2} = \phi F_b S K_x K_L \quad [9]$$

where,  $\phi$  = resistance factor of bending, 0.9;  $F_b = f_b (K_D K_H K_S K_T)$ ;  $f_b$  = specified strength in bending, in MPa;  $K_{zbg}$  = size factor glulam beams,  $(130/b)^{1/10} (610/d)^{1/10} (9100/L)^{1/10} \leq 1.3$ ;  $B$  = beam width (for single piece laminations), or width of the widest piece of lamination (for multiple piece laminations);  $L$  = length of the glulam beam from point of zero moment to zero moment;  $K_L$  = lateral stability factor;  $K_x$  = curvature factor ( $K_x = 1.0$  for straight members; and  $K_x \leq 1$  for curved member);  $S$  = section modulus.

The factored resistance to horizontal shear,  $V_r$ , of glulam beams can be calculated using equation 10 or 11, depending on the volume of the glulam beams.

$$V_r = \phi F_v 0.48 A_g C_v Z^{-0.18} \geq W_f \quad [10]$$

$$V_r = \phi F_v \frac{2A_g}{3} \quad [11]$$

where,  $\phi$  = resistance factor for shear, 0.9;  $F_v = f_v (K_D K_H K_S K_T)$ ;  $f_v$  = specified strength in shear, in MPa;  $A_g$  = gross cross-sectional area of member, in mm<sup>2</sup>;  $C_v$  = shear load coefficient;  $Z$  = beam volume, in m<sup>3</sup>; and  $W_f$  = the sum of all factored loads acting on the beam. Equation 10 can be used for any volume of glulam beam, while for beams of less than 2.0 m<sup>3</sup> in volume equation 11 is an alternative method.

Since all the beams are single-span, simply supported and loaded uniformly, they are subjected to positive bending moments only. The load duration is “standard” term, the service condition is “dry”, the construction provides lateral stability for the beams by the diaphragms, a size factor is applicable, and the beam is free of notches. Thus, the glulam beams were selected using the beam selection tables provided by wood design manual (CWC 2010) directly. In addition, the deflections of the selected glulam beams were checked, to make sure that the elastic deflection under the specified live load is no greater than span/360 (CSA 2014).

#### 3.3.2 Columns

The load-carrying capacity of an axially loaded wood compression member depends on the compression strength of wood and lateral stability which in turn depends on the stiffness property of the member. The design of a glulam column to support a given factored load involves the determination of an effective length, selecting a member size, grade and species group and calculating the factored compressive resistance parallel to grain. Generally the design is a trial and error process.

The factored compressive resistance parallel to grain,  $P_r$ , shall be taken as follows:

$$P_r = \phi F_c A K_{zcg} K_c \quad [12]$$

where,  $\phi$  = resistance factor for compression parallel to grain, 0.8;  $F_c = f_c(K_D K_H K_{Sb} K_c)$ ;  $f_c$  = specified strength in compression parallel to grain, in MPa;  $A$  = cross-sectional area of member, in  $\text{mm}^2$ ;  $K_{zcg} = \text{size factor, } 0.68(Z)^{-0.13} \leq 1.0$ ;  $Z$  = member volume, in  $\text{m}^3$ ; and  $K_c$  = slenderness factor and shall be taken as follows:

$$K_c = \left[ 1.0 + \frac{F_c K_{zcg} C_c^3}{35 E_{05} K_e K_T} \right]^{-1} \quad [13]$$

where,  $E_{05}$  = modulus of elasticity of member,  $0.87E$ ;  $C_c$  = slenderness ratio,  $K_e L/d \leq 50$ ;  $K_e$  = effective length factor;  $L$  = length associated with member dimension, in mm;  $d$  = dimension in direction of buckling (depth or width), in mm.

Since the effective length factor  $K_e$  is not equal to 1 i.e. the column does not have simple supports at both ends, the column selection tables provided by wood design manual (CWC 2010) cannot be used for this design. Instead, the factored compressive resistance parallel to grain was calculated using equation 12. The column is continuous for several storeys, but it can be treated as separate columns with length equal to a storey height and corresponding boundary conditions. Since the columns at the bottom (the 2<sup>nd</sup> storey) are effectively held in position at both ends, restrained against rotation at one end, while the columns at other storeys are effectively held in position and restrained against rotation at both ends. Thus, the effective length factors of the glulam column are 0.80 and 0.65 for the two cases, respectively (CSA 2014).

### 3.3.3 Walls

When providing resistance against gravity loads, the shear wall and the walls of the core are another kind of compression element with a very small depth/width ratio loaded by a uniform line load rather than a single load. Thus, only the stability of the walls in out-of-plate direction is required to be checked.

Because LSL is a proprietary product, its design properties are not provided by CSA O86-14 (CSA 2014) and wood design manual (CWC 2010). The LSL walls under compression are designed using equation 12 with specified compression strengths of 36.05 MPa and modulus of elasticity of 14,480 MPa (Grade 2.1E; CCMC 1994). Similar to the columns, the wall is continuous for several storeys, it was treated as separate walls with length equal to storey height and corresponding boundary conditions. Because the walls at the bottom (the 2<sup>nd</sup> storey) are effectively held in position at both ends, restrained against rotation at one end, while the walls at other storeys are effectively held in position and restrained against rotation at both ends. Thus, the effective length factors for the LSL walls are 0.80 and 0.65 for the two cases, respectively (CSA 2014).

## 3.4 DESIGN RESULTS

Based on the gravity plus wind or seismic loads with consideration of fire issue, the design results are discussed below.

SLT9 CrossLam™ of nine layers (309mm) and SLT5 CrossLam™

of five layers (169mm) with single span are used as roof and floor panel for 20<sup>th</sup> storey. The CLT panels of 3.0m in width are connected together using the joints shown in Fig. 6. TiComTec Glulam-concrete-composite deck, HBV – Vario system, made of 125mm concrete and 175 × 532mm glulam beam @ 800mm on centres is used as floor system, see Fig. 3. The adhesive used for the composite floor is a two-component epoxy glue by WEVO-CHEMIE GmbH, Stuttgart, Germany.

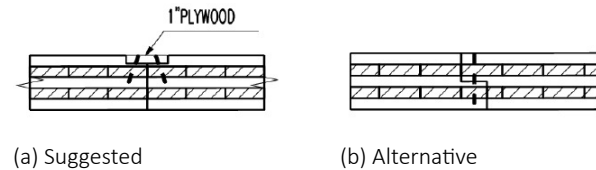


FIGURE 6: ROOF PANEL JOINTS OF CLT (STRUCTURLAM 2011)

Grade 2.1E TimberStrand® with dimensions of 19m (length) × 2.44m (width) × 89mm (thickness) is used to build the shear wall and core sub-system. The specified strengths are shown in Chapter 2, Table 7. Three layers of LSL panels are combined together to build the shear wall and the core with a total thickness of 267 mm.

Steel beam S5 × 10 of Grade 50 with a specified tensile strength of 345 MPa is used to connect the shear wall and core sub-system, Figs. 1 and 2. Beams and columns are grade 24f-E and 16c-E DFL glulam respectively. The cross sectional dimensions of beam are 315 × 532 mm. Two sizes of glulam columns are used at different locations. Their cross sectional dimensions are 365 × 418mm and 730 × 418 mm that is combined with two 365 × 418mm in the width direction. The specified strengths and modulus of elasticity of glulam are shown in Table 1. With increasing height, the vertical load carried by a column decreases, and a column with smaller cross section can be used at the upper storeys. In this design, however, the same cross-section of columns is used from bottom to top using balloon framing construction technique.

ITEMS	GRADE	
	24f-E	16c-E
Beanding moment (pos.), $f_b$	30.6	14.0
Beanding moment (neg.), $f_b$	23.0	14.0
Longitudinal shear, $f_v$	2.0	2.0
Compression parallel, $f_c$	30.2	30.2
Compression parallel combined with bending, $f_{cb}$	30.2	30.2
Compression perpendicular, $f_{cp}$		
(a) Compression face bearing	7.0	7.0
(b) Tension face bearing	7.0	7.0
Tension net section, $f_{tn}$	20.4	20.4
Tension gross section, $f_{tg}$	15.3	15.3
Tension perpendicular to grain, $f_{tp}$	0.83	0.83
Modulus of elasticity, E	12800	12400

TABLE 1: SPECIFIED STRENGTHS AND MODULUS OF DFL GLULAM, MPa

More details are provided in Appendix B, Structural Drawings.

## 4. PERFORMANCE UNDER GRAVITY LOAD

### 4.1 VIBRATION OF COMPOSITE FLOOR SYSTEM

The advent of stronger materials, lighter construction, more rigid cladding, smaller damping, longer spans and more accurate strength calculations, which takes into account the interaction of building components, means that vibrational serviceability has a greater influence on structural design of timber floor systems than before.

Two types of vibration problems arise in building construction: continuous vibrations and transient vibrations. Continuous vibration arises due to the cyclic forces of machinery or certain human activities such as dancing. This vibration can be considerably amplified when the cyclic forces are synchronized with a natural frequency of the floor – a condition called resonance. The walking action of occupants is the major cause of transient vibration in floor systems in buildings. Transient vibration typically decays at a rate that is dependent on the available damping.

Since this 20-storey tall wood building is a residential construction, transient vibration induced by walking is of interest. In this study, the performance criterion (equation 13) developed by Hu et al. (2001) and Hu (2007) to address walking vibration in wood floor systems is used to assess the vibrational serviceability of the long-span floors in the 20-storey building.

$$\frac{f_1}{d_{1kN}^{0.44}} > 18.7 \quad [14]$$

where,  $f_1$ =the fundamental natural frequency,  $H_z$ ;  $d_{1kN}$ =the deflection of the floor under a concentrate point load of 1 kN at the centre, in mm. As per equation 14, the fundamental natural frequency and the deflection of the floor are required for the assessment, therefore, the numerical simulation approach was used to estimate these parameters of the composite floor.

#### 4.1.1 Finite Element Model of Floor System

A three-dimensional (3D) detailed numerical simulation model of composite floor, shown in Fig. 7, was developed using ABAQUS (Hibbitt et al. 2011).

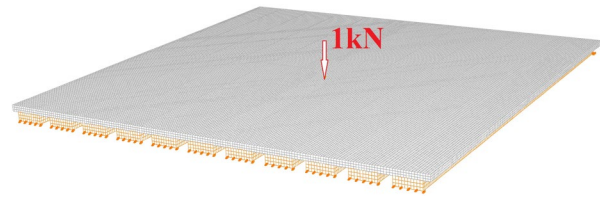


FIGURE 7: THREE-DIMENSIONAL FE MODEL OF COMPOSITE FLOOR

A surface-based constraint, TIE, was used to tie the contact surfaces between the concrete slab and the glulam beam together for the duration of the simulations, because the composite floor with near full composite action was designed using sufficient HBV connections. This floor was simply supported at two ends of glulam beams, Fig. 7.

Only a frequency analysis which is a linear perturbation procedure and a static stress analysis under 1kN which induces small elastic stress and strain were performed. Therefore, the constitutive models of glulam was assumed to be orthotropic elasticity while concrete was regarded as an isotropic elastic material. The parameters of these material models are shown in Table. 2.

MATERIAL	DENSITY, $\text{kg/m}^3$	MODULUS OF ELASTICITY, MPa	POISSON'S RATIO
Glulam	490	12,400	0.4
Concrete	2,400	30,500	0.3

TABLE 2: PROPERTIES OF GLULAM BEAM AND CONCRETE SLAB

The concrete slab and glulam beams were meshed using the 8-node linear brick stress/displacement element (C3D8R), reduced integration with hourglass control. The FE model was meshed with a total of about 14,000 elements.

### 4.1.2 Floor Vibration Analysis

The fundamental natural frequency of the composite floor was derived by performing natural frequency extraction using LANCZOS Eigen-solver. The fundamental natural frequency of the glulam-concrete composite floor is about 6.0 Hz, and the corresponding mode shape is shown in Fig. 8.

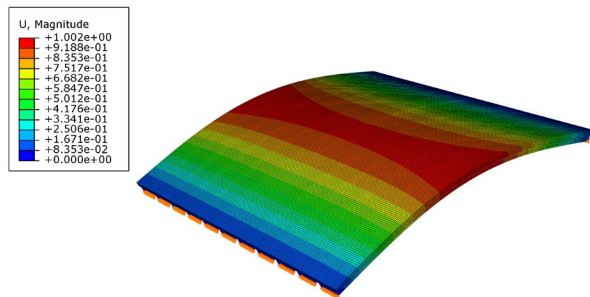


FIGURE 8: FIRST MODE SHAPE OF COMPOSITE FLOOR

In order to derive the deflection of the composite floor under a concentrate load of 1kN, a static stress analysis was conducted. The deformation of the glulam-concrete composite floor is shown in Fig. 9. The maximum deflection in the out-of-plane direction is 0.0639 mm.

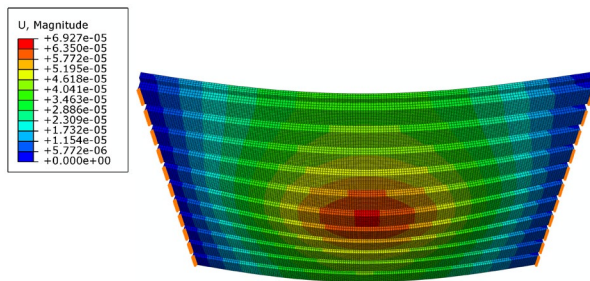


FIGURE 9: DEFORMATION OF COMPOSITE FLOOR UNDER 1KN SINGLE POINT LOAD

By substituting the fundamental natural frequency and the deflection of the glulam-concrete composite floor in to equation 14, a value of 20.1 was derived. It is larger than the threshold of 18.9, thus this composite floor is considered to have acceptable vibration performance.

## 4.2 GRAVITY-INDUCED RESPONSE

### 4.2.1 FE Model of GLRS

A 3D modeling approach was used to develop the FE model of the GLRS of the tall wood building based on ABAQUS (Hibbitt et al. 2011), in an attempt to investigate the load, stress and deformation distributions of the GLRS. The 3D FE model is shown in Fig. 10.

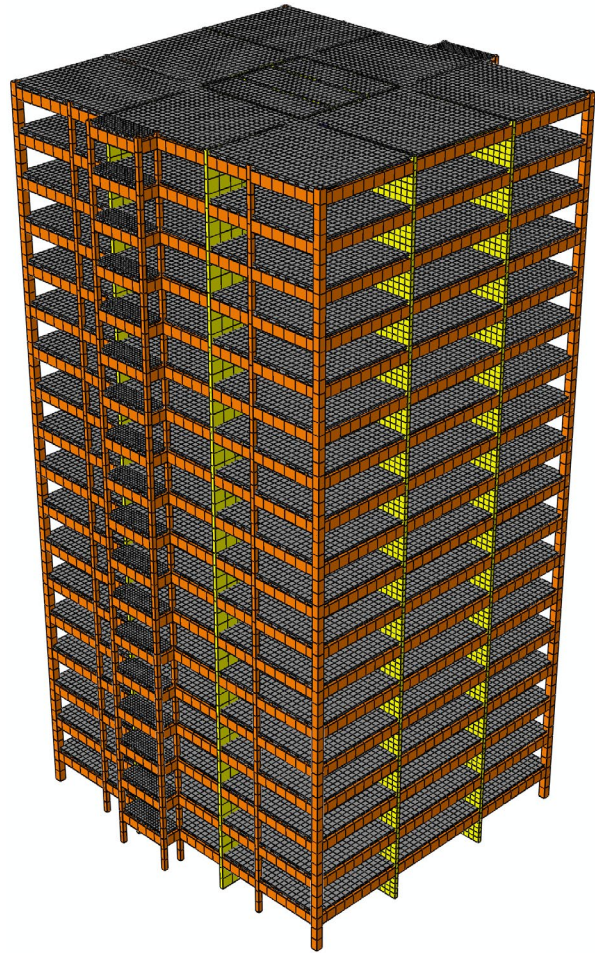


FIGURE 10: FE MODEL (3D) OF THE TALL WOOD BUILDING

The material, connection and interaction models of the 3D FE model is identical as those of the 2D FE model of the lateral load resisting system shown in Chapter 2. The joints between beam and column / shear wall, and floor and beam of timber structures were modeled as pinned joints.

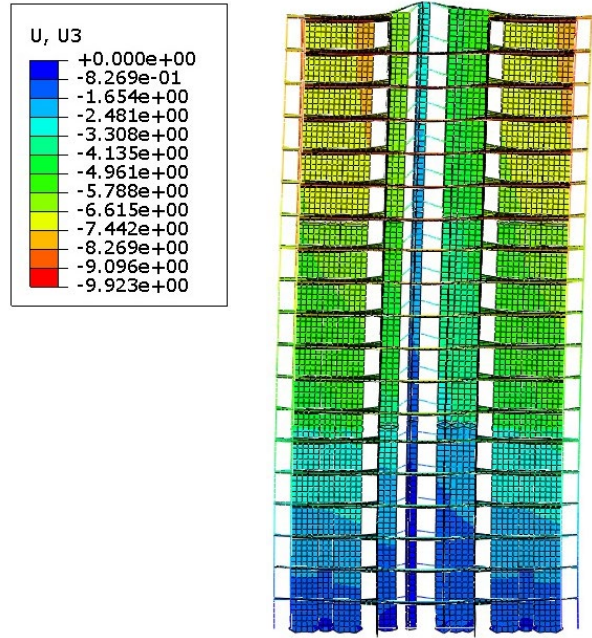
The shear core, shear walls and diaphragm were meshed using the 4-node doubly curved general-purpose shell element (S4R), reduced integration with hourglass control, and finite membrane strains. Glulam beams, columns and steel beams were modeled using the 2-node linear Timoshenko (shear flexible) beam element (B31). A 3D, 2-node connector element (CONN3D2) was used to simulate the vertical joints, shear connectors and hold-downs. Non-structural mass, which is a contribution to the model mass from features that have negligible structural stiffness, was lumped to the diaphragm (floor and roof) in the form of mass per unit area. The FE model was meshed with a total of about 90,000 elements, including the shell, beam, connector and mass elements.

**4.2.2 Performance of GLRS under Gravity Load**

Under gravity load, the vertical gravity resisting elements shorten. The shortening is due to short-term deformation, long-term creep and shrinkage. Generally, it will induce a lower storey height at the bottom storeys, which are of major concern. If there is a differential shortening between adjacent members, it will cause unlevel floor and induce additional stresses in members and joints. This phenomenon is referred to as ‘differential shortening’ in high-rise buildings.

In an attempt to investigate the ‘differential shortening’ on the GLRS of 20-storey tall wood building, numerical simulation of vertically compressive deformation was performed. In this analysis, only the short-term effect of gravity load (1.0D+1.0S and 1.0D+1.0L for the roof and floor, respectively, where D, S and L indicate the dead, snow and live load specified in Table 1 of Chapter 2) was analysed.

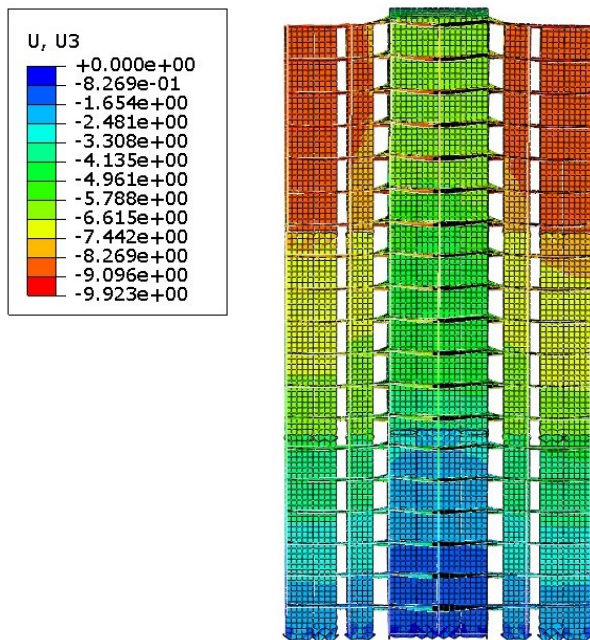
The static stress analysis procedure was adopted for conducting the FE analysis. Under the gravity load, the deformation profiles of the tall wood building are shown in Fig. 11. The largest compressive deformation occurs at near the bottom. However as the compressive deformation is cumulative from bottom to top, the largest movement occurs at the top storey with a maximum value of about 10 mm. The maximum ‘differential shortening’ happened at the top as well and is about 7.5mm. It appears that the differential shortening is caused by the relatively small compressive deformation in the core. The compressive deformation of the bottom storey is about 1-2 mm. It shows that the vertical compressive deformation and ‘differential shortening’ of the 20-storey tall wood building under short-term gravity load are very small and would not cause functional problems of the building. This indicates that using continuous vertical structural elements to construct the GLRS is effective in minimizing the vertical movement and differential shortening of the building under gravity loads.



(b) Y (N-S) direction

**FIGURE 11:** VERTICAL DEFORMATION UNDER GRAVITY LOAD (SCALE FACTOR = 250)

The stress distribution of 20-storey tall wood building under gravity is the inverse of the deformation distributions shown in Fig. 11. The maximum stress occurred at the bottom. The maximum vertical load and compressive stress of columns and walls are shown in Table 3. The factored resistance of these vertical components is listed in Table 3 as well. It can be found that the stresses in these components are substantially lower than their strengths. It indicates that the columns and walls were designed with a large superfluous resistance since the dimensions of the cross-section of these members were enlarged for fire issue.



(a) X (E-W) direction

ITEMS	GRADE	FACTORED LOAD, kN	STRESS, MPa	FACTORED RESISTANCE, kN
Column	730 × 418 mm	1,390	4.56	5,028
	365 × 418 mm	367	2.40	2,733
Wall, /m	Shear wall	752	2.80	5,175
	Core	846	3.17	5,175

**TABLE 3:** MAXIMUM LOAD AND STRESS IN COLUMNS AND WALLS

## 5. RECOMMENDATIONS

Based on the structural design and the FEA of this demonstration building, some recommendations are derived.

- (1) The gravity load resisting system consisting of continuous vertical elements and wood-concrete composite floor is suitable for the 20-storey high-rise wood building to address the vertical deformation and large-span diaphragm of tall wood buildings.
- (2) The 3D finite element modeling approach is appropriate to investigate the behavior of the gravity load resisting system under gravity load.
- (3) With respect to the vertical compression issue, only short-term loading analysis has been conducted, the long-term creep and shrinkage of the GLRS should be investigated. For taller high-rise wood buildings, this issue would be more significant.

## REFERENCES

- Canadian Construction Materials Centre (CCMC). (1994). TimberStand® LSL. Evaluation Report CCMC 12627-R. Weyerhaeuser, Boise.
- Canadian Standards Association (CSA). (2014). Engineering design in wood. CSA O86-14, Toronto.
- Canadian Wood Council (CWC). (2010). Wood design manual 2010. Eton System, Nepean.
- Chen Z.Y. (2011). Behaviour of typical joints and the structure of Yingxian Wood Pagoda. Ph.D. dissertation, School of Civil Engineering, Harbin Institute of Technology, Harbin.
- Chui. Y.H., and Barclay D.W. (1998). Analysis of three-layer beams with non-identical layers and semi-rigid connections. *Can. J. Civ. Eng.* 25: 271-276.
- Deutsches Institut für Normung, e.V. (DIN). (1994). Eurocode 5 : Entwurf, Berechnung and Bemessung von Holzbauwerken. Eurocode 5, DIN V ENV 1995-1-1, Berlin.
- Gagnou S., and Pirvu C. (2011). CLT handbook Canadian Edition. FPInnovations Special Publication SP-528E, Quebec.
- Green, M.C and Kash, J.E. (2012). The case for tall wood buildings. Forestry Innovation Investment (FII) report, Vancouver.
- Hibbitt D., Karlsson B., and Sorensen P. (2011). ABAQUS Analysis User's Manual (Version 6.11). Dassault Systemes Simulia Corp., Pawtucket.
- Hu, L.J., Chui, Y.H. and Onysko, D.M. (2001). Vibration serviceability of timber floors in residential construction. *Progress in Structural Engineering and Materials*, 3(3): 228-237.
- Hu, L.J. (2007). Design guide for wood-framed floor systems. Canadian Forest Service Report No. 32. Quebec: FPInnovations.
- NRC. (2010). National building code of Canada, Canadian Commission on Building and Fire Codes and NRC, Ottawa.
- Clouston, P, Bathon, L.A., Schreyer, A. (2005). Shear and Bending Performance of a Novel Wood-Concrete Composite System. *J. Struct. Eng., ASCE*, 131(9), 1404-1412.
- Structurlam. (2011). Cross Laminated Timber Design Guide – Ver. 7. Structural CLT Design Guide, Penticton.
- TiComTec GmbH. (2011). Load Bearing Constructions using Wood-Concrete-Composite Technique with glued-in HBVR – Shear Connectors. TiComTec GmbH technical report, Haibach.



# CHAPTER 4

## FIRE RISK ASSESSMENT

---

**Xiao Li** | Carleton University

**George Hadjisophocleous** | Carleton University

**Alejandro Medina** | Carleton University

**Andrew Harmsworth** | GHL Consultants

**Christian Dagenais** | FPInnovations

---

## 1. AIMS AND SCOPE

This chapter reports the fire risk assessment of the checker building using the quantitative fire risk assessment computer model CURisk. The objective of this work is to compare the fire risk of the proposed building of mass timber construction with the fire risk of a comparable building of non-combustible construction.

## 2. INTRODUCTION TO CURisk

CURisk is a quantitative fire risk assessment model that is being developed at Carleton University. It includes a system model and more than ten submodels. The system model deals with the system methodology and the basic structure of the model, the basic functions of each submodel, the relationship of all the submodels, as well as the data input and output of the whole model. CURisk comprises a number of submodels, including Fire Growth, Smoke Movement, Boundary Failure and Fire Spread, Smoke and Fire Detection, Occupant Response and Evacuation, Fire Department Response and Action, as well as Economic Loss submodel. The system model sets up a predetermined set of procedures to coordinate all the submodels. Finally, two decision-making parameters, the Expected Risk to Life and the Fire Cost Expectation are obtained. More detailed description can be found in CURisk Technical Report (Hadjisophocleous, et al 2011).

In the following, the basic methodology of the system model will be introduced, including the basic structure of the system model, a brief description of each submodel, and the input and output data of the system model and each submodel.

### 2.1 SYSTEM STRUCTURE OF THE RISK ASSESSMENT MODEL

This risk assessment model begins with the production of all the fire scenarios. For each scenario, a design fire is selected. Then, the Fire Growth submodel is run to predict the tenability conditions in the compartments that fire may spread to from the room of fire origin. The Smoke Movement submodel is used to predict tenability conditions in the compartments beyond the room of fire origin. The Fire Spread submodel is used to calculate the probability of fire spread from the room of fire origin to other compartments and to provide further information on tenability conditions. The information of the building tenability conditions are then sent to the submodels of Smoke and Fire Detection, Occupant Response, Occupant Evacuation, Fire Department Response and Action, and Life Loss to calculate the life loss of this scenario. Economic losses for this scenario are also calculated using the hazardous conditions. After finishing all the scenarios, the final two decision-making parameters, Expected Risk to Life and Fire Cost Expectation are obtained.

Figure 1 gives a schematic diagram of the system model, and Table 1 lists a description of the relationship of submodels. The following paragraphs provide a brief description of each submodel.

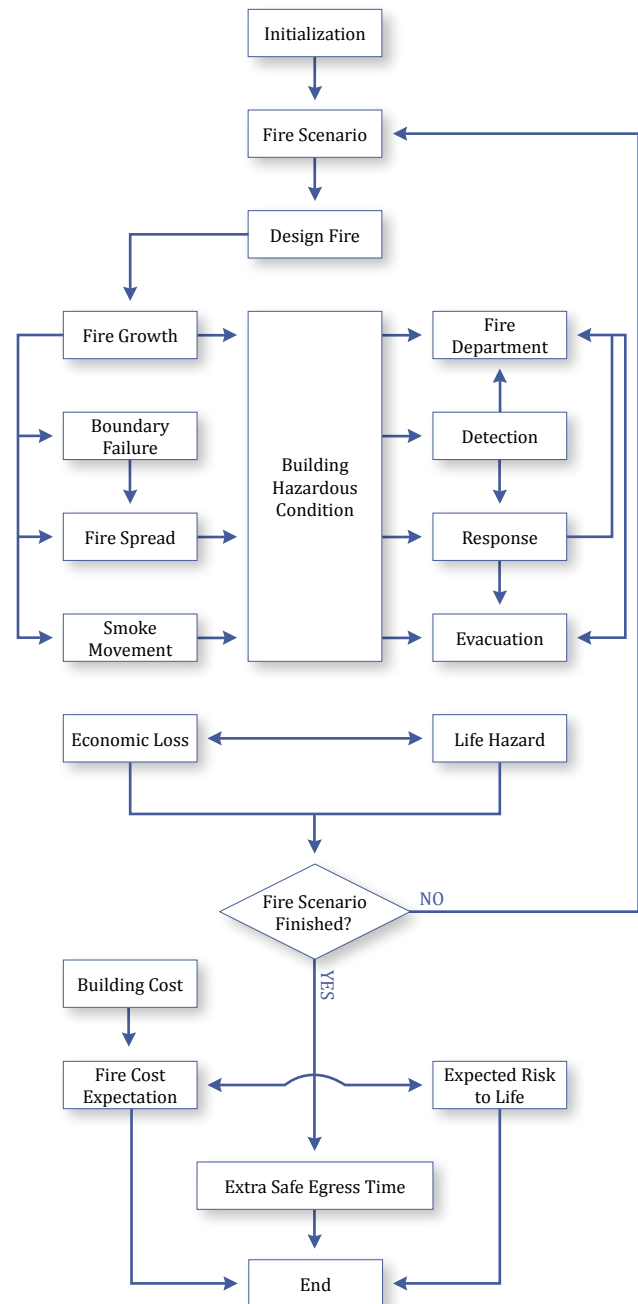


FIGURE 1: A SCHEMATIC OF THE FIRE RISK ASSESSMENT SYSTEM MODEL

SUBMODELS	INPUT SUBMODELS	OUTPUT SUBMODELS
Fire Scenarios	User Input	Expected Risk to Life Fire Cost Expectation
Design Fire	User Input	Fire Growth
Fire Growth	User Input Design Fire	Smoke Movement Boundary Failure Hazardous Conditions
Smoke Movement	User Input Fire Growth	Hazardous Conditions
Boundary Failure and Fire Spread	User Input	Hazardous Conditions
Smoke and Fire Detection	User Input Hazardous Conditions	Fire Department Response and Action Occupant Response
Occupant Response	User Input Smoke and Fire Detection Hazardous Conditions	Occupant Evacuation Fire Department Response and Action
Occupant Evacuation	User Input Hazardous Conditions Occupant Response	Life Hazard
Life Loss	Occupant Evacuation Fire Department Response and Action Hazardous Conditions	Expected Risk to Life
Fire Department Response and Action	User Input Occupant Response Smoke and Fire Detection Hazardous Conditions	Life Hazard
Hazardous Conditions	Fire Growth Smoke Movement Fire Spread	Smoke and Fire Detection Occupant Response Occupant Evacuation Fire Department Response and Action Economic Loss Life Hazard
Building Cost	User Input	Fire Cost Expectation
Economic Hazard	User Input Fire Scenarios Hazardous Conditions	Fire Cost Expectation
Risk to Life	Fire Scenarios Life Hazard	Final Output
Fire Cost Expectation	Fire Scenarios Building Cost Economic Loss	Final Output

TABLE 1: A LIST OF SUBMODELS

## 2.2 A DESCRIPTION OF MAJOR SUBMODELS

### 2.2.1 Fire Scenarios submodel

A scenario is composed of a number of well-defined events. In this model, the event tree is composed of the following events: room of fire origin, selection of design fire, sprinkler suppression, detectors and alarms, and firefighting. The first event is fire ignition or fire start at a specific location. According to the contents and characteristics of the fire compartment, the relevant design fire will then be selected for each type of fire and compartment. Whether the door of the room of fire origin is open or closed is the next event since it has a significant impact on the fire development and smoke movement. In addition, weather conditions also affect the fire development and smoke movement. The possibility and reliability of sprinkler and firefighting suppression are also considered which changes the heat release rate of the fire.

The Fire Scenario submodel produces the number of fire scenarios, and the probability of each scenario. The results of this submodel are used by Risk to Life submodel and Fire Cost Expectation submodel.

### 2.2.2 Design Fire submodel

This submodel is used to produce the design fire, defined as a typical fire reflecting the combustion characteristics of the fuel in the compartment. This submodel provides Fire Growth submodel with the composition of the fuel, ratios of smoke species production and consumption rates, and the nominal heat release rate. For this, the properties, arrangement, and amount of the fuel, and the geometry and dimension of the compartment are taken into account to obtain the required results. Details of the fire will be further computed with the Fire Growth submodel. The Design Fire submodel is only run once for each case study.

### 2.2.3 Fire Growth submodel

The Fire Growth submodel predicts the fire conditions in the compartment of fire origin. This submodel takes inputs from the Design Fire submodel. The required input parameters are the nominal heat release rate, the amount, arrangement, and composition of the movable fuels, ratios of species production rates, compartment geometry and dimension, and ventilation. The results of the submodel are to be used by the submodels of Smoke Movement, Smoke and Fire Detection, Boundary Failure, Fire Spread, and Hazardous Conditions. This submodel adjusts the nominal heat release rate from the design fire and provides species production rates based on the real conditions of combustion in the compartment. This submodel outputs the temperature of the gas layers and mass flow rates, by running the same two-zone fire model as used in the Smoke Movement submodel in each room. This model will be run only once for each compartment at the beginning of CURisk simulation.

### 2.2.4 Smoke Movement Submodel

The Smoke Movement submodel is a two-layer zone model

detailed in (Fu and Hadjisophocleous 2000). It is used to predict the tenability level of each non-fire compartment in the building, including smoke temperature, species concentrations, thickness of the smoke layer, heat flux to the boundaries, and smoke obscuration in each compartment based on the conditions of fire growth, building geometry and dimension, properties of boundary materials, ventilation system, and the environmental conditions. The Smoke Movement submodel is run once for each scenario. The results of the submodel are to be used by the submodel of Hazardous Conditions. A recent improvement has been done (Zhang and Hadjisophocleous 2013) to describe heat and mass transfer across the interface between the upper and lower layers as a result of the temperature difference between the two layers.

### 2.2.5 Boundary Failure and Fire Spread submodel

A new Fire Spread submodel (Cheng and Hadjisophocleous 2011) developed at Carleton University has been integrated into CURisk as the Barrier Failure and Fire Spread submodel. Barrier Failure and Fire Spread submodel is used to calculate the time at which the barrier will no longer fulfil its separating function and thus fire will spread to other compartments. The failure time depends on two factors, fire severity and fire resistance. When fire severity exceeds fire resistance, the barrier fails. A module inside the submodel is used to predict the failure time of the building barriers under the given design fire based on the Fire Resistance Ratings of the building barriers. The objective of this model is to provide a time-dependent probability of fire spread to any other compartment from the fire compartment for the given condition. Together with other hazardous information provided by Fire Growth and Smoke Movement submodels, this information will be used to calculate the number of deaths in the compartment to which fire spreads.

### 2.2.6 Smoke and Fire Detection submodel

This submodel is used to calculate the detection time of fire or smoke. It takes input from the submodel of Hazardous Conditions, and provides data for the submodels of Occupant Response and Evacuation, and Fire Department Response and Action. Fire alarm can be activated by the smoke temperature or smoke concentration at the location of the fire alarm. The Fire and Smoke Detection submodel checks temperatures and smoke concentration in each compartment to see whether the activation conditions are satisfied so that the activation time can be assessed.

### 2.2.7 Fire Department Response and Action

This submodel is used to estimate the arrival time of the fire department at the fire building and the room of fire origin as well as their efforts to perform their duty (fight the fire and rescue occupants). This submodel takes input from the submodels of Smoke and Fire Detection, and Hazardous Conditions, and outputs data for the submodels of Occupant Response and Evacuation, and Economic Loss. Intervention time is a very important parameter, which is defined as the

period of time from ignition to the first application of firefighting agent over the fire. This time is composed of the following intervals, detection, notification, dispatch, preparation, travel and set-up. This submodel calculates these times based on the properties of the fire building, characteristics of the fire department, and the distance between them and the environmental conditions. It is assumed that when the fire firefighter enters a compartment, the fire will be under control, and the occupants who are alive will be saved.

### 2.2.8 Hazardous Conditions Submodel

Hazardous Conditions submodel is used to collect all the information of hazardous conditions of each compartment in the building. This submodel collects data from the submodels of Fire Growth, Smoke Movement, and Fire Spread, and outputs data of temperature and species concentrations of gas layers, interface height, radiation flux, and temperature for the submodels of Smoke and Fire Detection, Occupant Response and Evacuation, Fire Department Response and Action, and Economic Loss.

### 2.2.9 Occupant Response submodel

The Occupant Response submodel is used to predict the response of occupants. This submodel takes input data from the submodels of Hazardous Conditions, Smoke and Fire Detection, and provides data for the Occupant Evacuation submodel. The Occupant response begins from receiving cues of fire or smoke. Some occupants will immediately begin to evacuate and other occupants will further check the conditions and then decide whether they should leave the compartment.

### 2.2.10 Occupant Evacuation submodel

The Occupant Evacuation submodel is used to calculate the evacuation of occupants. The evacuation model uses a coarse network approach to describe a building and an individual perspective to represent occupants (Gruchy 2004). The Monte Carlo methods repeats random variables including the occupants' gender, age, speed, exit selection, pre-evacuation time, and distance to be traveled to exit the initial compartment with uniform distributions (Zhang et al 2013). This submodel takes input data from the submodels of Hazardous Conditions, and then provides the data of the evacuation route and time of each occupant to the Life Hazard submodel. The Occupant evacuation submodel begins from the time when an occupant decides to evacuate. There will be different routes for them to select and different speeds for them to move based on their moving and judging ability as well as their familiarity with the building.

### 2.2.11 Life Hazard submodel

The Life Hazard submodel is used to calculate the expected number of casualties (injuries or deaths) in each fire scenario. This submodel takes input data from the submodels of Hazardous Conditions, Occupant Response and Evacuation, and Fire Department Response and Action, and then provides

the expected number of deaths and injuries to the submodel of Expected Risk to Life.

This submodel calculates the fractional effective dose of each occupant based on the hazardous conditions for each occupant as well as the information of occupant movement provided by the Occupant Response and Evacuation. In addition, once a fire in a compartment reaches flashover, the remaining occupants in that compartment are assumed to be immediately killed.

### 2.2.12 Building Cost submodel

The objective of this submodel is to calculate the capital cost of the passive and active fire protection systems and the maintenance cost of the active fire protection systems. These parameters will later be used by the Fire Cost Expectation submodel. It takes input data directly from users.

### 2.2.13 Economic Loss submodel

The objective of this submodel is to calculate the economic loss of each fire scenario. This parameter will later be used by the Fire Cost Expectation submodel. It takes the input data of fire conditions from Hazardous Conditions submodel, the data of economic values of contents, and damage criteria of contents from users to estimate the economic loss. A detailed description of this submodel can be found in reference (Esposito 2004).

## 2.3 FINAL DECISION-MAKING PARAMETERS

The primary focus of fire codes is life safety, thus in a quantitative fire risk assessment model, it is essential to determine a parameter to measure risk to life. In this model, the Expected Risk to Life (ERL) is one of the two final decision-making parameters, defined as the expected death frequency per year per individual of a building. ERL can be directly used as a decision-making parameter if there is available reference data or can be compared with that of another similar building deemed-to-satisfied the code objectives.

Fire Cost Expectation (FCE) is the other final decision-making parameter of CURisk. It is assumed that the fire costs are composed of three parts, fixed capital investment of active and passive fire protection systems, maintenance and inspection cost of the active fire protection systems, and the expected loss due to fire and smoke spread. The FCE does not include other costs such as the costs related to the impact on the environment of fire, and costs of fire department services. This model does not calculate the present worth of expected losses but directly calculate them based on the current data.

FCE is defined as a vector with four components: COSTFixed, the capital cost of the passive and active fire protection systems; COSTMaintain, the annual maintaining cost of the active fire protection systems; COSTLoss, the expected annual loss as a result of all probable fire incidents in the building; COSTTotal, as well as the total cost in the time span of the design life of the building.

### 3. BUILDINGS DESCRIPTION AND CURISK INPUTS

The buildings considered for comparison include the demonstration building of mass timber construction and a comparable building of non-combustible construction. The layouts of the two buildings are identical, and the differences are that the demonstration building has mass timber structural members. It was agreed that 15% of the room enclosure areas in the Checker building are exposed mass timber panels, and other areas are protected with non-combustible fire resistive linings. The comparable non-combustible construction is assumed to contain no combustible materials except the movable fuel loads (i.e., no combustible interior finish materials). Meanwhile it is noted that wood panelling is permitted in the non-combustible construction as per the code requirements.

According to the building design from the architecture group, the building is 20-storey tall. The ground floor is a concrete podium, as shown in Figure 2, which has a total floor area of 2250 m<sup>2</sup> and a floor height of 4.5 m. There are service and storage rooms, and four rooms (indicated as room 01 to room 04) intended for mercantile uses. Residents enter the lobby in the building through the courtyard, and they can also enter or exit the building through the two exits connected to the visitor parking lots.

The tower on top of the podium consists of 19 residential storeys. The general residential floor plan is shown in Figure 3. The floor plan of the 2<sup>nd</sup> floor (tower first floor) and the topmost 20<sup>th</sup> floor (penthouse) are slightly different with the general floor plan. Except the tower first floor (712 m<sup>2</sup>) and the penthouse (627 m<sup>2</sup>), each residential floor (see Figure 3) has a floor area of 712 m<sup>2</sup> and contains four 2-bedroom apartments and two 1-bedroom apartments. For the simplicity of CURISK input, it is assumed that all the residential plans (2<sup>nd</sup> to 20<sup>th</sup> floor) are same as shown in Figure 3.

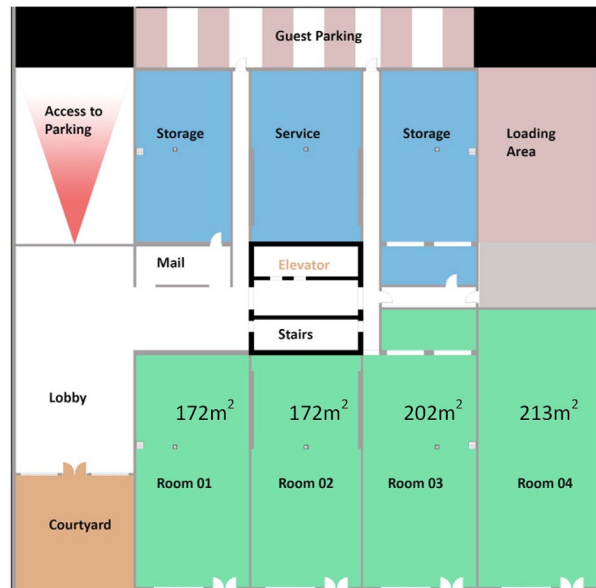


FIGURE 2: THE FLOOR PLAN OF PODIUM (FROM THE ARCHITECTURE GROUP)

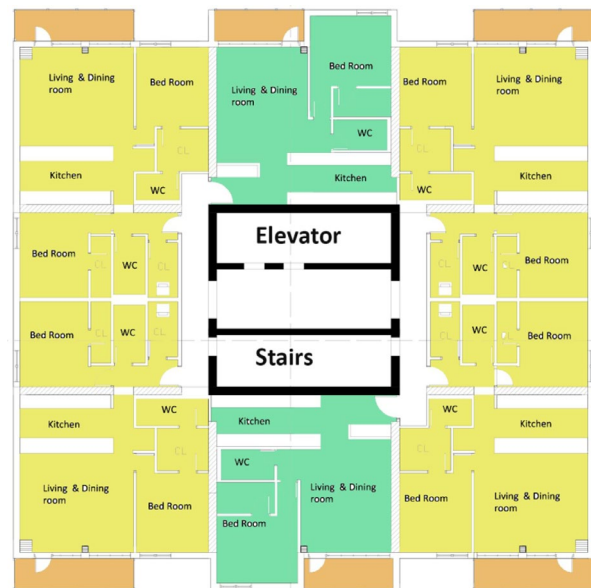
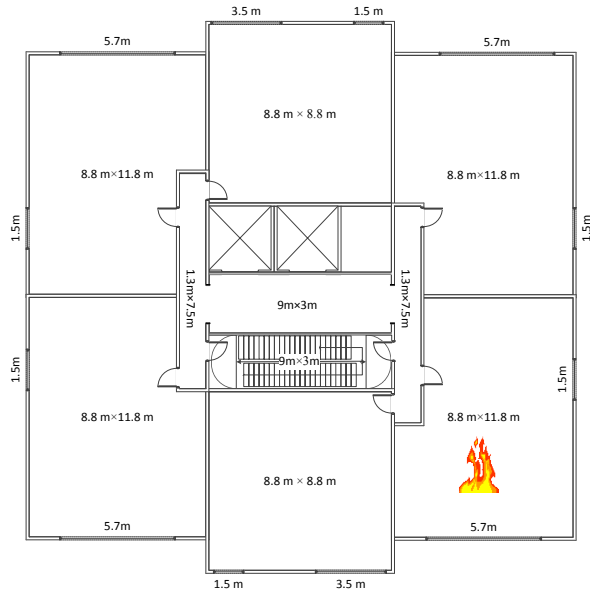


FIGURE 3: TOWER RESIDENTIAL STOREYS (FROM THE ARCHITECTURE GROUP)



**FIGURE 4:** OPTIMIZED RESIDENTIAL FLOOR PLAN AS CURisk INPUT

The floor plans in the demonstration building are optimized in order for creating the CURisk input files. The floor plan of the ground floor (or podium) is the same as the plan in Figure 2 but only lobby, building core and the four mercantile rooms are included in the simulation. Figure 4 shows the residential floor plan. Compared with the real floor plan, the optimized plan ignores the existence of partitions and balconies in each apartment, and simplifies the apartment area into rectangular squares. The reason for this treatment is to avoid creating too many rooms in CURisk and thus to reduce the CURisk computational time as well as maintain numerical stability. Besides, partitions inside apartments are not required to have a fire resistance rating, and without partitions CURisk would produce relatively conservative predictions as fire would grow barrierlessly inside the apartments. The fire-resistance rating of the building assemblies of the demonstration building are the same as that of the comparable building of non-combustible construction. As per the building code requirement, the fire-resistance rating of the structural wall assemblies and the floor assemblies is 2 hours, and fire-resistance rating of the non-structural fire separations is 1 hour. The positions and sizes of windows and doors are the same as the original design.

Occupant number and initial positions are the input data of CURisk. The Occupant Response submodel and the Occupant Evacuation submodel could predict the response and evacuation process of individual occupant and life risk can be predicted further by the Life Hazard submodel. The occupant distribution in the building is determined based on the description in the NBCC 2005, which specifies 2 occupants in each sleeping room of a dwelling, and 3.7 m<sup>2</sup>/person for mercantile uses. Therefore, 4 occupants reside in each 2-bedroom apartment and 2 occupants in each 1-bedroom apartment, for a total of 20 occupants per residential floor. No occupant is assigned in public areas such as corridors or stair rooms. On the ground floor (podium), the total area of the

commercial rooms (room 1 to 4) is 759 m<sup>2</sup>, and the maximum capacity is therefore taken as 205 persons. It is assumed that no person is distributed in other areas in the ground floor. Adding all the occupants together in the building, the total number of occupants is 585.

The Economic Loss submodel in CURisk can estimate the fire losses in a fire scenario based on the cost of building components and the severity of the fire scenario. The costs of the building include costs of passive and active fire protection systems and building contents. However, it is hard to precisely estimate the costs of building components in the demonstration building and the comparable building of non-combustible construction. To simplify the problem, the same costs are assigned to both the Checker building and the building of non-combustible construction. In this manner, the differences in the fire losses of two buildings are calculated totally based on the differences in the fire severities.

#### 4. FIRE SCENARIOS

CURisk is a scenario-based fire risk assessment model, and it can not only perform fire risk analysis of a specific fire scenario, but also can assess the overall fire risk of a building by considering all the possible fire scenarios. In CURisk, a fire scenario is defined as a fire incident that could possibly occur in reality. The determination of possible fire scenarios are based on a few factors, including location of fire origin, moveable fire loads, fire growth rates, opening conditions, availability of various fire protection options and so on. Furthermore, the probability of occurrence of a scenario can be calculated based on either statistical data or engineering judgement.

In this report, fire scenarios are divided into two different categories, one is the normal fire scenarios, and the other one is the extreme fire scenarios. Normal fire scenarios refer to the fire scenarios that could most probably occur and be easily predicted, such as fire in an apartment. Extreme fire scenarios means fires with lower probability of occurrence but potentially with greater consequences related to building damages and occupant safety. Examples of extreme fires are earthquake-induced fires or a arson fire initiating in the lobby.

The normal fire scenarios are fire incidents that occur in the apartments. Only the fire in the apartments is considered because of its relatively high probability of occurrence. Fires are unlikely to initiate in other places such corridor or staircases due to slim chances of ignition sources as well as limited fire loads. Multiple simultaneous fire sources in more than one apartment are ignored because chances are extremely low. In the residential building it can be assumed that fire occurs at each apartment with equal probability, and likewise fire occurs on each floor with equal probability. Technically speaking, to cover all the possible fire scenarios, fire in every apartment on all the 19 storeys should be simulated. However, it would take an extremely long time to run through all the possible fire scenarios. Thus, only typical and representative fire scenarios are taken into account.

The event tree method is used to establish the cluster of fire scenarios. The normal fire scenarios adopted in this report are illustrated in the event tree as shown in Figure 6. Events

that were included in the tree comprise the fire location, the availability of fire sprinklers, the availability of detectors/alarms and the availability of fire department action. It can be seen that all those events would greatly affect the fire development and consequences.

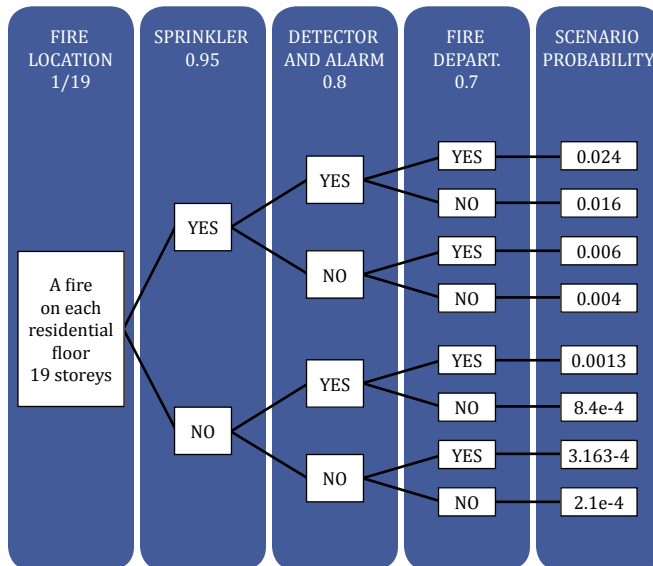


**FIGURE 5:** EVENT TREE SHOWING NORMAL FIRE SCENARIOS AND PROBABILITIES

The first event is the fire location. As mentioned earlier, it is not feasible to cover all the possible fire locations in the tower, and only one apartment on each residential floor is accounted as the fire source. As a matter of fact, close results of fire and smoke development are expected when the fire occur in any of the four 2-bedroom apartments because the floor plan is generally symmetrical vertically and horizontally. As such, it is decided that room of fire origin on each floor is located at the 2-bedroom apartment on the lower right in Figure 4. Based on the above discussion, in the normal scenarios, there are in total 19 fire locations in the tower and the probability of fire at each location is 1/19.

According to statistical data and engineering judgement, the reliability of sprinklers, detector/alarm and fire department action can be taken as 95%, 80% and 70%, respectively. Other factors such as the selection of design fire, fire loads and opening conditions of doors and windows could also largely affect the fire development. These factors are determined based on the statistical data and engineering judgement. In the CURisk simulation, the design fires are the well-known t-square fires and the fire growth rates in all the apartments are set to be fast ( $0.0469 \text{ kW/s}^2$ ) (Drysdale 1999). Fire load density in all the residential apartments is  $550 \text{ MJ/m}^2$ , according to a fire survey (Bwalya et al 2011). In the fire simulation by Fire Growth submodel and Smoke Movement submodel, windows are all assumed to be closed at the beginning of the fire and window glasses break when the room smoke upper layer temperature reach 300 Degree Celsius. All the doors, except

corridor doors, are assumed to be 50% open throughout the fire incident. Eventually, according to the event tree, a total of 152 fire scenarios are created for the normal fire scenario category.

In the extreme fire scenario category, two sub-categories are simulated: one is the fires in the lobby on the ground floor, and the other one is fires occurring at night in the apartments without fire protection systems. For the extreme fire scenario in the lobby, a fire load density same as that in the apartments ( $550 \text{ MJ/m}^2$ ) is given to the lobby area, which is not realistic but might happen in extreme conditions such as arson fire. For the fire occurring at night in the apartments without any suppression, 19 fire scenarios are created, in which 19 night fires occur on each floor.

## 5. CURISK SIMULATION RESULTS AND DISCUSSION

This section discusses the results of CURisk simulation. Firstly, the development of fire tenability conditions in the room of fire origin are presented considering the effects of construction types, heavy timber panel exposure areas and fire protection and suppression systems. Then the occupant response and evacuation results in the demonstration building as well as the building of non-combustible construction are demonstrated. Furthermore, the selected fire scenarios in the demonstration building are compared. After that the overall fire risk comparison is made between the demonstration building and the comparable building of non-combustible construction, and also shown are the fire risks of extreme fire scenarios. Finally the influences of reliability of fire sprinkler system on the building fire risk are discussed.

### 5.1 FIRE DEVELOPMENT IN THE ROOM OF FIRE ORIGIN

Fire development in a combustible construction may be different with a fire in a non-combustible construction. CURisk can simulate the fire development characteristics when the fire initiates in different types of room constructions. In order to show the feature of fire development in different types of constructions, five different room fires are simulated using CURisk. The five different types of room constructions are non-combustible, light timber frame protected with 1 layer gypsum board, heavy timber panels (HTP) (such as CLT and LSL, Laminated Strand Lumber) protected with 1 layer of gypsum board, heavy timber panels (HTP) with 1 wall unprotected (about 15% area of room enclosure), and non-combustible construction with 1 wall finished with 8 mm wood panelling (about 15% area of room enclosure). Figure 6 shows the results of fire development in the five different room constructions when fire is located on the second floor (tower first floor). Regarding to the performance of gypsum board, it is assumed that one layer of gypsum board would protect the inner structure for 15 minutes of fully developed fire.

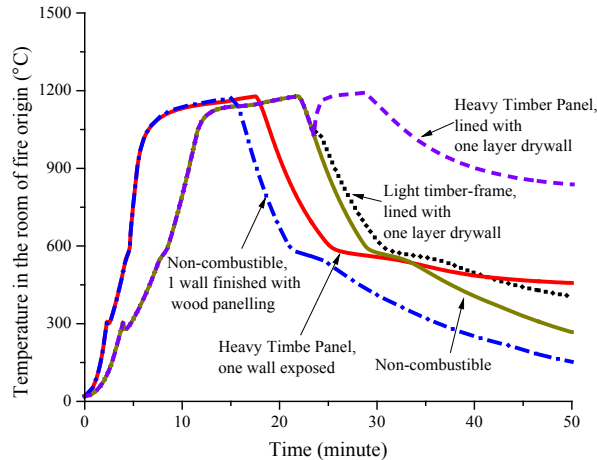


**FIGURE 6:** A COMPARISON OF FIRE DEVELOPMENT IN THE ROOM OF FIRE ORIGIN WITH DIFFERENT TYPES OF ROOM CONSTRUCTION, FIRE IN THE 2ND FLOOR WITHOUT FIRE SUPPRESSION

The red curve in Figure 6 shows the fire development in the room of fire origin when one HTP wall (15% of room enclosure area) is exposed while other room enclosure areas are well-protected through the fire. This is the proposed room setup in the Checker building. Compared with the initially protected rooms, the fire growth speed of the fires are higher in the HTP room with 1 wall unprotected and non-combustible room with 1 wall finished with wood panelling (before fully developed fire). This is because of the fire contribution of the exposed HTP wall or wood panels, and the simulation results is in line with the findings of the experimental tests performed at Carleton University (Li et al 2014). Fire growth phase is the golden period for occupant evacuation, the quicker fire growth means slightly shorter time of occupant evacuation in the room of fire origin. Moreover, the difference of the red curve (HTP with 1 wall exposed) with other curves in the later time of the fire is that the fire endures sustained burning or charring after all the movable fuels are consumed. The difference is minor compared with other fires given the area of exposed HTP walls, and this will not be a problem if firefighting is conducted at the appropriate time. In contrast, for the non-combustible room with wood panelling, its fully developed period is shorter than the HTP room with 1 wall exposed, because the 8 mm thick wood panel can only sustain a limited period of burning.

When the rooms are initially protected, the curves are basically overlapped before the failure of protective linings (gypsum boards), which means that the room structure has no influences on the fire development. The deviations of the fire curves appear after the failure of gypsum board, shown in the beginning of the decay phase in Figure 6. Taking the non-combustible curve as the baseline, the temperature curves in the decay periods of both light timer frame room and HTP room (protected with 1 layer of gypsum board) are above that baseline. The temperature of light timber frame room is a bit higher than the non-combustible room due to the burning of the wood studs but the contribution is limited because of the limited wood surface area. The significant contribution occurs in the HTP room. After the failure of gypsum board, the room

fire goes back to the fully developed phase and then enters a slower decay, which is apparently resulted from the heavily involvement of the HTP panels to the room fire.

## 5.2 EFFECT OF FIRE SUPPRESSION ON FIRE DEVELOPMENT

It is well acknowledged that without proper and timely suppression and firefighting fires in most cases will grow beyond control and lead to great damages and casualties. Fire prevention and protection systems are essential to mitigate the losses. Besides passive fire protection such as specifying fire resistance rating or flame spread ratings, etc., active fire protection plays a more important role in suppressing the fires. The common active fire protection measures are, for example, manual suppression, the adoption of fire sprinklers as well as firefighting from the fire department. The effects of fire sprinklers and fire department actions on the fire developments in the room of fire origin are simulated using CURisk as shown in Figure 7.

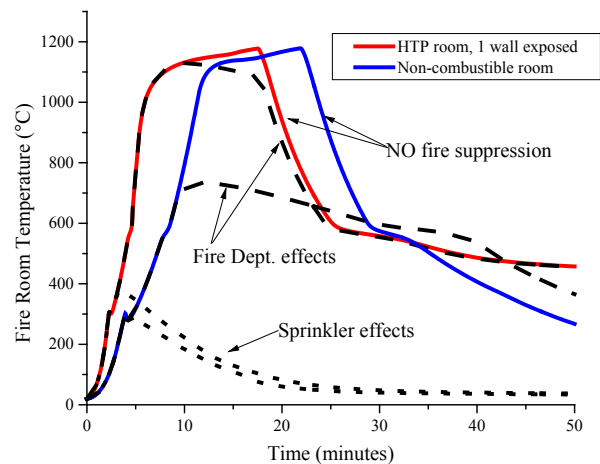


**FIGURE 7:** THE EFFECTS OF SPRINKLER OPERATION AND FIRE DEPARTMENT ACTION ON THE FIRE DEVELOPMENT IN THE ROOM OF FIRE ORIGIN (FIRE ON THE 2ND FLOOR)

In Figure 7, the room temperature developments in the demonstration building and in a comparable building of non-combustible construction are compared, and also shown together are the fire developments under the intervention of fire sprinklers and fire departments. Although fire in the demonstration building has a faster fire growth than the non-combustible construction, the operation of fire sprinklers could stop the fire in its early stage, before the fire grow to flashover conditions and spread beyond the room of fire origin. Apparently automatic sprinklers or other fast fire suppression tools are the most effective and widely used fire protection systems. It should be noted that fire sprinklers in this simulation are assumed to have 100% operational reliability. In reality the operational reliability may slightly below 100%, which means that there are chances when the sprinklers may not successfully operate and suppress the fire. This issue is considered when constructing the fire scenarios.

When sprinklers fail to stop the fire, fire departments can still

fight fires and save lives. The shortcoming of firefighting by the fire departments is that it takes time for fire department to respond to the fire, which includes notification time, travel time and setup time. For example, the average action time of fire department in Ottawa is about 8 minutes. The dash lines in Figure 7 show the room temperature variation after fire department takes action. Compared with fires without intervention, room temperature starts to decrease shortly before 10 minutes, at which time room fire already reaches flashover in both the demonstration building and the non-combustible building. The fire in the room of exposed combustible structures may reach flashover earlier than the room of non-combustible construction, but in both cases fire department has limited capabilities because it is known that post-flashover fire suppression is difficult, regardless of the types of construction.

### 5.3 THE IMPACT OF EXPOSURE AREA OF HEAVY TIMBER PANELS ON FIRE DEVELOPMENT

In the demonstration building it is agreed that one of the HTP wall is exposed without any protective lining. To learn the impact of wood panel exposure areas on the fire hazards, fire development in a room with four different wall exposure areas are simulated using CURisk, as shown in Figure 8. The room setup and fire load condition are on the basis of the two-bedroom apartment on the 2<sup>nd</sup> floor. One wall exposure means that 1/6 (about 17%) of the total room enclosure area are unprotected heavy timber panel (HTP) walls. Likewise, two to four wall exposures mean that 2/6 to 4/6 (33% to 67%) of the total room enclosure areas are exposed HTP walls. It is assumed that all other areas are well-protected during the fire. For comparison, the fire curve in a room of non-combustible construction (or well-protected room) is also provided in Figure 8.

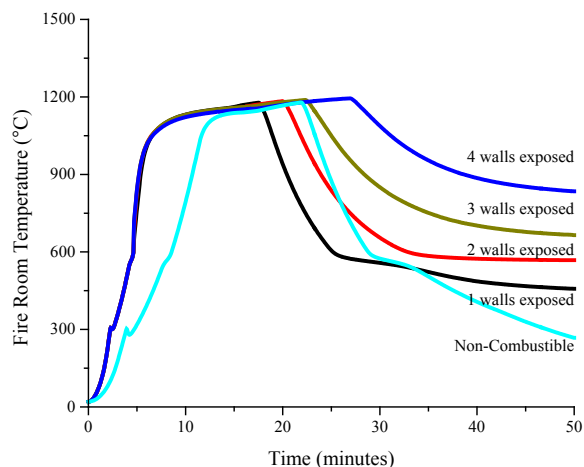


**FIGURE 8:** FIRE DEVELOPMENT IN THE ROOM OF FIRE ORIGIN COMPARING DIFFERENT HTP WALL EXPOSURE AREAS (FIRE ON 2<sup>ND</sup> FLOOR)

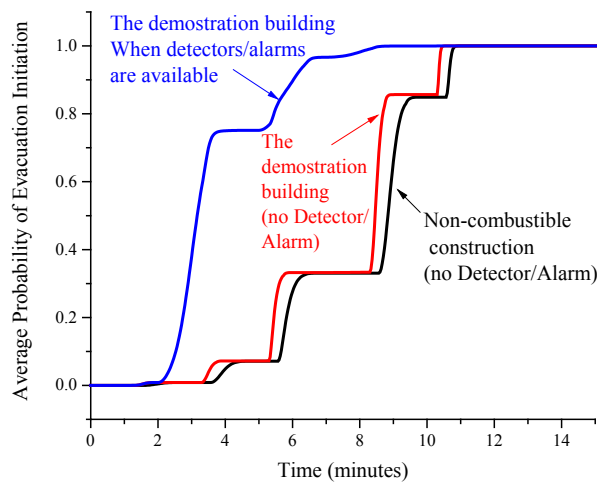
CURisk simulation results indicate that the HTP wall exposure mainly affects the fire growth speed and fire duration. As shown in Figure 8, the fire growth speed is relatively higher when part of the room enclosures is exposed with HTPs in comparison with a non-combustible room, because the release of paralysis gases from the HTPs after room gets hotter, which in turn increases the fire growth rate in the room. This is also found in the experimental tests (Li et al 2014). Furthermore, the exposed HTPs may be actively involved in the room fire as part of the fuel, and prolong the fully developed period. However, the room temperature is not much affected because the fire is controlled by the ventilation condition (i.e., ventilation controlled fire). After all the movable fuels (furniture) in the room are consumed in the fire, the fire in the non-combustible room enter decay phase and die out quickly. It is noted that the non-combustible room was lined with gypsum board only. It did not include combustible interior finish materials as allowed in NCBC, which would significantly impact fire growth. Whereas in the room with exposed HTPs, burning of HTPs leads to continuous release of heat and sustains the room temperature in certain level depending on the size of the exposure area. Lastly it should be noted that those fires are assumed to be not intervened by either fire sprinklers or Fire Department, which is unlikely in reality.

### 5.4 OCCUPANT RESPONSE AND EVACUATION

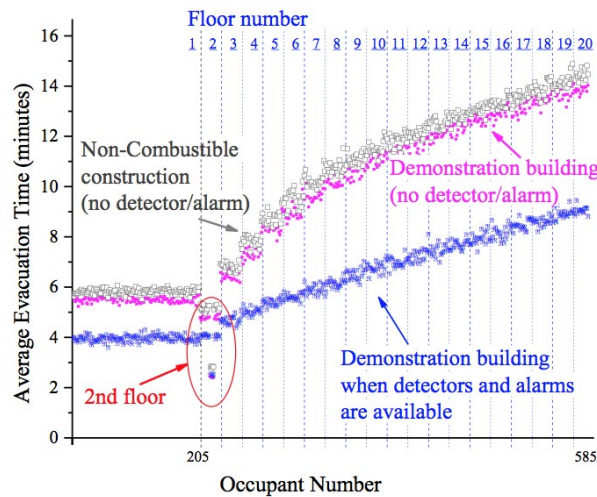
The Occupant Response submodel in CURisk can predict the occupant response probability as a function of time, based on the fire tenability conditions in the building and the availability of fire detection systems. The probability of evacuation initiation means the probability of an occupant takes action to move as a function of time, and the time duration before the evacuation initiation is called the response time.

Figure 9 demonstrates the average probability of evacuation initiation among all the occupants, when the fire occurs on the second floor in the demonstration building as well as in the building of non-combustible construction. The comparison is made between these two types of buildings when no fire detection and suppression systems are available, as indicated by the red curve and the black curve in Figure 9. Simulation results show that the average probability of evacuation initiation in the demonstration building is a bit higher than the comparable building of non-combustible construction, which mean that occupants would take slightly less time to respond to the fire. There are too many factors affecting the occupant response prediction in the submodel, thus it is difficult to say which factor lead to this results. But the most probably reason is that the occupants could receive a faster fire cue in the demonstration building, attributed to the faster fire growth rate in the room of fire origin. Another thing should be noted is that in some cases a few occupants may fail to respond to the fire and remain in their original position throughout the fire scenario (i.e., probability of evacuation initiation remains 0). This phenomenon is also simulated by CURisk but hard to identify in Figure 9 because it shows the average probability of evacuation initiation among all the occupants. The adoption of fire detectors and alarms can greatly reduce the occupant response time, and fire signals can be sent to occupants as

soon as the fires are detected. The blue curve in Figure 9 shows the average probability of evacuation when fire detector and alarm systems are available in the demonstration building.



**FIGURE 9:** PROBABILITY OF EVACUATION FOR OCCUPANTS IN THE BUILDING WHEN FIRE OCCURS ON THE 2ND FLOOR



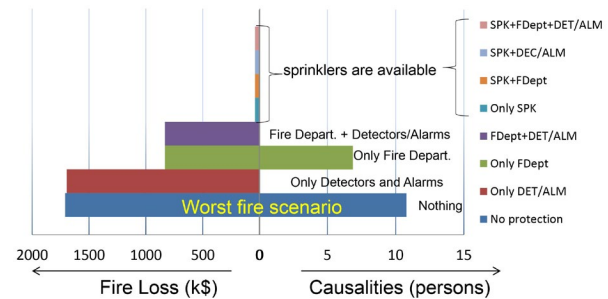
**FIGURE 10:** AVERAGE EVACUATION TIME FOR EACH OCCUPANT ON DIFFERENT FLOORS WHEN FIRE OCCURS ON THE 2ND STOREY

Figure 10 demonstrates the results of occupant evacuation simulated by the Occupant Evacuation submodel in CURisk. The Occupant Evacuation submodel is a network model incorporated with Monte Carlo simulation, and could predict the evacuation time of each occupant based on the occupant response times and fire tenability condition in the building. The evacuation time of each occupant refers to the time when an occupant safely evacuates out of the building. The mean evacuation time of each occupant averaged among Monte Carlo repetitions is illustrated in Figure 10. Each scattered symbol in the figure represents an occupant, and the occupants are numbered from the 1<sup>st</sup> floor to the 20<sup>th</sup> floor, and their original floor position is divided by the vertical dotted lines.

Similar to the probability of evacuation, when fire detector and suppression systems are not available, the evacuation times in the demonstration building are slightly shorter than the comparable building of non-combustible construction, while the contribution of fire detectors and alarms are significant as shown by the blue curve. The average total evacuation time for the demonstration building without detector/alarm system is about 14 minutes, and with detector/alarm system the average total evacuation time is reduced to about 9 minutes. Thus results indicate that the installation of detector/alarm system could reduce the total evacuation time by roughly 5 minutes. The result show that with the detectors and alarms all the occupants can exit the building within 9 minutes, by which time the fire is still contained in the room of fire origin.

### 5.5 FIRE SCENARIO COMPARISON IN THE DEMONSTRATION BUILDING

Building fires could cause significant property damages and occupant casualties; whereas economic loss and life risks can be reduced if appropriate active fire protection systems are used. Eight fire scenarios are simulated using CURisk to study the impact of different combinations of active fire protection options on the fire loss and life risk. The active fire protection systems include fire sprinkler (SPK), detector/alarm system (DET/ALM), fire department operation (FDept), which form eight combinations of active fire protection systems: SPK+FDept+DET/ALM, SPK+DEC/ALM, SPK+FDept, only SPK, FDept+DET/ALM, only FDept, only DET/ALM and No protection, as shown in Figure 11. The fire breaks out in the same apartment on the 2<sup>nd</sup> floor, and the eight active fire protection options forms eight different fire scenarios.



**FIGURE 11:** COMPARISONS OF FIRE LOSSES AND CASUALTIES IN EIGHT FIRE SCENARIOS WHEN FIRE OCCURS ON THE 2ND FLOOR IN THE DEMONSTRATION BUILDING

The results demonstrate that fire protection systems could significantly influence the consequences of the fire. The adoption of fire sprinklers plays the most important role in controlling the fire, and in most cases sprinkler operation could extinguish the fire in its infancy before the fire reach flashover and spread to other spaces. The four active fire protection combinations containing fire sprinkler (SPK) produced the minimum fire losses and no causality. Without the fire sprinklers or when they fail to operate or suppress the fire, further fire suppression should rely on the firefighting from the Fire Department. However, as was discussed before,

Fire Department usually takes time to arrive at the fire scene and fire may already grow too big and cause losses, as shown by the “Only FDept” bar. Nevertheless, fire spread may be stopped by the fire department and losses may be controlled. This can be found by comparing its fire loss with worst case fire scenario, i.e., no protection, as shown in Figure 11. Also shown in the graph is that the installation of detector/alarm system would greatly protect the life safety from the fire but may not reduce the property damages, which can be found by comparing the scenario “No protection” with scenario “Only DEC/ALM”.

### 5.6 FIRE RISK ANALYSIS OF THE DEMONSTRATION BUILDING IN NORMAL FIRE SCENARIOS

CURisk can not only provide the evaluation of different aspects of the fire incident such as fire and smoke spread and occupant evacuation, but also could evaluate the overall risk of the proposed building based on possible fire scenarios. The 152 normal fire scenarios have been constructed as shown in the event tree in Figure 5. The normal fire scenario cluster contains majority of the probable fire scenarios covering every residential floor as well as possible failure of active fire protection options. After looping through all the 152 normal fire scenarios, expected fire losses and casualties in each fire scenario are predicted by the Economic Loss submodel and Life Hazard submodel in CURisk. Then the overall fire risk of the normal fire scenarios is calculated by the two equations shown below,

$$\text{Expected Life Risk} = \sum_{\substack{\text{scenarios} \\ i=1 \text{ to } 152}} \text{Prob. } (i) \times \text{Casualty } (i)$$

$$\text{Expected Fire Loss} = \sum_{\substack{\text{scenarios} \\ i=1 \text{ to } 152}} \text{Prob. } (i) \times \text{Loss } (i)$$

In the above equations, Prob.(i) means the occurrence probability of scenario i; casualty (i) and Loss (i) refer to the predicted casualty and fire loss (in k\$) in scenario i, respectively.

In fact, the above two formulas indicate the calculation of “Risk”, which is the product of probabilities and consequences. To make it clear, the expected life risk shown by the equation means the expected total number of casualties if one fire occurs in the building. Likewise, the expected fire loss means the expected fire damages in the building if a fire occur (including damages of building construction and fire protection systems, building contents, downtimes costs, refer to Economic Loss submodel for details).

The expected life risk and expected fire losses of the normal fire scenarios are demonstrated in Figure 12. The general results are that the expected fire losses are roughly same for both the demonstration building and the comparable non-combustible construction, while the expected life risk in the demonstration buildings are somewhat higher than that in the non-combustible construction.

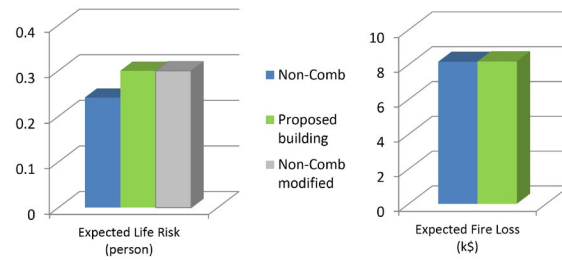


**FIGURE 12:** THE COMPARISON OF EXPECTED LIFE RISK AND EXPECTED FIRE LOSSES BETWEEN THE DEMONSTRATION BUILDING AND THE NON-COMBUSTIBLE CONSTRUCTION, AS WELL AS THE MODIFIED NON-COMBUSTIBLE CONSTRUCTION (WITH WOOD PANEL LININGS)

Although the results suggest that the fire risk of the demonstration building is somewhat higher, the assumptions behind all those CURisk simulations should be clarified. Most importantly, the principal assumption with the non-combustible construction is that the building is constructed with totally non-combustible materials except the moveable fuels such as furniture, whereas in the demonstration building one heavy timber panel wall in each apartment is unprotected and other areas are well protected. This difference would fundamentally affect the fire growth and smoke spread process, and further affect the life risk and fire damages. However, in reality combustible linings are widely used in the non-combustible buildings, so the assumption made for the non-combustible construction is not realistic. Taking this into consideration, the difference between the two types of buildings would most likely be very similar.

As discussed above, it might not be appropriate to assume the building of non-combustible construction as perfectly non-combustible. In order to show the influences of combustible linings, wood panels are added to the building of non-combustible construction. Similar to the building of mass timber construction, it is assumed that 15% of the apartment wall areas in the building of non-combustible construction are lined with 8 mm thick wood panels, and other room areas are well protected. In CURisk, it is assumed that wood panelling has the same combustible property (such as the charring rate) as the Heavy Timber panels, except that wood panel would burn away when the 8 mm panel was charred through.

For the modified building of non-combustible construction, the 152 normal fire scenarios are calculated again using CURisk and the overall fire risk of the modified building of non-combustible construction is then obtained. The results show that the expected risk to life of the modified building is extremely close to the risk of the demonstration building, as shown in Figure 12.

### 5.7 EFFECT OF RELIABILITY OF FIRE SPRINKLER SYSTEM

It is well acknowledged that fire sprinkler systems play a dominate role in protecting the building from potential fires. Compared with other active fire protection systems, fire sprinklers can detect and suppress the fire in very early stage before the fire cause any severe damages or life risks. It is appropriate to say that if the reliability of fire sprinklers

reaches 100%, then the fire risk in a building of combustible construction or in any other types of construction shall not be an issue, or in other words, the fire risks in a combustible construction shall be same as a non-combustible construction. However, in reality the reliability of fire sprinklers could never reach 100%. The problem is that sprinklers may malfunction at rare circumstances (operational reliability), and even if they operate properly in some cases the fire may not be effectively suppressed (performance reliability).

The reliability of fire sprinklers is the most important factor that affects the overall risk of the building, and the impact is studied through changing the reliability value in the event tree in Figure 5 while keeping other factors unchanged. Further, the expected life risk and expected fire losses of the demonstration building are calculated. The original reliability value of sprinkler was 95%, on the basis of which, the reliability value is increased to 99% as well as lowered to 90%, respectively. The results of the three different setups are compared in Figure 13, and all the calculated values are normalized by the original results when the reliability is 95%. From the figure it can be found that slightly changes in the reliability of sprinklers result in significant variations in the expected life risk and fire losses. Decreasing the reliability value by only 5% could lead to a double of the expected life risk and 56% increase in the expected fire loss. Similarly, if the reliability of fire sprinkler could increase by 4% to 99%, the expected life risk and fire losses could drop to 22% and 55% of the normal value, respectively. In this respect, the fire risk differences between the demonstration building and the comparable building of non-combustible construction shown by Figure 12 is rather insignificant, when comparing with the effect of sprinkler reliabilities.

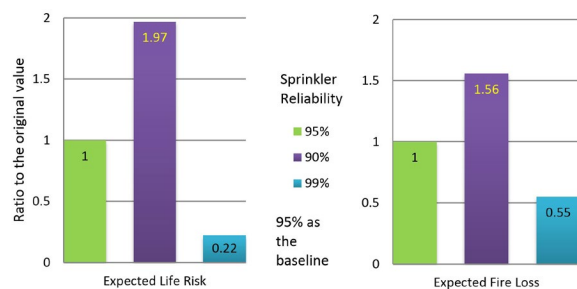


**FIGURE 13: THE EFFECT OF SPRINKLER RELIABILITIES ON THE FIRE RISK OF THE DEMONSTRATION BUILDING**

Besides the reliability of fire sprinkler system, following a same procedure as mentioned earlier, the effects of reliability of detector/alarm system as well as Fire Department action on the fire risk are also studied, respectively. For the detector and alarm system, the results indicate that when to vary the reliability values by  $\pm 10\%$ , the changes in both the expected risk to life and expected fire loss are far less than 1%. While varying the reliability values of Fire Department action by  $\pm 10\%$ , the expected risk to life is basically not largely affected (less than 1%), but the expected fire loss varies about 8%. Therefore, it can be concluded that the effects of above two

systems on the overall fire risk are far less sensitive than that of the fire sprinkler system. Nowadays, fire sprinkler system and detector / alarm system are indispensable tools to protect lives and properties. Maintaining and improving the reliability of those systems, especially the fire sprinkler system, are essential to mitigate the building fire risk.

## 5.8 EXTREME FIRE SCENARIOS

Extreme fire scenarios refer to the fire incidents that may not typically happen but would cause extremely severe fire consequences once they occur. Examples of those extreme fire scenarios include earthquake induced fires, arson fires, and fires occur at dangerous locations. Earthquake can cause damages of equipment and release of flammable or combustible materials, and they may result in fires when in touch with ignition sources such as electrical arcing. Post-earthquake fires are complicated and cannot be accurately predicted using a model like CURisk, thus CURisk simulation is not conducted toward earthquake-induced fires. In the following, fire in the lobby on the ground floor and fire at night without active fire protection systems are discussed based on CURisk calculations.

Fire in the lobby might cause significant losses if not under control. However, this is not likely to happen in reality because normally fire load in the lobby is low and could not sustain a big fire. But chances of arson exist. A fire scenario in the lobby is simulated using CURisk. In this fire scenario, a same fire load density as that in the apartments ( $550 \text{ MJ/m}^2$ ) is assumed, and all the doors in the building are assumed to be half open. The fire load and doorway opening status would provide a worst case scenario and thus conservative results. CURisk simulation results show significant casualties and a lot more damages than apartment fires due to fire spread to adjacent heavy-loaded shops. The fire smoke developed from the lobby fire quickly spreads all over the lobby and block all the building exits (see Figure 2). Even though lobby fire could cause significant outcomes, the fire scenario is probabilistically insignificant and will not much affect the overall fire risk.

Another extreme fire scenario is night fire without fire suppression systems. 19 night fire scenarios with a fire on each residential floor are modeled by CURisk, where sprinklers, detectors/alarms and fire department action are not available. Meanwhile, 19 daytime fire scenarios are also modeled for comparison. Then the expected life risk and expected fire loss are calculated for both cases. The results show the same expected fire losses, but the expected life risk of the night fires are more than two times of the daytime fire casualties.

## 6. CONCLUSION AND RECOMMENDATIONS

Possible fire scenarios are simulated on all the residential floors, and results showed that fire risk of the demonstration building is close to the comparable building of non-combustible construction. It is noted that 15% of the room enclosure areas in the demonstration building are exposed heavy timber panels while the non-combustible construction used for comparison does not contain combustible interior finish materials, which

yielded slightly lower risk to life and same expected fire loss. With that in mind, additional calculation was performed to a modified building of non-combustible construction which is applied 8 mm wood panelling on 15% of apartment wall enclosures, the expected risk to life of the modified building of non-combustible construction became same as that of the demonstration building.

Evacuation simulation results showed that occupants can evacuate out of the building with a reasonable time frame and occupant evacuation times in the demonstration building are slightly shorter than a comparable building of non-combustible construction. High reliability sprinklers (with good efficiency) can prevent the fire in its infancy, thus can avoid faster fire growth in the combustible compartment especially in the case where wood panels are exposed. Thus to minimize the fire risk, it is suggested that fast-response sprinklers with high reliability and suppression efficiency should be installed throughout the building. In addition, well-designed fire detector and alarm systems should be adopted in the building. Fires in extreme scenarios may cause significant life risks and fire losses though their occurrence probabilities are low. However, precautionary measures should be taken in advance to prevent those fires from occurring and mitigate the losses in case they happen.

---

## REFERENCES

Bwalya A, Lougheed G, Kashef A, Saber H (2011) Survey results of combustible contents and floor areas in canadian multi-family dwellings. *Fire Technol.* 4:1121-1140. DOI: 10.1007/s10694-009-0130-8

Cheng H, Hadjisophocleous GV (2011) Dynamic modeling of fire spread in building. *Fire Saf.J.* 4:211-224. DOI: DOI: 10.1016/j.firesaf.2011.02.003

Drysdale D (1999) *An introduction to fire dynamics.* John Wiley & Sons Ltd, Chichester, England

Esposito D (2004) *Economic impact of fires in buildings.* Dissertation/Thesis, Department of Civil and Environmental Engineering, Carleton University

Fu Z, Hadjisophocleous G (2000) A two-zone fire growth and smoke movement model for multi-compartment buildings. *Fire Saf.J.* 3:257-285. DOI: DOI: 10.1016/S0379-7112(99)00045-4

Gruchy D (2004) *Modelling occupant evacuation during fire emergencies in buildings.* Dissertation/Thesis, Carleton University

Hadjisophocleous G, Fu Z, Li X (2011) *Technical report on CURisk - A fire risk analysis model.* Department of Civil and Environmental Engineering, Carleton University, Ottawa, Ontario

Li X, Zhang X, Hadjisophocleous G, McGregor C (2014) Experimental study of combustible and non-combustible construction in a natural fire. *Fire Technol.* 1-28. DOI: 10.1007/s10694-014-0407-4

Zhang X, Hadjisophocleous G (2012) An improved two-layer zone model applicable to both pre- and post-flashover fires. *Fire Saf.J.* 0:63-71. DOI: <http://dx.doi.org/10.1016/j.firesaf.2012.06.014>

Zhang X, Li X, Hadjisophocleous G (2013) A probabilistic occupant evacuation model for fire emergencies using monte carlo methods. *Fire Saf.J.* 0:15-24. DOI: 10.1016/j.firesaf.2013.01.028



# CHAPTER 5

## FIRE RESISTANCE DESIGN

---

**Alejandro Medina** | Carleton University

**George Hadjisophocleous** | Carleton University

**Andrew Harmsworth** | GHIL Consultants

**Christian Dagenais** | FPInnovations

---

## 1. PROJECT DESCRIPTION

The project deals with a 20 storey wood building to be constructed in North Vancouver. The first storey of the building is made up of a concrete platform. The remaining 19 storeys sit atop of the concrete platform and are constructed out of mass timber wood slabs and glued-laminated (glulam) beams and columns. The building is classified as a high building under Subsection 3.2.6 of Division B of the BC Building Code (BCBC) (BC Office of Housing and Construction Standards 2012a). Combustible buildings higher than six storeys are not permitted by the prescriptive solutions of the building code, therefore an alternative solution is required.

The project is classified as a residential building (Group C major occupancy) although offices (Group D) will be located on the first storey. The objective of this work is to show that mass timber construction is safe for buildings higher than six storeys by demonstrating that the building design meets the fire resistance requirements.

## 2. APPLICABLE BUILDING CODE

The applicable Building Code for this project is the 2012 BCBC. All reference numbers indicated in this report refer to the 2012 BCBC, unless otherwise indicated.

## 3. BUILDING CHARACTERISTICS

This project will have the following characteristics:

Building Area (m <sup>2</sup> ):	750.8 m <sup>2</sup> /storey (including the area of the elevator core)
Building Height (storeys):	20
Streets Faced:	2
Occupancy:	C (major occupancy) / D (secondary)
Sprinklered:	Yes

## 4. FIRE SEPARATION REQUIREMENTS

The following fire separations will be provided between rooms and suites:

FIRE SEPARATION	FIRE RESISTANCE RATING REQUIREMENTS (HOURS)
Service room containing fuel fired appliance (sprinklered)	1
Service room	0
Emergency generator room	2
Combustible refuse storage	1
Main electrical equipment room (unsprinklered)	2
Electrical equipment room (sprinklered)	0
Janitors' rooms (sprinklered)	0
Between residential suites and corridors	1
Between suites and public corridors	0
Exit enclosures	2
Elevator shaft and elevator machine room	2
Between Apartments (Group C)	2

**TABLE 1:** FIRE RESISTANCE RATING REQUIREMENTS IN HOURS FOR MULTIPLE FIRE SEPARATION TYPES

## 5. STANDPIPE AND HOSE SYSTEMS

Since the building exceeds 3 storeys in height, a standpipe system needs to be provided as per BCBC 3.2.5. This system would be designed in accordance with NFPA 14 (NFPA 2013a).

Hose stations consisting of 63.5mm (2½ in) diameter hose connections would be provided within exit stairs near the entrance to each storey and roof. Where exit stairs do not serve roofs, NFPA 13 (NFPA 2013b) may require a roof hydrant.

The Fire Department siamese connections for the sprinkler and standpipe system needs to be coordinated with the Fire Department response points. Each connection will serve all portions of the building. These connections will be located within 45 m (150 ft.) of a fire hydrant. The hydrant serving connections will be located on site. The automatic sprinkler system does not require activation by the fire department.

## 6. FIRE ALARM AND DETECTION SYSTEM

This building would be equipped with a fire alarm and detection system as required by Sentence 3.2.4.1.(1) of Division B of the BCBC and designed in accordance with the requirements of Subsection 3.2.4. The system is designed to transmit a signal to the Fire Department using a method described in Sentence 3.2.4.7.(4) (i.e. central station monitoring).

Heat detection is provided by the sprinkler systems as permitted by Article 3.2.4.15. Smoke detectors are provided in exit stair shafts and within residential public corridors in accordance with Article 3.2.4.11.

Manual pull stations will be provided adjacent to each exit and at the principal entrance to the building as required by Article 3.2.4.17. Duct type smoke detectors would be provided for air handling systems serving more than one suite or storey (Article 3.2.4.12).

## 7. EMERGENCY LIGHTING AND POWER

In accordance with Article 3.2.7.3, emergency lighting would be provided at a minimum level of 10 lx at the floor in exits, principal access to exit routes, corridors serving the public, public corridors, service spaces, and individual service rooms.

Emergency power will be supplied to:

- Fire alarm and detection systems.
- Emergency lighting and exit signs.

Emergency power will be provided to emergency lighting and fire alarm systems in accordance with Article 3.2.7.9 by a generator for a duration of 24h for supervisory power and 2h under full load. Transfer to emergency power will occur automatically upon failure of the regular power supply.

## 8. EXTERIOR FAÇADE

For a building of this size, exterior walls with combustible components need to conform to the National Building Code of Canada (NBCC) article 3.1.5.5 of Division B (NRCC 2010)

A fire on an exterior wall of a building can result in human injuries and building damage due to fire spread through the wall cavities and fire spread on the exterior façade. To limit possible fire spread, the exterior cladding, making up the façade of the building, will be constructed using 70% noncombustible material and a maximum of 30% combustible material. Since the building consists of a mass timber structure, i.e. has components that are of combustible materials, the exterior wall assembly shall be tested to CAN/ULC-S134 (ULC 2013) [5] along with all of its components such as wall framing, non-combustible cladding, fasteners, expansion joints and caulking.

The wood cladding will only be used near balconies in order to maximize its visibility by the building occupants. Figure 1 illustrates the originally proposed 100% coverage wood cladding system.



**FIGURE 1:** PROPOSED FAÇADE BUILT USING ONLY WOOD CLADDING



**FIGURE 2:** MODIFIED VIEW OF THE BUILDING WITH PROPOSED REDUCED WOOD CLADDING



**FIGURE 3:** SOUTH VIEW OF THE BUILDING WITH REDUCED WOOD CLADDING TO LIMIT FIRE SPREAD

Figures 2 and 3 show the different elevation views of the building and the use of wood cladding on the balconies. In this scenario, the concrete balcony slab extending out from the building serves as a flame deflecting mechanism by breaking up the vertical wood cladding channel.

There are three primary means for an exterior wall to become involved in fire:

- An interior compartment fire with flames escaping through a building.
- A fire initiated near an exterior wall, such as that from a car near the building or a refuse bin
- A fire spreading from an adjacent building

Limiting the quantity of combustible components in the façade will reduce the risk of the exterior of a building becoming involved in fire and the severity and damages in case of a fire. The risk of a fire occurring in the interior compartment is not affected by the amount of combustibles in the building façade.

### 9. FIRE RESISTANCE OF ASSEMBLIES – GENERAL REQUIREMENTS

Wood is a material capable of maintaining a large proportion of its structural capacity under severe and prolonged fire conditions. As opposed to steel and concrete which are non-combustible materials, wood burns and chars when exposed to high temperatures. The biggest difference and advantage is that wood burns at a reasonably consistent and predictable rate. Although wood loses its physical and structural properties once it has charred, the unaffected area beneath the char layer (and the heated zone) remains at ambient temperature and maintains its full strength. Wood charring rates are well documented for exposure to standard fires such as ISO 834 (ISO 1999), ASTM E119 (ASTM 2012) and CAN/ULC-S101 (ULC 2007). Unlike steel used by itself or as reinforcement in concrete, which loses its structural properties once it reaches about 550°C and needs to be protected at all times, wood can sustain long lasting fires provided an adequate cross-sectional size is provided.

There are three criteria that are evaluated when determining the fire resistance rating of an assembly according to CAN/ULC S101 (ULC 2007):

- Structural Resistance: The assembly should withstand the applied load through out the duration of the fire.
- Integrity: The assembly must prevent the passage of flames, gases or smoke hot enough to ignite a cotton pad on the unexposed side.
- Insulation: The assembly must prevent a temperature rise of the unexposed side from reaching an average of 140°C or 180°C at any particular location, above the initial temperature.

The time at which any of the three criteria is no longer met, determines the fire resistance rating of the assembly, when exposed to the standard fire exposure, as per CAN/ULC S101.

In accordance with Annex B of CSA O86-14 (CSA 2014), when designing a structural element that will be subjected to fire, the specified strength shall be adjusted to the 50th percentile strength value with the use of the specified strength adjustment factor for fire design,  $K_{fi}$ , as shown in Table 2 for different products.

PRODUCT	$K_{fi}$
Solid Sawn Timber	1.5
Glued-Laminated Timber	1.35
Structural Composite Lumber	1.25

TABLE 2: SPECIFIED STRENGTH ADJUSTMENT FACTOR FOR FIRE DESIGN,  $K_{fi}$  (CSA 2014)

Figure 4 illustrates the different structural elements in one of the 20 storeys of the proposed building. These components include the glulam beams and columns and the Laminated Strand Lumber (LSL) panels used for the moment frame and for the elevator core. Figure 5 shows the floor plan of a storey in the building. The structural components used as well as the spacings between columns and beams are also shown in Figure 5.

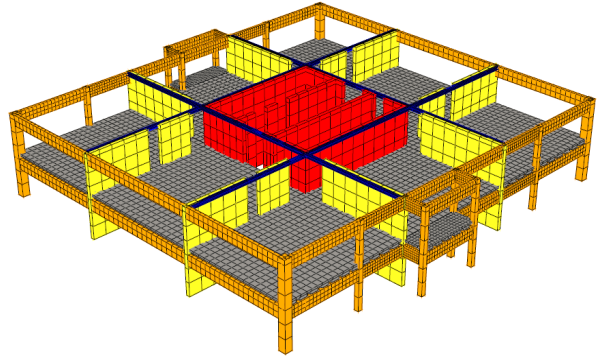


FIGURE 4: STRUCTURAL COMPONENTS IN ONE OF THE STOREYS OF THE BUILDING

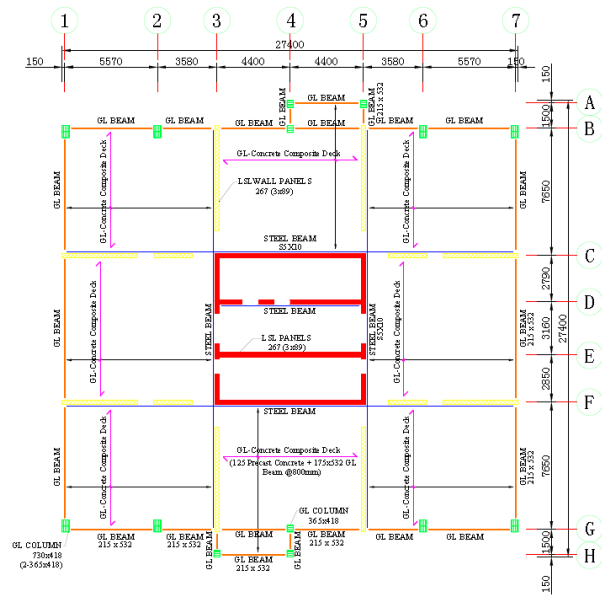


FIGURE 5: PLAN VIEW OF ONE OF THE STOREYS OF THE BUILDING

## 10. FIRE RESISTANCE CALCULATION OF GLULAM BEAMS

Two methods of calculation are investigated in this chapter. These are the new procedure presented in CSA O86-14 (CSA 2014) and the method given in Appendix D-2.11 of Division B of NBCC (NRCC 2010).

### 10.1 CSA O86-15 ANNEX B METHOD

A variety of glulam beams are used throughout the design of the building. To calculate the structural fire resistance of these beams, the recommendations found in the Annex B of CSA O86-14 standard was used. The fire resistance of the beam depends on the applied load as well as its cross sectional area which in turns depends on the time of fire exposure.

To calculate the fire resistance of the assembly the cross-sectional area that would not be affected by the fire and would remain at ambient temperature needs to be determined. To calculate the char layer, the time of exposure is multiplied by the charring rate of the wood. CSA O86-14 suggests the charring rates shown in Table 3, depending on assembly type and wood. Another important factor to consider is whether the beam is exposed to the fire from three or four sides. Figure 6 illustrates a three-sided and a four-sided charring behaviour of a timber beam or column.

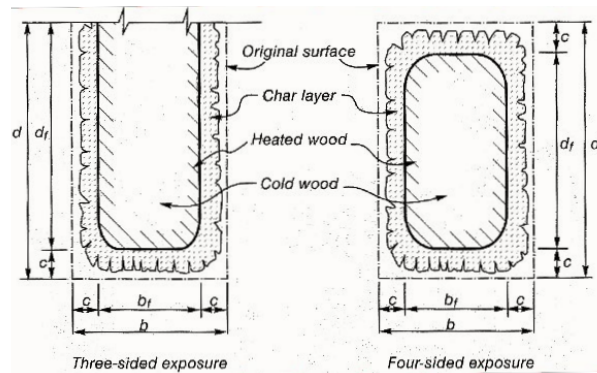


FIGURE 6: THREE-SIDED AND FOUR SIDED FIRE EXPOSURE OF A TIMBER BEAM OR COLUMN (BUCHANAN 2002)

	ONE DIMENSIONAL CHARRING RATE $\beta_0$	ONE DIMENSIONAL NOMINAL CHARRING RATE $\beta_n$
Solid Sawn Timber	0.65	0.80
Glued-Laminated Timber	0.65	0.70
Structural Composite Lumber	0.65	0.70

TABLE 3: DESIGN CHARRING RATES OF WOOD AND WOOD BASED PRODUCTS MM/MIN (CSA 2014)

The nominal charring rate ( $\beta_n$ ) is used to determine the char depth of a member when corner rounding is not explicitly taken into account. A value of 0.7 mm/min will be used to calculate the charring rate of the glulam beams and columns. For the LSL panels used as vertical slabs for the elevator core and shear walls, a one-dimensional charring rate ( $\beta_0$ ) of 0.65 mm/min will be used. The charring rates in Table 3 apply to cross-sections of wood products with the residual minimum dimension greater than 70 mm. When the residual minimum dimension is reduced to less than 70 mm, the charring rates will increase due to heating from both sides of the member.

Wood is considered to char once it has reached a temperature of 300°C. Beneath the char layer the temperature decreases from 300°C to the initial temperature. Given that many mechanical properties of wood start to decrease once temperature surpasses 100°C, the decrease in the strength of wood immediately beneath the char layer must be considered. To approximate this temperature gradient, Chapter 8 of the Cross Laminated Timber (CLT) Handbook (Dagenais 2014) recommends the use of a standard heated zone in which wood is assumed to have zero strength. The following equation is used to determine the depth of the heated zone:

$$d_o = \left( \frac{t}{20min} \right) \times 7mm \quad (for\ t < 20\ min)$$

$$d_o = 7mm \quad (for\ t \geq 20\ min)$$

Table 4 lists the geometric properties, number of fire exposed surfaces, and specified loads applied to glue-laminated beams used in the building. The specified live and dead loads of each building component were determined by the structural group responsible for conducting the structural analysis and design of the building. According to the Annex B of CSA O86-14, the load combination for fire design is as follows:

$$Specified\ Load = 1.0 (DL) + 1.0 (LL)$$

where LL is the design live load, and DL is the design dead load.

BEAM NO.	ORIGINAL DIMENSIONS	SPAN (m)	EXPOSED SIDES	SPECIFIED LOAD (kN/m)	FACTORED LOAD (kN/m)
1	GL 215 × 532 (G3-H3)	1.50	3	-	-
2	GL 215 × 532 (G5-G6)	3.58	2	26.39	34.81
3	GL 215 × 532 (G4-G5)	4.40	2	5.52	7.28
4	GL 215 × 532 (G3-G4)	4.40	2	-	-
5	GL 215 × 532 (H3-H4)	4.40	3	-	-
6	GL 215 × 532 (G6-G7)	5.57	2	26.39	34.81
7	GL 215 × 532 (F7-G7)	7.65	2	5.52	7.28
8	GL 215 × 532 (C7-F7)	8.80	2	5.52	7.28

TABLE 4: GLULAM BEAMS USED IN THE BUILDING

Loads resisted by roof: DL = 3.0 kPa, LL = 1.82 kPa, SL = 2.7 kPa (ULS), 2.4 kPa (SLS)

Loads resisted by floor: DL = 5.0 kPa, LL = 1.9 kPa

where SL is design snow load, ULS is ultimate limit states and SLS is the serviceability limit state.

The 2<sup>nd</sup> load combination (1.25DL + 1.5LL) and the 3<sup>rd</sup> load combination (1.25DL + 1.5SL + 0.5LL) govern the design (ULS and SLS) of floor and roof, respectively.

The specified and factored loads of the floors are heavier than those on the roof.

**Sample fire resistance calculation of a glulam beam**

Beam ID: GL 215 × 532 (Item No. 6)

24f-E D-Fir glulam

The glulam beams are positioned around the edges of the building therefore would only be exposed to the fire on two sides, the bottom and one of the two sides. The top and the other side of the beam would be shielded from the fire by the wall and ceiling assembly. Initial dimensions of the glulam beam are given below and the calculated modified dimensions presented in Table 5 after a 2 hour fire exposure.

Span: 5.57 m

Width: 215 mm

Depth: 532 mm

Fire exposure: 2 hours = 120 min

GL 215 × 532	EQUATION	VALUES
Total affected zone after 2 hours	$a_{char,eff} = \beta_n t + d_o$ $a_{char,eff} = 0.7mm/min \times 120min + 7mm$ $a_{char,eff} = 91mm$	$\beta_n = 0.7 mm/min$ $t = 120 min$ $d_o = 7 mm$
Effective new cross-sectional dimensions after exposure from 2 sides	$Modified\ Width = 215 - 1 \times 91 = 124mm$ $Modified\ Depth = 532 - 1 \times 91 = 441mm$	

TABLE 5: MODIFIED DIMENSIONS OF BEAM AFTER 2 HOUR FIRE EXPOSURE

**Moment of inertia**

$$I_{eff} = \frac{bh^3}{12} = \frac{124mm \times (441mm)^3}{12} = 0.89 \times 10^9 mm^4$$

**Effective section modulus**

$$S_{eff} = \frac{I_{eff}}{h_{fire} - \bar{y}} = \frac{0.89 \times 10^9 mm^4}{441mm - 220.5mm} = 4.02 \times 10^6 mm^3$$

**Moment resistance of the beam after 2 hour fire exposure from Annex B of CSA 086-14**

$$M_{r,fi} = \phi F_{b,fi} S_{eff} K_x \min(K_L, K_{zbg})$$

$$\phi = 1.0$$

$$F_{b,fi} = f_b (K_{fi} K_D K_H K_{sb} K_T)$$

$f_b$  = Specified bending strength of the wood (MPa), Clause 7.3, CSA 086

= 30.6 MPa for 24f-E D-Fir glulam

$K_{fi}$  = Strength adjustment factor, 1.35 as per Table 2

$K_D$  = Load duration factor, 1.15 (short-term duration for fire design)

$K_H$  = System factor, 1

$K_{sb}$  = Service condition factor, 1 for dry conditions

$K_T$  = Treatment factor, 1 for untreated wood

$K_L$  = Beam lateral stability factor (from reduced dimensions)

$K_{zbg}$  = Glulam size factor (from initial dimensions)

$K_x$  = Curvature factor

$$F_{b,fi} = 30.6 (1.35 \times 1.15 \times 1 \times 1 \times 1) = 47.5 MPa$$

$$K_{zbg} = \left(\frac{130}{B}\right)^{0.1} \left(\frac{610}{T}\right)^{0.1} \left(\frac{9100}{L}\right)^{0.1} = \left(\frac{130}{215}\right)^{0.1} \left(\frac{610}{532}\right)^{0.1} \left(\frac{9100}{5570}\right)^{0.1} = 1.01 (\leq 1.3)$$

$K_L = 1$  (assuming the slab provides full support of the compressive edge of the beam for the entire fire exposure)

$$M_{r,fi} = 1.0 \times 47.5 MPa \times 4.02 \times 10^6 mm^3 \times 1 \times 1.01 = 192.8 kNm$$

The moment resistance of the glulam beam is 192.8 kNm after 2 hours of fire exposure without added gypsum protection, assuming that lateral stability is provided through out from an appropriate fire-resistance rated slab (i.e.  $K_L = 1.0$ ).

The linearly distributed load on the beam is presented in Table 4 as 26.39 kN/m. The moment produced by this distributed specified load is calculated as follows

$$M_{applied} = \frac{w l^2}{8} = \frac{26.39kN/m \times (5.57m)^2}{8} = 102.34 kNm$$

The moment resistance of the beam after 2 hours is greater than the moment applied due to the expected linearly distributed load.  $M_{r,fi} > M_{applied}$

**10.2 LIE METHOD – NBCC DIVISION B – APPENDIX D-2.11**

Another calculation method for fire-resistance of glulam beams and columns is presented in Appendix D-2.11 of the NBCC which was derived by Lie (1977). This is a semi-empirical method for calculating the fire resistance of timber beams and columns. It was originally developed as a way to quickly assess the fire resistance before proceeding to more involved calculation methods.

Since the glulam beams are positioned around the edges of the building therefore they would only be exposed to the fire from two sides. The Lie Method only covers beams exposed from 3 or 4 sides. Calculations of a three-sided exposure will be presented for demonstration and comparison purposes. The same glulam beam as in 10.1 is evaluated here.

**Determine the load factor, f.**

Factored bending Moment = 102.34 kNm

$$F_{b,fi} = f_b (K_{fi} K_D K_H K_{sb} K_T)$$

From section 10.1, we obtain the following

$$F_{b,fi} = 30.6 (1 \times 1 \times 1 \times 1 \times 1) = 30.6 MPa$$

$$S = \frac{bh^2}{6} = \frac{215mm \times (532mm)^2}{6} = 10.1 \times 10^6 mm^3$$

$$M_r = \phi F_b S K_x K_{zbg}$$

$$M_r = 0.9 \times 30.6 MPa \times 10.1 \times 10^6 mm^3 \times 1.0 \times 0.99 = 278.5 kNm$$

(normal load duration)

$$M_{applied} = \frac{w \times l^2}{8} = \frac{34.81kN/m \times (5.57m)^2}{8} = 135 kNm$$

(from factored loads)

$$\frac{M_{applied}}{M_r} = \frac{135 \text{ kNm}}{278.5 \text{ kNm}} = 0.48$$

Load factor = 1.3

For a beam exposed to the fire from 3 sides, the following equation applies

$$FR = 0.1fB [4 - (B/D)] = 0.1 \times 1.3 \times 215 [4 - (215/532)] = 100.5 \text{ minutes}$$

The fire resistance of the beam using the Lie beam equation is 1 hour and 40 minutes. This time is less than what was predicted using the CSA O86-14 method for calculating the fire resistance. It is important to consider that for the Lie method, it was assumed that three sides of the beam would be exposed. In reality only two sides of the beam are exposed to the fire which makes the results obtained using the Lie method more conservative.

### 11. FIRE RESISTANCE CALCULATION OF GLULAM COLUMNS

Two methods of calculation are investigated in this chapter. These are the new procedure presented in CSA O86-14 (CSA 2014) and the method given in Appendix D-2.11 of Division B of NBCC (NRCC 2010).

#### 11.1 CSA O86-14 ANNEX B METHOD

Similarly as for the design of the glulam beams, factored specified loads are used for the fire design of the glue-laminated columns. The total load is calculated from the specified loads and tributary areas using a load factor of unity for the dead and the live loads. The specified loads on the floor are 5.0 kPa (Dead) and 1.9 kPa (Live). Since the live load on the floor is less than 4.8 kPa, the tributary area may not be reduced as per NBCC Division B 4.1.5.9. Table 6 lists the different glulam columns used in the proposed building with their respective specified loads and number of surfaces exposed to the fire. Although the columns are 20 meters in height, for fire safety design purposes and structural considerations such as buckling, it was considered that the columns were braced at every storey using a pin-pin connection which corresponds to 3 meters of unbraced length. Moreover, second order effects (P-Δ) from a combined bending and axial load have been considered. Columns exposed to fire will have their neutral axis moved as a function of charring (function of time), which will induce transient eccentricity leading to a reduced fire resistance. Designers should consider such effects when designing for fire-resistance of timber elements having their neutral axis shifted from its initial position.

COLUMN NO.	AXIS	B (mm)	T (mm)	UNBRACED LENGTH (m)	EXPOSED SIDES	SPECIFIED LOAD (kN)	FACTORED LOAD (kN)
9	G4	365	418	3.00	3	215.8	284.6
10	H3, H4	365	418	3.00	-	215.8	284.6
11	G1	730	418	3.00	2	1393.5	1837.7
12	G2	730	418	3.00	3	2289.1	3018.8

TABLE 6: GLUED-LAMINATED COLUMNS USED IN THE TALL WOOD BUILDING

#### Sample fire resistance calculation of a glulam column

The glulam column specifications are shown below and the calculated modified dimensions after a 2 hour fire exposure are summarized in Table 7.

Columns ID: GL 365 × 418 (G4)

24f-E D-Fir glulam

Unbraced Length: 3.00 m

Width: 365 mm

Depth: 418 mm

Fire exposure: 2 hours = 120 min

GL 365 × 418	EQUATION	VALUES
Total affected zone after 2 hours	$a_{char,eff} = \beta_n t + d_o$ $a_{char,eff} = 0.7 \text{ mm/min} \times 120 \text{ min} + 7 \text{ mm}$ $a_{char,eff} = 91 \text{ mm}$	$\beta_n = 0.7 \text{ mm/min}$ $t = 120 \text{ min}$ $d_o = 7 \text{ mm}$
Effective new cross sectional dimensions after exposure from 3 sides	$\text{Modified Width} = 365 - 2 \times 91$ $= 183 \text{ mm}$ $\text{Modified Depth} = 418 - 1 \times 91$ $= 327 \text{ mm}$	

TABLE 7: MODIFIED DIMENSIONS OF COLUMN AFTER 2 HOUR FIRE EXPOSURE

Reduced cross sectional dimensions: 183 × 327 mm

Effective Area (A<sub>eff</sub>) = 327 mm × 183 mm = 59,841 mm<sup>2</sup>

E = 13100 MPa

ϕ = 1.0

K<sub>SE</sub> = Service condition factor, 1 for dry conditions

$$F_{c,fi} = f_c (K_f K_D K_H K_{SC} K_T)$$

f<sub>c</sub> = 30.2 MPa

f<sub>b</sub> = 30.6 MPa

K<sub>n</sub> = 1.35, Strength adjustment factor as per Table 2

K<sub>D</sub> = Load duration factor, 1.15 (short-term duration for fire design)

K<sub>H</sub> = System factor, 1

K<sub>SC</sub> = Service condition factor, 1 for dry conditions

K<sub>T</sub> = Treatment factor, 1 for untreated wood

### Size factor, $K_{zcg}$

The size factor is determined using the original dimensions of the column (365 mm × 418 mm) and following the equation below from Clause 7.5.8.4.2, CSA O86

$$K_{zcg} = 0.68 (Z)^{-0.13} \leq 1.0$$

$$Z = \text{member volume} = 3 \times 0.365 \times 0.418 = 0.458 \text{ m}^3$$

$$K_{zcg} = 0.68 (0.458)^{-0.13} = 0.753$$

### Effective Moment of Inertia

$$I_{eff} = \frac{bh^3}{12} = \frac{183\text{mm} \times (327\text{mm})^3}{12} = 5.33 \times 10^8 \text{ mm}^4$$

### Effective Length

The effective length,  $L_e$ , is calculated from Clause 6.5.6.1 of CSA O86 as  $L_e = K_e \times L$  where  $K_e$  is the effective length factor.  $K_e$  is taken as 1 for pin-pin connections with no restraint against rotation as per Table A6.5.6.1 of the CSA-O86 standard. Provided the maximum unbraced length for these columns is the storey height, with pin-pin connections at every floor/ceiling, the effective length can be taken as 3m.

### Slenderness Ratio from CSA O86-14

$$C_c = \frac{L_e}{\sqrt{\frac{12 \times I_{eff}}{A_{eff}}}} = \frac{3000\text{mm}}{\sqrt{\frac{12 \times 5.33 \times 10^8 \text{ mm}^4}{59841\text{mm}^2}}} = 9.17$$

### Slenderness Factor

$$K_{c,fi} = \left[ 1 + \frac{F_{c,fi} \times K_{zcg} \times C_c^3}{35 \times E \times K_{SE} \times K_T} \right]^{-1}$$

$$K_{c,fi} = \left[ 1 + \frac{(30.2 \text{ MPa} \times 1.35 \times 1.15 \times 1 \times 1 \times 1) \times 0.753 \times 9.17^3}{35 \times 13100 \text{ MPa} \times 1 \times 1} \right]^{-1} = 0.94$$

### Compressive Resistance

$$P_{r,fi} = \phi F_{c,fi} A_{eff} K_{zcg} K_{c,fi} \geq P_f$$

$$P_{r,fi} = 1 \times (30.2 \text{ MPa} \times 1.35 \times 1.15 \times 1 \times 1 \times 1) \times 59841 \text{ mm}^2 \times 0.753 \times 0.94 = 1986 \text{ kN}$$

$$P_{r,fi} \geq P_f = 215.8 \text{ kN}$$

As explained previously, column assemblies are subjected to second-order effects (i.e. P-Δ) due to the charring of the fire exposed surface which creates transient eccentricity. It is strongly recommended to calculate the fire-resistance of members under compression using the procedures of Section 7.5.10 of CSA O86-14 for combined bending and axial load. Given that for a three sided exposure the load eccentricity occurs only in one axis, the following equation can be used. For bi-axial eccentricity created by a 2-sided fire exposure a different equation should be used.

$$\left( \frac{P_f}{P_{r,fi}} \right)^2 + \frac{M_f}{M_{r,fi}} \left[ \frac{1}{1 - \frac{P_f}{P_{E,fi}}} \right] \leq 1.0$$

$P_f$  = applied specified compressive axial load

$P_{r,fi}$  = specified compressive resistance parallel to grain in fire design

$$P_{r,fi} = \phi F_{c,fi} A_{eff} K_{zcg} K_{c,fi} = 1986 \text{ kN}$$

$M_f$  = applied specified moment in fire design

$$M_f = P_f \Delta$$

$M_{r,fi}$  = factored bending moment resistance in fire design

$$M_{r,fi} = \phi F_{b,fi} S_{eff} K_x K_{zbg}$$

$$F_{b,fi} = f_b (K_{fj} K_D K_H K_{sb} K_T) = 30.6 (1.35 \times 1.15 \times 1 \times 1 \times 1) = 47.5 \text{ MPa}$$

$$S_{eff} = \frac{I_{eff}}{h_{fire} - \bar{y}} = \frac{5.33 \times 10^8 \text{ mm}^4}{327 - 163.5 \text{ mm}} = 3.26 \times 10^6 \text{ mm}^3$$

$K_x$  = curvature factor, 1.0 for straight members

$$K_{zbg} = \left( \frac{130}{B} \right)^{0.1} \left( \frac{610}{T} \right)^{0.1} \left( \frac{9100}{L} \right)^{0.1} = \left( \frac{130}{365} \right)^{0.1} \left( \frac{610}{418} \right)^{0.1} \left( \frac{9100}{3000} \right)^{0.1} = 1.05 (\leq 1.3)$$

$K_L = 1$  (The columns are laterally supported by the perimeter building walls therefore  $K_L$  not less than 1)

$$M_{r,fi} = 1.0 \times 47.5 \text{ MPa} \times 3.26 \times 10^6 \text{ mm}^3 \times 1 \times 1.05 = 162.6 \text{ kNm}$$

In addition to the load eccentricity created during construction, two or three sided burning of a column creates an added eccentricity as the neutral axis constantly shifts due to charring. Figure 7 illustrates this behavior as it occurs in a structurally loaded wall.

$$e = \frac{h}{2} - \bar{y} = \frac{418\text{mm}}{2} - 163.5\text{mm} = 45.5\text{mm}$$

Added eccentricity due to P-Δ effect:

$$\Delta_f = \frac{(P_f e) L_e^2}{16 E I_{eff}} = \frac{(215800 \text{ N} \times 45.5 \text{ mm})(3000 \text{ mm})^2}{16 \times 13100 \text{ MPa} \times 5.33 \times 10^8 \text{ mm}^4} = 0.79 \text{ mm}$$

$$\Delta = e + \Delta_f = 45.5 \text{ mm} + 0.79 \text{ mm} = 46.3 \text{ mm}$$

$$M_f = P_f \Delta = 215.8 \text{ kN} \times 0.0463 \text{ m} = 9.99 \text{ kNm}$$

$$P_{E,fi} = \frac{\pi^2 E I_{eff}}{L_e^2} = \frac{\pi^2 \times 13100 \text{ MPa} \times 5.33 \times 10^8 \text{ mm}^4}{(3000 \text{ mm})^2} = 7657 \text{ kN}$$

Substituting the values in we obtain

$$\left( \frac{P_f}{P_{r,fi}} \right)^2 + \frac{M_f}{M_{r,fi}} \left[ \frac{1}{1 - \frac{P_f}{P_{E,fi}}} \right] = \left( \frac{215.8 \text{ kN}}{2416 \text{ kN}} \right)^2 + \frac{9.99 \text{ kNm}}{162.6 \text{ kNm}} \left[ \frac{1}{1 - \frac{215.8 \text{ kN}}{7657 \text{ kN}}} \right] = \mathbf{0.071} \leq 1.0$$

The combined axial load and bending moment equation yields a result much less than 1 meaning this column is capable of carrying the design loads after a 2 hour fire with the specified initial cross-section dimensions.

The axial capacity and moment resistance of all the glulam columns in the building were calculated using a spreadsheet. The spreadsheet was constructed using the equations shown in the above worked example. All the columns were evaluated using the spreadsheet and their axial and moment resistance were found to exceed their respective specified loads.

### 11.2 LIE METHOD – NBCC DIVISION B – APPENDIX D-2.11

Similar to glulam beams, the NBCC offers a method for calculating the fire resistance of glulam columns. For columns GL 365 × 418 exposed to fire on 3 sides, the fire resistance can be calculated as follows:

$$FR = 0.1fB \left[ 3 - \left( \frac{B}{2D} \right) \right]$$

where  $f$  = load factor

B = smaller (initial) cross-section dimension = 365 mm

D = larger (initial) cross-section dimension = 418 mm

The effective length,  $L_e$ , is

$$L_e = \frac{kL}{B} = \frac{1 \times 3000}{365} = 8.2 \leq 12$$

where  $k$  = the effective length factor = 1 for pin-pin columns

L = unbraced length of the column = 3000 mm

Factored Load = 284.6 kN

$$P_{r,fi} = \phi F_c A K_{zcg} K_c$$

$$K_{zcg} = 0.753$$

$$C_c = \frac{L_e}{B} = \frac{3000 \text{ mm}}{365} = 8.2$$

$$K_{c,fi} = \left[ 1 + \frac{F_c \times K_{zcg} \times C_c^3}{35 \times E_{05} \times K_{SE} \times K_T} \right]^{-1}$$

$$K_{c,fi} = \left[ 1 + \frac{(30.2 \text{ MPa} \times 1 \times 1 \times 1 \times 1) \times 0.753 \times 8.2^3}{35 \times (0.87 \times 13100 \text{ MPa}) \times 1 \times 1} \right]^{-1} = 0.97$$

$$P_{r,fi} = 0.8 \times (30.2 \text{ MPa} \times 1 \times 1 \times 1 \times 1) \times 365 \text{ mm} \times 418 \text{ mm} \times 0.753 \times 0.97 = \mathbf{2692 \text{ kN}}$$

$$\frac{\text{Factored Load}}{\text{Factored Resistance}} = \frac{284.6 \text{ kN}}{2692 \text{ kN}} = 0.11 \text{ or } 11\%$$

From Figure D-2.112.-A of the NBCC the corresponding load factor,  $f$ , for this column is 1.5, therefore

$$FR = 0.1fB \left[ 3 - \left( \frac{B}{2D} \right) \right] = 0.1 \times 1.5 \times 365 \times \left[ 3 - \left( \frac{365}{2 \times 418} \right) \right] = 140 \text{ minutes}$$

According to the Lie method the glulam column would be able to resist a fire for over 2 hours without collapse. It is noted that the Lie method does not account for the combined effect of bending and axial load. It assumes that the compression member is loaded axially during the fire exposure.

## 12. FIRE RESISTANCE CALCULATION OF LSL PANELS

LSL panels were designed to structurally support vertical loads as well as to provide stiffness to the building to resist lateral loads. The wood strands in the panel are oriented parallel to the vertical loads to provide maximum resistance. For the fire resistance calculation, it is assumed that the adhesive binding the strands remains intact allowing for full charring and no heat delamination. The LSL panels are also built up to a thicker section from a secondary gluing process. Again, it is assumed that the adhesive used in this secondary gluing does not exhibit heat delamination and allows the LSL panels to be treated as a solid element with a constant charring rate. Table 8 presents the height of the elevator core and shear wall panels and their design loads.

WALL	UNBRACED LENGTH (m)	SPECIFIED LOAD (kN/m)	FACTORED LOAD (kN/m)
Elevator Core 267mm (3 × 89mm)	3.00	641	846
Shear Wall 267mm (3 × 89mm)	3.00	570	752

TABLE 8: HEIGHT AND LOAD ON THE LSL WALLS IN THE BUILDING

**Sample fire resistance calculation of a LSL wall (elevator core)**

Wall ID: LSL 267mm (built-up panel from gluing 3 LSL panels of 89 mm in thickness)

Grade : 2.1E LSL Panel

Unbraced Height: 3.00 m

Width: 1000 mm strip

Initial Depth: 267mm

Fire exposure: 2 hours = 120 min

The charring rate for LSL panels used in this calculation is 0.65 mm/min as recommended by CSA O86-14 for 1-dimensional charring, Table 3. The depth of the heated zone beneath the char remains at 7 mm for exposures exceeding 20 minutes. Therefore the reduced thickness is,

$$Reduced\ thickness = 267mm - \left[ 120\ min \left( 0.65 \frac{mm}{min} \right) + 7mm \right] = 182mm$$

Properties of the LSL panels were obtained from CCMC Evaluation Report 12627-R on TimberStand® LSL (CCMC 1994). A one dimensional charring rate of 0.65 mm/min is used as there is no corner rounding to take into consideration. By evaluating a 1 m width of the wall the following properties are obtained:

$$Effective\ Area\ (A_{eff}) = 182mm \times 1000mm = 182000\ mm^2$$

E = 14480 MPa

K<sub>SE</sub> = Service condition factor, 1 for dry service conditions

$$F_{c,fi} = f_c(K_{fi}K_DK_HK_{SC}K_T)$$

f<sub>c</sub> = 36.05 MPa

f<sub>b</sub> = 50.0 MPa

K<sub>Fi</sub> = 1.25, Strength adjustment factor as per Table 2

K<sub>D</sub> = Load duration factor, 1.15 (short-term duration for fire design)

K<sub>H</sub> = System factor, 1

K<sub>SC</sub> = Service condition factor, 1 for dry service conditions

K<sub>T</sub> = Treatment factor, 1 for untreated wood

K<sub>Zc</sub> = Size factor, 1 for fire design calculations

**Effective Moment of Inertia**

$$I_{eff} = \frac{bh^3}{12} = \frac{1000mm \times (182mm)^3}{12} = 5.02 \times 10^8 mm^4$$

**Slenderness Ratio**

$$C_c = \frac{L_e}{\sqrt{\frac{12 \times I_{eff}}{A_{eff}}}} = \frac{3000mm}{\sqrt{\frac{12 \times 5.02 \times 10^8 mm^4}{182000 mm^2}}} = 16.5$$

**Slenderness Factor**

$$K_{c,fi} = \left[ 1 + \frac{F_{c,fi} \times K_{Zc} \times C_c^3}{35 \times E \times K_{SE} \times K_T} \right]^{-1}$$

$$K_{c,fi} = \left[ 1 + \frac{(36.05\ MPa \times 1.25 \times 1.15 \times 1 \times 1 \times 1) \times 1 \times 16.5^3}{35 \times 14480 MPa \times 1 \times 1} \right]^{-1} = 0.69$$

**Compressive Resistance**

$$P_{r,fi} = \phi F_{c,fi} A_{eff} K_{Zc} K_{c,fi} \geq P_f$$

$$P_{r,fi} = 1 \times (36.05 MPa \times 1.25 \times 1.15 \times 1 \times 1 \times 1) \times 182000 mm^2 \times 1 \times 0.69 = 6507.8\ kN\ per\ meter\ strip$$

$$P_{r,fi} \geq P_f = 641\ kN$$

Wall assemblies are subjected to second-order effects (i.e. P-Δ) due to the charring of the fire exposed surface which creates an additional eccentricity. It is strongly recommended to calculate the fire-resistance of members under compression using the procedures of Section 6.5.10 of CSA O86-14 for combined bending and axial load.

$$\left( \frac{P_f}{P_{r,fi}} \right)^2 + \frac{M_f}{M_{r,fi}} \left[ \frac{1}{1 - \frac{P_f}{P_{E,fi}}} \right] \leq 1.0$$

$P_f$  = applied specified axial compressive force in fire design

$P_{r,fi}$  = specified compressive resistance parallel to grain in fire design

$$P_{r,fi} = \phi F_{c,fi} A_{eff} K_{zc} K_{c,fi} = 6507.8 \text{ kN}$$

$M_f$  = applied factored moment in fire design

$$M_f = P_f \Delta$$

$M_{r,fi}$  = factored bending moment resistance in fire design

$$M_{r,fi} = \phi F_{b,fi} S_{eff} K_{zb}$$

$$F_{b,fi} = f_b (K_{fi} K_D K_H K_{Sb} K_T) = 50.0 (1.25 \times 1.15 \times 1 \times 1 \times 1) = 71.9 \text{ MPa}$$

$$S_{eff} = \frac{I_{eff}}{h_{fire} - \bar{y}} = \frac{5.02 \times 10^8 \text{ mm}^4}{182 - 91 \text{ mm}} = 5.52 \times 10^6 \text{ mm}^3$$

$$M_{r,fi} = 1.0 \times 71.9 \text{ MPa} \times 5.52 \times 10^6 \text{ mm}^3 = 396.9 \text{ kNm}$$

In addition to the load eccentricity created during construction, one-sided burning of a wall creates an additional eccentricity as the neutral axis constantly shifts due to charring. Figure 7 illustrates this behaviour as it occurs on a structurally loaded assembly.



FIGURE 7: SHIFT OF NEUTRAL AXIS IN A HEAVY TIMBER ASSEMBLY DUE TO UNEVEN BURNING (DAGENAI 2014)

$$e = \frac{h}{2} - \bar{y} = \frac{267 \text{ mm}}{2} - 91 \text{ mm} = 42.5 \text{ mm}$$

Added eccentricity due to P- $\Delta$  effect:

$$\Delta_f = \frac{(P_f e) L_e^2}{16 E I_{eff}} = \frac{(641000 \text{ N} \times 42.5 \text{ mm})(3000 \text{ mm})^2}{16 \times 14480 \text{ MPa} \times 5.02 \times 10^8 \text{ mm}^4} = 2.1 \text{ mm}$$

$$\Delta = e + \Delta_f = 39.0 \text{ mm} + 2.1 \text{ mm} = 41.1 \text{ mm}$$

$$M_f = P_f \Delta = 641 \text{ kN} \times 0.0411 \text{ m} = 26.3 \text{ kNm}$$

$$P_{E,fi} = \frac{\pi^2 E I_{eff}}{L_e^2} = \frac{\pi^2 \times 14480 \text{ MPa} \times 5.02 \times 10^8 \text{ mm}^4}{(3000 \text{ mm})^2} = 7971.3 \text{ kN}$$

Substituting the values into the interaction equation we obtain

$$\left(\frac{P_f}{P_{r,ff}}\right)^2 + \frac{M_f}{M_{r,ff}} \left[\frac{1}{1 - \frac{P_f}{P_{E,ff}}}\right] = \left(\frac{641 \text{ kN}}{6507.8 \text{ kN}}\right)^2 + \frac{26.3 \text{ kNm}}{396.9 \text{ kNm}} \left[\frac{1}{1 - \frac{641 \text{ kN}}{7971.3 \text{ kN}}}\right] = 0.08 \leq 1.0$$

### 13. FIRE RESISTANCE CALCULATION OF PRECAST CONCRETE COMPOSITE DECK

The composite deck is constructed out of a 125 mm concrete slab supported by glulam beams GL 175 × 532 spaced at 0.8 m on center. The glulam beams are oriented on their weak axis (i.e. laminations are oriented on their edges). Figure 8 illustrates the Wood-Concrete-Composite System (HBV-System) used in the building.

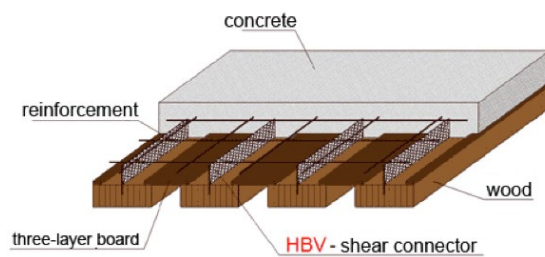


**FIGURE 8:** HBV WOOD-CONCRETE-COMPOSITE SYSTEM (HOLZ-VERBUND-SYSTEME 2014)

The fire resistance of the hybrid composite floor slab can be calculated by considering the tensile resistance of the glulam beam and the compressive resistance of the concrete slab. In this report we focus solely on the moment resistance of the glulam beam. To do so, the same methodology as the one used to calculate the fire resistance of glulam floor beams in Section 10 is used. The calculations assume that the char layer will not reach the HBV shear connector allowing for full composite action of the slab during the fire. Table 9 shows the moment resistance capacity of the glulam beams used in the hybrid slab after 2 hours of fire exposure.

MODIFIED DIMENSIONS AND RESISTANCE AFTER 2 HOUR FIRE (3 SIDE EXPOSURE)						
Original Dimensions	Width (mm)	Depth (mm)	Span (m)	I (mm <sup>4</sup> )	S (mm <sup>3</sup> )	M <sub>r</sub> (kNm)
GL 532 × 175	350	84	8.8	1.7E+07	4.1E+05	19.5

**TABLE 9:** MOMENT RESISTANCE OF GLULAM BEAM IN THE COMPOSITE FLOOR SYSTEM AFTER 2 HOURS OF FIRE EXPOSURE

The applied moment of each glulam member is 53.4 kNm. Each beam on the composite deck can support an applied moment 19.5 kNm after a 2-hour fire. The addition of the concrete slab increases the overall moment capacity of the deck to above the applied moment of 53.4 kNm. The composite deck relies heavily on the integrity of the HBV shear connector during the fire. Charring rate calculations suggest that the HBV steel connector would not suffer a major temperature increase during a 2 hour fire exposure. The embedded depth of the HBV connector is greater than the predicted char layer (91 mm) after 2 hours, therefore the metal will not be compromised by the fire.

### 14. ADDED FIRE PROTECTION

The previous fire resistance work examples assume that the assemblies are bare without added protection at the time of the fire (i.e. fully exposed). These calculations are based on a worst case scenario in which the sprinklers are unreliable or ineffective and there is no gypsum board protection. Given that these protection systems will be implemented in the building, the fire resistance of the structural elements would likely be much higher. If gypsum board is applied on the fire-exposed sides, the following time can be added to the unprotected member failure time (Dagenais 2014):

- a) 15 minutes to the Fire Resistance Rating (FRR) with one layer of 12.7 mm (½”) type X gypsum board;
- b) 30 minutes to the FRR with one layer of 15.9 mm (⅝”) type X gypsum board;
- c) 40 minutes to the FRR with two layer of 12.7 mm (½”) type X gypsum board, and;
- d) 60 minutes to the FRR with two layers of 15.9 mm (⅝”) type X gypsum boards.

### 15. FIRE SAFETY DURING CONSTRUCTION

Buildings are at their most vulnerable to fire during construction due to the lack of fully operational life safety systems such as sprinklers, fire alarms and fire compartmentation. Mitigating the risk of a fire occurring during construction requires the development and implementation of a plan. Section 5.6, Division B of the British Columbia Fire Code (BCFC) (BC Office of Housing and Construction Standards 2012b) requires a Construction Fire Safety Plan (CFSP) prior to construction, renovation or demolition of a building. For a building located in North Vancouver, the following fire safety standards and references apply:

Section 2.8, 5.2 and 5.6 “Construction and Demolition Sites”, Division B of the 2012 BC Fire Code’

- Part 8, Division B “Safety Measures at Construction and Demolition sites” of the 2012 BC Building Code
- Office of the Fire Commissioner of BC, OFC Bulletin
- Standata Fire Code Interpretation FCI-09-03

- City of Vancouver
  - City of Vancouver Building By-law (VBBL) 2007, Division B, Part 8
  - City of Vancouver Fire By-law (VFBL) 2000, Section 2.14 and 5.2

The minimum requirements for fire safety during construction are highlighted in the BCFC, Div B, 5.6.1.3 / 2.8.2.1 as follows:

- Designation of personnel responsible for carrying fire safety duties
- Establishing emergency procedures such as
  - Fire Alarms. Procedures once alarm sounds
  - Notification of fire department and definition of firefighting procedure
- Documentation of type, location and operation of fire emergency systems
- List of response numbers as well as names, addresses and telephone numbers of personnel to be contacted during and after working hours in case of emergency

Prior to construction, there are a number of features that need to be coordinated. Each floor level is to have an unobstructed stair that will discharge occupants to the grade level in case of emergency. All temporary heating equipment shall be listed and used in accordance to manufacturer’s instructions. High standards of housekeeping shall be kept on site at all times. The contractor is responsible for providing a 1 hour fire separation between occupied areas and areas under construction. In addition to the passive fire protection techniques, the building is to be equipped with the following active protection systems during construction.

An activated or charged standpipe shall be installed progressively with building construction. The standpipe must be accessible at all times and shall not be blocked by other equipment. See Figure 9.



**FIGURE 9:** ACTIVE STANDPIPE (CWC 2012).

An active sprinkler system must be established upon installation of the ceiling membrane. The system should be activated when construction is not taking place but may be turned off during operating hours. See Figure 10.



**FIGURE 10:** ACTIVE SPRINKLER SYSTEM (CWC 2012)

Onsite fire protection stations that may include portable fire extinguishers possibly supplemented by a garden hose for ease of use by all personnel. Clear notion of the location of such protection stations is mandatory by all staff members. See Figure 11.



**FIGURE 11:** PORTABLE FIRE EXTINGUISHERS (CWC 2012)

Early installation of fire pumps where required for fire protection water supply. Fire hydrants shall be visible and accessible at all times to the fire department. See Figure 12.



**FIGURE 12:** FIRE HYDRANT (CWC 2012)

## 16. CONCLUSION

Mass wood elements such as solid sawn timber, glued-laminated timber (glulam), cross-laminated timber and structural composite lumber can provide excellent fire-resistance, comparable or better to that afforded by traditional non-combustible materials. This is due to the inherent nature of massive wood members to char slowly when exposed to fire allowing the building assemblies or members to maintain significant structural capacity for a target duration under fire conditions.

The structural elements analyzed in this chapter show that massive wood buildings can be safely designed for fire conditions and in some instances might perform better than other traditional materials. Provided that a Construction Fire Safety Plan is rigorously followed, the risk of fire during construction should be diminished. The building at hand demonstrates that the use of combustible structural components can be used for midrise and tall buildings.

## REFERENCES

ASTM. 2012. Standard Test Methods for Fire Tests of Building Construction and Materials, ASTM E119-12. American Society for Testing and Materials, West Conshohocken, PA, USA.

BC Office of Housing and Construction Standards. 2012a. British Columbia Building Code. Building and Safety Standards Branch, Government of British Columbia. Victoria, BC.

BC Office of Housing and Construction Standards. 2012b. British Columbia Fire Code. Building and Safety Standards Branch, Government of British Columbia. Victoria, BC.

Buchanan, A. H. 2001. Structural Design for Fire Safety. John Wiley & Sons Ltd, Chichester, UK.

Canadian Construction Materials Centre (CCMC). (1994). TimberStand LSL. Evaluation Report CCMC 12627-R. Weyerhaeuser, Boise.

CSA. 2014. Engineering Design in Wood. CSA O86-14: Canadian Standards Association, Toronto, ON.

CWC. 2012. Fire Safety and Security. A Technical Note on Fire Safety and Security on Construction Sites in British Columbia. Canadian Wood Council, Ottawa, ON.

Dagenais, C. 2014. CLT Handbook (Canadian 2011 Edition). Chapter 8 - Fire Performance of Cross-Laminated Timber Assemblies. FPInnovations, Quebec City, PQ.

Lie, T. T. 1977. A method for assessing the fire resistance of laminated timber beams and columns. Can. J. Civ. Eng., Vol. 4, pp. 161-169.

ISO. 1999. Fire-Resistance Test - Elements of Building Construction - Part 1: General Requirements. ISO 834-1: International Organization for Standardization, Geneva, Switzerland.

NFPA. 2013a. NFPA 14 Standard for the Installation of Standpipe and Hose Systems. NFPA Standard 14. National Fire Protection Association, Quincy, MA, USA.

NFPA. 2013b. Standard for the Installation of Sprinkler Systems. NFPA Standard 13. National Fire Protection Association, Quincy, MA, USA.

NRCC. 2010. National Building Code Canada. National Research Council, Canada, Ottawa, ON.

T. Holtz-Verbund-Systeme. 2014. [http://www.ticomtec.de/hbv/decken\\_vario\\_e.htm](http://www.ticomtec.de/hbv/decken_vario_e.htm).

ULC. 2013. Standard Method of Fire Test of Exterior Wall Assemblies. CAN/ULC S134. Underwriters Laboratories of Canada, Toronto, ON.

ULC. 2007. Standard Method of Fire Endurance Tests of Building Construction Materials. CAN/ULC S101. Underwriters Laboratories of Canada, Toronto, ON.

# CHAPTER 6

## DESIGN OF ENERGY EFFICIENT AND DURABLE ENVELOPE

---

**Hua Ge** | Concordia University

**Sabrina D'Ambra** | Concordia University

**Lin Wang** | Concordia University

---

## 1. INTRODUCTION

A properly designed and constructed building envelope is extremely important for the success of tall wood buildings. Their structural wooden elements must be protected from the environmental conditions, especially sustained moisture and temperature that may cause moisture damages and durability issues. A 20-storey wood building is proposed in North Vancouver, an area with a high amount of wind-driven rain. Taller buildings experience higher wind induced pressure, stack effect, therefore, higher possibility of air leakage, and higher amount of wind-driven rain. Good moisture management when designing building envelopes for taller, especially wood buildings, is essential for ensuring its long-term durability.

Over the past couple of decades, research efforts have been made to advance the understanding of building science and moisture management. As a result, a series of best practices have been published by CMHC, BC Housing HPO branch and FPInnovations.

The method employed in developing the building envelope design for the conceptual 20-storey tall wood building with a concrete podium is applying sound building science principles and following the best practices. The “Technical guide for the design and construction of tall wood buildings in Canada” is used as one of the main references.

The primary functions of building envelopes are (Hutcheon, 1963):

- Control of heat flow
- Control of air flow
- Control of water vapour flow
- Control of rain penetration
- Control of light, solar and other radiation
- Control of fire
- Control of noise
- Structural integrity
- Durable
- Aesthetically pleasing
- Economically sound

The building envelope design principles to be followed:

- Continuity of thermal insulation and elimination of thermal bridges
- Continuity of air barrier
- Proper placement and choice of vapour retarder
- Two lines of defense: 1<sup>st</sup> line of defense-water shedding layer; 2<sup>nd</sup> line of defense-drainage plane, i.e. water resistive barrier (WRB), flashing, etc.
- Ensuring the drying capacity greater than the wetting potential
- 4D principles: deflection, drainage, drying and durability
- Properly designed joints to accommodate movement

The design of building envelopes for the tall wood building

focuses on durability, energy efficiency, constructability, maintenance, and cost-effectiveness. This design has tried to use wood over other materials wherever possible.

## 2. WALL ASSEMBLY: CONCEPTUAL DESIGN

In the coastal area of BC, a rainscreen wall assembly is mandated for part 9 low-rise residential buildings (BCBC, 2012). The presence of an air gap behind the cladding provides a capillary break for rain penetration, a drainage plane for any incidental water passing through the cladding, i.e. the first line of defense, to drain, drying through ventilation if both bottom and top vents are provided. The implementation of such a design in tall wood buildings would not be different than following the current best practices for the rainscreen design typically used in lower multi-unit residential buildings. A pressure-moderated, ventilated cavity of sufficient air change rate is highly recommended. The influence and required air cavity ventilation rate for the design will be investigated through hygrothermal simulations in section 4.

Three wall assembly alternatives were considered for the tall wood building’s envelope: 1) Cross Laminated Timber (CLT) wall assembly with exterior insulation; 2) simple stud wall; and 3) split-insulated stud wall.

Since the structural sub-team decided to use Glulam columns, and a shear core wall moment frame as the main load bearing elements, the perimeter walls were determined to be non-load bearing. As such, mass timber paneling in the envelope was unnecessary. The split-insulated wall option offers many more advantages than the simple stud wall. The exterior insulation will reduce thermal bridging effect and keep the wood structural elements at higher temperature and thus reduced risks for condensation due to vapour diffusion or air leakage, and higher drying potential should incidental rainwater penetration occur. Therefore, the split-insulated wall assembly alternative was selected and will now be considered for use in the proposed tall wood building. Figure 1 shows a typical configuration of split-insulated wall assembly, which will be used as the basis for the wall assembly design.

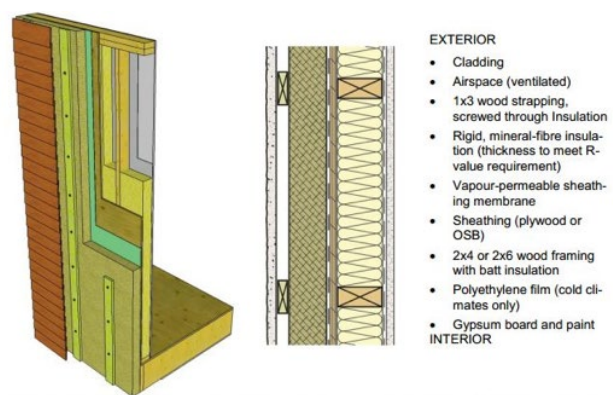


**FIGURE 1:** WALL SECTION ELEMENTS BASED ON THE SPLIT-INSULATED WOOD-FRAME WALL ASSEMBLY WITH EXTERIOR RIGID MINERAL-FIBER INSULATION FROM THE GUIDE FOR DESIGNING ENERGY-EFFICIENT BUILDING ENCLOSURES (FPINNOVATIONS)

## 2.1 ENERGY CODE REQUIREMENTS

North Vancouver is located in a cold climate zone 4 with a heating degree-day less than 3000HDD. The prescriptive path of the National Energy Code for Buildings (NECB, 2011) for building envelope design is followed. Table 1 lists the minimum required effective thermal resistance for wall and roof assemblies in ASHRAE 90.1, NECB 2011 and ASHRAE

189.1-2011. Table 2 lists the range of minimum effective RSI for wood-frame wall and roof assemblies required by various current standards and building codes. Table 3 lists the range of minimum effective RSI for wall and roof assemblies for high-performance wood-frame enclosures. Table 4 lists the minimum effective RSI selected for the proposed tall wood building.

	ASHRAE 90.1 — 2010 ENERGY STANDARD FOR BUILDINGS EXCEPT LOW-RISE RESIDENTIAL BUILDINGS	NECB 2011 NATIONAL ENERGY CODE OF CANADA FOR BUILDINGS	ASHRAE 189.1 — 2011 STANDARD FOR THE DESIGN OF HIGH PERFORMANCE, GREEN BUILDINGS EXCEPT LOW-RISE RESIDENTIAL BUILDINGS
Above-grade timber frame wall	2.7	3.17	3.5
Wood-frame roof- insulation entirely above deck	3.7	4.41	4.5

TABLE 1: MINIMUM EFFECTIVE THERMAL RESISTANCE (RSI IN m<sup>2</sup>-K/W): ABOVE-GRADE WOOD FRAME WALL

CLIMATE ZONES	WOOD-FRAME, ABOVE GRADE WALL	WOOD-FRAME ROOF – INSULATION ENTIRELY ABOVE DECK
	R-value (RSI)	R-value (RSI)
4 to 5	2.6 to 4.1	4.4 – 6.2

TABLE 2: RANGE OF EFFECTIVE RSI-VALUE TARGETS FOR MINIMUM COMPLIANCE WITH VARIOUS ENERGY CODES

CLIMATE ZONES	WOOD-FRAME, ABOVE GRADE WALL	WOOD-FRAME ROOF – INSULATION ENTIRELY ABOVE DECK
	R-value (RSI)	R-value (RSI)
4 to 5	3.9 - 4.9	5.3 – 7.0

TABLE 3: RANGE OF EFFECTIVE RSI-VALUE TARGETS FOR EXCEEDING MINIMUM COMPLIANCE WITH ENERGY CODES: HIGH PERFORMANCE WOOD-FRAME BUILDING ENCLOSURES

	WOOD-FRAME, ABOVE GRADE WALL	WOOD-FRAME ROOF – INSULATION ENTIRELY ABOVE DECK
	RSI	RSI
<b>PRESENT</b> Meets minimum NECB requirements	3.2	4.4
<b>FUTURE*</b> 25% above present minimum requirements	4.0	5.5

\* The minimum requirements at a future date would be likely closer to the high-performance requirements of today

TABLE 4: SELECTED DESIGN REQUIREMENTS FOR PRESENT & FUTURE TALL WOOD BUILDING

As per the prescriptive requirement by the NECB 2011, the accepted maximum fenestration and door area to wall area ratio (FDWR) is 40% for climates with HDD less than 4000. Therefore, a FDWR of 40% is selected for this design. For climate zone 4, the maximum overall thermal transmittance of fenestration is 2.4 W/m<sup>2</sup>·K.

**2.2 MATERIAL SELECTION AND RATIONALE**

Table 5 lists the materials selected for the proposed wood frame wall assembly. To lessen the environmental impact of the project, as much as possible, recycled, plantation or third-party certified timbers for non-load bearing framing members, should be selected for use.

WALL SYSTEM	SPLIT-INSULATED
Cladding (combustible)	Silva Panel: 3 ply, cross-laminated, Western red cedar engineered solid wood panels, thickness 20mm (Silva Panel Canada Ltd.)
Cladding (Non-Combustible)	Fibre reinforced cement panels, (SWISSPEARL)
Air cavity	Ventilated 20mm air gap
Exterior insulation	Semi-rigid mineral wool (ROXUL CavityRock), (25-50mm), R4.2/inch
WRB/Air-barrier system	Self-adhered vapour permeable water resistive barrier membrane/air barrier
Exterior wall sheathing	Plywood/exterior grade gypsum board
Stud wall	38x140 mm studs @ 400 mm on center (o.c.) (nominal 2x6 in studs @ 16 in. o.c.)
Stud-cavity insulation	Mineral wool batt (ROXUL Comfortbatt), R4.0/inch
Vapour retarder	6 mil polyethylene film
Interior finish	Gypsum board with paint

TABLE 5: CONFIGURATION OF PROPOSED WOOD-FRAME WALL ASSEMBLY

**2.2.1 Cladding**

**Combustible cladding**

To increase the wood content of the proposed tall wood building, wood cladding was considered. To meet fire requirements, the fire design team suggested to limit the wood cladding to 30% of the total cladding area, and preferably installed in horizontal spandrels with non-combustible cladding providing fire separation between the wood spandrel panels. A checker-

board pattern was chosen at the end to satisfy both aesthetic and fire requirements. However, the checker-board pattern may present some difficulties and challenges for recoating and maintenance of the wood cladding.

The wood cladding system chosen is 3-ply cross-laminated western red cedar engineered solid wood panel with a thickness of 20mm by Silva Panel Canada Ltd. The same product was used in the CIRS building at UBC. Western red cedar is highly durable, naturally resistant to decay, dimensionally stable, light in weight and easy to work with. With pre-finished coating and the proper regular maintenance, the cladding can last a long time.

**Non-combustible cladding**

Cement fibre-reinforced composite panels were selected for the non-combustible cladding. A panel thickness of 12mm was selected. Effectiveness of the system depends on a clear minimum cavity of 25 mm (depending on height of building) and on ventilation openings at the base and top of the cladding area, windows, etc. (SWISSPEARL, 2013)

**Panel joints**

Panel joints need to be minimum 3/16 in. (5 mm) wide for vertical joints, and 3/12 in. (6 mm) wide for horizontal joints. A typical joint width is 5/16 in. (8 mm).

The connection between the different types of claddings needs to be designed and installed properly. The joints allow water to shed and accommodate movement due to thermal and moisture expansion/contraction, and other structural loads to maintain the integrity of the cladding. The sealant must be compatible between the cladding materials it is in contact with. The application of current standard practices for joint detail design is acceptable for the case of a tall wood building.

**Cladding-attachment strategy**

Optimizing structural cladding attachment is important for improving the thermal efficiency of wall assemblies, while minimizing exterior insulation and overall wall thicknesses. Intermittent thermal spacers (which pass through the exterior insulation) were selected to support the vertical batten (i.e. strapping) upon which the cladding is to be attached. Figure 2 shows an example of the cladding attachment strategy.

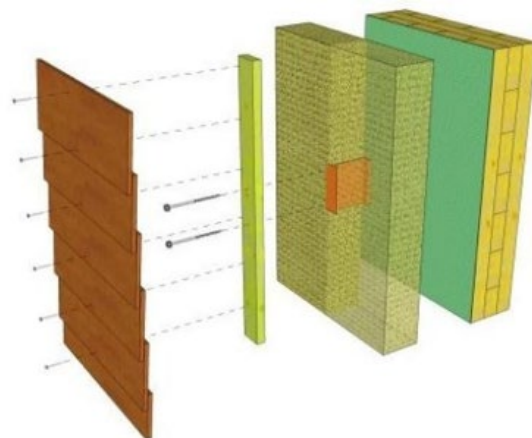


FIGURE 2: EXAMPLE OF THE SELECTED ATTACHMENT STRATEGY (FPINNOVATIONS)

### 2.2.2 Air space

A 20mm air space behind the cladding will be created by properly preservative-treated wood strapping or z-girt. The air cavity may be compartmentalized by cross-cavity flashing at each floor to facilitate pressure moderation and control of vertical fire spread through the air cavity. Openings will be provided at both bottom and top of the cladding.

### 2.2.3 Insulation

Mineral wool was selected as the preferred insulation for its non-combustible and drainable properties as both exterior and stud cavity insulations. ROXUL COMFORTBATT is chosen as the stud cavity insulation and the semi-rigid mineral wool (ROXUL CavityRock) for the exterior insulation.

### 2.2.4 Air barrier strategy

Self-adhered vapour permeable Water Resistive Barrier membrane is chosen to serve as both WRB and exterior air barrier systems. Because of the higher wind pressure and stack effect, thus higher potential of air leakage for taller buildings, a good quality of air barrier is very important for the durability and energy efficiency of tall wood buildings. The WRB membrane will be applied to the plywood or gypsum board sheathing and protected by the mineral wool exterior insulation. This system has the advantages of easier installation and maintaining the continuity at various joints, rigid support between sheathing and exterior insulation, and cost effective serving as WRB as well.

### 2.2.5 Vapour retarder

A 6 mil polyethylene film is chosen as the vapour retarder to control the vapour diffusion through building envelope assemblies. For the relatively mild climate of North Vancouver, low-permeance paint would satisfy the requirement for vapour diffusion control as well if it can be applied properly. The suitability of using poly as the vapour retarder will be further investigated through hygrothermal simulations reported in section 4.

## 2.3 CALCULATION OF THE EFFECTIVE RSI-VALUE

The parallel-path method is followed to calculate the effective thermal resistance of the wall assemblies proposed (ASHRAE 2013). A framing factor of 25% is assumed for a split-insulated 2x6 stud wall at 16 in. o.c. wall assembly. The placement of a continuous exterior insulation reduces the effect of thermal bridging.

The wood columns (Glulam), which take the structural load along the perimeter, are to be placed on the interior side of the wall assembly, making them visible to the occupants. This architectural feature reduces the effect of thermal bridging in the enclosure, and ensures the columns are kept warm all year long (reducing condensation concerns during the cold season).

To meet the current NECB code requirements of RSI 3.2, a minimum of 1" exterior insulation will be needed. To meet the

future high-performance enclosure requirements of RSI 4.0, a 1.5" exterior insulation will be needed. The achieved effective thermal resistance with a 2" semi-rigid mineral wool insulation of the proposed wall assembly is RSI 4.8.

## 3. ROOF ASSEMBLY: CONCEPTUAL DESIGN

A flat roof with a minimum of 2% slope is proposed for the tall wood building. The 7-ply CLT panels will be used as the roof deck. A 2 x 6 wood structure will be built between the CLT panels and insulation boards to provide natural ventilation for the mass timber and the 2% slope required for drainage. Both conventional and protected membrane roof assemblies are considered.

The design and choice of materials need to meet the building code and energy code requirements. Figure 3 shows the proposed roof assemblies. Materials chosen for this roof assembly are listed in Table 6. The effective thermal resistance achieved for the proposed roof assembly is RSI 5.9 for the conventional roof assembly using 4" polyiso insulation and RSI5.7 for the protected membrane roof assembly using 4" XPS insulation. The roof/parapet wall connection details are provided in section 5.

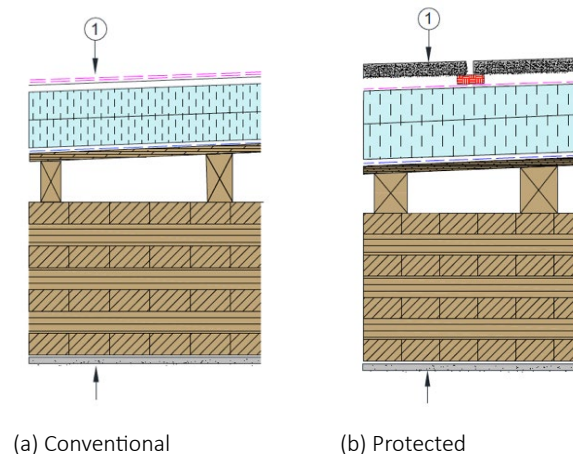


**FIGURE 3:** CONFIGURATION OF A) CONVENTIONAL AND B) PROTECTED MEMBRANE CLT ROOF ASSEMBLY (ADAPTED FROM TECHNICAL GUIDE FOR TALL WOOD BUILDING DESIGN IN CANADA).

CONVENTIONAL ROOF ASSEMBLY	MATERIALS
Roof membrane	2-ply modified SBS bituminous membranes, torched on or mechanically fastened
Protection board	DensDeck protection board, ½"
Roof insulation	Two layers of polyisocyanurate (2") with staggered joints and tapered to provide roof slope
Air/vapour barrier	adhered or torched on membrane
Built-up wood structure to provide ventilation space	2 × 6 with plywood sheathing
CLT roof deck	7-ply CLT (180mm)
Ceiling finish	Gypsum board with paint

**TABLE 6 A:** CONFIGURATION OF A CONVENTIONAL CLT ROOF ASSEMBLY

PROTECTED MEMBRANE ROOF ASSEMBLY	MATERIALS
Ballast	Gravel or concrete paver
Filter fabric	
Roof insulation	Two layers of XPS (2") with staggered joints
Roof membrane	Adhered or torched on membrane function as waterproofing, air and vapour barrier
Built-up wood structure to provide drainage slope and ventilation space	2 × 6 with plywood sheathing
CLT roof deck	7-ply CLT (180mm)
Ceiling finish	Gypsum board with paint

**TABLE 6 B:** CONFIGURATION OF A PROTECTED MEMBRANE ROOF ASSEMBLY

### 3.1 OVERHANG CONSIDERATION

Initially we considered including a roof overhang to help reduce wind-driven rain exposure for the 20-story tall wood building. Field measurements have shown that the provision of overhang even for tall buildings can significantly reduce wind-driven rain exposure at the upper level of the façade for this particular climate characterized with mild wind speed and rainfall intensity but long period of rain (Ge & Krpan, 2009). Many of the damaging water ingress issues we have experienced on all types of construction on the west coast originate at the parapet, where higher amount of wind-driven

rain is deposited.

However, the provision of an overhang adds complexity to the roof design, such as the requirement of a special anchoring system of the overhang into the CLT deck or a built-up wood structure to provide the overhang. It can contribute to roof upturning from wind-loads adding to the elevated wind pressures for the flat roof at corners and edges. From the drainage perspective, using a single-sided 2% slope (flat-roof) as the main water shedding system would require a less standard drainage system for a high-rise, such as gutters and downspouts, which may be less easy to implement and maintain on a tall building. These added complexities would lead to added design costs, and possibly, make such a building less appealing to build.

The roof overhang is beneficial in reducing the durability risks from wind-driven rain wetting and rain penetration for façade but may not be critical. A well-designed and constructed rainscreen wall assembly should be able to manage water ingress successfully without the overhang. Therefore, the overhang is not included in the final design.

## 4. HYGROTHERMAL PERFORMANCE EVALUATION OF THE PROPOSED BUILDING ENVELOPE DESIGN

The proposed 20-story wood building is located in North Vancouver, an area with an annual rainfall of about 1.8m. Therefore it is important to design the building to minimize wind-driven rain exposure and robust building envelopes to manage wind-driven rain and rain penetration.

Historical weather data were obtained from Environment Canada for weather stations in North Vancouver. Data from stations with hourly wind speed, wind direction and rainfall intensity are selected for analysis. Prevailing wind direction during all hours and rain hours are plotted. The airfield wind-driven rain indices for eight orientations at three building heights 10m, 30m and 60m are calculated.

Among the 16 years of data available, hourly wind speed, wind direction, rainfall intensity of year 1999 is chosen to generate the customized weather data file for hygrothermal simulations since year 1999 has the highest amount of rain and the complete hourly weather data.

### 4.1 WIND-DRIVEN RAIN EXPOSURE OF THE PROPOSED BUILDING

The prevailing wind directions during all hours and rain hours are plotted in Figure 4. As shown in Figure 4, the prevailing wind direction is from North and East during all hours while during rain hours the wind is predominately from the ENE with 40% of frequency. Therefore the North and East façade will expose to higher amount of wind-driven rain. Figure 5 shows the wind speed distribution during all hours and rain hours. Typically the wind speed is greater during rain. Eighty percent of the time the mean wind speed is less than 3m/s during all hours and about 5m/s during rain hours.

Figure 6 shows the mean annual wind speed and direction

and Figure 7 shows the mean annual precipitation for Metro Vancouver region (Oke & Hay, 1998). These contours show that due to the unique local topography, wind and rain varies significantly within a small distance in metro Vancouver region. Therefore, site specific wind-driven rain exposure is important for designing durable building envelopes.

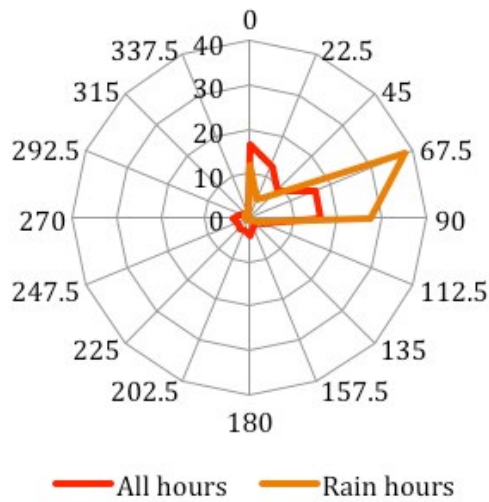


FIGURE 4: PREVAILING WIND DIRECTION DURING ALL HOURS AND RAIN HOURS FOR THE PROPOSED BUILDING SITE.

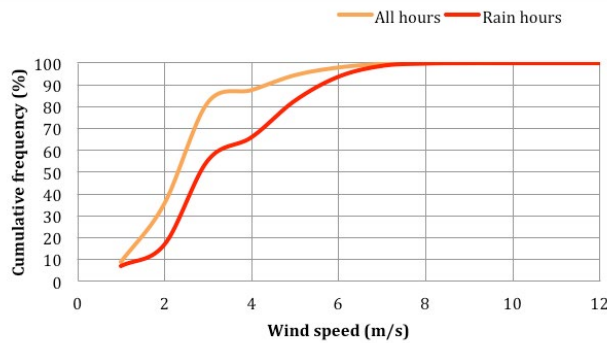


FIGURE 5: FREQUENCY DISTRIBUTION OF MEAN WIND SPEED DURING ALL HOURS AND RAIN HOURS FOR THE PROPOSED BUILDING SITE (10M ABOVE GROUND).

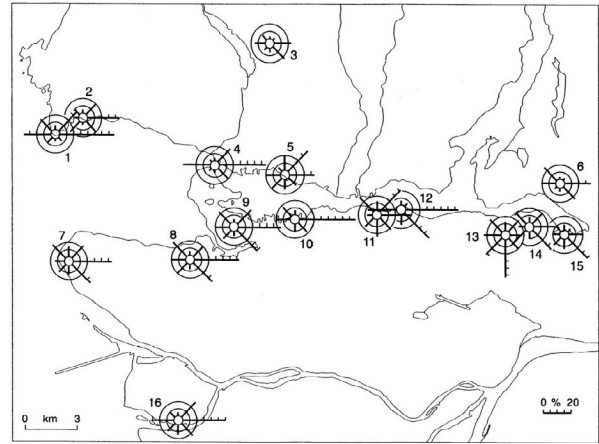


FIGURE 6: THE ANNUAL MEAN WIND SPEED AND DIRECTION FOR METRO VANCOUVER (OKE & HAY, 1998). STATION 5: NEIGHBORHOOD OF PROPOSED BUILDING (NORTH VANCOUVER)

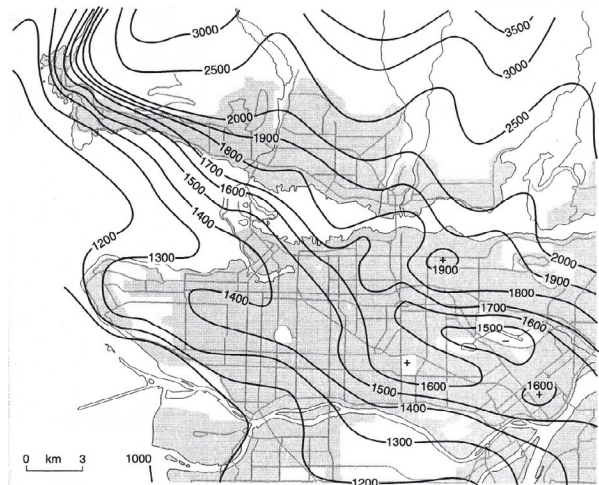


FIGURE 7: MEAN ANNUAL PRECIPITATION (MM) FOR METRO VANCOUVER. SOURCE: (OKE & HAY, 1998)

To quantify the wind-driven rain exposure on façade, the airfield and wall indices are calculated following the procedure prescribed by ISO standard 5927-3 (ISO, 2009).

#### 4.1.1 Airfield driving rain index

The annual airfield annual index (IA) can be calculated using equation 1 (ISO: 15927):

$$I_A = \frac{2}{9} \frac{\sum U * R_h^{0.9} \cos(D - \Theta)}{N} \quad [1]$$

where,

$U$  = hourly mean wind speed (m/s)

$R_h$  = hourly rainfall (mm)

$D$  = hourly mean wind direction from North

$\Theta$  = wall orientation relative to North

$N$  = number of years of available data

The summation is taken over all hours for which  $\cos(D - \Theta)$  is positive. Sixteen years of hourly values of wind speed, wind direction and rainfall for weather stations near to the proposed building location were used.

Typically higher amount of rain deposited at the upper level of façade and at corners and edges of the building due to higher wind speed and the change of direction of wind flow. Airfield wind-driven rain indices at three building heights of 10m, 30 and 60m are calculated.

The weather data obtained from Environment Canada was recorded at 10m above ground. The power law correlation is used to estimate wind speed at building height  $h$ ,  $U(h)$ :

$$U(h) = U_{10} \cdot (h/10)^\alpha \quad [2]$$

where,

$U_{10}$  = standard wind speed at 10 m above grade, normally reported by weather stations (m/s); and

$h$  = height above grade (m)

The recommended exponent  $\alpha = 0.25$  for a suburban terrain is used since the proposed building site is located in a relatively open urban area.

#### 4.1.2 Wall indices: wind driven rain impinged on the wall

The airfield indices are the annual amount of wind-driven rain passing through an imaginary vertical plane. To estimate the actual amount of rain deposited on a specific location of façade, wall indices need to be calculated by taking into account the influence of terrain roughness, topography, obstructions and spatial distribution on the façade.

According to the procedure prescribed by ISO: 15927, the annual wind-driven rain on wall surface:

$$I_{WA} = I_A C_R C_T O W \quad [3]$$

where,

$C_R$  = terrain roughness factor that takes into account the variability of the mean wind speed at the site due to the height above the ground and the upstream roughness of the terrain;

$C_T$  = topography factor that accounts for the increase of the mean wind speed over isolated hills and escarpments;

$O$  = obstruction factor that takes into account the shelter by the nearest obstacle of similar dimensions to the wall; and

$W$  = wall factor that takes into account the variation of wind-

driven rain over the surface of the wall.

Since the weather station is located in an area similar to the proposed building site,  $C_R$  is assumed to be 1.0. There is no isolated hills or escarpments at the building site, therefore  $C_T$  is assumed to be 1.0 as well. On the proposed building site, there are a few high-rise buildings within 50m of the 20-storey wood building, therefore, an obstruction factor of  $O = 0.6$  is chosen. There are no detailed wall factors available for tall buildings. According to ISO standard, a wall factor can be taken as 0.5 for the top 2.5m and 0.2 for the remainder. Field measurements in this region showed that 0.5 is a reasonable value to be used (Ge & Krpan, 2009). The calculated annual airfield WDR indices and the estimated wall indices are listed in Table 7. The East orientation receives the highest amount of wind-driven rain followed by the NE and North orientations. For the proposed building, the east façade will experience the highest wind-driven rain exposure. Typically North façade receives less solar radiation, thus less drying, therefore, North façade may experience higher moisture loads as well. The hygrothermal performance of cladding and plywood sheathing will be evaluated for the North, East, and South façade.

	AIRFIELD 60M ANNUAL INDEX (L/m <sup>2</sup> )	WALL SURFACES (L/m <sup>2</sup> )		AIRFIELD 30M ANNUAL INDEX (L/m <sup>2</sup> )	WALL SURFACES (L/m <sup>2</sup> )		AIRFIELD 10M ANNUAL INDEX (L/m <sup>2</sup> )	WALL SURFACES (L/m <sup>2</sup> )
N	667.1	200.1	N	561.0	67.3	N	426.3	51.2
NE	1733.3	520.0	NE	1457.5	174.9	NE	1107.5	132.9
E	1824.2	547.3	E	1534.0	184.1	E	1165.6	139.9
SE	884.8	265.4	SE	744.0	89.3	SE	565.3	67.8
S	31.7	9.5	S	26.6	3.2	S	20.2	2.4
SW	15.9	4.8	SW	13.4	1.6	SW	10.2	1.2
W	31.0	9.3	W	26.1	3.1	W	19.8	2.4
NW	66.2	19.8	NW	55.6	6.7	NW	42.3	5.1

TABLE 7: ANNUAL AIRFIELD AND WALL INDICES FOR THE PROPOSED BUILDING AT THREE BUILDING HEIGHTS.

## 4.2 HYGROTHERMAL SIMULATIONS USING WUFI PRO 5.1

To evaluate whether the proposed wood-frame wall assembly typically used for low-rise residential buildings will be suitable for the tall wood building with higher wind-driven rain exposure and air leakage potential, hygrothermal simulations are carried out using WUFI Pro 5.1.

### 4.2.1 Exterior climatic conditions

Hourly weather data selected for year 1999, i.e. wind speed, wind direction, temperature, relative humidity, and solar radiation are used to generate the customized weather file for the simulations. No weather station located in North Vancouver has record of solar radiation, therefore, the solar radiation data from the weather station at UBC was used.

### 4.2.2 Interior moisture load

A normal moisture load according to standard EN15026 (2007), which correlates the indoor temperature and relative humidity to outdoor conditions, is specified for indoor climate. The resulting interior relative humidity and temperature are shown in Figure 8.

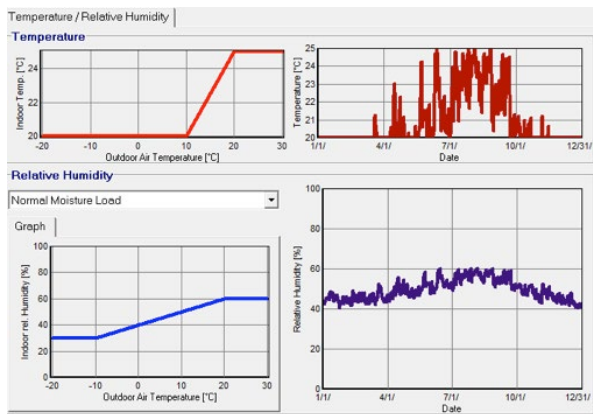


FIGURE 8: INTERIOR CONDITIONS SPECIFIED IN WUFI SIMULATIONS

### 4.2.3 Wind-driven rain model

The default wind-driven rain model in WUFI Pro is used.

$$R_{\text{wdr}} = R_h \cdot (R1 + R2 \cdot U) \quad [4]$$

where,

$R_{\text{wdr}}$ , rain deposited on vertical façade, L/m<sup>2</sup>

$R_h$ , horizontal rainfall intensity from weather data file, L/m<sup>2</sup>

$R1$ , driving rain coefficients, zero for vertical surface

$R2$ , driving rain coefficients, depending on the specific location on façade; 0.2 is used for the reference cases

$U$ -wind speed, from weather data file, m/s

### 4.2.4 Parameters investigated

Parameters investigated are listed in Table 8. The parameters studied include orientation, design variables for the wood-frame wall assembly, cavity ventilation rates and three different types of moisture loads, driving rain coefficient and water absorption coefficient of cladding.

Based on the on-site wind-driven rain exposure analysis, the east façade will receive the highest amount of wind-driven rain, the North façade will receive the second-highest amount of wind-driven rain but with the least solar radiation, and the South will receive the least amount of wind-driven rain but with the highest solar radiation available in the winter rainy season. The west façade will receive similar amount of wind-driven rain as the South façade. Therefore, three orientations (east, north, and south) are investigated.

In terms of wall assembly design, two types of cladding materials i.e. western red cedar wood siding and fiber cement panel, and two types of sheathing i.e. plywood and exterior grade gypsum board are included. The appropriateness of using polyethylene as vapour barrier is investigated to evaluate whether there is any risk for inward solar driven condensation during the summer time, cases with and without polyethylene films are included. The proposed wall assembly uses vapour permeable WRB with vapour permeable mineral

wool insulation, having a combined vapour permeance of 975 ng/Pa s m<sup>2</sup> outboard of the sheathing. Two additional design variables are included to investigate the influence of vapour permeability of the exterior insulation and WRB, i.e. vapour permeable WRB with EPS as exterior insulation having a combined vapour permeance of 64.4 ng/Pa s m<sup>2</sup> and vapour impermeable WRB with mineral wool insulation having a combined vapour permeance of 1.6 ng/Pa s m<sup>2</sup>.

Cavity ventilation is beneficial for drying of wet absorptive cladding or under conditions with strong solar radiation. Given the unique climatic characteristics of the coastal British Columbia, rainy winter with limited availability of solar radiation, the effect of cavity ventilation may not be that significant. Therefore, the influence of cavity ventilation with a range of 0-200 ACH is also investigated.

Three levels of moisture loads are investigated, i.e. vapour diffusion only, introduced air leakage and introduced rain leakage, to evaluate the robustness of the wall assembly in

handling risks for moisture damage. An air leakage rate of 1.5L/m<sup>2</sup>·s, which represents an average air tightness for building envelope assembly is introduced into the wood stud cavity. According to ASHRAE 160P (ASHRAE, 2009), 1% of wind-driven rain deposited on wall surface is assumed to penetrate and deposited into the wall assembly. Two deposition locations are investigated, one in compliance with ASHRAE 160P onto the WRB, and the second location assuming the rainwater penetrating the 2<sup>nd</sup> line of defense of WRB and deposited directly onto plywood sheathing.

The sensitivity of MC of western red cedar cladding to the driving rain and water absorption coefficients of the cladding is investigated by varying the driving rain coefficient R<sub>2</sub> by a factor of 2 and the water absorption coefficient of 50%.

All layers are assumed with an initial MC at 80%RH and 20°C temperature. Three years of simulations are performed to remove the influence of the assumed initial conditions. The simulation starts from October.

<b>ORIENTATION</b>	N, E, S
<b>WALL ASSEMBLIES</b>	With/without poly
	Plywood/Exterior grade gypsum board sheathing
	Western red cedar wood siding/fiber cement panel cladding
	Permeable WRB+mineral wool insulation (with a combined permeance of 975 ng/Pa.s.m <sup>2</sup> )
	Permeable WRB+EPS insulation (with a combined permeance of 64.4 ng/Pa.s.m <sup>2</sup> )
<b>CAVITY VENTILATION</b>	Impermeable WRB+mineral wool insulation (with a combined permeance of 1.6 ng/Pa s m <sup>2</sup> )
	0, 10, 50, 100 and 200 ACH
<b>MOISTURE LOAD</b>	Vapour diffusion only
	Air leakage (1.5L/m <sup>2</sup> ·s) into the stud cavity
	1% rain leakage deposited onto the WRB/directly to sheathing
<b>WATER ABSORPTION COEFFICIENTS OF CLADDING</b>	Default value: 0.001 kg/m <sup>2</sup> ·s <sup>0.5</sup>
	Half value: 0.0005 kg/m <sup>2</sup> ·s <sup>0.5</sup>
<b>DRIVING RAIN COEFFICIENT R<sub>2</sub></b>	Default value, R <sub>2</sub> =0.2
	Half value, R <sub>2</sub> =0.1
	Double value, R <sub>2</sub> =0.4

**TABLE 8:** PARAMETERS INVESTIGATED IN WUFI SIMULATIONS

#### 4.2.5 Simulation results

The moisture content of wood siding, the moisture content of plywood sheathing, the relative humidity at the interface of plywood sheathing and stud cavity insulation, and the relative humidity at the interface of stud cavity insulation and the interior gypsum board are used as indicators to evaluate the hygrothermal performance of the proposed wall assembly.

**4.2.5.1 Effect of polyethylene as the vapour barrier**

- Solar-driven inward vapour diffusion:** since polyethylene film is used as vapour barrier, there might be concerns for solar-driven inward vapour diffusion induced condensation at the interface of polyethylene and the stud cavity insulation during the summer time. However, given the particular climate in Metro Vancouver, which is relatively dry during the summer time, the simulations showed that the relative humidity at the interface of the polyethylene film and the stud cavity insulation is around 40-60% RH year around, there is no risks of solar-driven condensation at this location for the cases both with and without poly for all three orientations. Figure 9 shows the relative humidity plots at polyethylene film for both North and South orientation as examples.

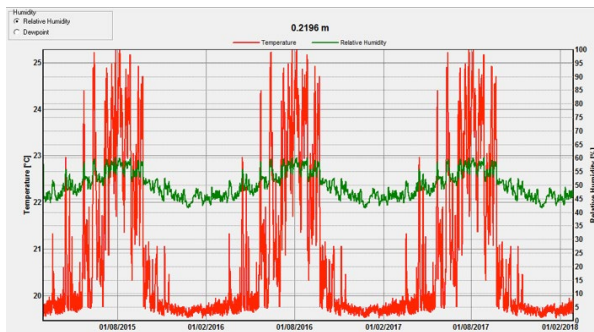


**FIGURE 9 A:** NORTH ORIENTATION: RH AT THE INTERFACE OF STUD CAVITY INSULATION AND POLYETHYLENE FILM (POLY WITH RAIN LEAKAGE)

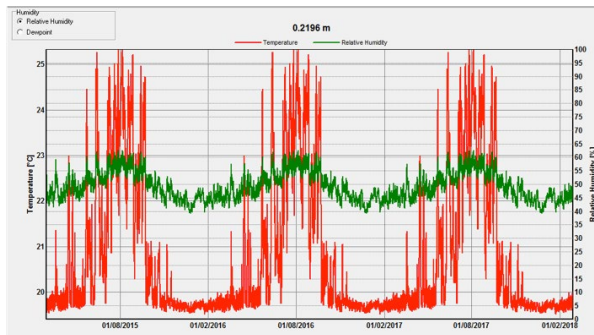


**FIGURE 9 B:** SOUTH ORIENTATION: RH AT THE INTERFACE OF STUD CAVITY INSULATION AND POLYETHYLENE FILM (POLY WITH RAIN LEAKAGE)

- Vapour diffusion control during the wintertime:** cases without poly showed higher moisture content level in plywood sheathing during the wintertime for all three moisture load scenarios for the wall assembly with permeable WRB and mineral wool exterior insulation. Table 9 shows the maximum MC in plywood sheathing over the three-year simulation period. For all the moisture load scenarios except for 1% rain leakage deposited directly onto the plywood, the MC in plywood

sheathing is below 15%. The MC level in plywood for the North orientation is slightly higher than that in the East and South orientation. Generally, the MC in plywood without poly is about 1.5-3.5% higher than the cases with poly for all three moisture load scenarios except the case with 1% rain leakage on the East façade, for which the MC level is slightly decreased by 2% when poly is removed. Therefore, for the Metro Vancouver climate, vapour retarder is required to control vapour flow. The use of a class I vapour barrier, i.e. polyethylene does not inhibit the drying given that the rainy season is in the winter time when the vapour flow is from indoor to outdoor. The permeable exterior insulation and WRB allows drying outwards. A vapour retarder with higher vapour permeance may be appropriate. Figure 10 and 11 shows the MC in plywood for the cases with 1% rain leakage deposited directly onto plywood with permeable WRB and mineral wool insulation for the North and East orientation.

	VAPOUR DIFFUSION ONLY		AIR LEAKAGE		RAIN LEAKAGE			
	w/ poly	w/o poly	w/ poly	w/o poly	1% on WRB		1% on plywood (200ACH) w/ poly	
					w/ poly	w/o poly	w/ poly	w/o poly
N	10.6	14.3	12.1	14.0	10.7	14.3	36.4	38.3
E	10.2	13.6	10.4	13.4	10.2	13.6	102.1	100.0
S	9.6	12.3	10.8	12.3	9.8	12.4	9.8	12.5

**TABLE 9:** MAXIMUM MC (%) IN PLYWOOD SHEATHING WITH PERMEABLE WRB AND MINERAL WOOL EXTERIOR INSULATION

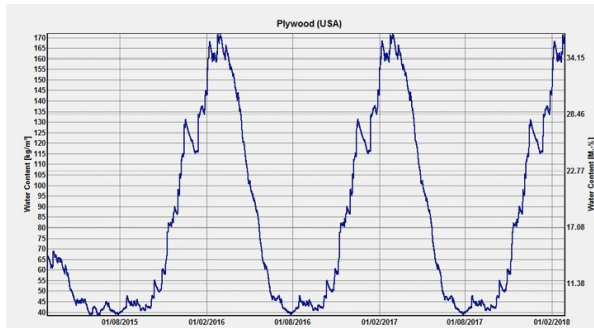


**FIGURE 10 A:** NORTH ORIENTATION: MC IN PLYWOOD FOR THE CASE WITH POLY, 1% RAIN LEAKAGE ON PLYWOOD

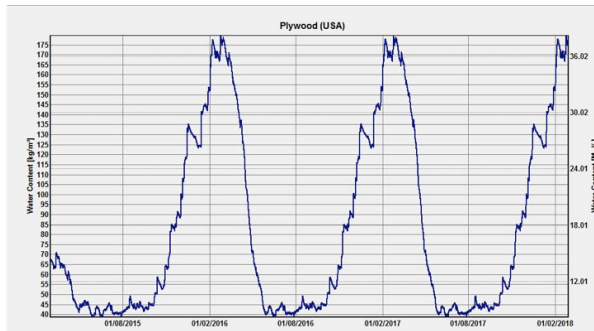


**FIGURE 10 B:** NORTH ORIENTATION: MC IN PLYWOOD FOR THE CASE WITHOUT POLY, 1% RAIN LEAKAGE ON PLYWOOD

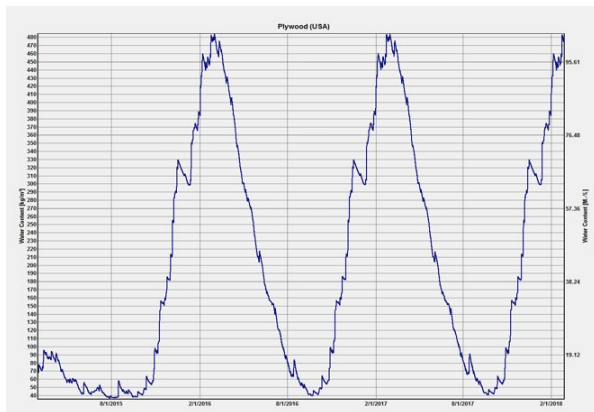


**FIGURE 11 A:** EAST ORIENTATION: MC IN PLYWOOD FOR THE CASE WITH POLY, 1% RAIN LEAKAGE ON PLYWOOD

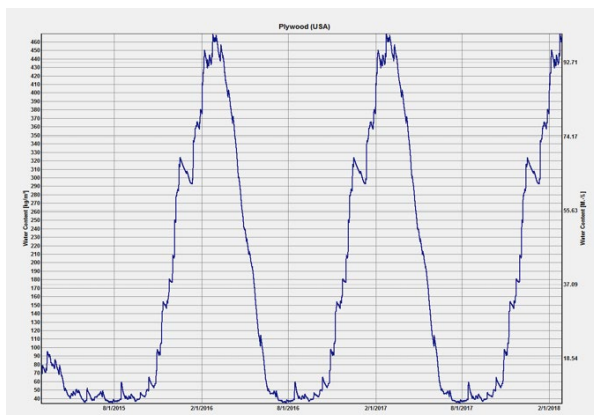


**FIGURE 11 B:** EAST ORIENTATION: MC IN PLYWOOD FOR THE CASE WITHOUT POLY, 1% RAIN LEAKAGE ON PLYWOOD

Tables 10 and 11 show the Maximum MC in plywood sheathing for the assembly with impermeable WRB and mineral wool exterior insulation, and for the assembly with permeable WRB and EPS exterior insulation, respectively. In general, the MC level in plywood sheathing for these two wall assemblies is higher than the case with permeable WRB and mineral wool exterior insulation when the poly is removed for both vapour diffusion and air leakage cases. The North orientation is the worst case for all moisture loads except for when 1% rain leakage directly deposited on the plywood sheathing. With 1% rain leakage introduced, the removal of poly helps significantly reduce the MC level in plywood for North and the South orientations for the impermeable WRB assembly since drying towards indoor is the only path. However, the MC level is still extremely high for North orientation at the end of 3-year simulation period while for the South orientation the MC level is within the safe range. For the East orientation, the removal of polyethylene only slightly reduces the MC level in plywood probably due to the significantly high wind-driven rain exposure in this orientation and the drying potential is much smaller than the wetting. For the permeable WRB with EPS exterior insulation, the effect of removing polyethylene film for the North and East orientation is similar to that for the wall assembly with impermeable WRB, however, the MC level is increased for the south orientation. The level of vapour permeability of the EPS exterior insulation will allow the introduced 1% rain leakage to dry towards outside to a safe level given the much smaller amount of wind-driven rain on South façade. Similar to the moisture load cases with vapour diffusion and air leakage, the removal of poly will bring in additional moisture from indoor and elevate the MC level in plywood sheathing from 10% to 14.5%.

Therefore, it is a safe choice of using a vapour permeable WRB and permeable exterior insulation with polyethylene vapour retarder as the proposed wall assembly. Given the high wind-driven rain load for this climate, the wall assembly won't be able to handle the 1% rain leakage load directly onto plywood for the North and East orientation. Therefore, care should be given in design and construction of the connection details to minimize the chances of rain penetration through the 2<sup>nd</sup> line of defense.

	VAPOUR DIFFUSION ONLY		AIR LEAKAGE		RAIN LEAKAGE, 1% ON PLYWOOD	
	w/poly	w/o poly	w/poly	w/o poly	w/poly	w/o poly
N	13.8	17.2	10.0	16.6	117.0	71.3
E	13.8	16.6	9.7	16.0	121.3	116.0
S	13.8	14.9	9.3	14.5	33.0	15.5

**TABLE 10:** MAXIMUM MC IN PLYWOOD SHEATHING WITH IMPERMEABLE WRB AND MINERAL WOOL EXTERIOR INSULATION

	VAPOUR DIFFUSION ONLY		AIR LEAKAGE		RAIN LEAKAGE, 1% ON PLYWOOD	
	w/ poly	w/o poly	w/ poly	w/o poly	w/ poly	w/o poly
N	10.2	16.2	10.6	15.8	101.0	59.6
E	9.9	15.5	10.3	17.9	115.9	115.9
S	9.5	13.9	9.8	13.6	10.0	14.5

**TABLE 11:** MAXIMUM MC IN PLYWOOD SHEATHING WITH PERMEABLE WRB AND EPS EXTERIOR INSULATION

Figure 12 and Figure 13 show the MC in plywood over the three-year simulation period for the wall assembly with impermeable WRB and the wall assembly with permeable WRB and EPS exterior insulation for the North and South orientation. The plots for the East orientation are similar to North orientation.

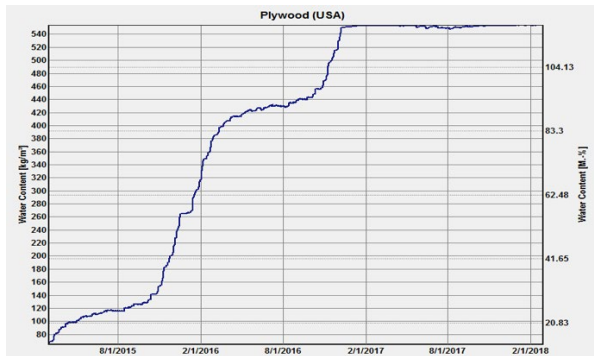


**FIGURE 12 A:** NORTH ORIENTATION: MC IN PLYWOOD SHEATHING WITH IMPERMEABLE WRB, 1% RAIN LEAKAGE ON PLYWOOD, WITH POLY

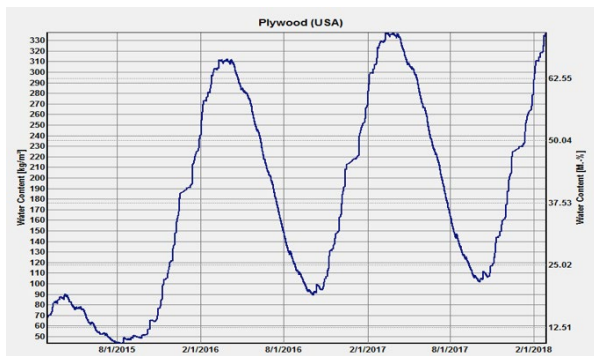


**FIGURE 12 B:** NORTH ORIENTATION: MC IN PLYWOOD SHEATHING WITH IMPERMEABLE WRB, 1% RAIN LEAKAGE ON PLYWOOD, WITHOUT POLY



**FIGURE 12 C:** SOUTH ORIENTATION: MC IN PLYWOOD SHEATHING WITH IMPERMEABLE WRB, 1% RAIN LEAKAGE ON PLYWOOD, WITH POLY

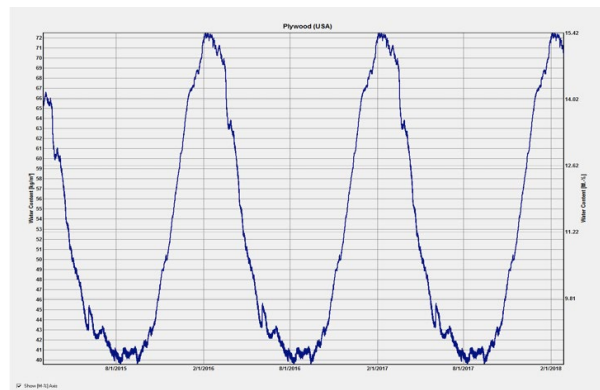


**FIGURE 12 D:** SOUTH ORIENTATION: MC IN PLYWOOD SHEATHING WITH IMPERMEABLE WRB, 1% RAIN LEAKAGE ON PLYWOOD, WITHOUT POLY

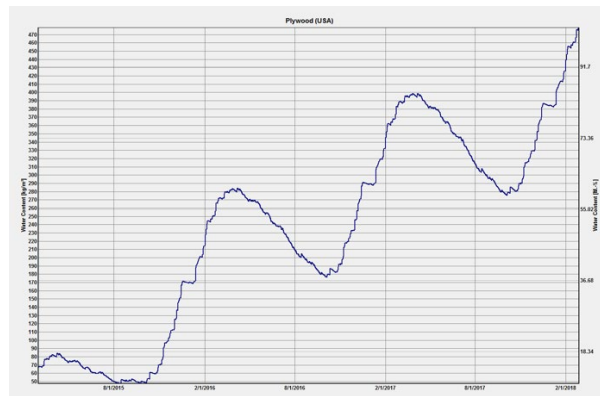


**FIGURE 13 A:** NORTH ORIENTATION: MC IN PLYWOOD SHEATHING WITH PERMEABLE WRB AND EPS EXTERIOR INSULATION, 1% RAIN LEAKAGE ON PLYWOOD, WITH POLY

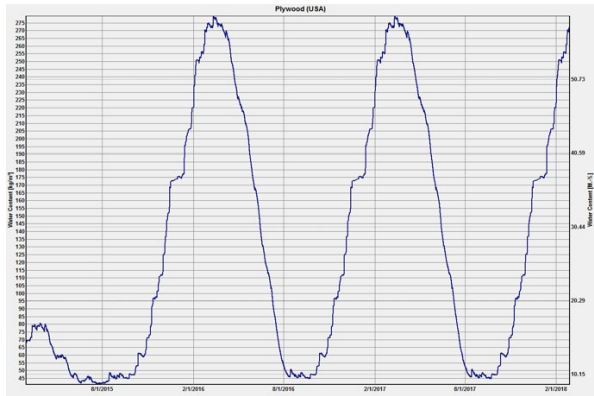


**FIGURE 13 B:** NORTH ORIENTATION: MC IN PLYWOOD SHEATHING WITH PERMEABLE WRB AND EPS EXTERIOR INSULATION WITH 1% RAIN LEAKAGE ON PLYWOOD, WITHOUT POLY

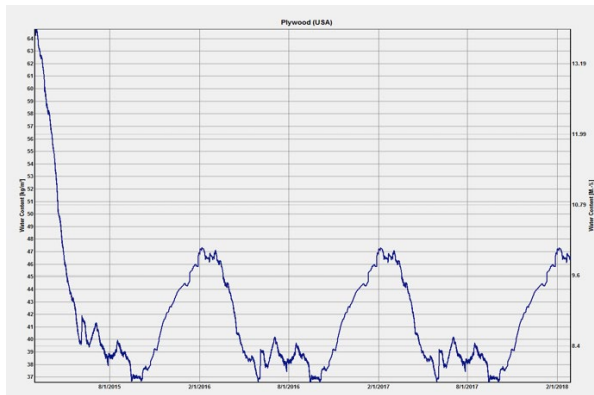


**FIGURE 13 C:** SOUTH ORIENTATION: MC IN PLYWOOD SHEATHING WITH PERMEABLE WRB AND EPS EXTERIOR INSULATION, 1% RAIN LEAKAGE ON PLYWOOD, WITH POLY

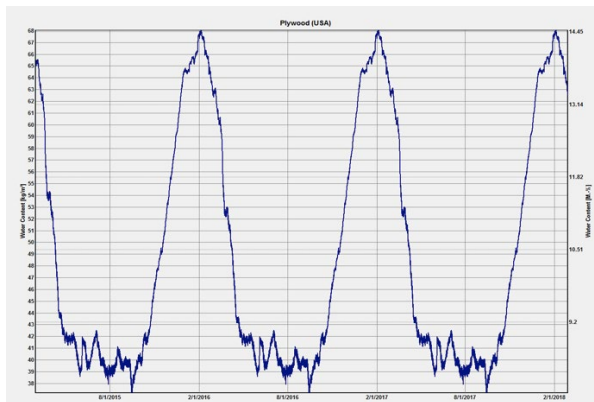


**FIGURE 13 D:** SOUTH ORIENTATION: MC IN PLYWOOD SHEATHING WITH PERMEABLE WRB AND EPS EXTERIOR INSULATION, 1% RAIN LEAKAGE ON PLYWOOD, WITHOUT POLY

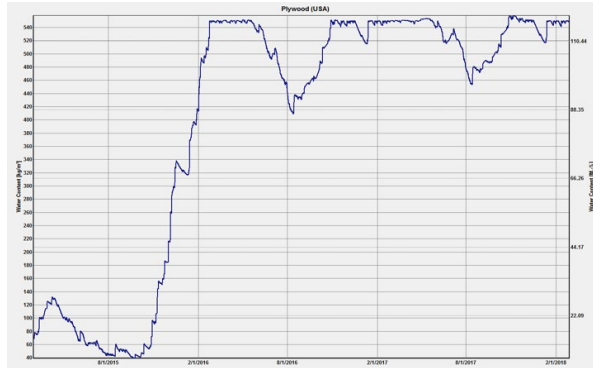
#### 4.2.5.2 Effect of cavity ventilation

Table 12 shows the maximum MC in the wood siding and the maximum MC in plywood sheathing when 1% rain leakage directly deposited onto plywood for the proposed wall assembly under different cavity ventilation rates. It can be seen that:

- For the South orientation, the increase of cavity ventilation from 0 ACH to 10ACH reduces the MC of the wood siding by 5.7%MC while further increase of cavity ventilation has little influence on the MC in wood siding. For the East and North façades, the increase of cavity ventilation from 0 ACH to 50ACH significantly reduces the MC of the wood siding from 94% to 27% for the North façade and from 74% to 29% for the East façade while further increase of cavity ventilation has little influence on the MC in wood siding. Therefore, for this particular climate, cavity ventilation helps keep the wood cladding drier for the façade receiving higher wind-driven rain, i.e. the East and the façade receiving higher solar radiation i.e. the South, however the effect is not as significant when the cavity ventilation rate is greater than 50ACH. Given that an air gap exists behind the wood cladding, even when no intentional top vent is provided, there will always be some air movement in the air cavity. Therefore, it is most unlikely that the MC level of the wood cladding MC level reaches as high as over 94%. The provision of rainscreen wall is more important to provide effective drainage for this climate. Given the damp conditions in the winter time, cavity ventilation may increase the moisture content level of plywood sheathing although very slightly. This is for the case when permeable WRB and permeable insulation is used without rain leakage.
- Cavity ventilation helps drying of the plywood when it is wet by rain penetration for the North facade more significantly when the cavity ventilation rate increased from 0 to 10ACH, further increases has little influence. As for the East orientation with the highest amount of wind-driven rain, the effect of ventilation drying is minimal. Figure 14 shows the MC in plywood over the three-year simulation period for 0ACH and 50ACH for the East orientation.

	MC IN WOOD CLADDING					MC IN PLYWOOD SHEATHING WITH 1% RAIN LEAKAGE ON PLYWOOD WITH POLY				
	0	10	50	100	200	0	10	50	100	200
N	94.3	45.7	27.1	26.6	25.7	115.9	42.5	37.8	36.4	36.4
E	74.3	48.6	29.3	27.1	27.1	120.2	117.0	110.6	106.4	102.1
S	17.7	12.0	12.6	12.0	12.0	10.9	9.4	9.6	9.8	9.8

**TABLE 12:** MAXIMUM MC (%) IN THE WOOD SIDING AND PLYWOOD SHEATHING IN THE PROPOSED WALL ASSEMBLY UNDER DIFFERENT CAVITY VENTILATION RATES



**FIGURE 14 A:** MC IN PLYWOOD SHEATHING WITH 1% RAIN LEAKAGE DEPOSITED ON PLYWOOD FOR THE EAST ORIENTATION WITHOUT CAVITY VENTILATION.

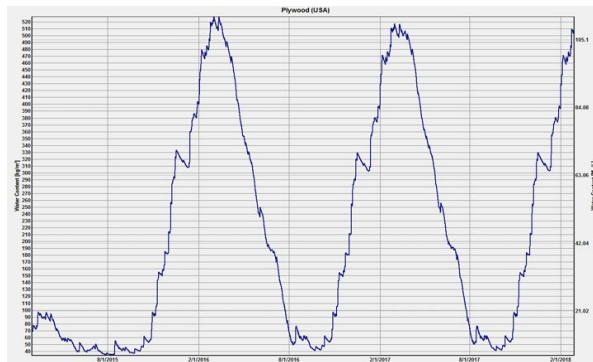


**FIGURE 14 B:** MC IN PLYWOOD SHEATHING WITH 1% RAIN LEAKAGE DEPOSITED ON PLYWOOD FOR THE EAST ORIENTATION WITH CAVITY VENTILATION OF 50ACH.

#### 4.2.5.3 Effect of air leakage

The air leakage amount of  $1.5\text{L}/\text{m}^2\cdot\text{s}$  representing the airtightness of an average building envelope assembly (ASHRAE, 2013) under 75 Pa is introduced into the stud cavity. Field measurements showed that at the 24<sup>th</sup> floor, the sustained air pressure due to stack effect could be as high as 150Pa under a 40°C temperature differential (-18°C outdoor and 21°C indoor) (Ganguli and Dalglish, 1988). Therefore an assumption of air leakage rate under 75Pa is reasonable for the proposed tall wood building for Vancouver climate, which is mild in the winter. It is assumed that the amount of air leakage deposited in the centre of the stud cavity. As shown in Table 9 - 11, the introduction of air exfiltration is insignificant

on the MC of plywood sheathing and the trend is inconsistent for wall assemblies with different configurations. For the proposed wall assembly with permeable WRB and mineral wool insulation and the wall assembly with permeable WRB and EPS insulation, the introduction of air exfiltration slightly increases the MC level in plywood when poly is used as vapour barrier while decreases the MC level in plywood when poly is removed. For the wall assembly with impermeable WRB wall assembly, the introduction of air exfiltration slightly decreases the MC level in plywood for both cases with and without poly as vapour retarder. The reason for decreasing MC in plywood is probably due to the heat brought by the air exfiltrated from indoor increased the sheathing temperature, therefore reduced MC level under the conditions that the plywood sheathing temperature is above the dew point of indoor air and there is no risk for condensation (Figure 15). For permeable wall assembly and EPS wall assembly, the higher permeability allows moisture being brought in from outdoor as well.

Analysis comparing the surface temperature of the interior side of the plywood to the dew point of indoor air (Figure 15) indicate that the plywood interior surface temperature is always higher than the dew point of indoor air, therefore, there is no risk for condensation at plywood sheathing due to the elevated plywood temperature by the application of 50.8mm exterior insulation.

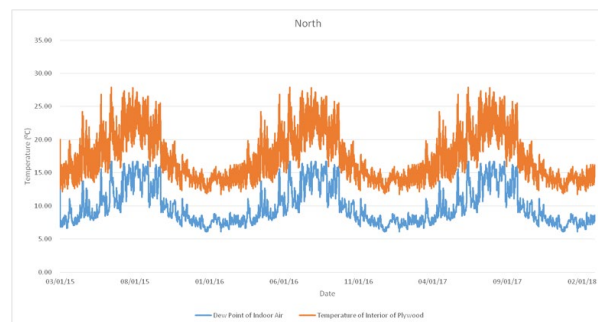


**FIGURE 15:** CONDENSATION RISK CHECK AT THE INTERIOR SURFACE OF PLYWOOD DUE TO AIR EXFILTRATION FOR NORTH ORIENTATION.

#### 4.2.5.4 Effect of rain leakage

According to ASHRAE 160P (ASHRAE, 2009), 1% of rain deposited on the façade is assumed to have passed through the first line of defense and deposited on the WRB. A second scenario assuming that the 1% of rain has passed through the second line of defense, the WRB, deposited directly on the sheathing. As indicated by the maximum MC in plywood sheathing listed in Table 9, simulation results showed that

- The 1% of rain deposited on the WRB can be well-managed by the wall assemblies, there is no noticeable increase of MC in the plywood sheathing.
- When 1% of rain deposited directly onto plywood sheathing, depending on the orientation, significantly higher MC observed in the plywood sheathing for the North and East façade. As shown in Figure 10 and 11, for the North façade, the MC is as high as 36.4% in plywood sheathing, while for the East façade, the MC is as high as 102.1% in the plywood sheathing. For the South façade, there is no difference than the case without rain leakage. This is because of the much less wind-driven rain exposure of the south façade. As shown in Table 7, the WDR on the south façade is only 5% of the amount on the North façade and 2% of the amount on the East façade. With the much smaller amount of rain and higher level of solar radiation, the plywood sheathing can remain at safe MC level.

#### 4.2.5.5 Effect of vapour permeability of exterior insulation and WRB

As discussed in the section “effect of vapour barrier”, in general the MC level in plywood sheathing for the wall assembly with impermeable WRB and the assembly with permeable WRB and EPS exterior insulation is higher than the case with permeable WRB and mineral wool exterior insulation when the poly is removed for both vapour diffusion and air leakage cases. The North orientation is the worst case for all moisture loads except for when 1% rain leakage directly deposited on plywood sheathing.

As shown in Tables 9-11, with 1% rain leakage deposited directly onto plywood sheathing, these two assemblies have extremely high MC level in plywood sheathing after the three-year simulation periods for the North and East orientation. The removal of polyethylene helps drying towards inside, but the effect is minimal for the East orientation and considerable for North orientation but the level of MC is still in the range of 60-70%MC. For the South orientation because of the much smaller amount of wind-driven rain exposure, the wall assembly with permeable WRB and EPS exterior insulation can handle the 1% moisture penetration and the MC in plywood is below 15% while for the wall assembly with impermeable WRB, only when the polyethylene is removed, the MC in plywood can reach a safe level of 15.5%.

Therefore, the safer choice of wall assembly is to use a vapour permeable WRB and permeable exterior insulation with polyethylene vapour barrier. The impermeable or less permeable wall assembly has less capacity handling the introduced rain leakage moisture load. Given the high wind-

driven rain load for this climate, especially the high wind-driven rain exposure in the North and East orientation, the impermeable or less permeable wall assembly won't be able to handle the rain leakage load even when a “double vapour barrier” situation is avoided by removing polyethylene. The coincidence of rainy season with cold temperature does not allow much drying towards indoor.

#### 4.2.5.6 Effect of wind-driven rain exposure and cladding water absorption coefficients

Both the driving rain coefficient R2 and water absorption coefficient of the cladding are changed to investigate the sensitivity of cladding MC to the wind-driven rain exposure. Silvia Western Red Cedar is chosen as the wood cladding. Given that no detailed hygric material properties available for this specific product and the default material properties in WUFI database is specified. The western red cedar has a water absorption coefficient of  $0.001 \text{ kg/m}^2 \cdot \text{s}^{0.5}$  (A-value listed in Table 13). A protection coating is typically applied on the wood siding, assuming this protection coating will reduce the water absorption coefficient of the western red cedar siding by half while other material properties remains the same.

As shown in Table 13, for the South orientation both doubling the driving rain coefficient and cladding water absorption coefficient have minimal influence on the MC of cladding, while the effect of doubling driving rain and cladding water absorption coefficients is similar for the North and East orientations and the influence of water absorption coefficient is more significant than the driving rain coefficient. For example, the doubling of driving rain load increases the cladding MC by about 1.4% while doubling the water absorption coefficient increases the cladding MC by 7.0% for the North façade. The effect on the East façade is similar.

Figure 16 shows the MC profile in western red cedar cladding. For North and East façades the MC level in the wood siding remains above 20% over the winter months. When the water absorption coefficient of the wood siding is reduced by half, the maximum MC in the cladding is at about 20%, therefore, the MC level in the wood siding remains within a safe range. The MC level in South façade is within a safe range year round. Detailed hygric material properties for the specific produce is needed to obtain more accurate analyses.

A-VALUE	WESTERN RED CEDAR, A = 0.001 kg/m <sup>2</sup> ·s <sup>0.5</sup>			WESTERN RED CEDAR A = 0.0005 kg/m <sup>2</sup> ·s <sup>0.5</sup>		
	default	half	double	default	half	double
R2						
N	25.7	22.8	27.0	18.8	17.7	20.0
E	26.3	24.3	27.4	18.8	17.1	20.0
S	12.0	11.7	12.0	11.4	11.4	11.5

TABLE 13: MAXIMUM MC (%) IN THE WOOD SIDING WITH RESPECT TO DRIVING RAIN COEFFICIENTS AND WATER ABSORPTION COEFFICIENTS

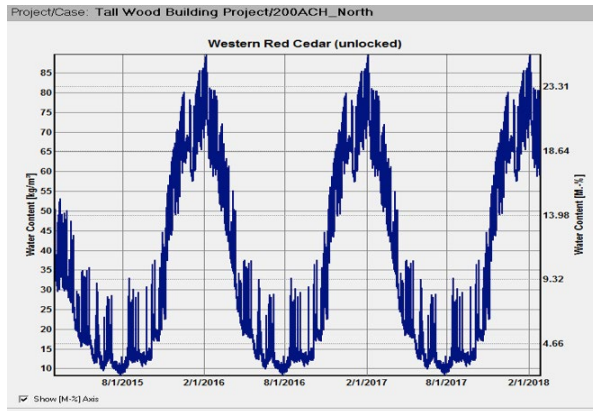


**FIGURE 16 A:** NORTH FAÇADE: MOISTURE CONTENT IN THE WESTERN RED CEDAR WOOD SIDING

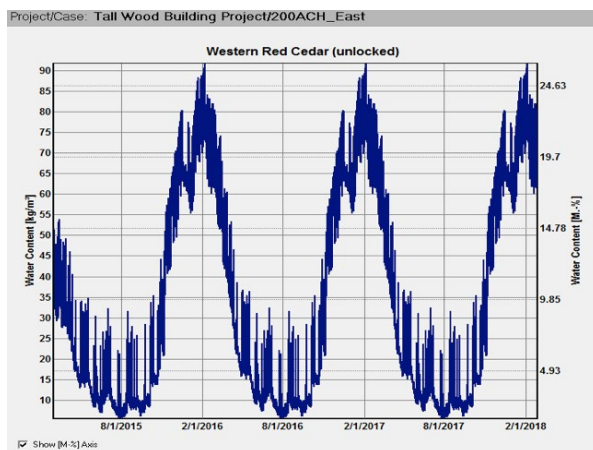


**FIGURE 16 B:** EAST FAÇADE: MOISTURE CONTENT IN THE WESTERN RED CEDAR WOOD SIDING

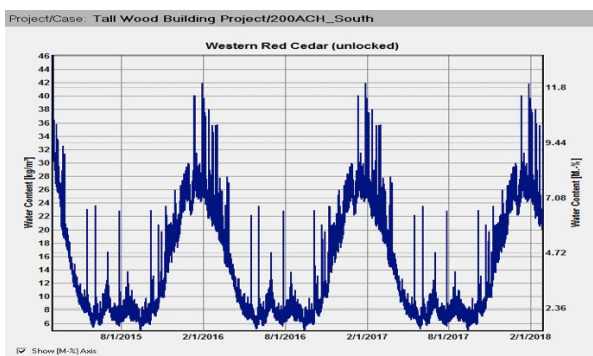


**FIGURE 16 C:** SOUTH FAÇADE: MOISTURE CONTENT IN THE WESTERN RED CEDAR WOOD SIDING

In summary, the proposed wall assembly can manage the moisture loads from vapour diffusion, air leakage and rain penetration passing through the first line of defense i.e. cladding. The critical aspect of the building envelope design is to manage the rain penetration passed through the 2<sup>nd</sup> line of defense, i.e. WRB, the rain water deposited directly on the

sheathing. Given this particular site, East and North façade have the highest risks with rain leakage induced moisture damage because of the higher amount of wind-driven rain in the East orientation and lower solar radiation available for drying in the North orientation. For the South and West façade, 1% of rain can be well managed by the wall assembly.

The application of impermeable WRB or less permeable exterior EPS insulation will reduce significantly the drying outwards when 1% rain leakage is assumed on the plywood sheathing although these two wall assemblies can handle the vapor diffusion and air leakage moisture loads similarly well to the proposed permeable wall assembly. The MC level in plywood remained extremely high after three-year simulation periods for both North and East façades even when the polyethylene as the vapour barrier is removed to eliminate “double vapor barrier” situation. For this particular climate where the rainy season is in the wintertime, there is little drying potential towards indoor. Therefore, for the tall wood building located in North Vancouver, a permeable exterior insulation and WRB with an interior vapour retarder is recommended to allow incidental rainwater leaked to the sheathing to dry to outside.

The MC levels in the western red cedar wood siding remained above 20% over the winter months for the North and East façade. The MC in wood siding can be reduced to below 20% when the water absorption coefficient of the wood siding is half of the default value. To maintain a durable cladding, a permeable protection coating that reduces the water absorption but does not inhibit drying of the wood siding should be applied. To extend the lifetime of the finish, the wood siding should also be back primed if possible (FPL, 2004).

Given the high amount of wind-driven rain exposure on North and East façade, the reduction of wind-driven rain exposure by building form and details such as overhangs, balcony projections, canopies should be considered. In this proposed tall wood building, the provision of balconies on the North side can help reduce the wind-driven rain exposure. Most importantly, great efforts should be made to ensure that the building envelope is well constructed to avoid any rainwater leakage passing through the 2<sup>nd</sup> line of defense.

## 5. FINAL DESIGN DETAIL DRAWINGS

This section presents the design details of building envelopes. A well-designed and constructed connection detail is critical for the durability of building envelopes. Building science principles and best practices are closely followed for the development of these connection details, in particular Chapter 6-Building Envelope Design: Technical guide for the design and construction of tall wood buildings in Canada.

As discussed earlier, sound building science principles should be followed to design any type of building envelopes. The challenge for the tall wood building design is to make sure that the wood-frame building envelope systems typically used in low-rise residential building can handle the greater environmental loads, i.e., wind, rain, and air leakage. Therefore, it is critical for the success of tall wood building to ensure the integrity of building envelopes through proper detailing. The

connection details need to provide:

- continuity of insulation to minimize thermal bridges
- continuity of air barrier to minimize air leakage
- continuity of drainage planes, i.e. 2<sup>nd</sup> line of defense including WRB, flashing, etc.
- accommodation for movement

### 5.1 ACCOMMODATION FOR MOVEMENT

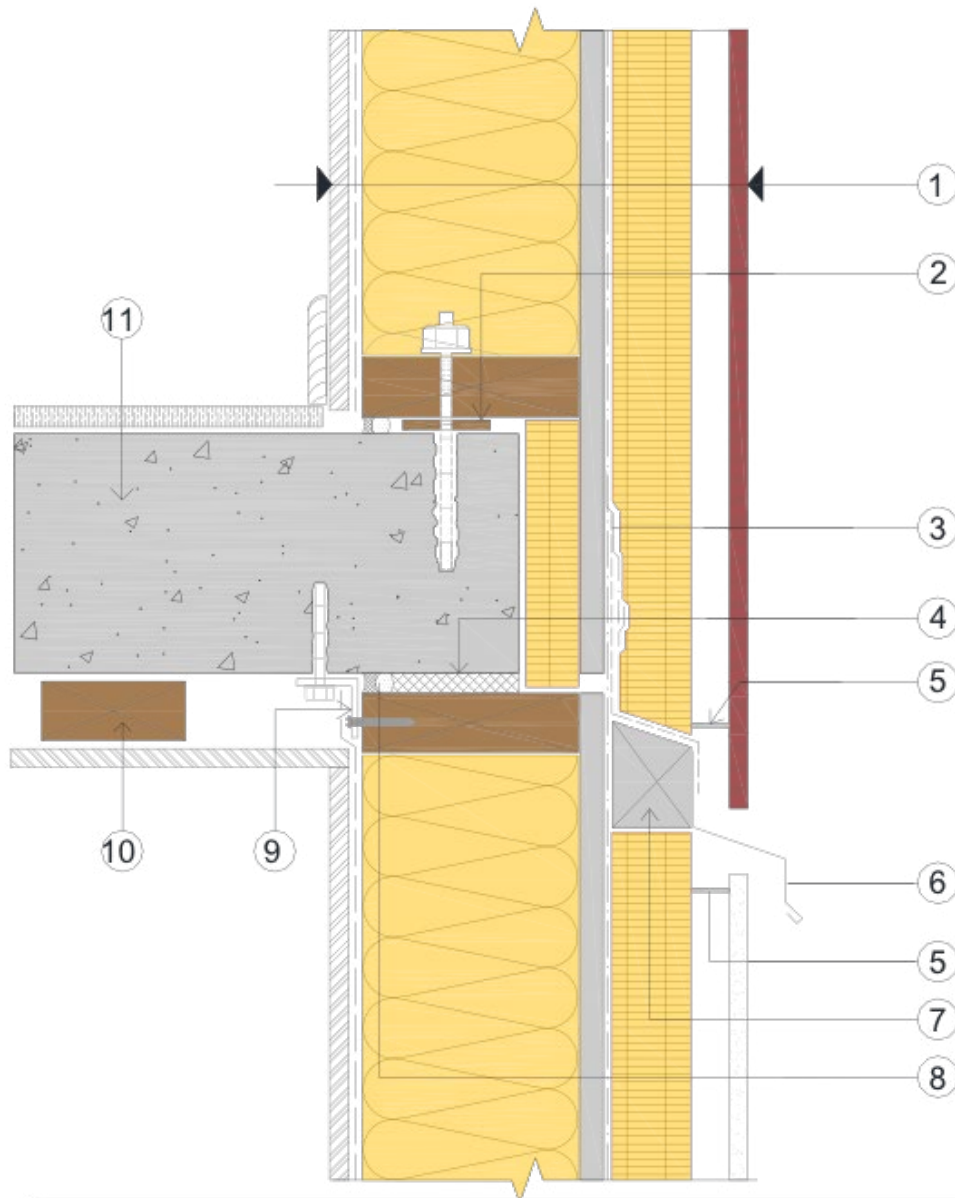
Lack of movement joints, or improperly designed, installed and maintained joints are one of the common causes for building envelope failures. Wood as a hygroscopic material, its moisture content changes with the change of ambient relative humidity, which results in its dimensional change. The compatibility of wood framing with materials that have different characteristics need to be considered. As per building code's requirement, S-Dry lumber should be used (MC < 19%) to minimize shrinkage. Most importantly, wood-frame needs to be kept dry to avoid moisture damage and dimensional changes.

The wood-frame wall assembly proposed in this tall wood building is used as a non-load bearing infill wall, which is similar to low-rise construction and the expected shrinkage resulted from bottom and top plates should be similar to low-rise buildings. The wall connection details, however, need to accommodate the movement of the primary structure. The final proposed floor is a combined glulam and concrete structure, therefore, the shrinkage resulted from the floor should consider the initial dimension change of concrete slab due to curing and creep in addition to the dimensional change due to structural loads. The wood-frame is a non-load bearing infill wall, therefore, soft joints need to be provided between wood frame and concrete slab, and between horizontal cladding panels to accommodate the movement due to thermal and moisture expansion/contraction, and structural loads.

### 5.2 DETAILING AT CRITICAL ENCLOSURE INTERFACES

The connection details included in this section are adapted from drawings presented in "Technical guide for the design and construction of tall wood buildings in Canada, Ch. 6-building envelope design". The connection details at critical enclosure interfaces include:

- Wall and floor slab connection
- Window/wall sill
- Window/wall head
- Window Jam
- Roof parapet walls



**LEGEND**

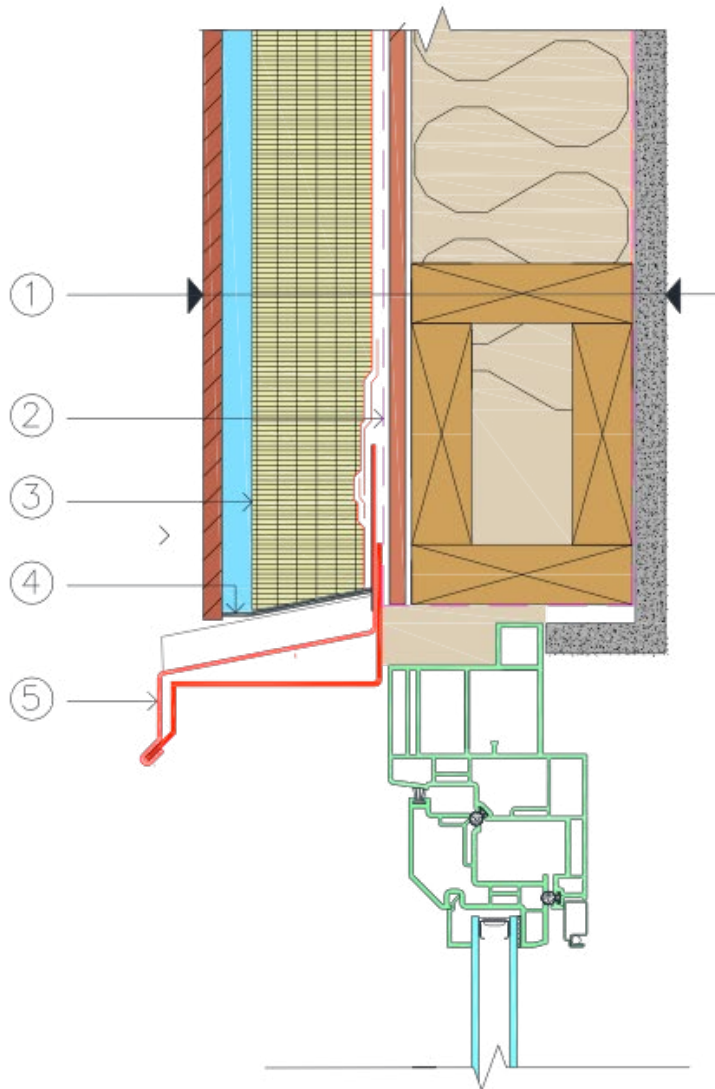
**1. Wall Assembly**

- Cladding (Top: Engineered wood; Below: Fibre cement panel)
- 20 mm Ventilated air space & wood strapping
- 50.8 mm (2") Semi-rigid mineral wool insulation
- Vapour permeable sheathing membrane
- 13 mm Plywood Sheathing
- Wood framing 38X140mm (2X6)
- 140 mm Mineral wool batt insulation
- Polyethylene
- 12.5mm Gypsum board

**2. Shims**

- 3. Vapour permeable sheathing membrane lapped over & taped to membrane flashing
- 4. Movement allowance joint
- 5. Insect screen
- 6. Pre-finished metal flashing
- 7. Shear block
- 8. Backer rod & sealant
- 9. Slotted metal attachment clip
- 10. Wood furring
- 11. Concrete structural slab

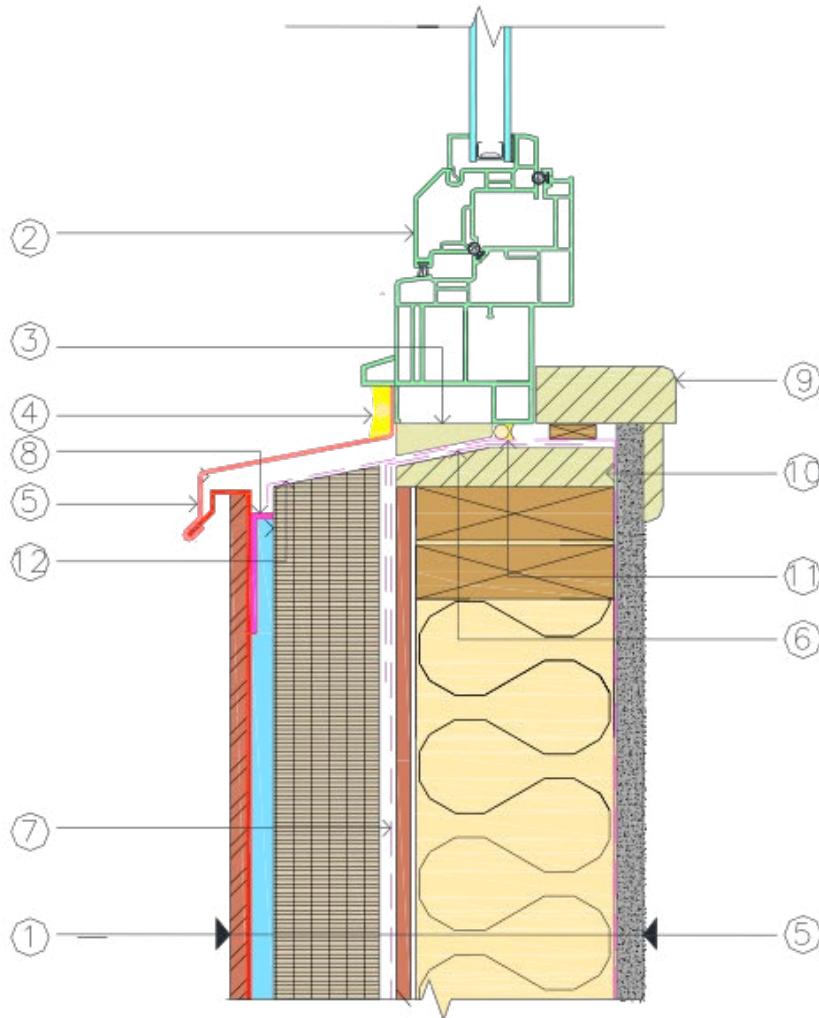
Floor slab/wall connection



**LEGEND**

1. Wall Assembly
  - Cladding (Top: Engineered wood; Below: Fibre cement panel)
  - 25 mm Ventilated air space & wood strapping
  - 50.8mm (2") Semi-rigid mineral wool insulation
  - Vapour permeable sheathing membrane
  - Plywood Sheathing
  - Wood framing 38X140mm (2X6)
  - Mineral wool batt insulation
  - Polyethylene
  - Gypsum board
2. Vapour permeable sheathing membrane lapped over & taped to membrane flashing
3. Shear block
4. Insect screen
5. Pre-finished metal flashing

WINDOW HEAD


**LEGEND**
**1. Wall Assembly**

Cladding (Top: Engineered wood; Below: Fibre cement panel)  
 25 mm Ventilated air space & wood strapping  
 50.8mm (2") Semi-rigid mineral wool insulation  
 Vapour permeable sheathing membrane  
 Plywood Sheathing  
 Wood framing 38X140mm (2X6)  
 Mineral wool batt insulation  
 Polyethylene  
 Gypsum board

**2. Window assembly**

5. Pre-finished metal flashing with end dams

6. Sub-sill foil-faced membrane flashing

7. Vapour permeable sheathing membrane

8. Insect screen

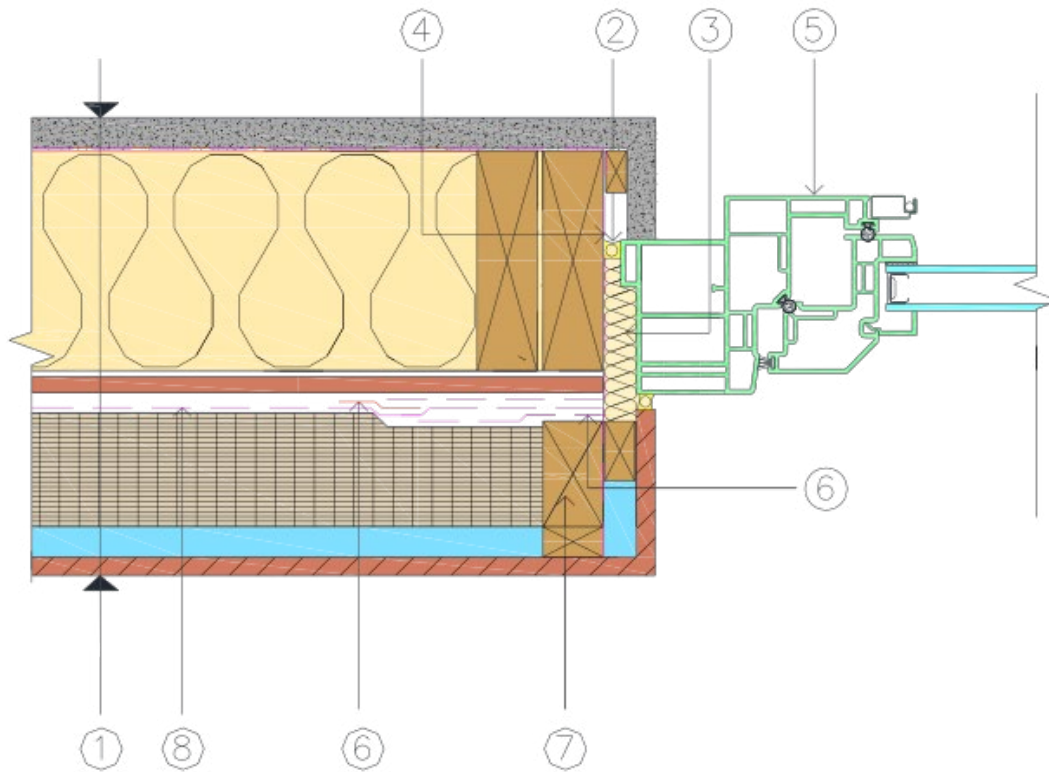
10. Sloped blocking

11. Backer rod & sealant

12. Foil-faced membrane skirt flashing

**3. Intermittent shims**
**4. Sealant**

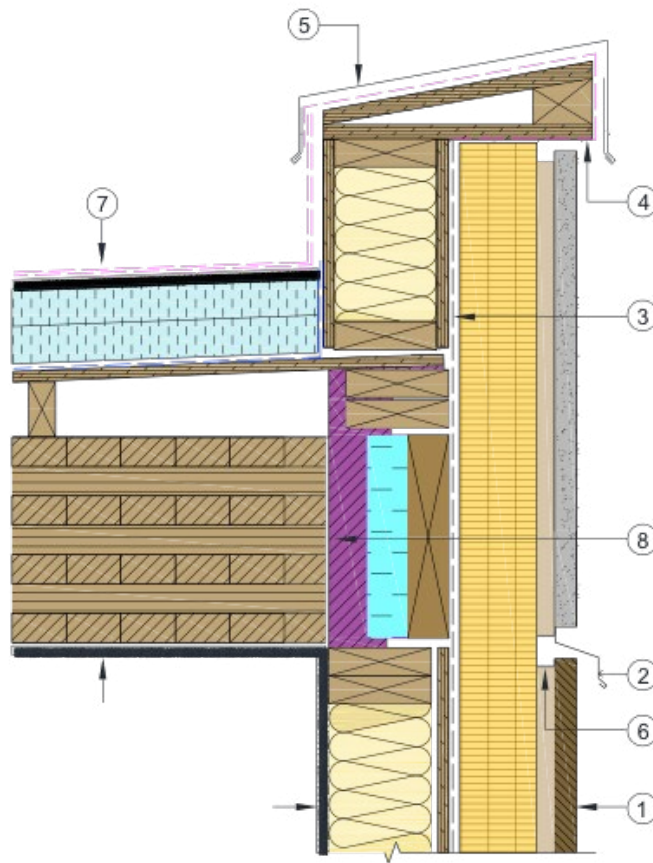
## WINDOW SILL



LEGEND

1. Wall assembly
  - Cladding (Top: Engineered wood;Below: Fibre cement panel)
  - 25 mm Ventilated air space & wood strapping
  - 50.8mm (2") Semi-rigid mineral wool insulation
  - Vapour permeable sheathing membrane
  - Plywood Sheathing
  - Wood framing 38X140mm (2X6)
  - Mineral wool batt insulation
  - Polyethylene
  - Gypsum board
2. Backer rod & sealent
3. Insulation
4. Foil tape
5. Window assembly
6. Tape
7. Wood blocking (p.t)
8. Vapour permeable sheathing membrane

WINDOW JAMB

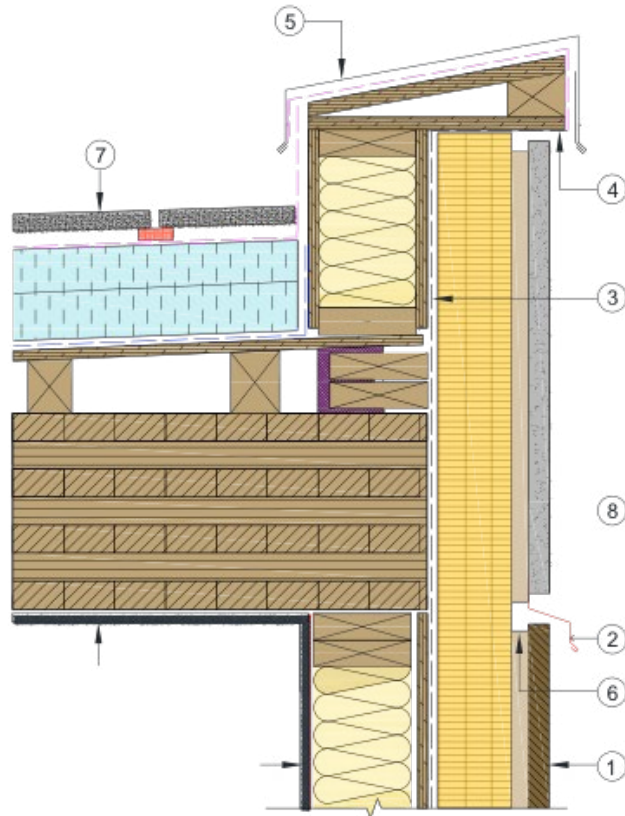

**LEGEND**
**1. Wall Assembly**

Cladding (Top: Fibre cement; Below: Engineered wood)  
 19 mm wood strapping  
 50.8 mm (2") Semi-rigid mineral wool insulation  
 Vapour permeable sheathing membrane  
 13 mm Plywood Sheathing  
 Wood framing 38X140mm (2X6)  
 140 mm Mineral wool batt insulation  
 Polyethylene  
 12.5mm Gypsum board

**2. Cladding transition flashing**
**3. Sheathing membrane lapped and taped**
**4. Foil faced self adhered membrane**
**5. Metal cap flashing**
**6. Insect screen**
**7. Roof Assembly**

Roof membrane  
 Protection board  
 102 mm Polyisocyanurate insulation  
 Self adhered membrane  
 Sheathing  
 Air cavity with cross purlins to provide roof slope  
 CLT 7-ply  
 Gypsum board

**8. Extruded polystyrene insulation and spray-in-place foam at edges**
**CONVENTIONAL ROOF**



**LEGEND**

**1. Wall Assembly**

- Cladding (Top: Fibre cement; Below: Engineered wood)
- 19 mm wood strapping
- 50.8 mm (2") Semi-rigid mineral wool insulation
- Vapour permeable sheathing membrane
- 13 mm Plywood Sheathing
- Wood framing 38X140mm (2X6)
- 140 mm Mineral wool batt insulation
- Polyethylene
- 12.5mm Gypsum board

**2. Cladding transition flashing**

**3. Sheathing membrane lapped and taped**

**4. Foil faced self adhered membrane**

**5. Metal cap flashing**

**6. Insect screen**

**7. Roof Assembly**

- Concrete paver
- Filter fibre
- 102 mm Extruded polystyrene insulation
- Self adhered membrane
- Sheathing
- Air cavity with 2X6 wood frame to provide roof slope
- CLT 7-ply
- Gypsum board

**8. Extruded polystyrene insulation and spray-in-place foam at edges**

**INVERTED ROOF**

## 6. CONCLUSIONS AND FUTURE WORK

The building envelope design is carried out for a conceptual twenty-story tall wood building situated in North Vancouver, a location with high wind and rain exposure. Sound building science principles and best practices are applied in selecting materials, building envelope components and systems to ensure long-term durability in addition to meeting higher energy efficiency, fire, structural, architectural, and maintenance requirements. The wall assembly chosen is an infill wood-frame with split insulation with an effective R-value 25% better than the requirements by NEBC 2011. Non-combustible fiber cement board is chosen as the main cladding material with 30% engineered wood cladding. A CLT roof assembly, with two options, conventional and protected membrane, is designed. Chapter 6 of the “Technical guide for designing tall wood buildings in Canada” is used as the main reference for developing the connection details

Historical weather data from Environment Canada was acquired for the analysis of the wind-driven rain exposure of the proposed building site. Extensive hygrothermal simulations were carried out to evaluate the moisture damage risks for the proposed wood-frame wall assemblies. Recommendation on the proper design and selection of building envelope assemblies for the proposed tall wood building is provided.

- The proposed wall assembly can manage the moisture loads from vapour diffusion, air leakage and rain penetration passing through the first line of defense i.e. cladding. The critical aspect of the building envelope design is to manage the rain penetration passed through the 2<sup>nd</sup> line of defense, i.e. WRB, the rainwater deposited directly on the sheathing. Given this particular site, East and North façade have the highest risks with rain leakage induced moisture damage because of the higher amount of wind-driven rain in the East orientation and lower solar radiation available for drying in the North orientation. For the South and West façade, 1% of rain can be well managed by the wall assembly. Therefore, for the tall wood building located in North Vancouver, a permeable exterior insulation and WRB with an interior vapour barrier is recommended to allow incidental rainwater leaked to the sheathing to dry to outside.
- The MC levels in the western red cedar wood siding remained above 20% over the winter months for the North and East façade. The MC in wood siding can be reduced to below 20% when the water absorption coefficient of the wood siding is reduced to half of the default value. To maintain a durable cladding, a permeable protection coating that reduces the water absorption but does not inhibit drying of the wood siding should be applied. To extend the lifetime of the finish, the wood siding should also be back primed if possible.
- Given the high amount of wind-driven rain exposure on North and East façade, the reduction of wind-driven rain exposure by building form and details such as overhangs, balcony projections, canopies should

be considered. Most importantly, great efforts should be made to ensure that the building envelope is well constructed to avoid any rainwater leakage passing through the 2<sup>nd</sup> line of defense.

### Future work

- The current architectural design includes balconies on the North façade allowing residents to enjoy the mountain view, which can reduce the wind-driven rain exposure. There is no balcony or canopy included on the east façade, which has the highest wind-driven rain exposure. Overhangs could be considered to add to the east façade to reduce the wind-driven rain exposure, especially at the upper level of the façade. Coordination with structural team is required to ensure that the overhang will be properly designed to sustain wind loads.
- A CLT balcony is suggested for consideration. Further design of the balcony connection detail is required to ensure sound structural connection with the concrete slab, elimination of thermal bridges, provision of capillary break between concrete slab and the CLT balcony, waterproofing and provisions for easy repair and replacement. Moisture damage risk analyses could also be carried out through 2-D hygrothermal simulations to ensure moisture safety.
- For more accurate prediction of the hygrothermal performance of the wood-frame wall assembly, a typical low-rise wall assembly, to be used on a twenty-story tall building, detailed hygric material properties for the specific product such as the Sivia western red cedar siding will be needed.

In conclusion, durable wood-frame envelope systems with higher energy efficiency are possible for tall wood building for a high moisture load region with a properly designed, carefully constructed, and properly maintained building envelope system.

## 7. ACKNOWLEDGEMENTS

We would like to acknowledge the consultation received from Mr. Robert Drew from Perkins+Will, and Dr. Jieying Wang from FPIInnovations. We also thank graduate students at Concordia University, Mr. Uzzwal Kumar Deb Nath, Ms. Angel Lam and Ms. Stuti Bhatkulikar for their assistance in carrying out the wind-driven rain and hygrothermal analyses, and providing the AutoCad drawings.

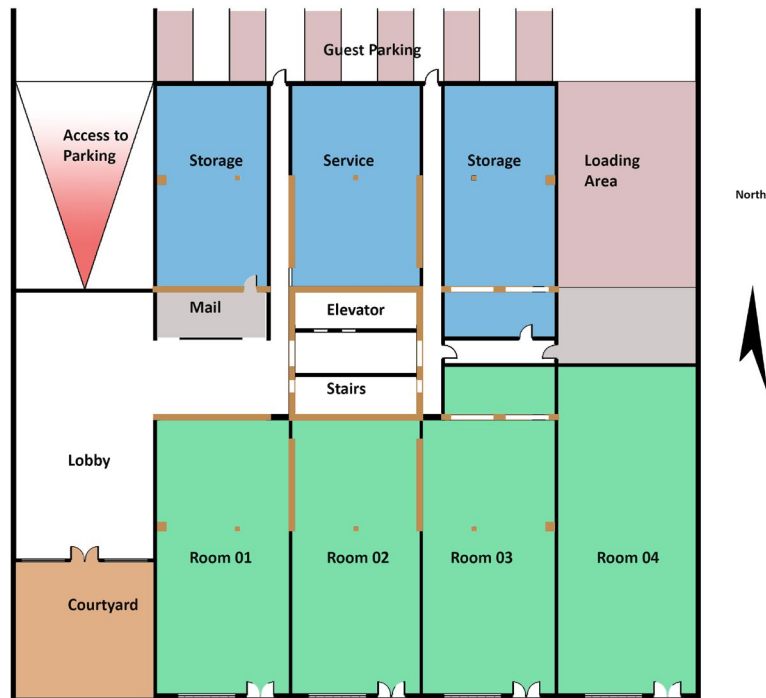
## REFERENCES

- ASHRAE. (2009). Criteria for moisture-control design analysis in buildings. ANSI/ASHRAE Standard 160-2009. American Society of Heating, Refrigeration and Air Conditioning Engineers, Atlanta, GA.
- ASHRAE. (2009). Handbook of Fundamentals. American Society of Heating, Refrigeration and Air Conditioning Engineers, Atlanta, GA.
- ASHRAE. (2011). Standard for the design of high performance, green buildings except low-rise residential buildings. ASHRAE 189.1-2011. American Society of Heating, Refrigeration and Air Conditioning Engineers, Atlanta, GA.
- ASHRAE. (2013). Energy Standard for Buildings Except Low-Rise Residential Buildings. ANSI/ASHRAE/IES Standard 90.1-2013. American Society of Heating, Refrigeration and Air Conditioning Engineers, Atlanta, GA.
- British Columbia Building Code (2012). Office of Housing and Construction Standards. Ministry of Energy, Mines and Natural Gas, Province of British Columbia.
- Hutcheon N B (1963). Canadian Building Digest 48: requirements for exterior walls. IRC, National Research Council. Retrieved from [http://web.mit.edu/parmstr/Public/NRCan/CanBldgDigests/cbd048\\_e.html](http://web.mit.edu/parmstr/Public/NRCan/CanBldgDigests/cbd048_e.html)
- EN15026-2007. (2007) Hygrothermal performance of building components and building elements. Assessment of moisture transfer by numerical simulation. European standard.
- FPIinnovations (2013). Guide for Designing Energy-Efficient Building Enclosures for Wood-Frame Multi-Unit Residential Buildings in Marine to Cold Climate Zones in North America. FPIinnovations.
- Ganguli U, Dalgliesh W A (1988). Wind pressure on open rainscreen walls: Place Air Canada. Journal of Structural Engineering, Vol. 114, No.3, pp. 642-656.
- Ge H, Krpan R (2009) Wind-driven Rain Study in the Coastal Climate of British Columbia. British Columbia Institute of Technology. Internal research report.
- ISO (2009). Hygrothermal performance of buildings - Calculation and presentation of climatic data - Part 3: Calculation of a driving rain index for vertical surfaces from hourly wind and rain data. ISO 15927-3:2009, International Standards Organization, Geneva, Switzerland.
- NECB 2011. National Energy Code of Canada for Buildings. National Research Council Canada, Ottawa, ON.
- Oke, T R, Hay J E, (1998). The climate of Vancouver (2nd ed., Vol. 50). Department of Geography, University of British Columbia, Vancouver, BC
- WUFI Pro 5.1. Fraunhofer IBP. (2010). Retrieved 05 20, 2012, from WUFI: <http://www.wufi-pro.com/Silva Panel Canada Ltd.> (n.d.). Retrieved from <http://silvapanel.com>
- SWISSPEARL. (2013). SWISSPEARL Design and Installation Manual. Retrieved from <http://swisspearl.com>

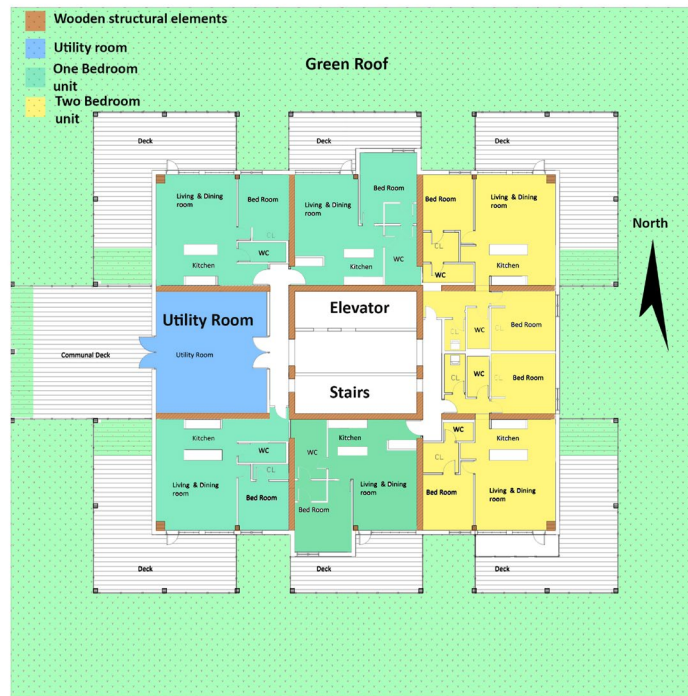
APPENDIX A

# ARCHITECTURAL DRAWINGS

---



Podium Floor Plan  
Scale: 1/50



Tower Floor Plan Level One  
Scale: 1/50



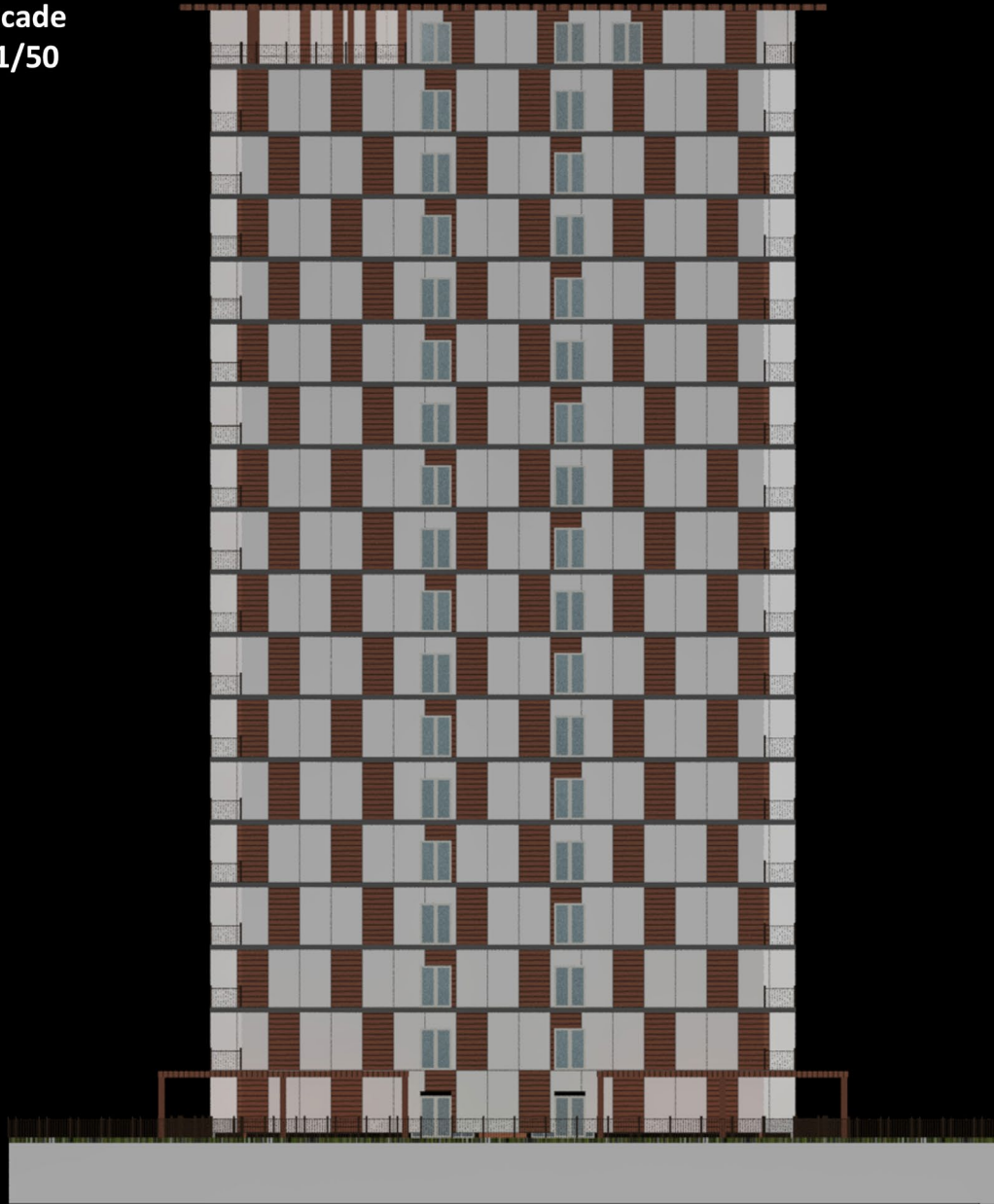
**Tower Floor Plan Level Two - Eighteen**  
 Scale: 1/50



**Penthouse Floor Plan**  
 Scale: 1/50



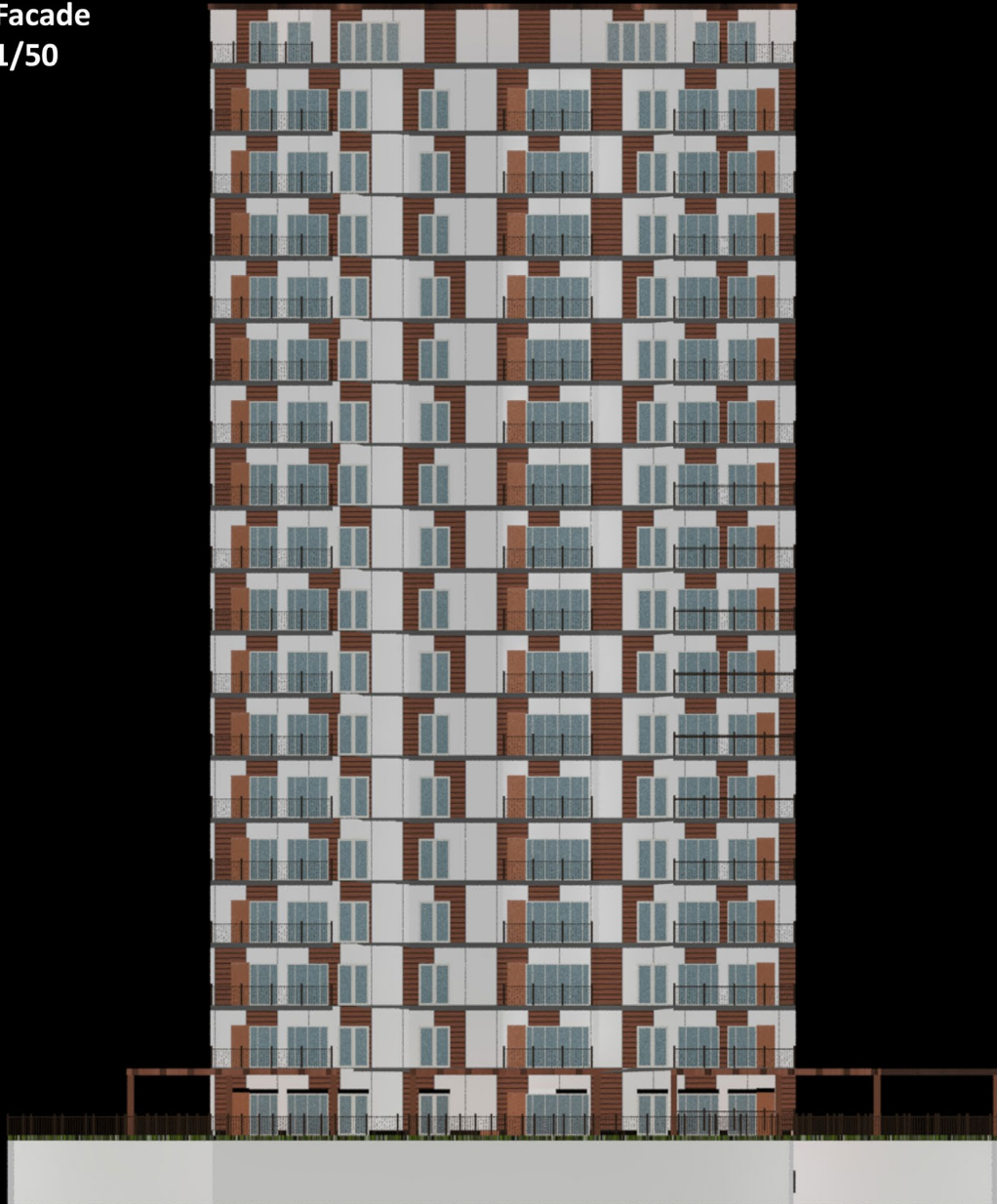
East Facade  
Scale: 1/50



1m 2m 5m 10m



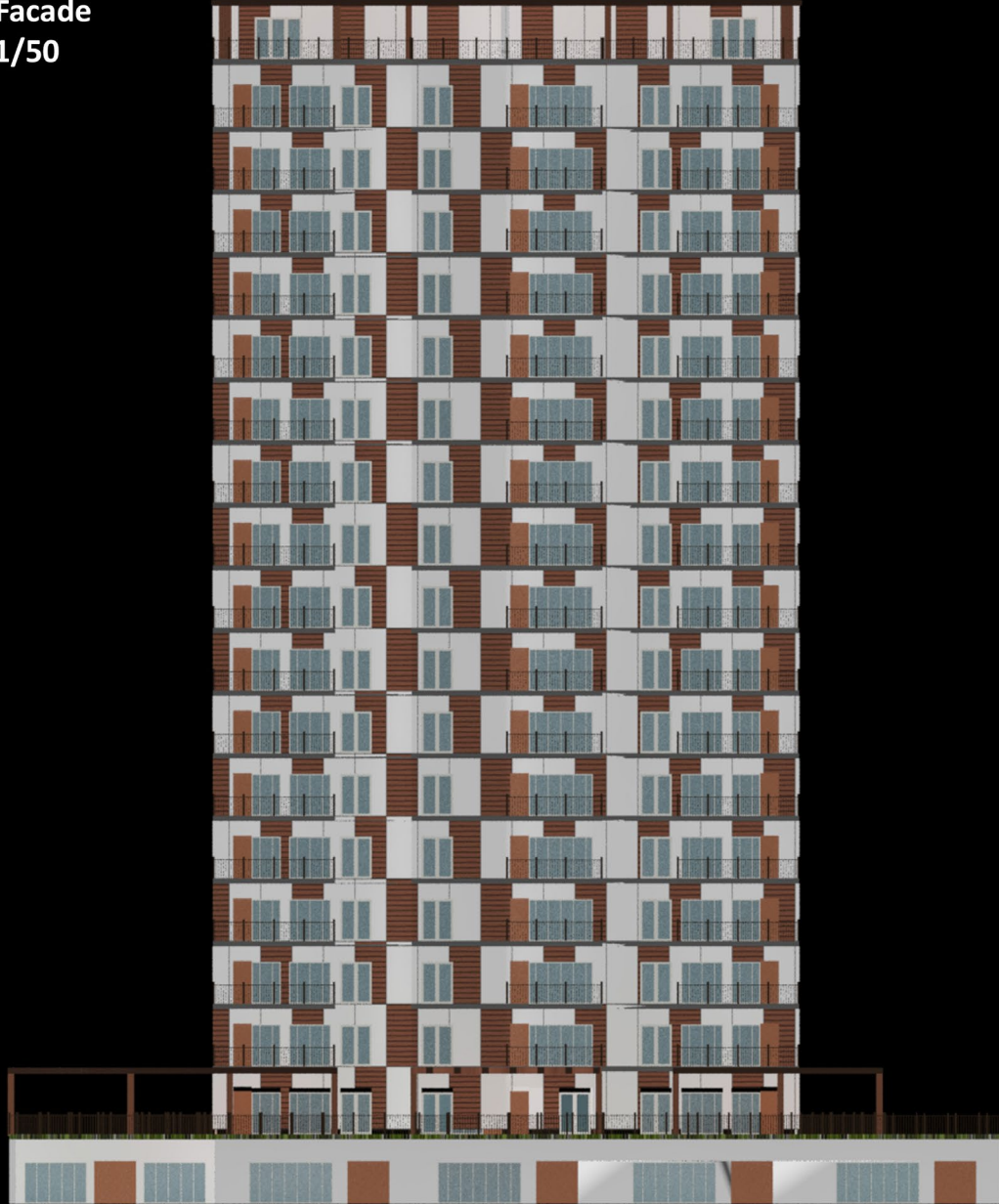
North Facade  
Scale: 1/50



1m 2m 5m 10m

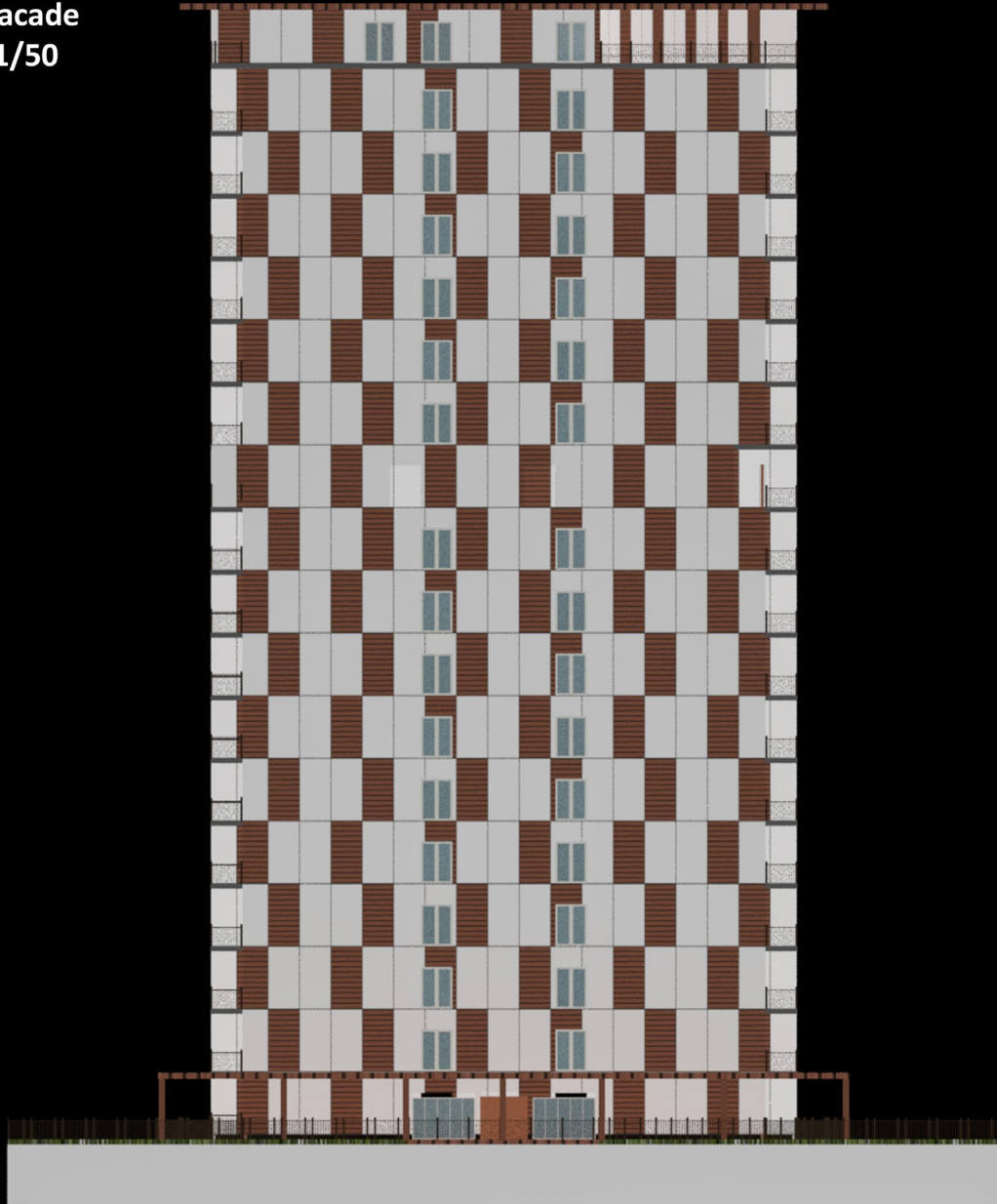


South Facade  
Scale: 1/50



1m 2m 5m 10m

West Facade  
Scale: 1/50



1m 2m 5m 10m





**Interior view of one of the units**



**Southeast Perspective**



**Southwest Perspective**

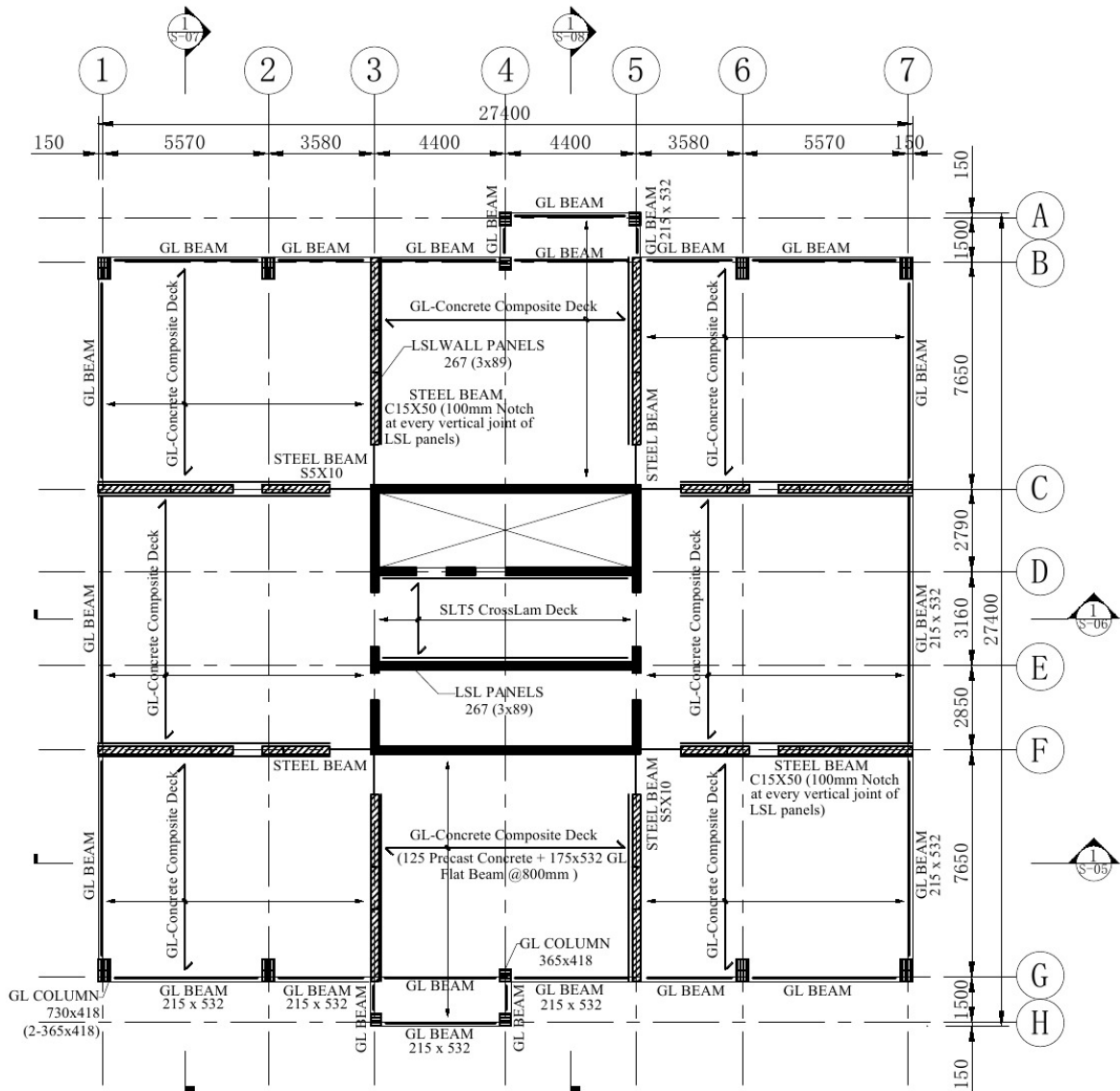


**Southeast Lower Perspective**

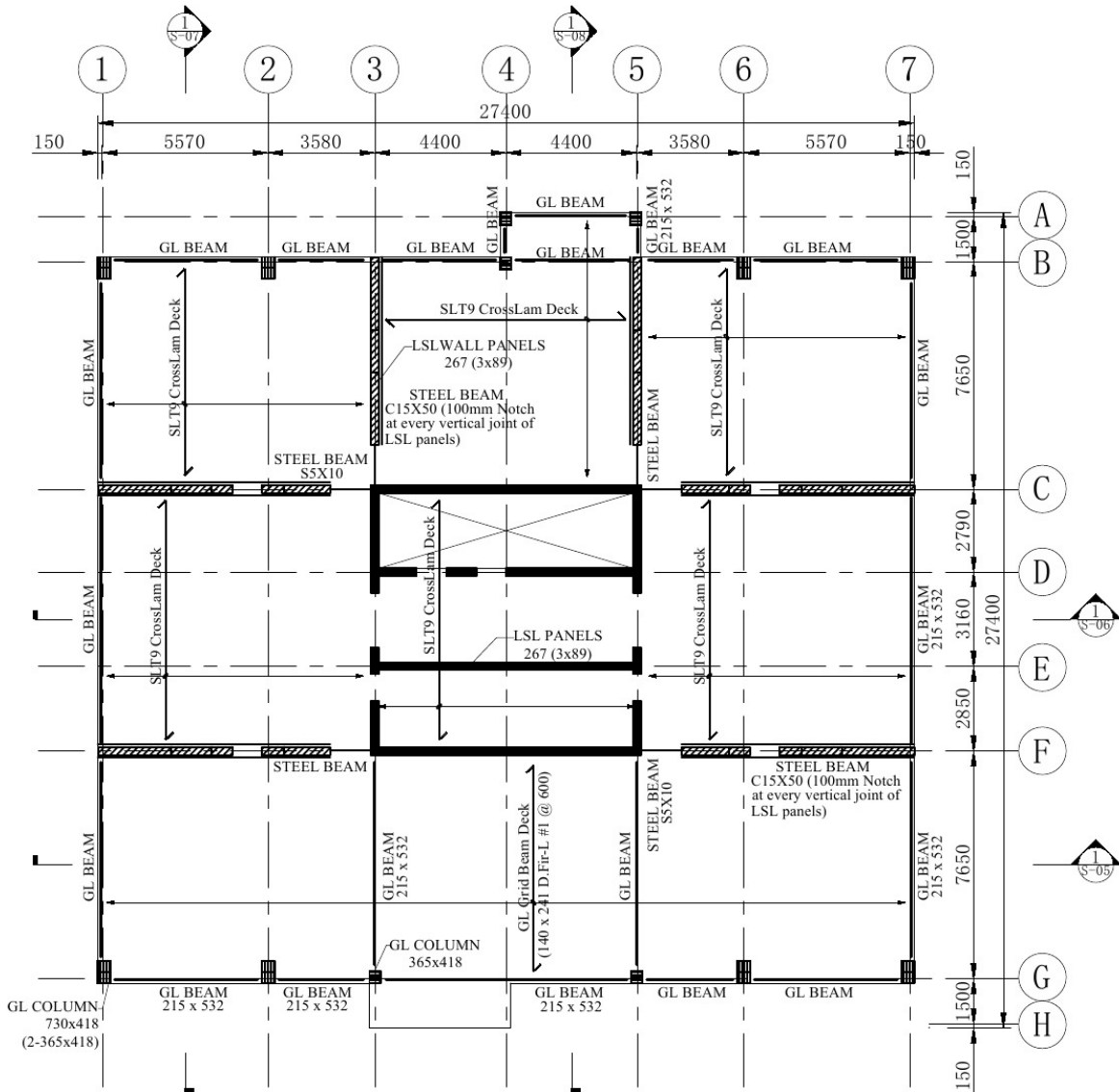
APPENDIX B

# STRUCTURAL DRAWINGS

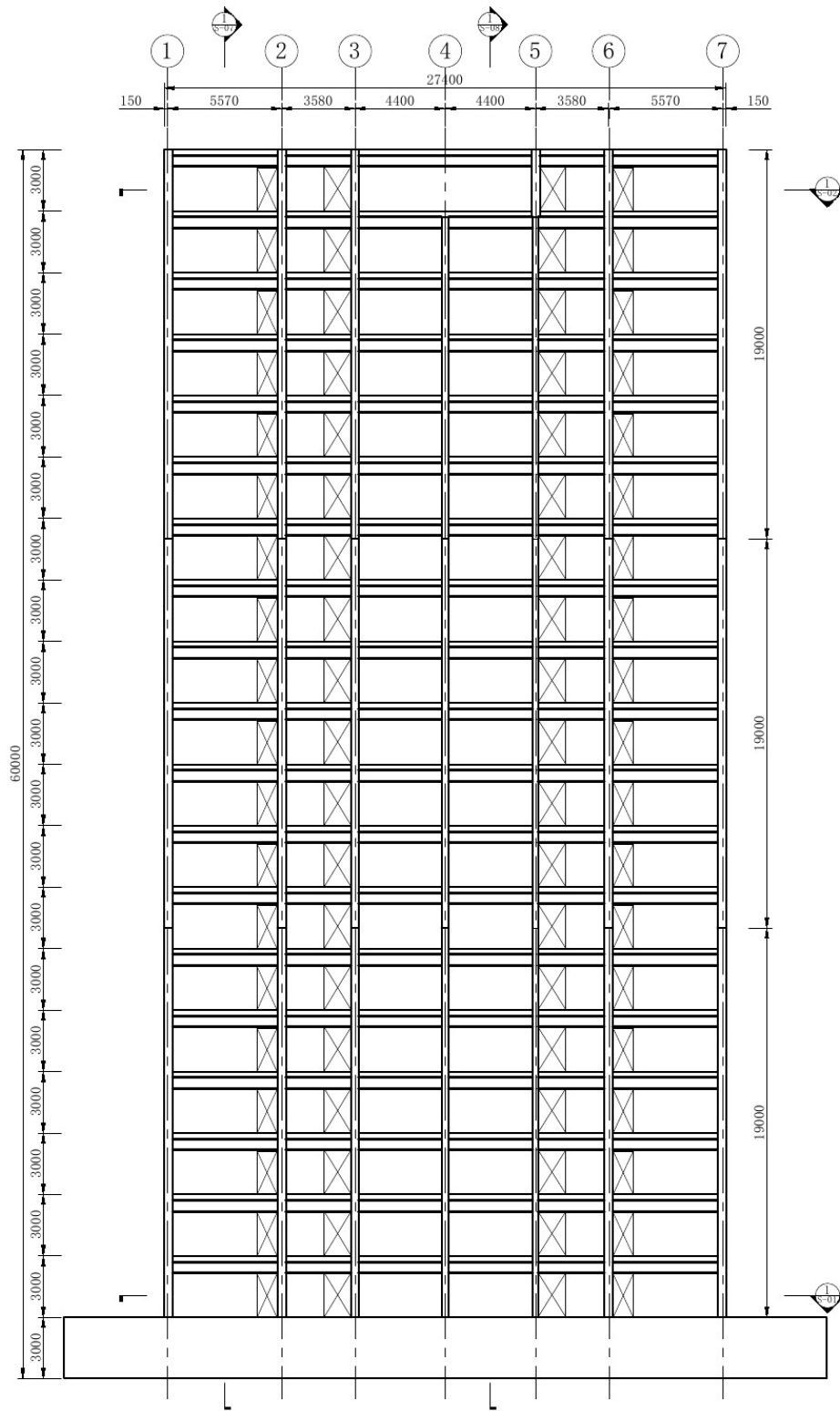
---



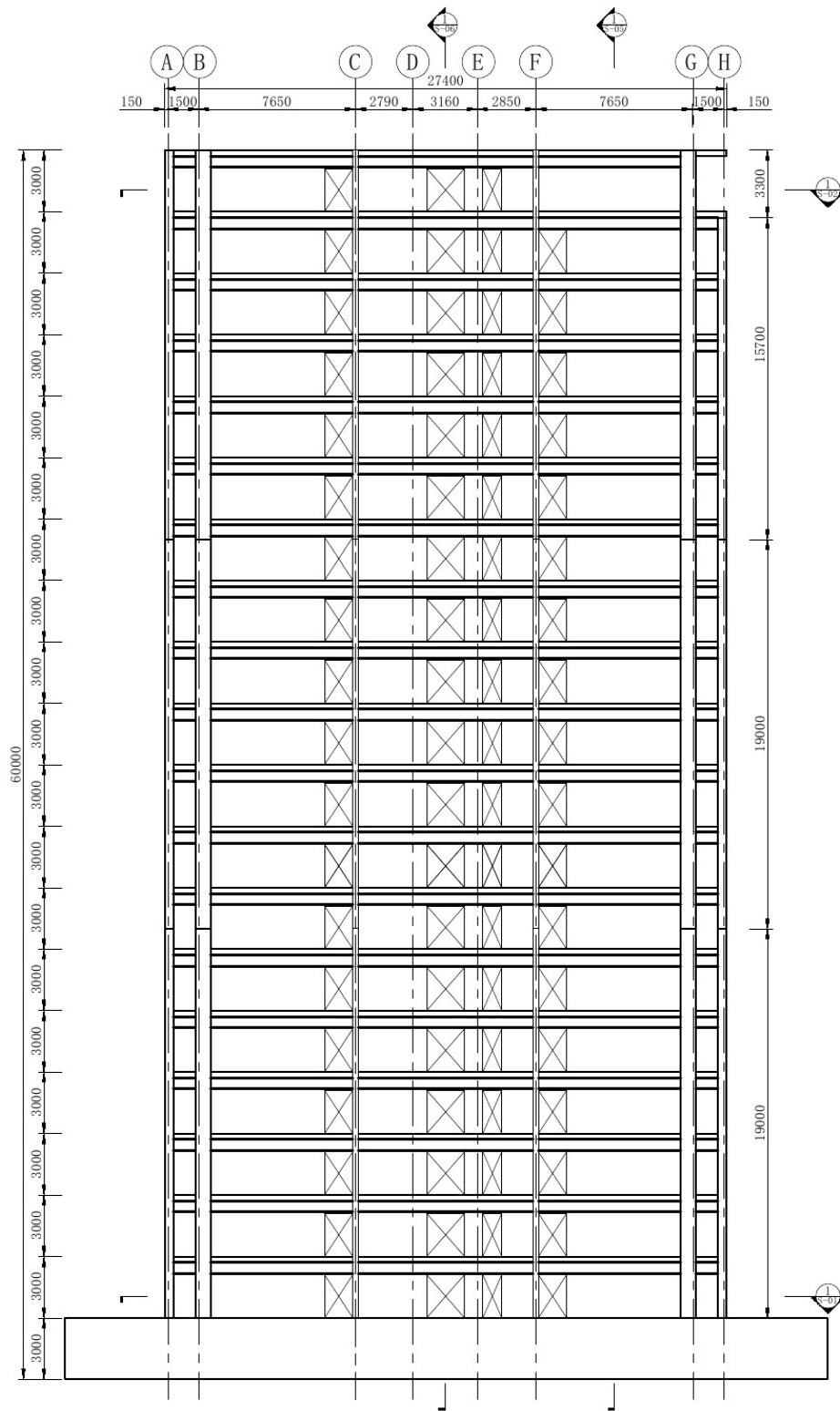
**1** TYPICAL FLOOR PLAN  
1:200



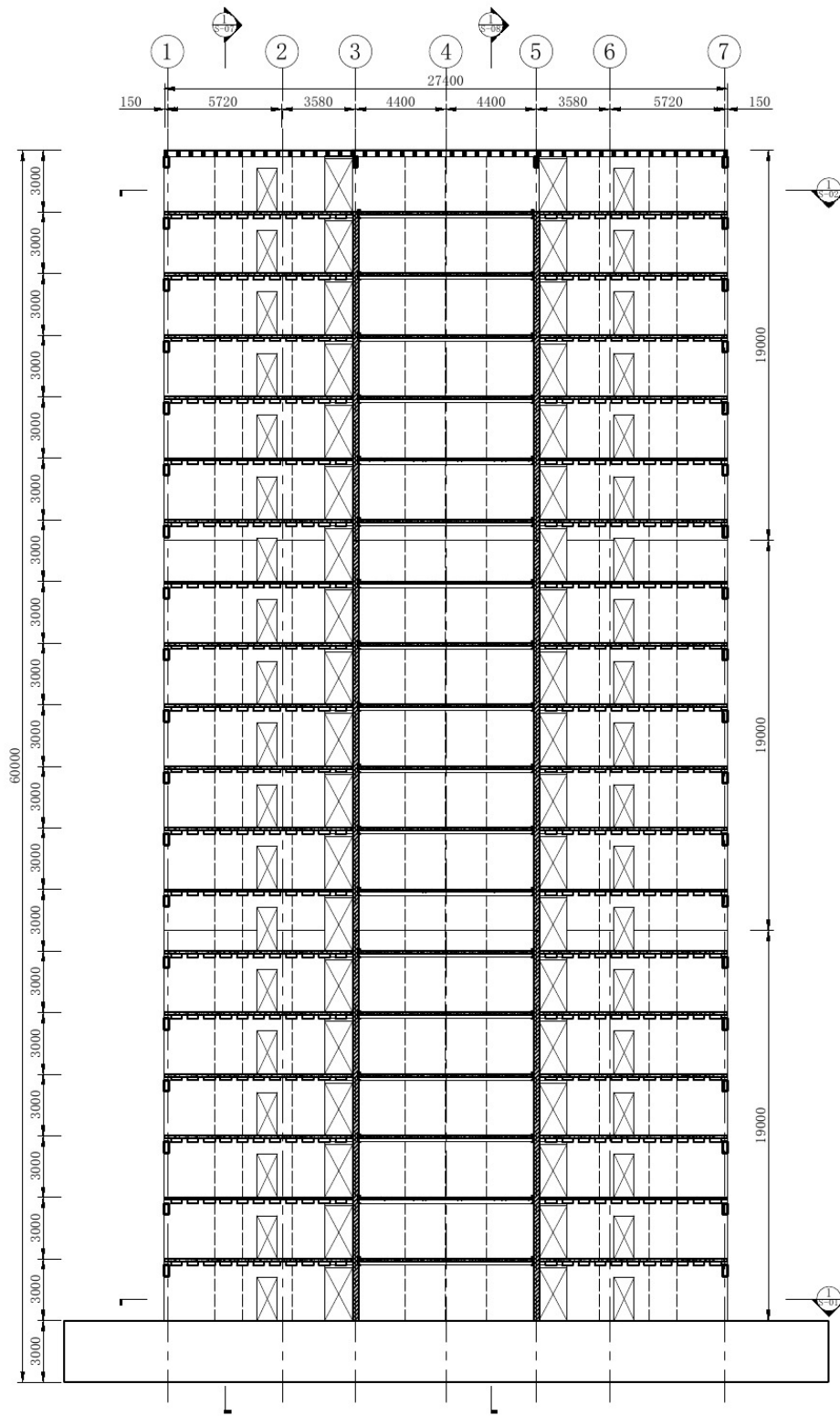
**1** 20th FLOOR PLAN  
1:200



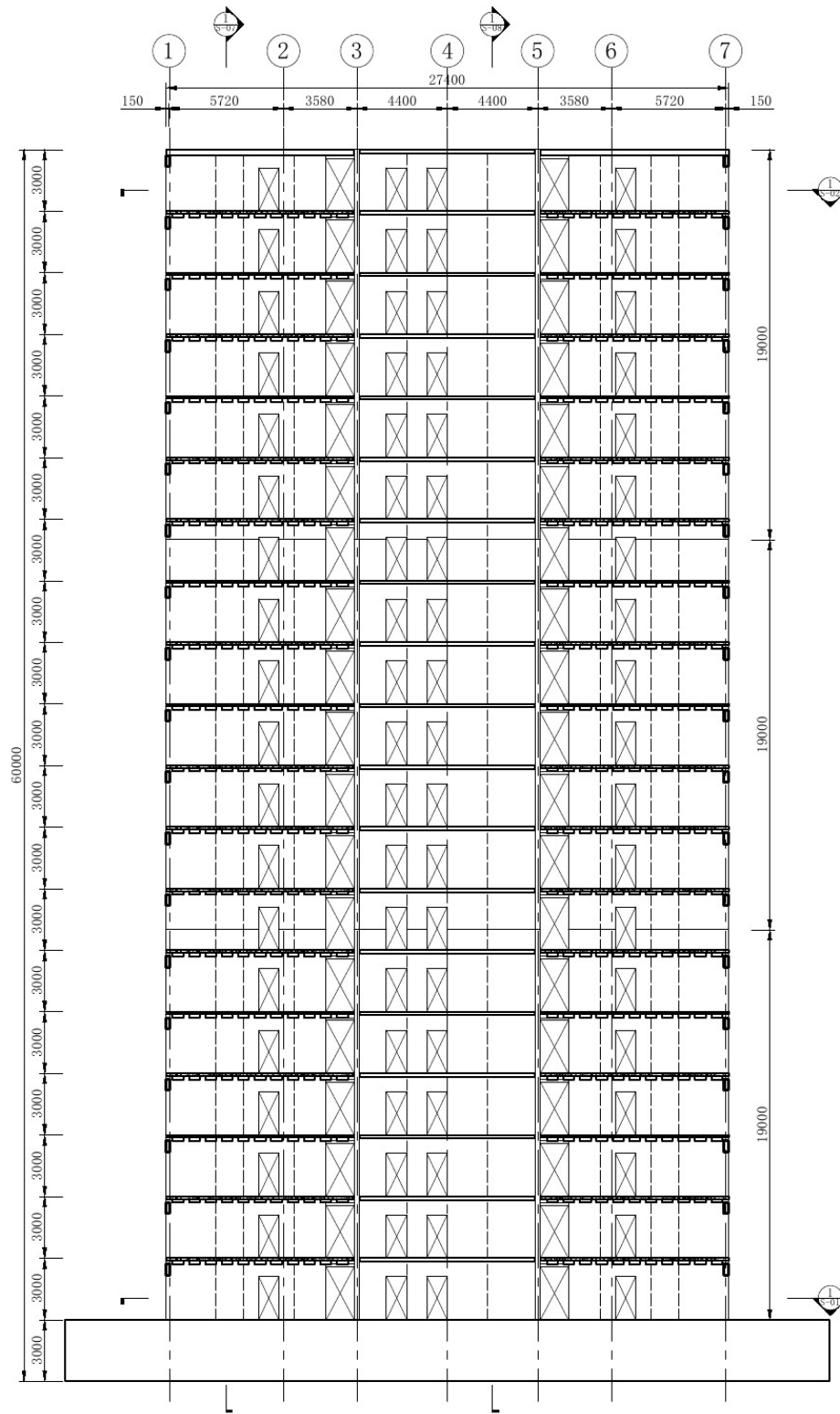
**1** SOUTH ELEVATION  
1:200



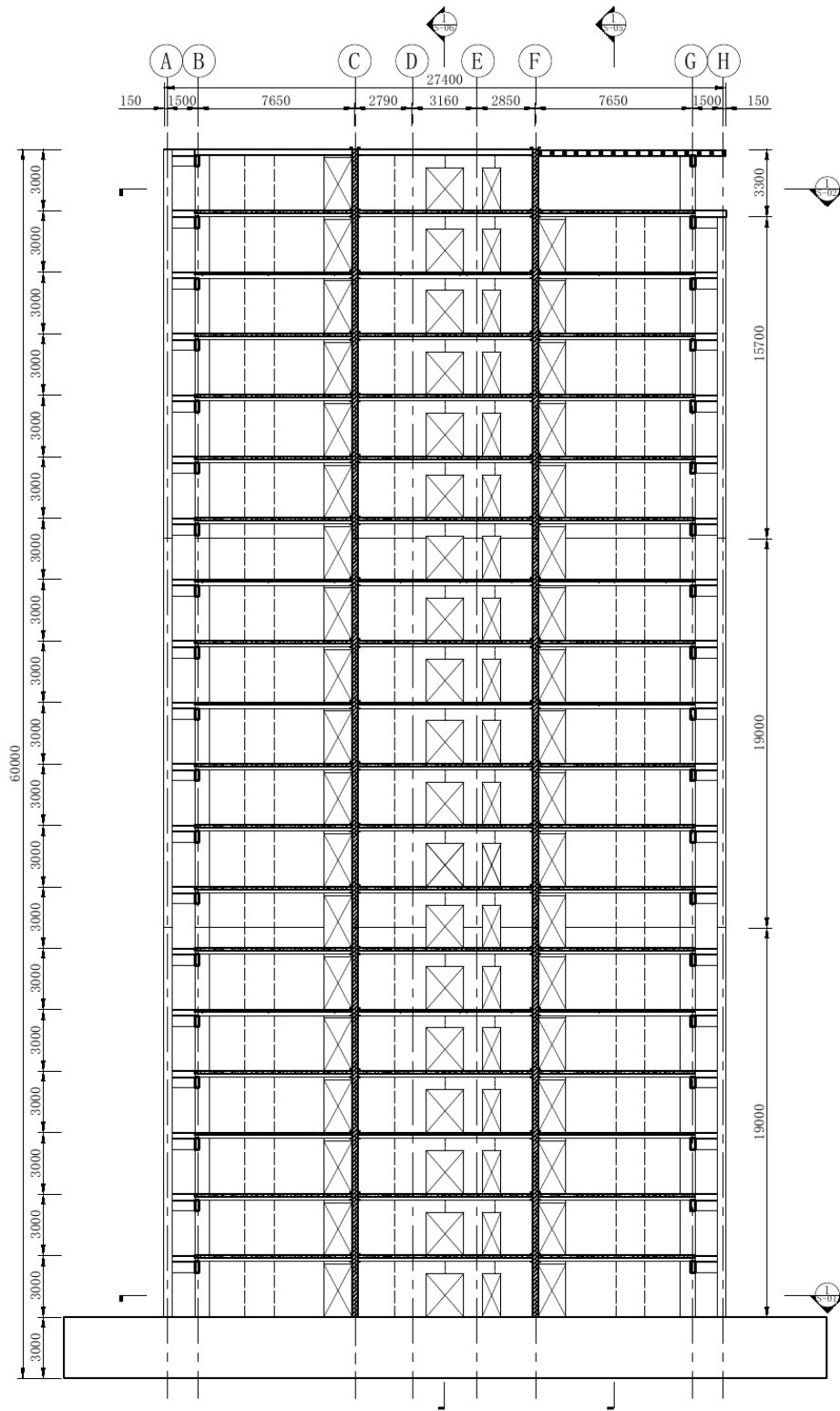
**1** WEST ELEVATION  
1:200



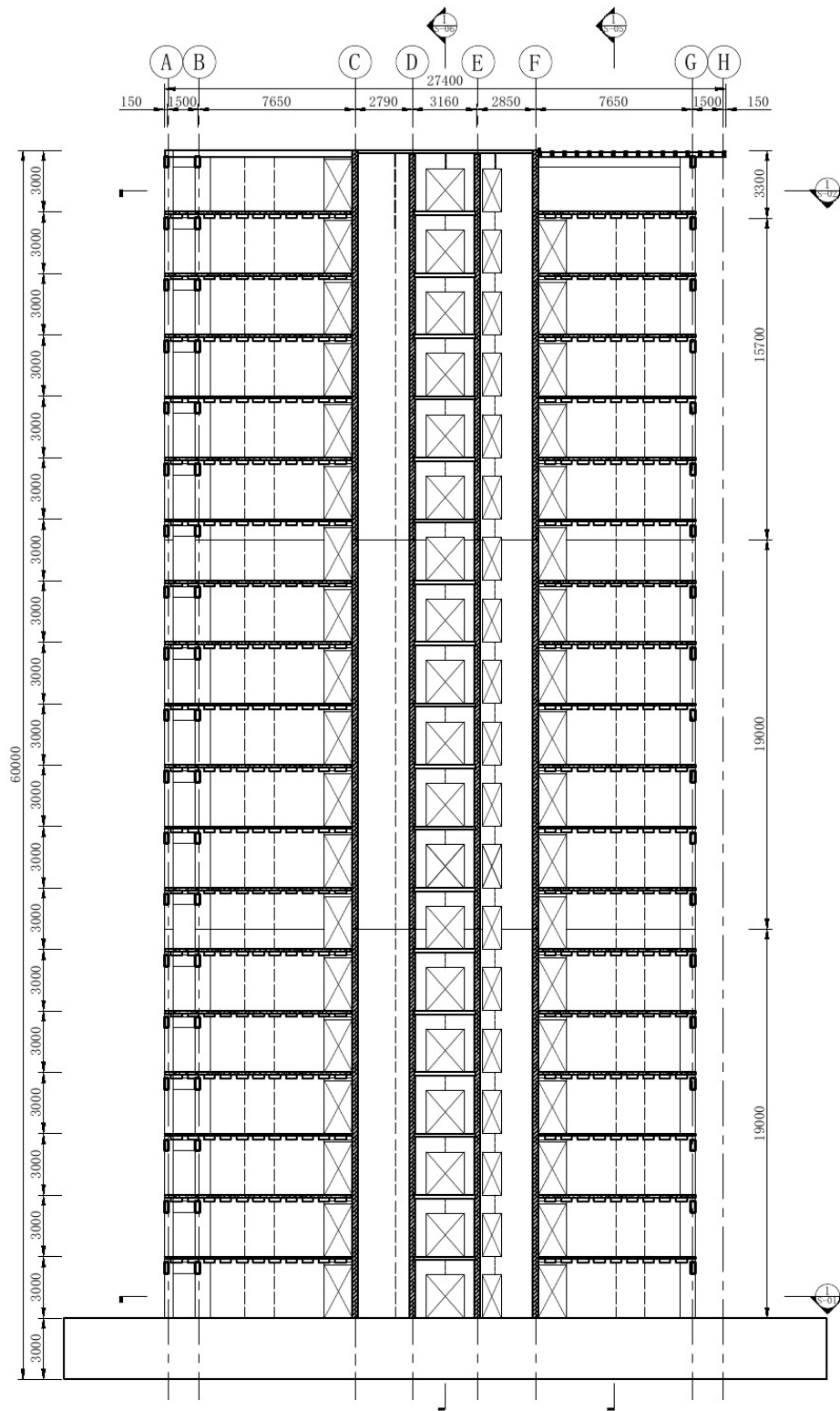
**1** EAST-WEST BUILDING SECTION I  
1:200



**1 EAST-WEST BUILDING SECTION II**  
1:200

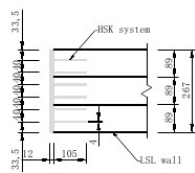


**1** SOUTH-NORTH BUILDING SECTION I  
1:200

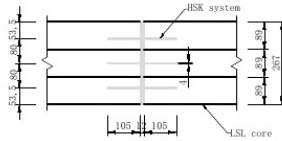


**1** SOUTH-NORTH BUILDING SECTION II  
1:200

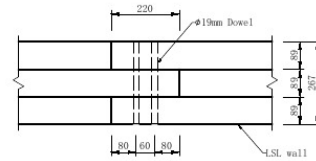




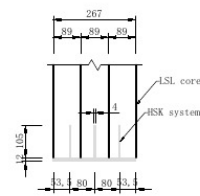
**1 HOLD-DOWN CONNECTION**



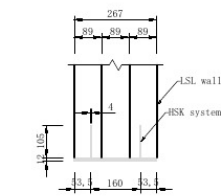
**2 VERTICAL JOINT OF CORE**



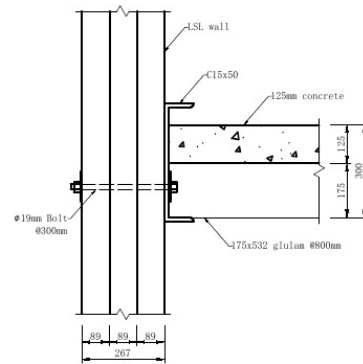
**3 VERTICAL JOINT OF SHEAR WALL**



**4 SHEAR CONNECTOR OF CORE**



**5 SHEAR CONNECTOR OF SHEAR WALL**



**6 FLOOR TO WALL CONNECTION**